N° :_____

Université Lille1
Sciences et Technologies

THESE DE DOCTORAT

Contribution of nanoparticles to the flame retardancy of epoxy resins

Présentée et soutenue publiquement à
L'UNIVERSITE LILLE 1 SCIENCES ET TECHNOLOGIES

pour obtenir le grade de
DOCTEUR
Spécialité : Molécules et Matière Condensée

par
Caroline GERARD
Ingénieur ENSCL

Thèse dirigée par **Prof. Serge Bourbigot et Dr. Gaëlle Fontaine**

Soutenue le 21 juin 2011 devant la Commission d'Examen composée de :

Prof. Jean-Marc LEFEBVRE, Université Lille 1	Président du jury
Prof. Manfred DÖRING, Karlsruhe Institut für Technologie/Heidelberg University	Rapporteur
Prof. Jean-François GERARD, INSA de Lyon	Rapporteur
Dr. Kenneth SCOBBIE, Huntsman Advanced Materials	Examinateur
Prof. Serge BOURBIGOT, ENSCL	Directeur de thèse
Dr. Gaëlle FONTAINE, ENSCL	Co-directrice de thèse

N° :_____

Université Lille1
Sciences et Technologies

THESE DE DOCTORAT

Contribution of nanoparticles to the flame retardancy of epoxy resins

Présentée et soutenue publiquement à
L'UNIVERSITE LILLE 1 SCIENCES ET TECHNOLOGIES

pour obtenir le grade de
DOCTEUR
Spécialité : Molécules et Matière Condensée

par
Caroline GERARD
Ingénieur ENSCL

Thèse dirigée par **Prof. Serge Bourbigot et Dr. Gaëlle Fontaine**

Soutenue le 21 juin 2011 devant la Commission d'Examen composée de :

Prof. Jean-Marc LEFEBVRE, Université Lille 1	Président du jury
Prof. Manfred DÖRING, Karlsruhe Institut für Technologie/Heidelberg University	Rapporteur
Prof. Jean-François GERARD, INSA de Lyon	Rapporteur
Dr. Kenneth SCOBBIE, Huntsman Advanced Materials	Examinateur
Prof. Serge BOURBIGOT, ENSCL	Directeur de thèse
Dr. Gaëlle FONTAINE, ENSCL	Co-directrice de thèse

Acknowledgements

The work described in this thesis has been carried out in the laboratory UMET (CNRS UMR 8207), led by Pr. Alexandre Legris, and more precisely in the team Ingénierie des Systèmes Polymères led by Dr. Jean-Marc Lefebvre. I would like to thank them for giving me the opportunity to integrate this laboratory and work on this challenging project.

I am especially grateful to Pr. Serge Bourbigot and Dr. Gaëlle Fontaine, who guided me along these years. Their never-ending suggestions and support when unexpected results kept appearing, and their patience towards my own numerous questions helped me enormously during this work. More than that, our discussions and trips for meetings abroad made me grow up.

I thank once more Dr. Jean-Marc Lefebvre, who agreed to chair this jury. I also thank Pr. Manfred Döring and Pr. Jean-François Gérard, who accepted to spend their time and competencies to review this thesis. I also acknowledge Dr. Kenneth Scobbie who agreed to be part of this jury.

I would also like to thank Pr. Jean Grimblot, director of the Ecole Nationale Supérieure de Chimie de Lille (ENSCL), which partly hosts the laboratory.

During the LAYSA project, I have met many people and I would like to thank them for the knowledge they provided to me and the good atmosphere of our meetings. The European Commission is also acknowledged for its financial support.

During this PhD, many people have helped me by transmitting their technical knowledge and carrying out special experiments. Therefore, I thank the NMR team from the Centre Commun de Mesures, and especially Pierre Watkin, Marc Bria and Bertrand Revel who worked with me for the characterization of carbon nanotubes and degraded

materials. I am also deeply indebted towards Dr. Anne-Sophie Mamède, who carried out the XPS experiments. Maxence Vandewalle is also acknowledged for the XRD analysis. I especially thank Dr. Séverine Bellayer, who carried out most of the microscopic analyses and answered my sometimes strange questions, but also shared her knowledge on carbon nanotubes with me.

I also would like to thank the technical and administrative departments of the ENSCL, who provided helpful support during these years, and especially Philippe Lambourg, who printed this manuscript.

I sincerely thank all members of the laboratory for all the moments we shared. I am particularly indebted towards Fabienne and Aurore, who have become more than colleagues, for their support, their humour and all the fits of the giggles that came out during our discussions. I thank Antoine for standing my frequent questions and remarks about almost everything (!). Pierre is acknowledged for is neverending good mood and helpfulness. I also thank Sophie, for her even temper and her answers to my numerous questions. Maryska and Clémence, don't give up sports, going with you helped me through this last year. Many thanks to the current members of the laboratory: Bastien, Ghassan, Hassan, Jérémie, Marion and the former ones: Christelle, Damien, Fatima, Hélène, Jérémy, Louis, Mathilde F., Mounim, Nico, Nadine, Oriane, Thomas, Virginie and Yohan. Mathilde C., Charaf, Maude, Michel, thank you for your support. I am also indebted towards the two interns I was responsible for: Olivier, for his enthusiasm, and Wen, for teaching me that sometimes 'yes' means 'no'. Finally, I owe many thanks to Brigitte for her constant helpfulness and good mood.

I would finally thank my family: my parents, who made it possible for me to study, my brother, Caroline and my nephew, my friends, for their support during these years. I owe a special acknowledgement to Thibault for his patience and help.

Contents

Résumé (Français)

Cette thèse porte sur l'ignifugation d'une résine époxyde grâce à l'incorporation de nanoparticules.

Depuis leurs premières synthèses au cours du XIXe siècle, l'utilisation des polymères s'est considérablement développée et est désormais courante dans notre quotidien. On les retrouve en effet dans des domaines aussi variés que le secteur de l'emballage, de la construction, des transports ou de l'électronique. Parmi eux, les résines époxydes, apparues au cours des années 1930, sont des matériaux thermodurcissables dont l'essor a également été considérable. La production de pièces composites à matrice polymère pour les secteurs automobile et aéronautique offre également de nouveaux débouchés pour ces matériaux. Actuellement, 50 % du volume d'une voiture (équivalent à 10 % de son poids) et 27 % de la masse du nouvel Airbus A380 sont faits de plastiques. Dans les avions actuellement en développement, ce niveau atteint 50 % en masse.

Cependant, les nombreux avantages offerts par l'utilisation de polymères ne doivent pas cacher un de leurs défauts majeurs : ils brûlent facilement. Ce sont en effet des matériaux organiques, et de ce fait, ils produisent des composés volatils inflammables lorsqu'ils sont soumis à une source de chaleur. Si les conditions sont réunies, ceci peut résulter en l'inflammation du matériau et de son environnement. Ce type de danger ne peut être ignoré dans le domaine aéronautique, étant donné que les passagers ne peuvent pas quitter les lieux facilement en cas d'incendie. De plus, en cas d'inflammation, les polymères alimentent non seulement l'incendie, mais ils libèrent aussi des gaz toxiques et des fumées, ce qui limite la mobilité des passagers et engendre la panique. La question du retard au feu n'est donc pas négligeable pour ce type d'applications.

Les matériaux composites vont donc vraisemblablement être utilisés de plus en plus souvent dans les avions, ils offrent de nombreuses possibilités mais peuvent également contribuer au développement d'un incendie. Le projet LAYSA (Multifunctional Layers for Safer Aircraft Composite Structures) a été élaboré à partir de ce constat. Ce programme financé par l'Union Européenne vise à étudier la faisabilité de composites à matrice polymère combinant plusieurs fonctions :

- la prévention de la formation de glace et son élimination lorsque l'avion est à haute altitude
- l'amélioration de la réaction au feu des composites étudiés
- la mesure de la température et de contraintes mécaniques (élongation) à travers des variations de conductivité électrique.

Un des objectifs du projet est d'aboutir à ces propriétés principalement à travers l'utilisation de nanoparticules, et en particulier de nanotubes de carbones (CNTs). Ce type de charges permettrait notamment de réduire le poids final de la structure, ce qui conduirait à des économies de carburant. Douze partenaires, universitaires ou industriels, se sont associés pour mener à bien ce programme. Le travail a été subdivisé en trois grandes étapes. Tout d'abord, différentes matrices et nanoparticules ont été identifiées dans la littérature et des tests préliminaires portant sur les trois propriétés ont été effectués. Les systèmes ont ensuite été optimisés et modélisés pour chaque propriété à l'échelle laboratoire, avant d'être combinés pour obtenir le système multifonctionnel. Le développement final du système à l'échelle intermédiaire est encore en cours.

Cette thèse s'attache à l'évaluation de la réaction au feu de différentes nanoparticules dans une résine époxyde modèle, aux méthodes mises en œuvre pour étudier les mécanismes associés et au développement d'une résine époxyde ignifugée.

Le premier chapitre de cette thèse expose les principes généraux de l'ignifugation des polymères. La dégradation thermique des résines époxydes y est décrite ainsi que les modes d'actions des retardateurs de flamme traditionnels. Les récentes avancées concernant l'utilisation de nanoparticules pour ignifuger les polymères (aussi bien thermoplastiques que thermodurcissables) ainsi que le concept d'intumescence sont particulièrement décrits.

Le deuxième chapitre de cette thèse vise à procurer au lecteur tous les détails pratiques concernant la préparation des résines époxydes chargées et celle de CNTs fonctionnalisés. Les méthodes de caractérisation des matériaux obtenus, ainsi que celles destinées à évaluer leur réaction au feu sont ensuite présentées. Enfin, les techniques ayant permis l'élucidation du comportement au feu de ces composites sont décrites.

Le troisième chapitre présente les propriétés de résines époxydes chargées avec différentes nanoparticules. Une première partie cherche à évaluer le potentiel de

nanoparticules commerciales en tant que retardateurs de flamme (Polyhedral Oligomeric Silsequioxanes (POSS) et nanotubes de carbone). Dans la seconde partie, les CNTs sont fonctionnalisés, caractérisés puis incorporés dans la matrice et la réaction au feu des matériaux obtenus est évaluée.

Le quatrième chapitre présente les résultats obtenus en combinant un retardateur de flamme phosphoré traditionnel (APP) avec deux nanoparticules identifiées comme prometteuses dans le chapitre précédent.

Enfin, dans le cinquième chapitre, les mécanismes d'action des formulations identifiées dans le quatrième chapitre sont étudiés.

La première des actions menées au cours de cette thèse a été l'évaluation du potentiel de nanoparticules commerciales (POSS et CNTs) pour l'ignifugation de la résine modèle. Le Tableau 1 présente les différentes charges testées dans cette partie et leur taux d'incorporation. Les quatre types de POSS diffèrent par les fonctions organiques présentes aux sommets des cages de POSS.

Tableau 1: Formulations des époxy chargées en nanoparticules commerciales

Désignation de l'échantillon	Charge	Taux de charge (% massique)
Epoxy vierge	-	-
Epoxy_aminopropylisobutylPOSS-5	AminopropylisobutylPOSS	5
Epoxy_trisilanolphenylPOSS-5	TrisilanolphenylPOSS	5
Epoxy_FQ-POSS-5	Firequench 1286	5
Epoxy_OMPOSS-5	OctamethylPOSS	5
Epoxy _CNT-0.5	CNTs	0,5

Dans un premier temps, la dispersion de ces charges dans la matrice ainsi que le taux de réticulation des matériaux ainsi obtenus ont été caractérisés. L'étude de la dispersion des nanoparticules dans le polymère montre qu'elle diffère selon le type de POSS utilisé : l'échantillon contenant le trisilanolphenylPOSS peut être considéré comme un nanocomposite (Figure 1) alors que l'aminopropylisobutylPOSS est microdispersé (Figure 2). Les OMPOSS et les FQ-POSS présentent un comportement intermédiaire.

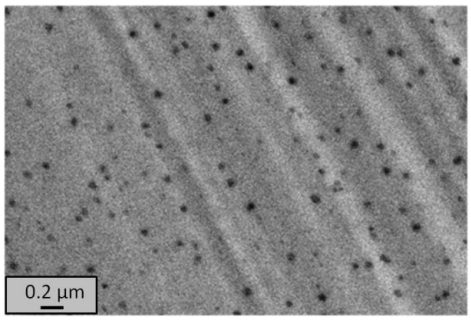

Figure 1: Image de l'échantillon Epoxy_trisilanolphenylPOSS-5 en microscopie électronique à transmission

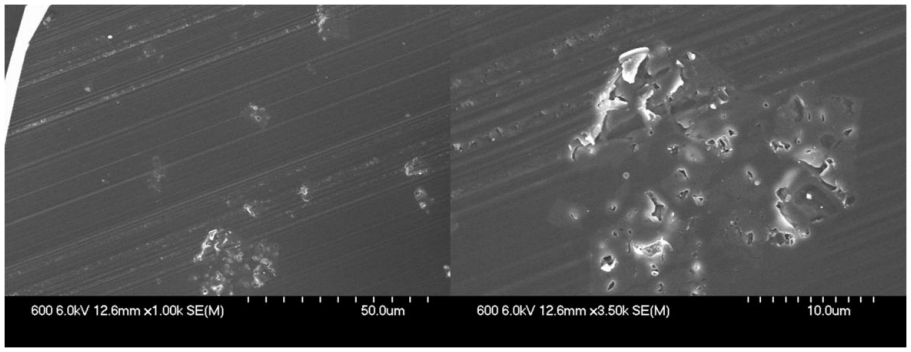

Figure 2: Images de l'échantillon Epoxy_aminopropylisobutylPOSS-5 en microscopie électronique à balayage

La dispersion des nanotubes de carbone n'est pas homogène (Figure 3). En effet, certaines zones présentent une forte densité en CNTs (Figure 3a et b), d'autres sont presque vides (Figure 3c) et l'on peut voir de gros agrégats à d'autres endroits (Figure 3d).

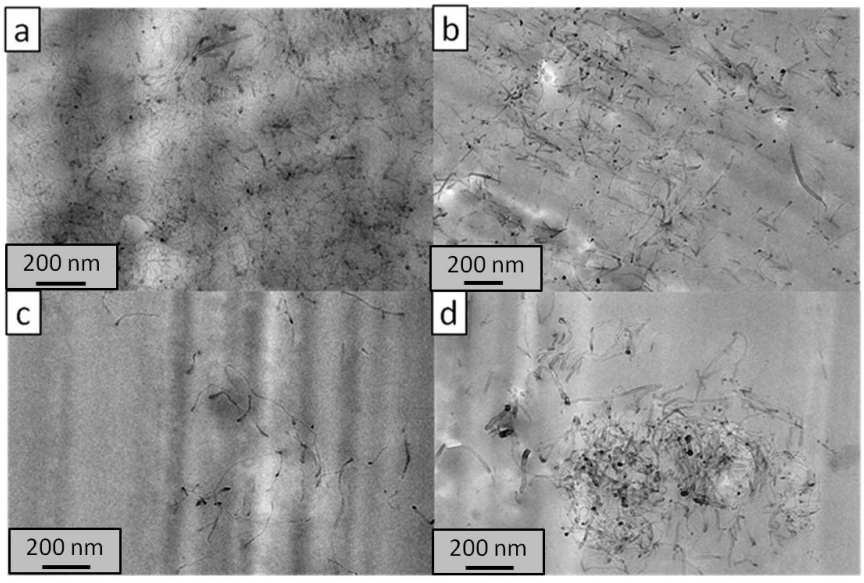

Figure 3: Images de l'échantillon Epoxy_CNT-0.5 en microscopie électronique à transmission

Les températures de transition vitreuse, mesurées par calorimétrie différentielle à balayage, sont similaires pour tous les échantillons (130-132 °C). Etant donné que le taux de réticulation et la température de transition vitreuse sont reliés par l'équation de di Benedetto (III.1.1.b, p.120), le taux de réticulation des différents matériaux doit être similaire. Cette hypothèse est en effet confirmée par la mesure du taux de réticulation en infrarouge à transformée de Fourier : il est compris entre 72 et 82 % pour tous ces matériaux. Un spectre type de la résine époxyde est présenté Figure 4.

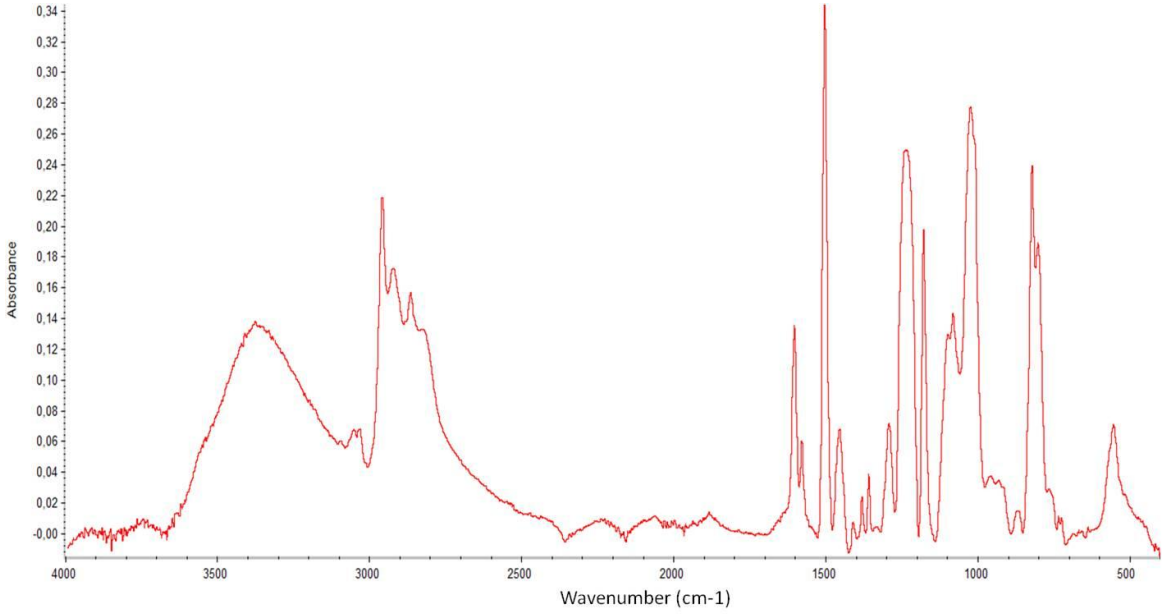

Figure 4: Spectre infrarouge de l'Epoxy vierge

La stabilité thermique des matériaux chargés a ensuite été évaluée par analyse thermogravimétrique en atmosphère thermo-oxydante. Cette étude révèle que la présence de nanocharges entraîne un début de décomposition du système à plus basse température que pour la résine vierge. Cependant, la température pour laquelle la vitesse de dégradation est maximale est significativement déplacée vers de plus hautes températures avec certains POSS (particulièrement avec le trisilanolphenylPOSS et l'OMPOSS). On observe également un effet sur les quantités de résidus intermédiaires : la présence de CNTs, d'aminopropylisobutylPOSS ou de FQ-POSS augmente la quantité de résidu intermédiaire (respectivement 65 wt.%, 56 wt.% et 50 wt.% au lieu de 40 wt.% pour la résine vierge). Au contraire, l'incorporation de trisilanolphenylPOSS ou d'OMPOSS diminue la quantité de résidu intermédiaire (respectivement 30 wt.% et 24 wt.%).

Lors de tests de réaction au feu par calorimétrie à cône (mass-loss), on observe une faible amélioration du comportement au feu des matériaux dans de nombreux cas (Figure 5). Parmi les POSS, les OMPOSS donnent les meilleurs résultats (46 % de diminution de débit calorifique). Il y a donc un rôle de la nature des fonctions organiques des POSS sur les performances feu du matériau final. Quant aux CNTs, ils diminuent le débit calorifique de 27 %.

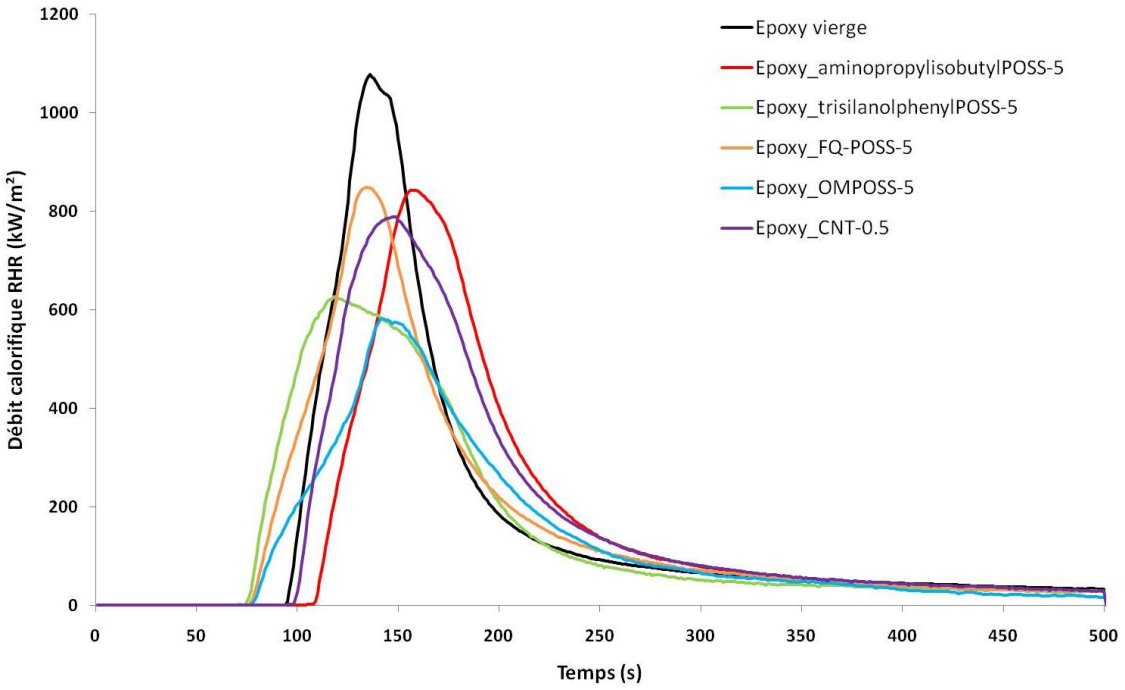

Figure 5: Débit calorifique en fonction du temps pour les époxy chargés en nanoparticules commerciales (irradiance : 35 kW/m², épaisseur : 5 mm, distance : 25 mm)

Etant donné que la dispersion dans la matrice des nanoparticules n'est pas satisfaisante même si les propriétés feu sont améliorées, notre approche a été de fonctionnaliser les nanotubes de carbone afin d'augmenter cette dispersion en greffant à leur surface deux fonctions potentiellement retardatrices de flamme (mélamine et POSS) (Figure 6). Les CNTs sont tout d'abord oxydés dans du mélange sulfonitrique afin de créer des fonctions acide carboxylique servant de points d'ancrage dans la suite de la réaction (CNT-COOH). Ces fonctions sont ensuite activées par du chlorure de thionyle (CNT-COCl) et réagissent immédiatement avec des amines (CNT-amine et CNT-POSS). Dans le cas de la fonctionnalisation par la mélamine, une étape supplémentaire est

nécessaire : la diamine greffée sur le CNT réagit avec de la 6-chloro-2,4-diamino-1,3,5-triazine pour conduire aux CNT-mélamine.

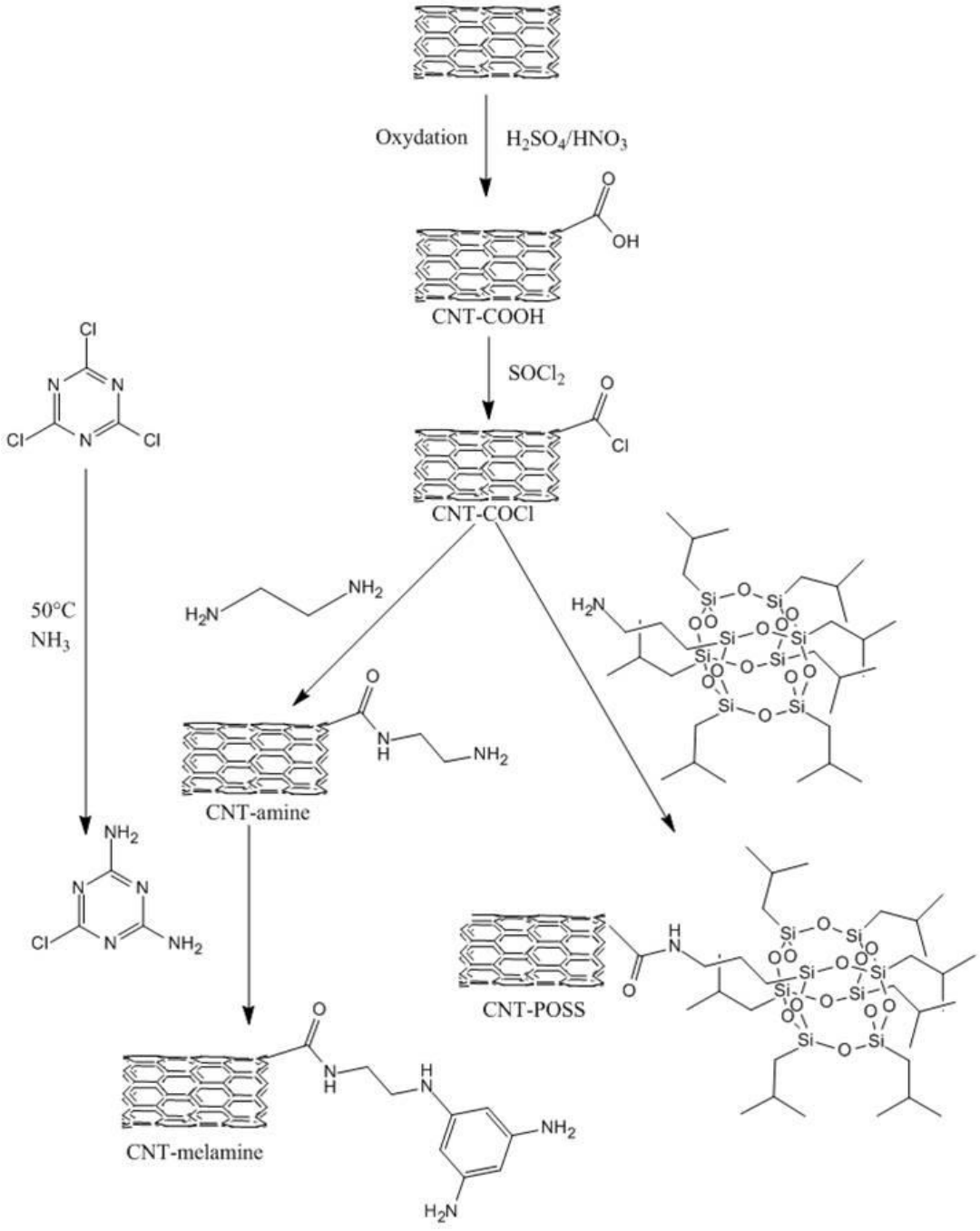

Figure 6: Schéma de la fonctionnalisation des CNTs

Les CNTs fonctionnalisés ont été caractérisés par IRTF, Résonance Magnétique Nucléaire (RMN) du liquide et spectroscopie de photoélectrons induits par rayons X (XPS), ce qui a permis d'établir que des liaisons covalentes ont été bien été créées entre les CNTs et les différentes fonctions. La stabilité thermique de ces nouvelles charges a

également été évaluée : elle établit également que le greffage a eu lieu et suggère que ces charges sont suffisamment stables pour être incorporées dans la matrice. Malheureusement, les meilleures performances au feu obtenues en utilisant ces nanotubes modifiés sont similaires à celles que l'on obtient avec les nanotubes commerciaux. Des mesures réalisées sur la résine vierge et celle contenant les nanotubes commerciaux montrent également que la conductivité thermique du matériau n'est pas augmentée en présence de CNTs. Ceci est attribué à la mauvaise dispersion des CNTs, qui limitent la circulation des phonons lorsqu'ils sont agglomérés.

L'utilisation de nanoparticules seules, qu'elles soient commerciales ou modifiées en laboratoire, a un effet sur la réaction de la résine époxyde. Cependant, les performances des matériaux obtenus ne sont pas suffisantes pour l'application visée. La deuxième action menée a donc été la recherche d'un système plus performant.

Les systèmes intumescents sont régulièrement utilisés dans la littérature pour ignifuger les polymères [1]. Ces systèmes agissent par la formation d'une couche charbonnée expansée qui isole du feu le polymère non dégradé et limite l'émission de combustibles alimentant la flamme. Ils se sont montrés particulièrement efficaces dans les résines époxydes [2]. De plus, des effets de synergies ont été rapportés lorsqu'ils sont combinés avec des nanoparticules [3-5].

Il a donc été décidé de combiner du polyphosphate d'ammonium (APP) avec les OMPOSS (identifiés précédemment comme les nanoparticules les plus prometteuses) et les CNTs (étant donnés l'intérêt particulier du Consortium pour ces nanoparticules et les performances feu obtenues précédemment). Les formulations utilisées sont décrites dans le Tableau 2.

Tableau 2: Formulations des matériaux époxy intumescents

Désignation de l'échantillon	Charge 1	Taux de charge (% massique)	Charge 2	Taux de charge (% massique)
Epoxy vierge	-	-	-	-
Epoxy_OMPOSS-5	OMPOSS	5	-	-
Epoxy_APP-5	APP	5	-	-
Epoxy_APP-4.5_CNT-0.5	APP	4.5	CNTs	0.5
Epoxy_APP-4_OMPOSS-1	APP	4	OMPOSS	1

Une fois encore, le degré de réticulation des matériaux obtenus ne semble pas affecté par la présence des charges (valeurs comprises entre 78 et 83 %). La dispersion des charges a également été caractérisée. Elle semble assez homogène, même si la dispersion des particules n'est pas nanométrique. La conductivité thermique des matériaux a été mesurée : la présence d'APP augmente la diffusivité thermique des formulations, probablement à cause de la cristallinité de l'APP (les phonons circulent plus rapidement dans les cristaux). La stabilité thermique a également été évaluée en atmosphère thermo-oxydante (Figure 7).

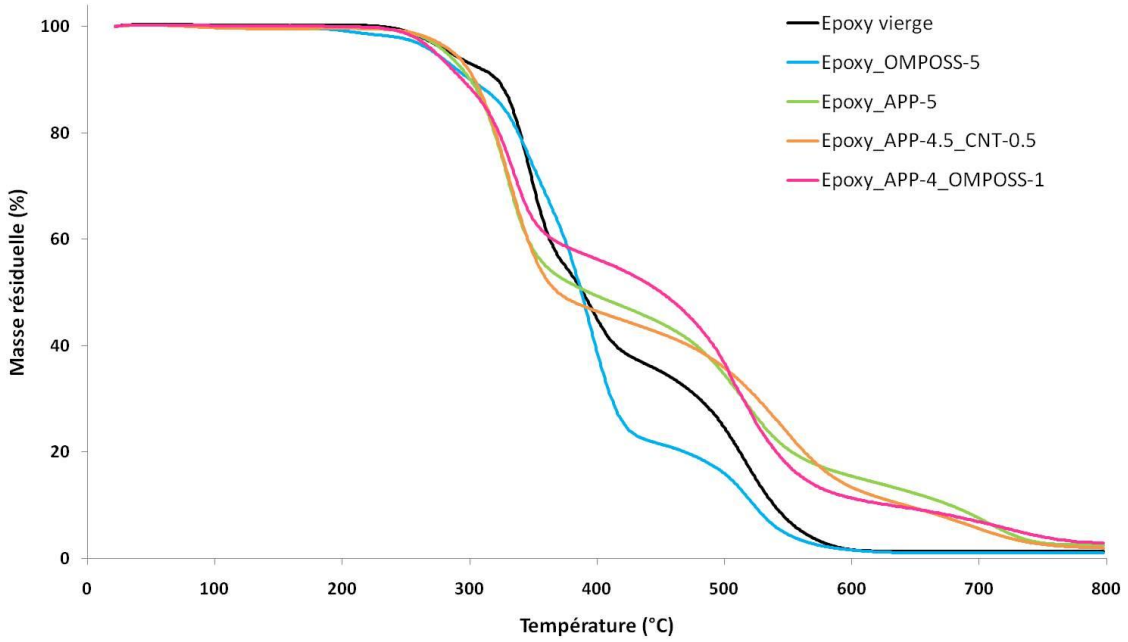

Figure 7: Dégradation thermo-oxydante des époxy intumescents (Air, 10 °C/min)

On peut voir que la présence d'APP déstabilise le système à basse température (décomposition en acide polyphosphorique et ammoniac à T<280 °C)[1] mais que cela permet la formation précoce d'un résidu charbonné qui limite la dégradation ultérieure du matériau. L'association des CNTs à l'APP ne modifie pas la première étape de dégradation, mais le résidu intermédiaire obtenu est plus faible. Quant à la combinaison APP/OMPOSS, elle permet d'obtenir un résidu intermédiaire plus important.

Ces formulations ont été testées pour leur réaction au feu en calorimétrie à cône (Figure 8).

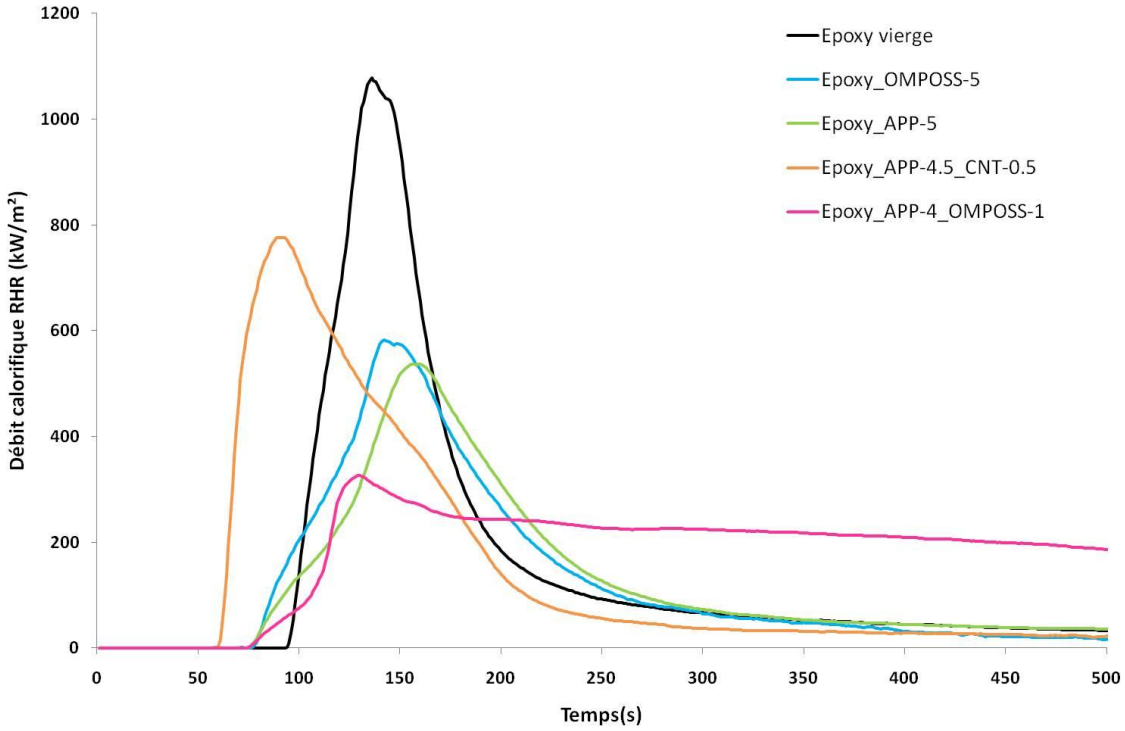

Figure 8: Débit calorifique en fonction du temps pour les époxy intumescents (irradiance : 35 kW/m², épaisseur : 5 mm, distance : 25 mm)

On peut voir que le débit calorifique est diminué de 50 % par rapport à la résine vierge lorsque l'APP est utilisé seul. Les CNTs ont un effet antagoniste avec l'APP puisque la réduction n'est plus que de 28 % (les CNTs utilisés seuls apportent une réduction de 27 %). Au contraire, l'utilisation d'OMPOSS en combinaison avec l'APP est bénéfique puisque la réduction atteint 68 %, alors que l'OMPOSS utilisé seul n'apporte que 46 % de réduction.

La morphologie des résidus après combustion apporte des informations sur les comportements précédemment observés (Figure 9). La résine époxyde non chargée ne laisse presque pas de résidus (l'aluminium utilisé pour envelopper l'échantillon est encore visible, mais percé par endroits). Lorsque les OMPOSS sont incorporés seuls dans la matrice, on observe la formation d'un résidu fragile après combustion : il est composé de fines couches blanchâtres, probablement dues à la présence de silice issue de la dégradation du POSS. Avec l'APP, on obtient un résidu charbonné expansé, mais avec des zones de vide à l'intérieur. Lorsque l'APP est combiné avec les CNTs, le résidu est fait de grosses cellules et est très friable. Au contraire, l'ajout d'OMPOSS au système Epoxy_APP-5 permet de renforcer le résidu obtenu avec l'APP seul : il est formé de

nombreuses petites bulles, sans que l'on observe des fissures comme dans la formulation Epoxy_APP-5.

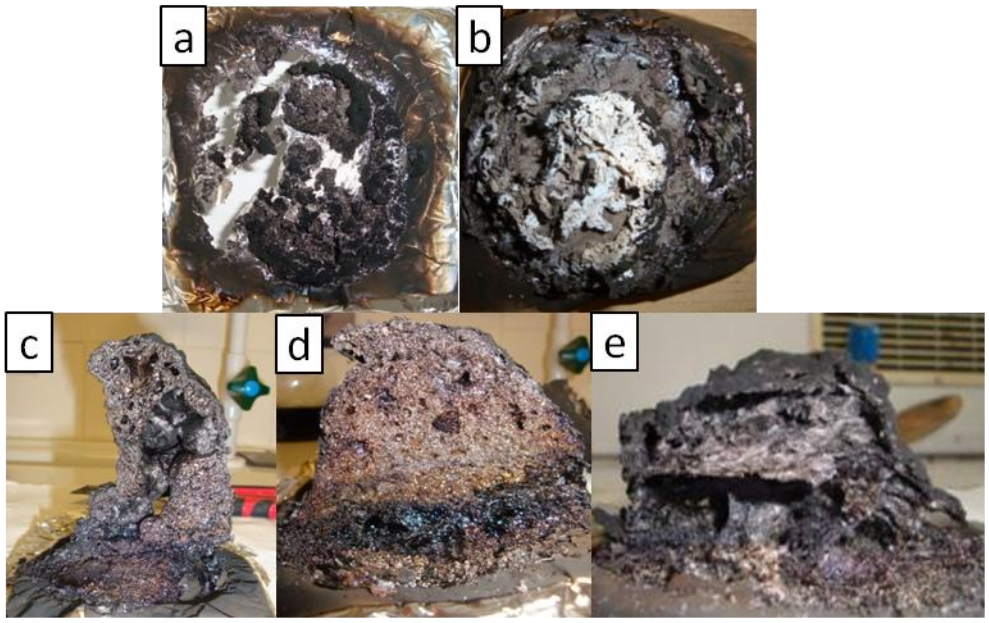

Figure 9: Résidus obtenus après les tests réalisés au calorimètre à cône – a : Epoxy vierge (vue de dessus), b : Epoxy_OMPOSS-5 (vue de dessus), c : Epoxy_APP-5 (vue en coupe), d : Epoxy_APP-4_OMPOSS-1 (vue en coupe), e : Epoxy_APP-4.5_CNT-0.5 (vue en coupe) (irradiance : 35 kW/m², épaisseur : 5 mm, distance : 25 mm)

Ces résultats concordent avec la mesure de la chaleur totale dégagée par combustion et avec la mesure de la perte de masse en fonction du temps. Enfin, l'énergie produite par la combustion des gaz dégagés lors de la pyrolyse des échantillons est similaire entre les échantillons (test au Pyrolysis Combustion Flow Calorimeter), ce qui suggère que les effets observés sont principalement des phénomènes en phase condensée.

La dernière partie de ce manuscrit concerne l'élucidation des effets de synergie et antagonismes précédemment observés. Dans un premier temps, la combustion de ces systèmes est stoppée à des moments clés (durant le gonflement pour les formulations intumescentes, au maximum de débit calorifique et après combustion pour l'ensemble des formulations) et les résidus sont analysés. L'aspect général de ces résidus au cours du temps fournit plusieurs informations : on obtient un résidu plein de bulles plus tôt avec la formulation Epoxy_APP-4_OMPOSS-1 qu'avec celle ne comportant que l'APP. Au contraire, l'association Epoxy_APP-4.5_CNT-0.5 ne forme jamais de bulles. L'analyse des

résidus par RMN du solide ne suggère pas la présence d'espèces chimiques supplémentaires dans ces systèmes. Cependant, la dégradation du mélange APP/OMPOSS seul dans un four à haute température suggère qu'il est possible d'obtenir des silicophosphates issus de la réaction entre ces deux espèces. Il est donc envisageable que la réaction ait lieu de manière limitée dans le résidu du matériau formulé, mais que la concentration soit si faible que les silicophosphates ne puissent pas être détectés par RMN dans le résidu fortement expansé. S'ils sont effectivement obtenus dans la matrice dégradée, il est probable qu'ils contribuent au renforcement mécanique du résidu sans pour autant être le phénomène majeur expliquant le meilleur comportement au feu.

Les systèmes intumescents ont donc été étudiés d'un point de vue dynamique. Tout d'abord, des mesures de viscosité apparente ont été effectuées. En effet, la dégradation thermique des résines époxydes s'accompagne d'une chute de viscosité. Si la viscosité est trop faible lorsque les gaz de dégradation sont relargués, ils ne pourront être piégés et donc contribuer au développement de la structure intumescente. Au contraire, si elle est trop élevée, le résidu va se fissurer lors de la libération des gaz à cause d'une pression interne trop forte. Ainsi, une viscosité adaptée est essentielle pour le bon développement de l'intumescence. La Figure 10 illustre le développement de l'intumescence en fonction du degré de conversion de la dégradation (noté α).

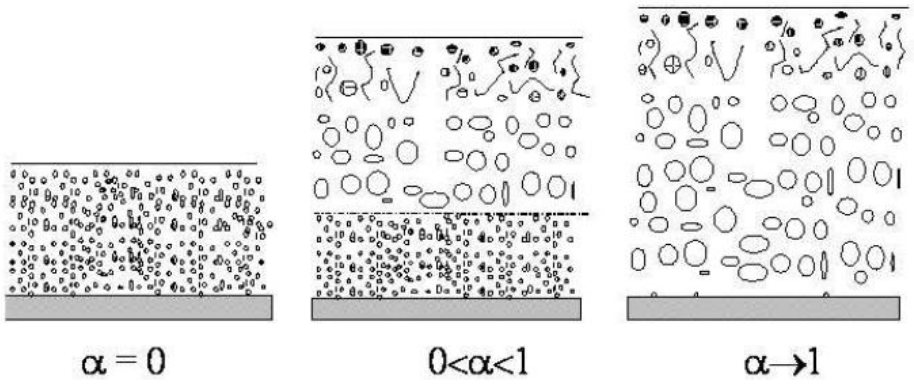

Figure 10: Développement de l'intumescence (α= degré de conversion)

La Figure 11 présente la viscosité en fonction de la température pour la résine vierge et les formulations intumescentes. Pour toutes les formulations, la viscosité reste stable jusqu'à 320-350 °C. La viscosité de la résine vierge chute après 350 °C et augmente après 370 °C. Lorsqu'APP est incorporé seul dans la résine, la chute a lieu à plus basse température (330 °C) et la viscosité minimale est similaire à celle de la résine vierge. Le

comportement est semblable lorsqu'il y a des CNTs. Au contraire, la formulation contenant à la fois l'APP et l'OMPOSS est stable à plus haute température (chute à 340 °C) et sa valeur de viscosité minimale est la plus élevée parmi les formulations testées. On peut donc supposer que cette viscosité plus élevée de la formulation Epoxy_APP-4_OMPOSS-1 permet une meilleure capture des gaz de dégradation, qui contribuent au foisonnement du résidu charbonné.

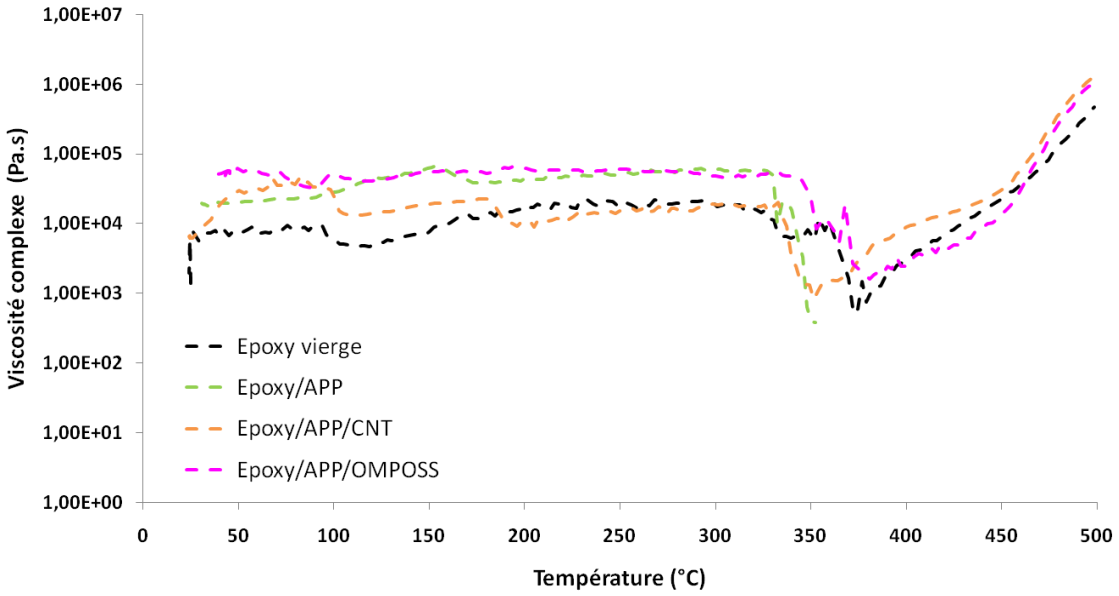

Figure 11: Viscosité apparente des époxy intumescents en fonction de la température (10 °C/min)

Les tests au calorimètre à cône ont été instrumentés de façon à pouvoir mesurer la vitesse de gonflement des formulations et les températures dans les résidus en fonction de la chaleur dégagée. Un exemple de courbe obtenu est présenté Figure 12.

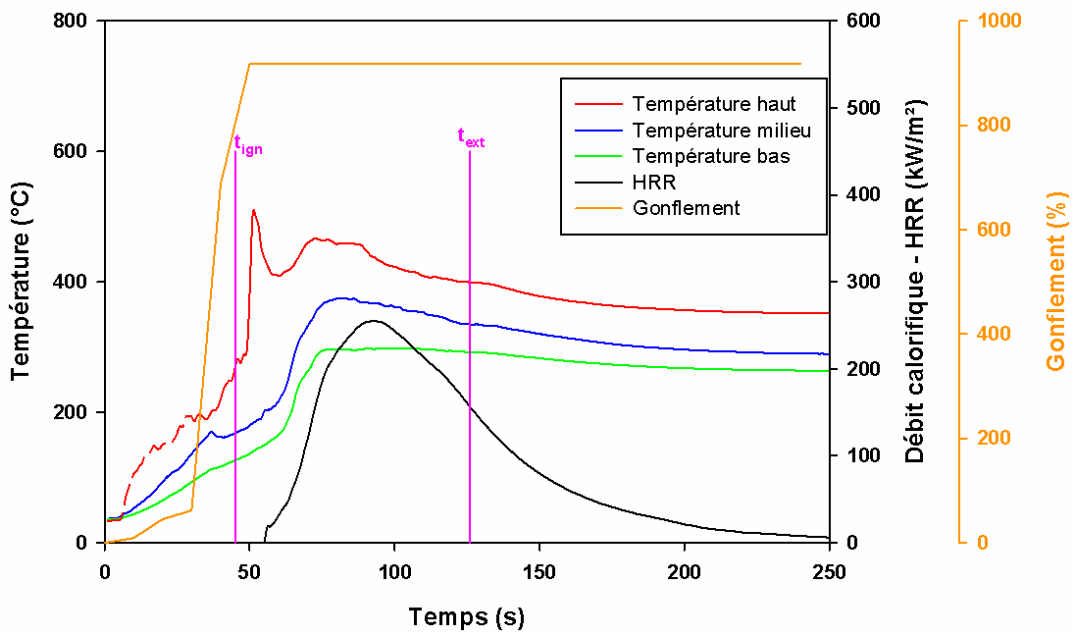

Figure 12: Débit calorifique, températures au sein du matériau et gonflement en fonction du temps pour la formulation Epoxy_APP 4_OMPOSS 1 (t_{ign} and t_{ext} représentent respectivement les temps d'ignition et d'extinction) (irradiance : 35 kW/m², épaisseur : 2.5 mm, distance : 35 mm)

Les résultats obtenus permettent de mettre en évidence le fait que l'ajout d'OMPOSS dans le système intumescent Epoxy_APP 5 augmente le volume des gaz dégagés permettant le gonflement (sublimation du POSS associée à la dégradation de l'APP), modifie la viscosité de façon à mieux encapsuler les gaz et peut éventuellement entraîner la formation de silicophosphates qui renforcent la structure du résidu. Au contraire, les CNTs sont néfastes au mélange Epoxy_APP 5. Ils n'augmentent pas la viscosité de façon à piéger les gaz de dégradation et rigidifient le résidu, qui craque sous la pression des gaz et ne protège pas le polymère restant.

En conclusion, la première partie de cette thèse présente le potentiel de différentes nanoparticules en tant que retardateurs de flammes. Malgré la modification de CNTs par greffage covalent, l'utilisation de nanoparticules seules ne permet pas d'ignifuger efficacement la résine époxyde étudiée. Dans la deuxième partie de cette thèse, des interactions entre nanoparticules et un retardateur de flamme phosphoré sont mises en évidence. La combinaison APP/OMPOSS est bénéfique alors que l'association APP/CNTs est néfaste. La troisième partie de l'étude a permis de comprendre ces interactions.

Différentes perspectives peuvent être envisagées pour poursuivre ce travail et élargir son champ d'action. La littérature n'indique pas clairement si les OMPOSS se subliment

lorsqu'ils sont chauffés ou si les gaz dégagés sont des produits de décomposition. Notre travail suggère que les gaz dégagés et analysés par spectroscopie infrarouge ne sont pas des POSS intacts. L'étude de la dégradation précise de ces charges peut être envisagée, notamment par chromatographie en phase gazeuse couplée à la spectrométrie de masse. Un autre aspect de cette étude a été l'identification des espèces présentes dans les résidus après combustion. Il a été possible de réaliser des cartographies de la répartition des espèces phosphorées par microsonde de Castaing. La même étude n'a pas pu être réalisée pour les espèces silicées, dont la concentration était trop faible. Des analyses élémentaires pourraient apporter une solution.

D'un point de vue applicatif, cette étude a été menée au sein du projet LAYSA et il serait intéressant d'observer comment les CNTs présents dans le composite multicouche final agissent dans ce cas. Les échantillons testés lors de ce travail étaient uniquement des matériaux massifs. Un revêtement protecteur pourrait cependant être formulé avec de l'APP et des OMPOSS. Enfin, maintenant que le mode d'action de ce système a été décrypté, sa transposition à d'autres polymères peut être envisagée.

List of figures

List of tables

Abbreviations

APP: Ammonium PolyPhosphate

APT: Attached Proton Test

ATH: Aluminum TriHydroxide

ATR: Attenuated Total Reflectance

BGPPO: Bis-(3-Glycidyloxy)PhenylPhosphine Oxide

BSE: Back Scattered Electrons

CCD: Charge-Coupled Device

CNT(s): Carbon Nanotube(s)

- SWNT: Single-Wall carbon Nanotubes
- MWNT: Multi-Wall carbon Nanotubes
- CNT-COCl: Carbon nanotubes reacted with thionyl chloride
- CNT-COOH: Oxidized carbon nanotubes
- CNT-amine: Carbon nanotubes reacted with ethylene diamine
- CNT-melamine: Carbon nanotubes reacted with ethylene diamine and 6-chloro-2,4-diamino-1,3,5-triazine
- CNT-POSS: Carbon nanotubes reacted with aminopropylisobutylPOSS

CP: Cross-Polarization (Solid-state NMR)

DDM: DiaminoDiphenylMethane

DETA: DiEthyleneTriAmine

DEPT: Distortionless Enhancement by Polarization Transfer

DGEBA (or BADGE): DiGlycidylEther of Bisphenol A

DGMPS: DiGlycidyloxyMethylPhenylSilane

DOPO: 9,10-dihydro-9--oxa-10-phosphaphenanthrene

DSC: Differential Scanning Calorimetry

DTA: Differential Thermal Analysis

EPMA: Electron Probe Micro-Analysis

FIGRA: Fire Growth Rate Index

FTIR: Fourier-Transform Infrared Spectroscopy

HMQC: Heteronuclear Multiple Quantum Coherence

HRR: Heat Release Rate

pHRR: peak of Heat Release Rate

k: thermal conductivity

LDH: Layered Double Hydroxide

LOI: Limiting Oxygen Index

MAS: Magic Angle Spinning (Solid-state NMR)

MMT: MontMorilloniTe

OMMT: Organo-modified MontMorilloniTe

NMR: Nuclear Magnetic Resonance

OSU: Ohio State University test

PCFC: Pyrolysis Flow Combustion Calorimetry

PGPSQ: Poly(Glycidoxypropyl)PhenylSilsesQuioxane

PMLR: Peak Mass Loss Rate (Cone-calorimeter under nitrogen)

PGSQ: PolyGlycidoxypropylSilsesQuioxane

POSS: Polyhedral Oligomeric Silsesquioxane

OMPOSS: OctamethylPOSS

FQ-POSS: Firequench

SEM: Scanning Electron Microscopy

SSA: Self-crosslinked Silicone Acrylate

TGDDM: TetraGlycidylether of DiaminoDiphenylMethane

TEM: Transmission Electron Microscopy

TEOS: TetraEthylOrthoSilicate

T_g: Glass transition temperature

TGA: ThermoGravimetric Analysis

tign: Time to ignition (mass-loss calorimetry)

THR: Total Heat Release (mass-loss calorimetry)

WXRD: Wide angle X-Ray Diffraction

WDS: Wavelength Dispersive X-ray Spectrometer

XPS: X-ray Photoelectron Spectroscopy

General Introduction

Since the development of polymer industry in the 20th century, plastics have spread to many fields of our everyday life. Figure 13 shows that the world production of plastics has dramatically increased since 1950 [6]. Indeed, they have partly substituted steel and wood in many applications, and new markets, where they are the main available solution, have been developed (e.g. packaging). Since 2000, the progression is not as spectacular as before, but the growing rate is still significant. 2008 and 2009 were the only years where the production has been reduced (by 9 % and 7 % respectively), due to the loss of activity linked to the current financial crisis. An activity recovery has been recorded in 2010 [7] (full data on year 2010 are not available yet).

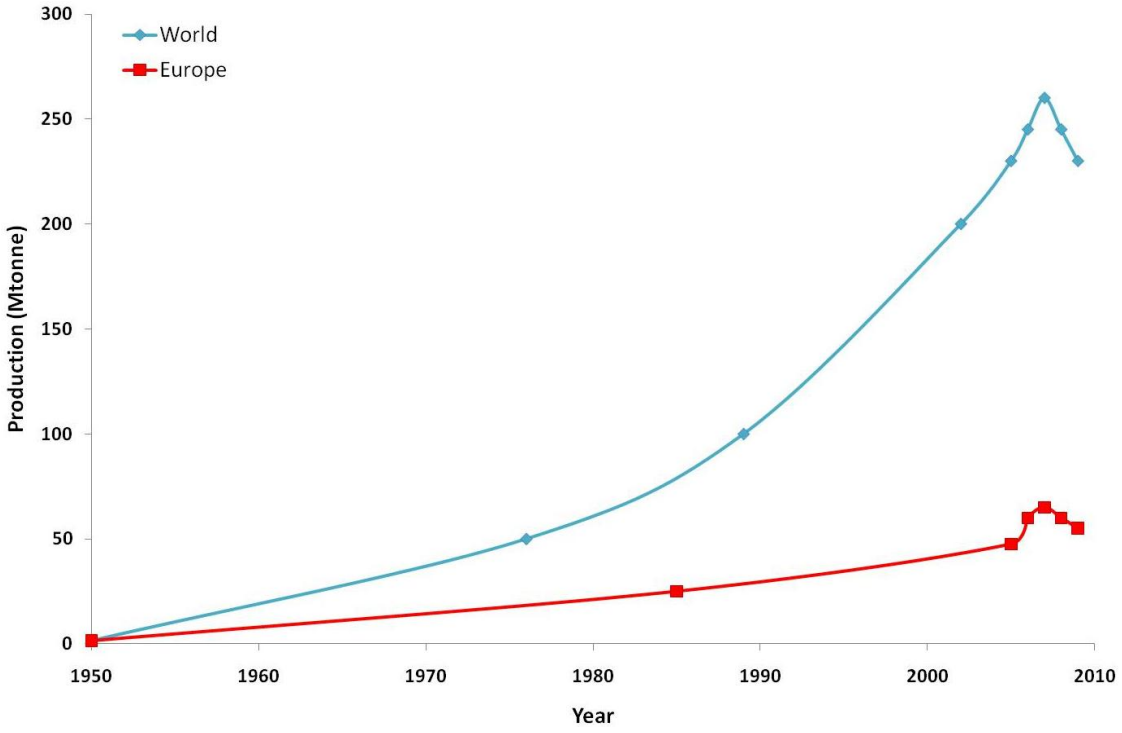

Figure 13: World and European plastics production (data cover thermoplastics, polyurethanes, thermosets, elastomers, adhesives, coatings, sealants and polypropylene-fibers)

Because of their great versatility, plastics are nowadays used in many applications sectors. Figure 14 presents the repartition of the demand for plastics for different applications fields in Europe. Packaging is the main sector using plastics (40.1 %), followed by the building and construction market (20.4 %). The transportation area is also an increasing outlet (7.0 %) and applications linked to electronics are not negligible (5.6 %). Finally, 26.9 % are used in niche markets such as sport, leisure, agriculture and machinery engineering.

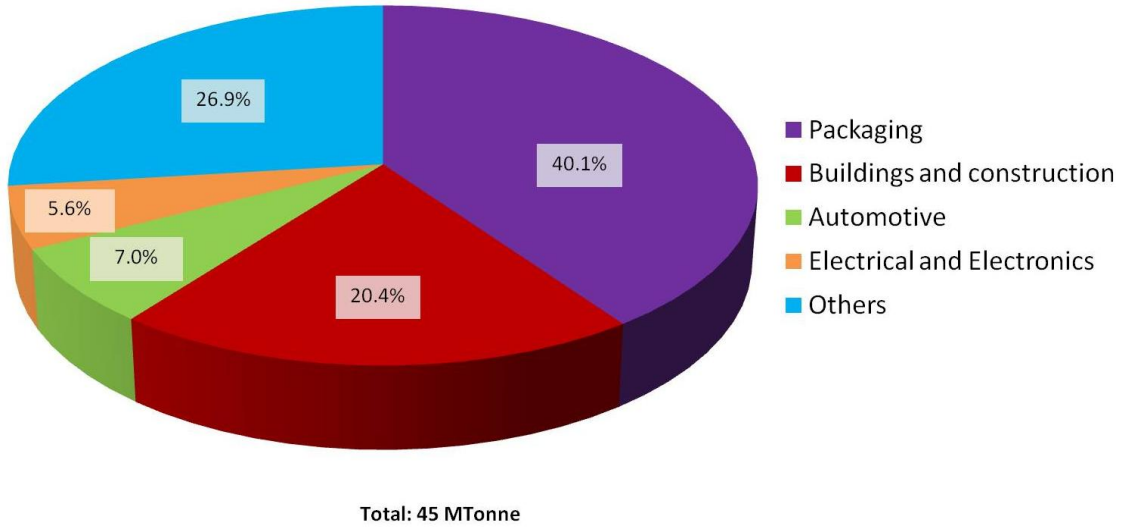

Figure 14: Europe plastics demand by segments in 2009

Among plastics, thermoset epoxy resins have been considerably developed since their first synthesis in 1930's. Epoxy sales increased rapidly in the 1970's and the rise continued in the 1980's, as new applications were developed (annual growth rate >10 % in the US market). More recently, the slower growth rates (3–4 %) of the U.S., Japanese, and European markets in the 1990s were made up for by the higher growth rate (5–10 %) in the Asia-Pacific markets outside of Japan, particularly in Taiwan and China [8]. More recently, the epoxy market has shrunken due to the crisis and the global sales have gone back to the level of 2005. In 2010, industry has regained confidence and annual growth rates of 3.5-4 % are projected until 2015 [9]. Nowadays, epoxy resins are not only used for the production of sport devices, coatings or electronic printed wiring boards, but also in the design of structural parts in the automotive or aeronautic industry. This latter application is especially growing since technical issues about the production of parts for cars or aircrafts are progressively solved. Furthermore, the reduction of oil stocks reinforces the interest for economical modes of transportation. One way to adapt traditional ones is to reduce their weight. Indeed, 50 vol.% (corresponding to only 10 wt.%) of an average car and 25 wt.% of the new A380 aircraft from Airbus are already made of plastics. In the future, polymers will account for 50 wt.% of Airbus A350 (expected in 2013) and Boeing 787 (under early production, first flight in 2009) global weight.

The numerous advantages of polymers should not hide one of their major drawbacks: their high flammability. In fact, polymers are organic materials, and as such,

they produce volatile combustibles when submitted to a heat source. If suitable conditions are fulfilled, this can result in the inflammation of the material and its surrounding. This hazard is especially to take into account for aircrafts, as people cannot escape fire during a flight. Indeed, in-flight fires and post-crash fires account for 20 % of the fatalities resulting from airplane accidents [10]. Furthermore, in case of ignition, polymeric materials do not only fuel the fire, but they also release gases and smokes, some of them being toxic, which incapacitate passengers or make them panic because of a reduced visibility. Special effort is therefore required for increasing the fire safety in aircrafts.

The high flammability of polymers, combined with the development of their use in aircrafts, is one of the starting points of the LAYSA project (Multifunctional Layers for Safer Aircraft Composite Structures) [11]. This program is funded by the European Union and aims at developing multifunctional polymeric composites. Three main functionalities are especially considered:

1. Prevention of ice formation on aircraft when flying at high altitude.
2. Improved reaction to fire
3. Sensing of temperature and stress by electrical conductivity variation measurements.

The goal is to achieve these performances by using mainly nanomaterials, and especially carbon nanotubes. Using such fillers would impressively decrease the weight of the aircraft structure. Twelve partners have been associated to reach these objectives. Universities provide their knowledge on specific properties during the different steps of the composite design. The Centre de Recherche Paul Pascal (CRPP, Bordeaux, France) and the University of Pau and Pays de l'Adour (UPPA-CANBIO, joint-laboratory between the Centre National de la Recherche Scientifique and Arkema, France) have an important knowledge on the process of carbon nanotubes. The University of Cranfield (United Kingdom) is specialized in aircraft de-icing, whereas the Ecole Nationale de Chimie de Lille investigates the reaction to fire of materials. The prediction of the different performances is carried out by the University of Patras (Greece), which models composite structures. Integrated Aerospace Sciences Corporation (INASCO, Greece) focuses on the assessment and design of the sensing

device. Concerning the preparation of materials combining three functionalities, industrial partners are called upon for the preparation and testing of materials at larger scale. Huntsman supplies base resin materials. The formulation of batches and composites is carried out by Inasmet-Tecnalia (Spain), Swerea-Sicomp (Sweden) and Advanced Composites Group (ACG, United Kingdom). Finally, the Consortium also includes Aries Complex (Spain) and Aernnova (Spain), which directly manufacture aircraft parts and are therefore end-users.

The work has been divided into three main parts. First, the potential of different nanofillers and matrices has been evaluated from literature and preliminary tests. Then, for each functionality, optimized systems have been developed, modeled and combined into a multifunctional system. The final development of this system at medium-scale is still under work.

This thesis is focused on the assessment of different nanofillers as flame retardants in a model epoxy resin (easily processed at lab-scale), as well as the methodology for investigating the associated mechanism of action. Furthermore, a new flame-retarded epoxy resin formulation is developed.

The first chapter provides the reader with a global knowledge on why polymers burn and the solutions available for limiting their contribution to fire. The thermal degradation mechanisms involved in epoxy resins are described. Traditional flame retardants, as well as their mode of action, are detailed, and a special focus is drawn on the most recent advances in the incorporation of nanoparticles in polymers (thermoplastics and thermosets) for fire safety issues.

The second chapter first presents the materials evaluated in this study. The functionalization of carbon nanotubes is described, as well as the preparation of filled epoxy resins. All methods concerning the characterization of the obtained materials and their reaction to fire are then described. Finally, experimental techniques used for the elucidation of the protection mechanisms are depicted.

The third chapter focuses on the properties of epoxy filled with different types of nanoparticles. First, commercial nanoparticles are incorporated in the resin. Then, the functionalization of carbon nanotubes as well as their incorporation in the matrix is examined. For each formulation, the matrix general properties as well as the reaction to fire are assessed.

The fourth chapter emphasizes the use of intumescent systems containing nanomaterials. Combinations between nanoparticles and traditional fillers providing intumescence are evaluated in terms of reaction to fire. Their morphology and general properties are also evaluated.

Finally, the fifth chapter is devoted to the comprehension of the behaviors observed in the fourth chapter. The composition of the systems is analyzed at characteristic times of the burning. Then, their evolution during the burning is characterized. Based on these results, mechanisms of action are proposed.

A general conclusion is drawn from all these results in the last part of this thesis and further developments of the chosen system are also considered.

Chapter I - State of the art: flame retardancy of epoxy resins

The credit for the first synthesis of epoxy resin is generally given to P. Castan in 1936 and to S.O. Greenlee in 1939 [12]. As explained in the general introduction, they are nowadays used in various fields of application, with different specifications for each of them. Many systems have been developed in order to meet these requirements and have contributed to the creation of a large range of available epoxy resins. The importance of fire issues in some application fields of these polymers has also been emphasized. Therefore, this chapter presents how epoxy resins are produced and how they degrade when submitted to a heat source. Then, the strategies developed for protecting polymers against fire are described. When possible, examples with epoxy resins are used, and a special focus is drawn on the use of phosphorus-based systems and nanocomposites.

I.1. EPOXY RESINS

I.1.1. Synthesis and processing

Epoxy resins are thermoset polymers. They result from the reaction between a prepolymer comprising epoxide rings at its ends and another molecule called hardener, which is generally an amine or an anhydride. This reaction produces a tridimensional network whose geometry partly rules the final properties of the materials (Figure 15). Epoxide rings are able to react with the hardener and ether groups enhance the resistance against hydrolysis. Hydroxyl groups provide adhesion and the aliphatic chains are flexible segments. Finally, the presence of bisphenol A units enhances different properties such as resistance against corrosion, thermal stability and stiffness. The following paragraphs aim at providing a general knowledge of epoxy networks.

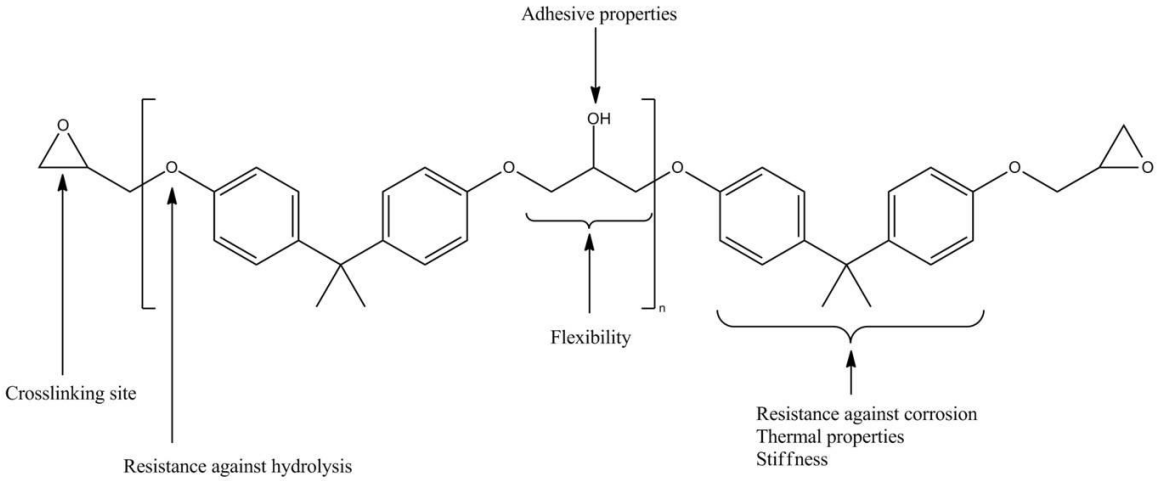

Figure 15: Links between an epoxy prepolymer (Bisphenol A diglycidyl ether) and material properties [13]

I.1.1.a. Epoxy prepolymers

Depending on their functionality, different types of epoxy prepolymers should be distinguished. The most common one is bisphenol A diglycidylether (DGEBA or BADGE): 75 % of the resins currently used worldwide are derived from this monomer [12]. It is obtained through the reaction between epichlorhydrin and bisphenol A in the presence of sodium hydroxide (Taffy process, Figure 16). The polymerization degree and thus the viscosity are controlled, among other parameters, by the stoichiometry between epichlorhydrin and bisphenol A. This issue is not negligible since it has a direct effect on the processability of resin batches.

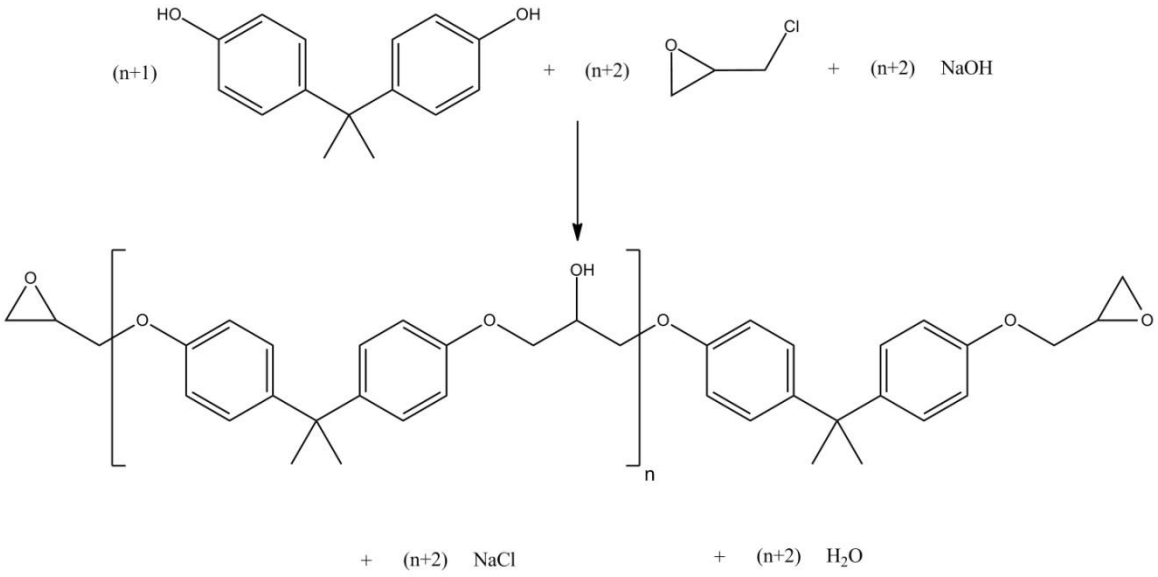

Figure 16: DGEBA synthesis via Taffy process [13]

Apart from DGEBA, other prepolymers such as tetraglycidylether of diaminodiphenylmethane (TGDDM) or triglycidylether of paraaminophenol are used for the production of airplanes structural parts (Figure 17).

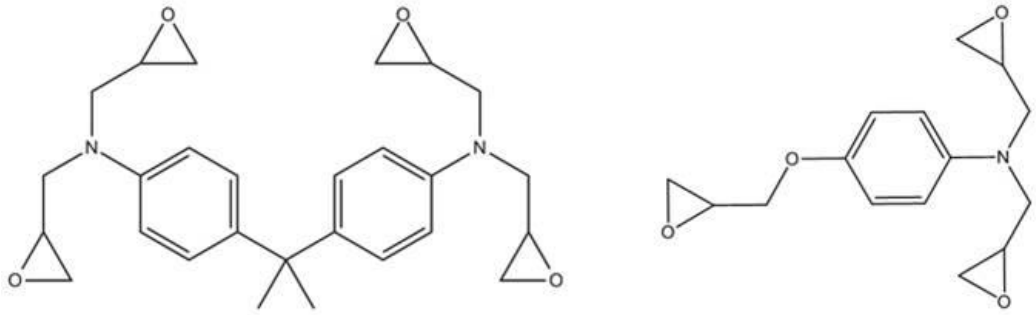

Figure 17: Chemical structures of tetraglycidylether of diaminodiphenylmethane (left) and diglycidylether of paraaminophenol (right)

I.1.1.b. Hardeners

Hardeners react with the epoxy rings of the prepolymer in order to create a tridimensional final network. Because epoxy rings are easily reactive compounds, the range of available hardeners is relatively large. However, the most commonly used are amines (either aliphatic or aromatic, 50 % of the US market in 2001) and anhydrides (9% of the US market in 2001)[12]. Table 3 describes the different major types of available hardeners and the specificities linked to each of them. Due to the special interest for amine hardeners in this thesis, they will be described in details in the next part.

Table 3: Common hardener types and associated specificities

Hardener	Advantages	Drawbacks	Major applications
Aliphatic amines	- Low viscosity - Room temperature cure - Slightly colored - Low cost	- Short pot life - Some of them are moderately toxicity - High moisture absorption - Blush, carbonation - Limited high temperature performance (<100°C)	- Flooring, - Civil engineering, - Marine and industrial coatings - Adhesives - Small castings
Polyamides	- Pot life - Room temperature cure - Flexibility - Low volatility and toxicity	- High viscosity - Low temperature performance, - Poor color - High cost	- Marine and maintenance coatings - Civil engineering - Castings - Adhesives

Aromatic amines	- Excellent elevated temperature performance (150°C) - good chemical resistance, - long pot life - low moisture absorption	- Solid - Long cure cycles at high temperature(150°C) - Toxicity	- High performance composites and coatings - adhesives - electrical encapsulation
Mercaptans	- Room temperature rapid cure - Flexible systems - Moisture insensitive	- Poor performance at high temperature - Odorous	- Consumer adhesives - Sealants - Traffic paints
Anhydrides	- Low exotherm - Good thermal (high Tg) mechanical, electrical properties - Low shrinkage and viscosity - Long pot life, slightly colored	- Long cure cycles at high temperature (200°C)	- Composites, - Castings - Potting - Encapsulation

I.1.1.c. Cure reaction

The curing is when the prepolymer and the hardener react together and create a tridimensional infusible and insoluble network (Figure 18).

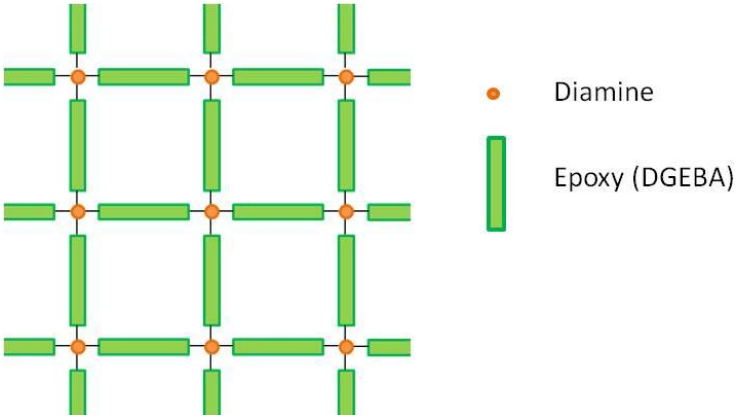

Figure 18: Schematic idealized epoxy network

However, different possibilities coexist for the reaction between a primary amine and epoxy groups. In fact, the final geometry of the network depends on the relative rates of different reactions.

Ring-opening addition of amines

The first step of the network creation is the heteromolecular reaction between the primary amine and epoxy prepolymer, which leads to the creation of a secondary alcohol and a secondary amine (Figure 19). This reaction is highly exothermic. Successive polyaddition reactions lead to chain extensions and/or ramifications. Then, the obtained secondary amines react with remaining epoxies and produce tertiary amines and secondary alcohols [13].

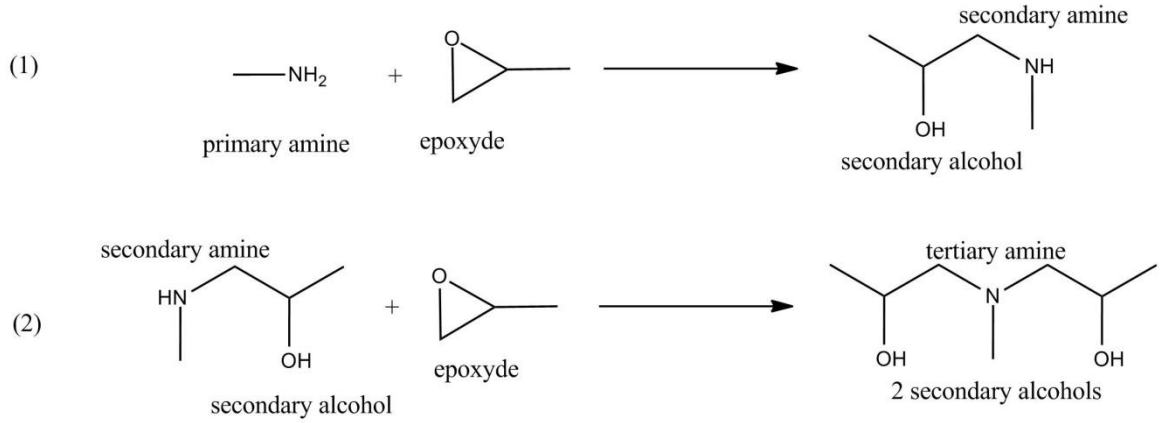

Figure 19: Main reactions occurring during the curing of epoxy by amines

The amine reactivity depends on its basicity, aliphatic amines being more reactive than aromatic ones. Furthermore, reactions 1 and 2 (Figure 19) follow similar mechanisms. However, there are more steric hindrance issues with secondary amines than with primary ones. Reaction rates for the two reactions may therefore differ. Various factors influence these parameters: type of amine, temperature, presence of compounds with hydroxyl groups which can act as catalyzers (since alcohols are obtained during curing, this reaction is autocatalyzed), presence and nature of solvent [12, 13].

Etherification

This reaction corresponds to the homopolymerization of epoxy groups (Figure 20). Secondary alcohols obtained after the addition of amines react with remaining epoxide rings. In systems containing an excess of epoxy groups, etherification occurs when there is no more primary or secondary amines. In stoichiometric systems or when there is an excess of amine functions, the relative importance of etherification compared to the two

other reactions (Figure 19) depends on the amine type and curing temperature, but it is generally considered as negligible [13].

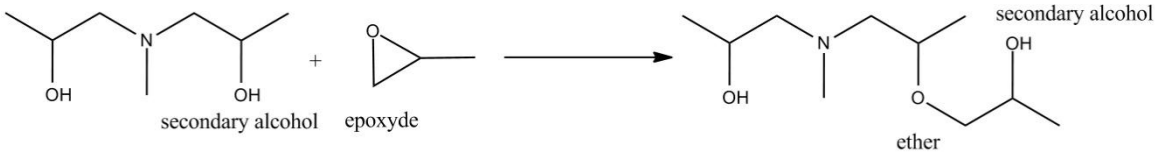

Figure 20: Secondary reaction during crosslinking: etherification

Processing

Some particularities of the curing reaction require specific conditions for the processing of epoxy resins. The polycondensation reaction is an exothermic reaction. In the case of amines that can react at ambient temperature, the curing may occur rapidly, before casting the material in its mould. Complete curing of an epoxy resin requires a definite amount of energy. In order to get suitable materials, this energy should be brought gradually, so that the reaction is progressively initiated in the whole part. On the contrary, if the curing temperature is too high, the reaction begins violently and the maximum temperature reached is higher than in the previous case. It results in internal stresses or cracks in the cured material [14].

I.1.2. Thermal decomposition of epoxy networks

The previous part provided general knowledge about the wide range of available epoxy systems, the reactions involved in the curing reactions and the importance of the curing cycle on the morphology of the final material. This part aims at understanding how the created networks thermally degrade.

The thermal behavior of polymers influences their reaction to fire: flame retardants may act at a specific temperature, degradation products may participate in the creation of a thermal protection or in evolving more fuel for burning. Therefore, understanding how epoxy resins degrade is important for designing flame retardant systems.

Before describing the degradation pathway of epoxies, the effect of the constituents of epoxy systems on their thermal stability was studied. Levchik et al. [15] reported that literature data concerning the effect of crosslinking density on the thermal stability of epoxy resins are contradictory. Dyakonov et al. [16] studied epoxy cured with different aromatic amines and observed an increase of the thermal stability of the obtained

materials when the crosslinking density was higher. Iji et al. [17] reported in 2001 that previous attempts for enhancing the heat resistance of epoxy were based on the restriction of molecular segments movements inside the epoxy networks. Concerning the effect of the nature of the hardener, in general, aromatic amines provide better stability that aliphatic ones, even though the crosslinking density may be lower (steric hindrance). Therefore, the composition of epoxy systems has an influence on their thermal stability. It is controlled by many parameters such as curing cycle or hardener type, and it is therefore difficult to predict the exact thermal behavior of a given system.

I.1.2.a. Decomposition of base resin

The study of the thermal degradation of epoxy resins is a relatively old issue. Authors generally refer to publications dating back to the 1960's, but this question has been widely reviewed, and scientists agree on general degradation mechanisms. Because of the materials later studied in this thesis, the degradation of epoxy cured with amines will be especially exposed. The initial degradation step is the dehydration of secondary alcohols, which leads to the production of vinylene ethers (Figure 21). Competitive dehydrogenation of secondary alcohol has also been reported by Bishop et al.[18]. However, it seems that this reaction has been mostly observed in particular conditions (hot-wire pyrolysis), where the presence of metal can catalyze it.

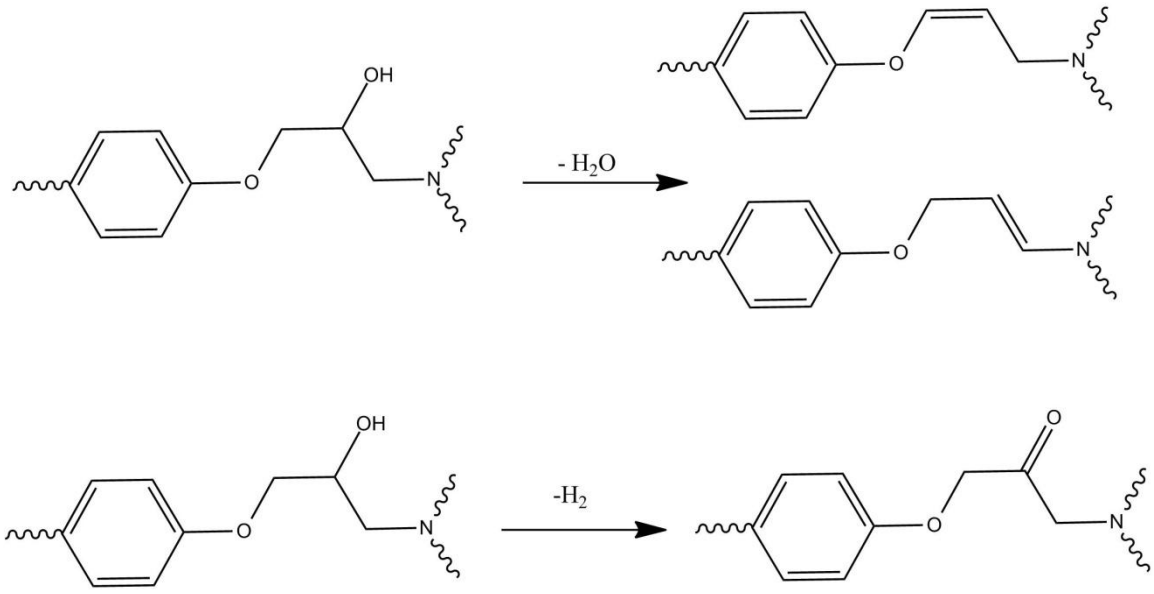

Figure 21: Dehydration and dehydrogenation of epoxy network

The C-O bond from allylic ether resulting from dehydration is less stable than the initial C-O, therefore this initial dehydration results in the breaking of chains mainly at the allylic position. In the particular case of epoxy/amines, the presence of C-N bonds adds another degradation path (Figure 22). C-N bonds are less stable than C-O and the degradation is also initiated near them. Homolytic or heterolytic scission mechanisms were reported in the literature. Keenan and Smith [19] suggested than homolytic ones are preponderant.

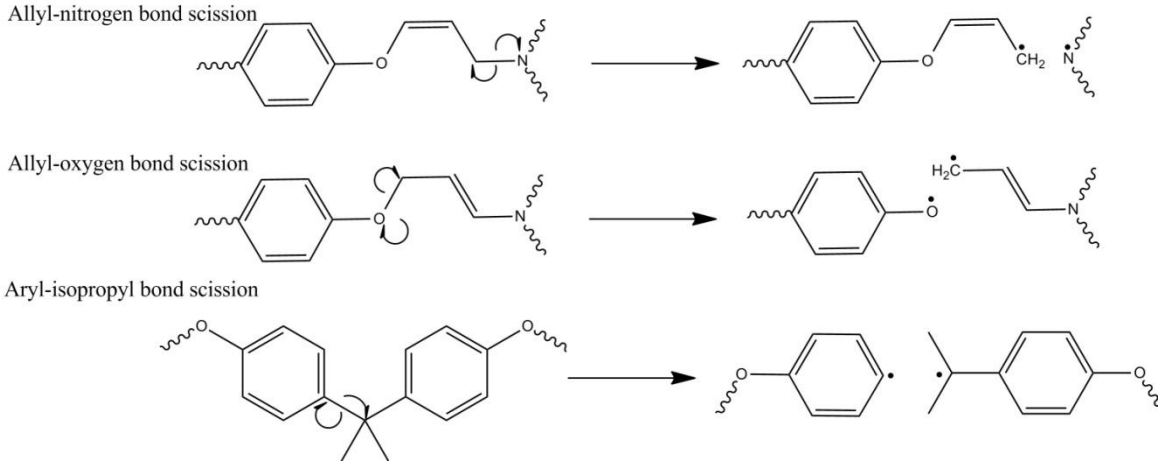

Figure 22: Homolytic scissions occurring after initial dehydration

Another possible reaction is the liberation of hardener through the breaking of the secondary amine created after the curing reaction. However, this hypothesis has not been verified since gas phase measurement showed that amines are a minor part of thermal decomposition products [15]. In fact, it seems that they are not released individually but linked to broken chains, or incorporated in the solid residue.

During these first steps, the main degradation products are methane, carbon dioxide, formaldehyde and hydrogen [20].

An additional mechanism at higher temperature is Claisen's rearrangement, occurring on the allylic ethers or amides formed after dehydration (Figure 23). Paraphenylene groups are changed into 1,2,4-trisubstituted benzenes, which have a higher thermal stability. This mechanism is not supposed to be observed at the beginning of the degradation because of steric hindrance in the crosslinked network. It is more likely to occur after the primary scission of N-allyl groups.

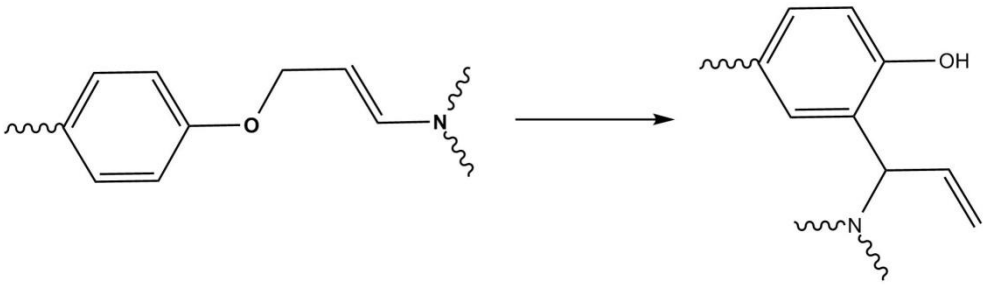

Figure 23: Claisen's rearrangement after dehydration

The previously described mechanisms are considered as major reactions during the thermal decomposition of epoxy networks. Secondary ones have also been reported and will be described in the next paragraph. Among them, cyclization of aliphatic chain ends, instead of breaking, can contribute to the charring and then to fire retardancy (Figure 24).

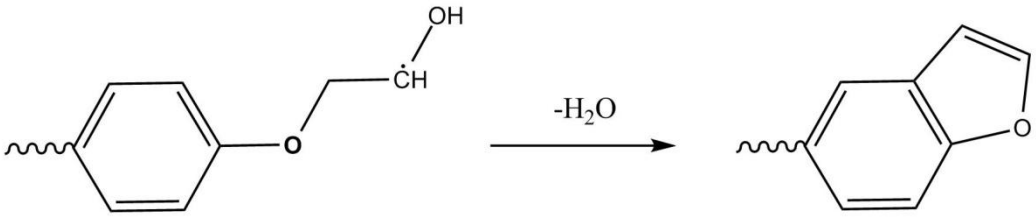

Figure 24: Cyclization of aliphatic chain ends

At very high temperature, polyaromatic structures are obtained by further aromatization. In addition to this, the recombination of radicals may also lead to formation of aromatic structures. For examples, two phenyl radicals may react together to form biphenyl.

At high temperatures, aliphatic chain release light combustible gases (methane), ethylene, propylene, allyl alcohol, acetone, and acetaldehyde. The aromatic segments of the polymer also produce phenol, benzene, toluene, *o*- and *p*-cresols and phenols with a higher molecular weight [20].

The considerable crosslinking and subsequent charring which occur during the thermal degradation of epoxy resins is therefore the consequence of different phenomena: dehydration, creation of insaturations and presence of long-life radicals.

I.1.2.b. Thermo-oxidation

Levchik et al.[15] have summarized the thermo-oxidative phenomena into three main mechanisms, which lead to the formation of carbonyl groups in the two first cases and isomerisation in the third case:

- Oxygen attacks methylene groups obtained after the initial dehydration. This results in an auto-oxidation sequence leading to the formation of hydroperoxide. This latter species reacts further to create aldehydes, which have been observed by Fourier Transform Infrared spectroscopic analysis (FT-IR). The reaction leading to the production of aldehydes is also responsible for the network breakdown.
- Tertiary carbons in the aliphatic chain may be oxidized. Abstraction of the hydrogen atom of tertiary carbon in the presence of oxygen results in the creation of hydroperoxides. They further decompose to form amide-containing compounds.
- Oxygen attacks nitrogen atoms in the case of epoxy/amine. Burton [21] suggested that in this case, chain cleavage may occur via a Cope reaction that produces hydroxylamines and either alkenes or methyl ketones (rearranged from enols).

The obtained carbonyls then decompose and result in chain splitting. These mechanisms are supported by experimental results which reveal the presence of carbonyls and amides during oxidative decomposition.

As a conclusion, numerous reactions are involved in the thermal degradation, either in air or nitrogen. Under nitrogen, dehydration marks the beginning of the degradation process. It is followed by chain scissions and recombinations which lead to the production of aliphatic gaseous products, carbon monoxide, carbon dioxide, … Solid residues are also obtained in the condensed phase. They result from successive condensation mechanisms which promote the carbonization of the material. When in a thermo-oxidative environment, different areas of the macromolecule can be oxidized, leading in particular to the production of aldehydes and amide-containing compounds.

I.2. FLAME RETARDANCY OF EPOXY RESINS

The previous section has shown that a wide range of epoxy resins could be synthesized and that different hardeners are available, leading to many different epoxy systems. This variety of formulations associated to the system complexity results in numerous reactions involved in the thermal degradation of these systems. However, fire protection strategies developed for polymers in general are applied to epoxy systems. The following part presents the mechanisms involved in the combustion of polymers and the different flame-retardant strategies developed, with a special focus on epoxy systems when available.

I.2.1. Why do polymers burn? Fire retardancy concepts

The combustion process can be divided into four major steps: heating, decomposition, ignition and flame spread. Indeed, when submitted to a heat source, the material softens, or even melts in the case of thermoplastics. Then, when the energy given to the material is higher than that needed for its degradation, decomposition products are released in the gas phase. These flammable gases are mixed with oxygen from the air and when the system reaches a critical concentration, ignition occurs. Part of the energy of the flame is given back to the material, so that the combustion process continues without help of external energy. As long as degradation products are evolved and oxygen remains in sufficient amount, there is an auto-fed flame which can propagate to its surroundings.

This combustion involves radicals' production in the flame. Figure 25 describes the main reactions occurring in the flame.

Initiation:	$RH + O_2 \rightarrow HO^{\bullet} + RO^{\bullet}$
Propagation:	$RH + HO^{\bullet} \rightarrow H_2O + R^{\bullet}$
Branching :	$R^{\bullet} + O_2 \rightarrow RO^{\bullet} + O^{\bullet\bullet}$ $O^{\bullet\bullet} + H_2 \rightarrow HO^{\bullet} + H^{\bullet}$
Termination:	$H^{\bullet} + HO^{\bullet} \rightarrow H_2O$

Figure 25: Combustion mechanisms occurring in the flame (R=polymer)

Figure 26 summarizes the different phenomena observed during the combustion of polymers and shows where a fire-retardant action can be carried out.

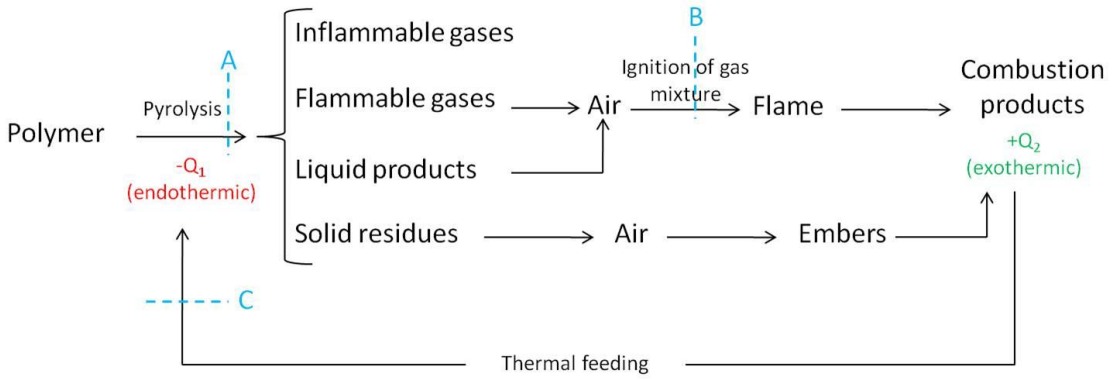

Figure 26: Steps of the combustion cycle of polymers

Indeed, fire retardancy consists in the diminution of heat supplied to the polymer, so that the system remains below the critical level that ensures flame stability. This can be achieved by stopping the combustion cycle at different steps:

- Modification or suppression of the degradation process of the polymer (A, Figure 26)
- Flame extinction (B, Figure 26)
- Diminution of heat transfer between the flame and the polymer (C, Figure 26)

In practical terms, the encountered solutions are:

- use of inherently flame-retarded polymers such as poly(tetrafluoroethylene), polyoxazoles, polyimides or benzoxazines [22, 23]. Simple enhancement of the reaction to fire of epoxy resins can be gained by controlling the final crosslinking degree. A low crosslinking leaves free unreacted moieties and leads to a stronger combustion [24]. On the contrary, it has been observed that a very high crosslinking could make the network structure too rigid to produce intumescent[1] charred layers during combustion, therefore being detrimental for flame retardancy [25].
- chemical modification of existing polymers: preparation of organic/inorganic epoxy resin prepared from silsesquioxane [26], curing of mixed phenolic/epoxy resins [27], synthesis of phosphorus-based epoxy monomers [15].
- incorporation of flame retardants in the polymer.

[1] Intumescent systems produce a cohesive and insulating layer on the surface of the polymer, which is blown by the gases produced during the decomposition of the underlying polymer (more details page 87).

The two first solutions are quite interesting, since they permit to produce unique material adapted for each application. However, the main drawback is that this results in higher production costs. The most commonly used solution is therefore the incorporation of flame retardants in the materials.

The market concerning flame-retardants has considerably evolved in recent years. Some common fillers have been banned from different countries and new solutions have taken significant importance. Indeed, some halogenated compounds, among them many polybrominated diphenyl ethers, that were commonly used 15 years ago have been progressively banned from European and North American markets since 2004. Furthermore, alternative solutions are required by possible restrictions due to REACH enforcement [28]. REACH stands for Registration, Evaluation and Authorization of Chemicals and this directive from the European Commission will influence the choice of the components used in many areas, in particular in plastics. Figure 27 shows the repartition of types of flame retardants depending on the volume produced or on the value for the European markets. Major types of flame retardants are metal hydroxides, halogenated compounds, phosphorus-based products and nitrogen-containing solutions.

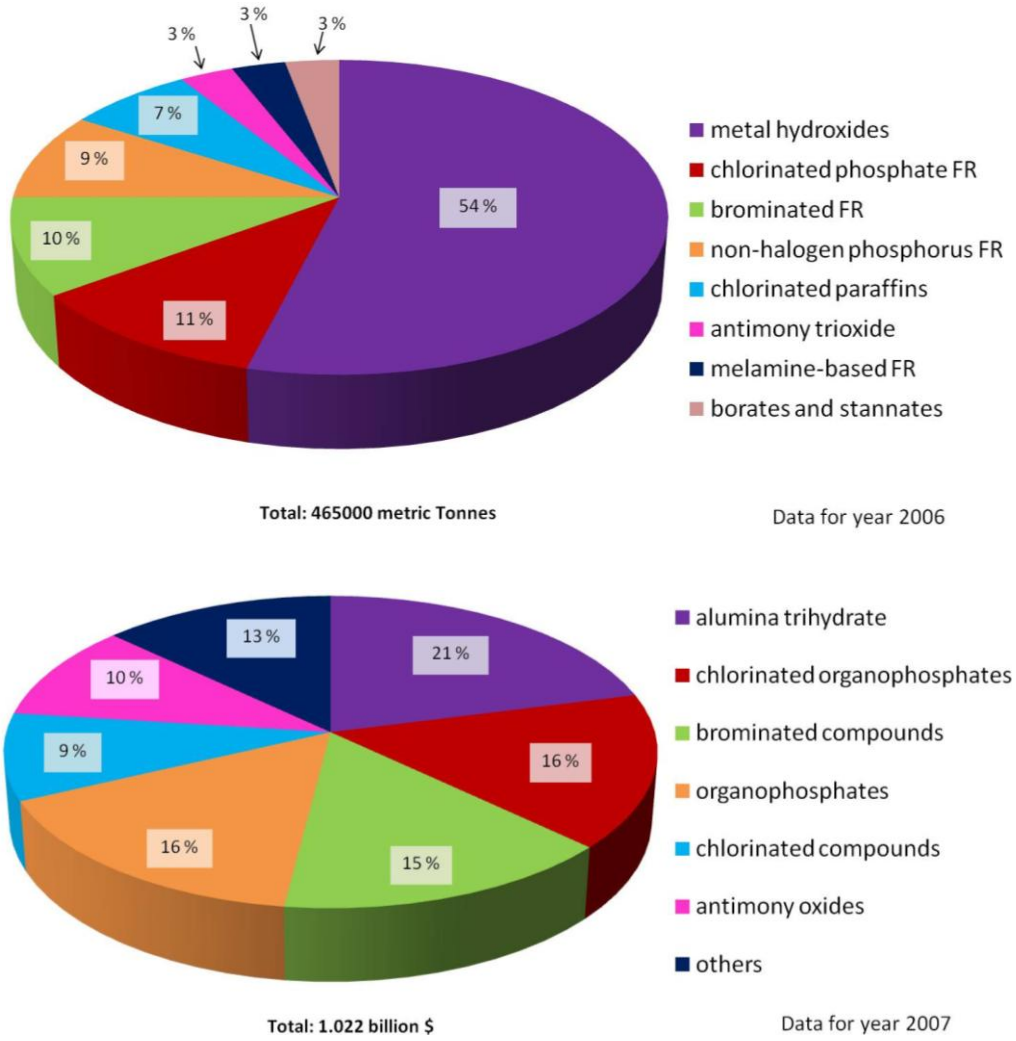

Figure 27: European consumption of flame retardants in volume (up) and in values (bottom) [29, 30]

Depending on the flame-retardant type, different modes of actions coexist in the gas phase or in condensed phase (Figure 28).

Mode of action		Flame retardant
<u>Gas phase</u>		
Radical inhibition	→	Halogen- or phosphorus-based compounds, antimony trioxide
Dilution causing the decrease of the flame temperature	→	Compounds releasing carbon dioxide, water or ammonia
<u>Condensed phase</u>		
Endothermic degradation of flame-retardant	→	Metallic hydroxides
Dilution	→	Inert fillers (talc, chalk)
Creation of a thermal barrier limiting heat exchanges with the flame	→	Intumescent or vitrifying systems

Figure 28: Flame-retardant modes of action

The next section gives further details on the different types of used flame-retardants.

I.2.2. Conventional flame retardants

This section is divided in four sub-sections: halogen-containing flame retardants, metallic hydroxides, melamine and derivatives and compounds containing boron or silicon.

I.2.2.a. Halogen-containing flame retardants

This type of flame retardants offers a wide range of available compounds. From the four halogen atoms, only chlorine and bromine are used for the production of common flame retardants. Fluorinated compounds have an excessive stability, whereas iodinated ones have a low thermal stability that limits the polymers in which they can be incorporated.

Brominated and chlorinated flame retardants are generally incorporated in polymers at 20 and 40 wt.% respectively [31]. The use of brominated resins as a copolymer in epoxy systems is also common. In this case, part of the standard resin has to be replaced by the bromine-containing monomer, leading to bromine contents between 20 to 55 wt.%.

Halogen-containing compounds act mainly in the gas phase [32]. They are able to release radicals or hydrogen halides during their decomposition at temperatures below that of the polymer. Their action therefore stems from a dilution of the gas phase, which decreases combustibles and oxygen concentrations, associated to reactions with radicals from the flame. Indeed, these fillers release halogenated radicals which recombine immediately with hydrogen atoms coming from the flame retardant itself or from the polymer (Figure 29) [33].

$$R\text{-}X \rightarrow R^{\bullet} + X^{\bullet}$$
$$X^{\bullet} + \text{-}CH_2\text{-}CH_2\text{-} \rightarrow \text{-}^{\bullet}CH\text{-}CH_2\text{-} + H\text{-}X$$
$$\text{-}^{\bullet}CH\text{-}CH_2\text{-} \rightarrow \text{-}CH{=}CH\text{-} + H^{\bullet}$$

Figure 29: Radicals generation by halogen-based flame retardants

When no synergy agent is present in the system, halides volatilize and go in the flame where they react quickly with hydrogen or hydroxyl radicals (Figure 30). The

trapping of these very energetic radicals modifies the thermal balance, therefore limiting the progress of combustion [34].

$$H\text{-}X + H^{\bullet} \rightarrow H_2 + X^{\bullet}$$
$$H\text{-}X + OH^{\bullet} \rightarrow H_2O + X^{\bullet}$$

Figure 30: Interactions between halides and radicals from the flame

When synergists are added to the flame-retarded material, e.g. metallic oxides, metallic salts, compounds containing phosphorus, nitrogen or zinc, the filler loading is decreased. These mixtures release metallic halides when they degrade and these species inhibit the flame more efficiently than hydrogen halides [35].

I.2.2.b. Metallic hydroxides

The major part of the production of flame retardants is represented by metallic hydroxides: aluminium trihydroxide (ATH) and magnesium hydroxide. They provide good fire properties to these systems while being relatively cheap. Epoxy resins used for the manufacturing of printed wiring boards often contain ATH as flame retardant. This is an alternative solution to the use of tetrabromobisphenol A. However, loadings over 60 wt.% are needed to reach suitable flame retardancy and this often affects other properties such as soldering-heat resistance and dielectric properties [36].

Another drawback of ATH is its decomposition at relatively low temperature (Figure 31). ATH is therefore commonly used in elastomers, thermoset resins and thermoplastics. However, it cannot be used for polymers being processed at temperatures higher than 200 °C [37]. In this case, magnesium hydroxide is better suited.

$$2\ Al(OH)_3 \xrightarrow{180\text{-}200^{\circ}C} Al_2O_3\ (s) + 3H_2O\ (g) \qquad \Delta H = 1.3 kJ/g$$

Figure 31: Endothermic dehydration of aluminium trihydroxide

During their thermal degradation, metallic hydroxides undergo an endothermic dehydration (Figure 31).When incorporated to a polymer, they can therefore act as a “heat sink” and delay ignition. Furthermore, once the polymer is burning, they create at its surface a protective ceramic layer which acts as a thermal shield [38].

I.2.2.c. Melamine and derivatives

This class of flame retardants consists in melamine itself, its derivatives and its homologues. Derivatives are organic or inorganic acid salts such as boric, cyanuric, (poly)phosphoric acid. Homologues are represented by melam, melem and melon (Figure 32)[34].

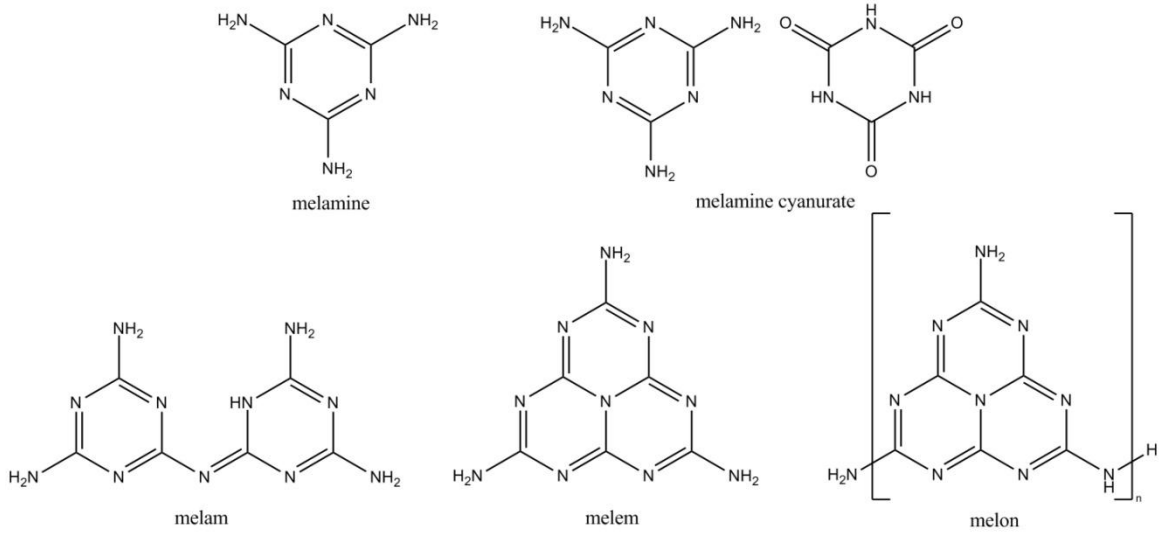

Figure 32: Melamine-based flame retardants

Melamine-containing compounds have different possible actions: chemical reaction, heat sink, carbonization, intumescence, dilution. Furthermore, they do not release large amounts of toxic or corrosive fumes and are relatively cheap.

Melamine itself can delay the ignition of the polymer by acting as a heat sink. Indeed, endothermic dissociation and sublimation of this filler occur around 350°C. Melamine vapors (obtained after sublimation) can also decompose endothermically. Furthermore, ammonia and later nitrogen gas are formed during the combustion and act by dilution in the gas phase.

This filler can also act in the condensed phase, especially for the reinforcement of intumescent structures. The char is reinforced by cyclic structures of melem and melon formed during melamine condensation. The stability is further reinforced by the presence of chlorinated or phosphorated compounds [39]. In intumescent systems, melamine also acts as a blowing agent.

I.2.2.d. Boron or silicon containing systems

Borax ($Na_2B_4O_7$, 10 H_2O) and boric acid ($H_3BO_{3)}$ have been used for years for flame-retarding cellulosic materials. Zinc borate is also commonly used in thermoplastics and epoxy resins [40]. However, the loadings needed to achieve flame retardant properties are high: zinc borate incorporated at 5 wt.% in an aerospace epoxy system decreases the peak of heat release rate[2] (pHRR) by only 3 % while 40 wt.% loading provides a 55 % decrease [41]. Boron-containing compounds act as heat sink: they decompose into boric acid or boron oxide (H_3BO_3) and water. When combined with metallic hydroxides, they are able to create a protective vitrified layer on top of the polymer.

Silicon-based products have proven to be flame-retardant. Synthesis of hybrids based on epoxy and silicon has also been developed. Recent work in this field will be reviewed in the next part: organic-inorganic networks obtained by mixing an epoxy prepolymer with a silicon-containing monomer are often encountered.

Mercado et al. [42] mixed DGEBA with diglycidyloxymethylphenylsilane (DGMPS, Figure 33) and cured the obtained resin with diaminodiphenylmethane.

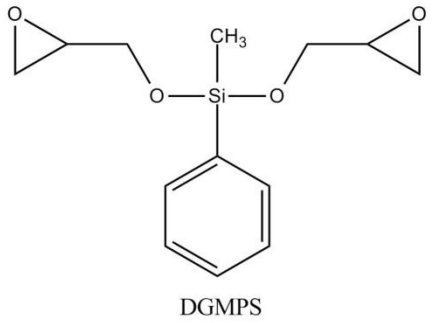

Figure 33: Structure of diglycidoxymethylphenylsilane

Several DGMPS/DGEBA molar ratios were used in order to obtain silicon contents varying from 0 to 8 wt.%. It is important to note that the 8 wt.% silicon content corresponds to a material based only on DGMPS (without DGEBA). The curing cycle was modulated taking into account the modified reactivity of the system when DGEBA is substituted by DGMPS. Mixed epoxy systems exhibit a single Tg, suggesting a

[2] More details on heat release rate and mass-loss calorimetry page 103.

homogeneous material. The flammability was evaluated by means of LOI[3]. It is increased when silicon is incorporated in the epoxy network: 24.1 vol.% for the virgin epoxy, 26.1 vol.% for the composite made from the 50 wt.% DGEBA/50 wt.% DGMPS mixture and 36.0 vol.% for the sample made from DGMPS only. Even if outstanding values are claimed, the best results are obtained for the sample without DGEBA but only the silicon-bearing part of the formulation. The increase for the sample DGEBA 50%/DGMPS 50 % is far less impressive: 2 %. The silicon-based resin therefore appears as an alternative to more common epoxy resins.

Harada et al. [43, 44] studied silsesquioxane derivatives bearing epoxy rings. First, polyglycidyloxypropyl silsesquioxane (PGSQ) was mixed with titanate and cured with diaminodiphenylmethane. Two different shapes of titanate were used: an organo-layered and a spherical titanate. DGEBA was prepared in the same way for comparison. Horizontal UL-94[4] tests were conducted in order to evaluate the flammability of the materials. DGEBA/organo-layered titanate and PGSQ/spherical titanate (5 wt.%) burnt completely without self-extinguishing, but the PGSQ/organo-layered titanate system extinguished after 8 s and was classified V-0. Scanning Electron Microscopy (SEM) showed aggregates in the composite containing layered titanate. On the contrary, the spherical titanate showed a uniform dispersion. These results highlight the importance of the shape of the used particles for flame-retardant purpose: different shapes for similar materials can lead to completely different dispersions. In a further study, Harada et al. [44] chose poly(glycidyloxypropyl)phenylsilsesquioxane (PGPSQ), mainly because of the reported capability for enhancing flammability properties of phenyl groups. PGPSQ was then mixed with the same organo-titanate as before and cured with DDM. Similarly to what was observed for the PGSQ system, Transmission Electron Microscopy (TEM) micrographs indicated that a microscopic phase separation occurred. UL-94 horizontal burning test showed that the self-extinguishing behavior was achieved with only 1 wt.% titanate in the PGPSQ system. In order to obtain a hybrid material, DGEBA

[3] Limiting Oxygen Index is the minimum concentration of oxygen, expressed as a percentage, that will support combustion of a polymer. It is measured by passing a mixture of oxygen and nitrogen over a burning specimen, and reducing the oxygen level until a critical level is reached (ASTM D2863 – ISO 4589).

[4] UL 94 is a plastics flammability standard released by Underwriters Laboratories. The standard classifies plastics according to how they burn in various orientations and thicknesses. The sample passes the horizontal test if it burns slowly (burning rate < 76 mm/min for thickness < 3 mm).

was mixed with PGPSQ and the titanate. Up to 10-20 wt.% DGEBA in the system increases the extinguishing time but the samples are still classified as V-0. For the composite containing 30 wt.% DGEBA, no self-extinguishing behavior could be observed, whatever the titanate content. These studies show the potential of silicon in epoxies. However, the enhancement of the fire performance is often very limited and the best materials are often those containing very small amounts of epoxy resin.

I.2.3. Nanocomposites

The incorporation of nanoparticles into polymers has attracted much interest in the last ten years. Indeed, apart from providing fire properties to the materials, low loadings achieved do not modify the other properties or even enhance some of them, such as mechanical properties [45]. Survey of the literature with SciFinder® for different keyword combinations helps to identify the tendencies in the use of nanoparticles. The incorporation of nanoparticles in epoxies for enhancing mechanical properties is widely described (Figure 34, 'epoxy' and 'nanoparticle'). An overview of the literature shows that the occurrences are more limited when coming to the incorporation of nanoparticles in epoxy for flame retardancy ("epoxy" and 'nanoparticle' and 'flame retardant'). However, the use of nanoparticles as flame retardants in other polymers is well-known ('nanoparticle' and 'flame retardant'). The following section is therefore devoted to a screening of the different nanoparticles commonly used as flame retardants, then the results obtained for nanoparticles incorporated in epoxies and the expected developments in this field.

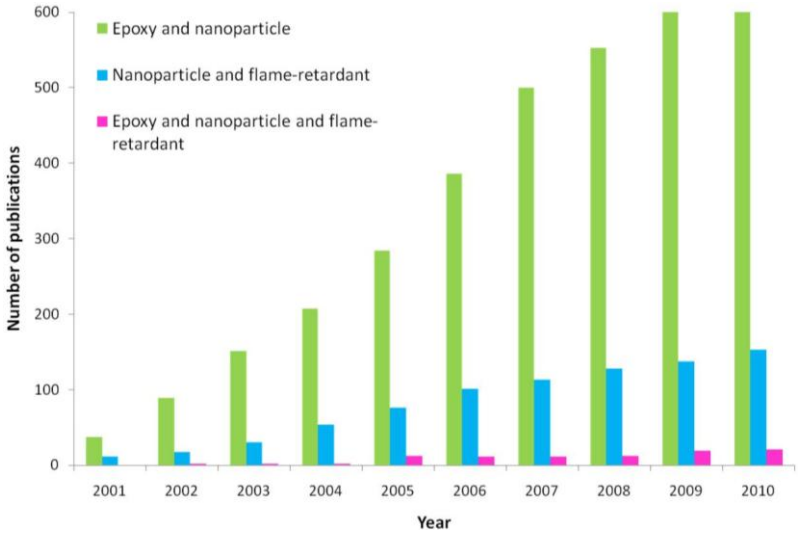

Figure 34: Number of publications per year for different keyword combinations (Scifinder®, April 2011).

A wide range of nanoparticles has been incorporated in epoxies. The effect of the incorporation of layered silicates, then the potential fire retardant properties of layered double hydroxides, polyhedral oligomeric silsesquioxanes and carbon nanotubes will be discussed.

I.2.3.a. Organoclays

Nanoclays are widely used in polymers because of their flame-retardant properties. They are layered silicates (phyllosilicates), which gives them the possibility to develop particular morphologies in polymers. Montmorillonite clay is widely used for its flame-retardant properties in polymer nanocomposites. It is an aluminium hydrosilicate, in which the proportion of silicic acid to alumina is about 4:1. The individual layers feature a total of three layers. As shown in Figure 35, the two outer layers are silica sheets, composed of SiO_4 tetrahedra. They envelope a central sheet of aluminium ions, with the result that each aluminium cation is surrounded in octahedral form by oxygen atoms of the silicate groups as shown in Figure 35.

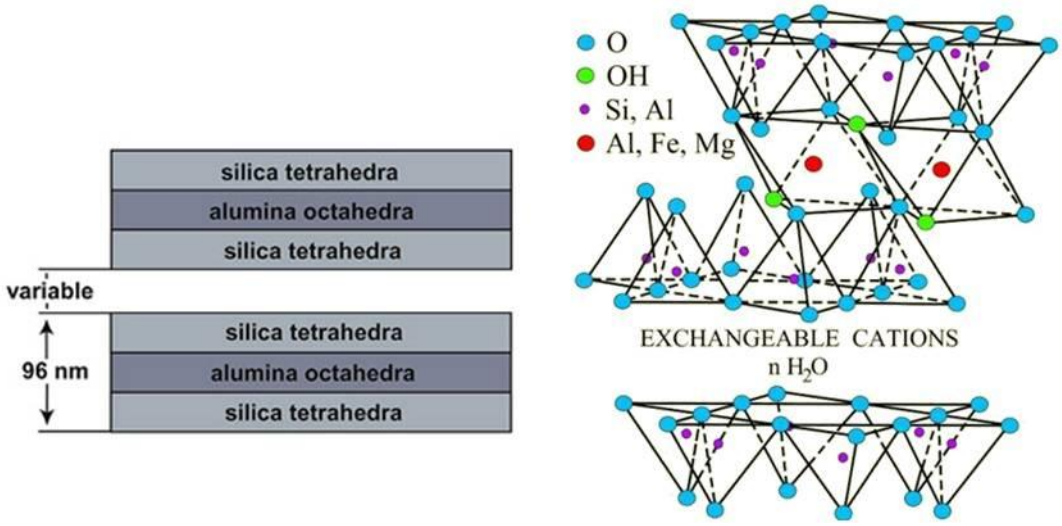

Figure 35: Montmorillonite structure [46, 47]

Three categories of montmorillonite composites are generally distinguished (Figure 36): (a) microcomposites: there is no penetration of the polymer into the clay lamellae; (b) intercalated composites: the insertion of polymer into the clay structure occurs so as to increase the spacing between platelets in a regular fashion; (c) exfoliated composites: the individual clay layers are dispersed as single platelets into a continuous polymer matrix.

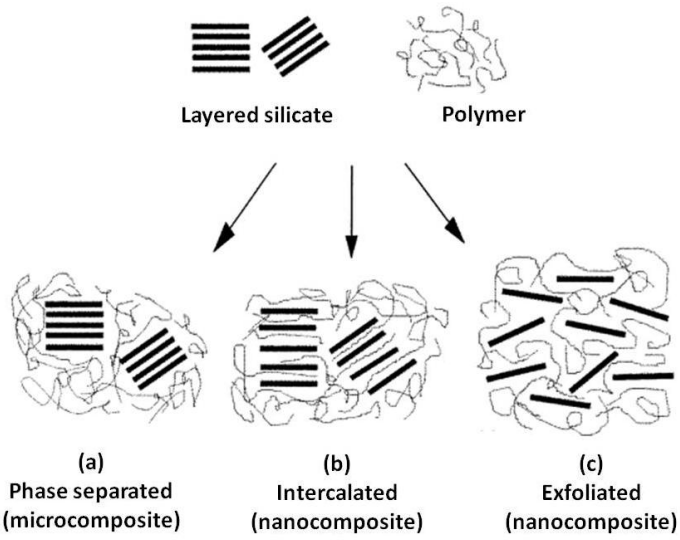

Figure 36: Scheme of different types of composite arising from the interaction between layered silicates and polymer: (a) phase separated microcomposite ; (b) intercalated nanocomposite and (c) exfoliated nanocomposite [48]

Samyn et al.[49] reported that if nanodispersion is achieved at a reasonable level, polymer/clay nanocomposite should exhibit fire retardant properties. Furthermore, they observed that the morphology of the composite (exfoliated, dispersed and presence of tactoids) in polyamide-6 does not play a significant role on the flammability of the composite.

Capability of layered silicates for being exchanged with organic cations at commercial level led to an easier dispersion in various polymers, especially in epoxies. Hartwig et al.[50] reported the combustion behavior of clay-filled epoxies. Two different bentonites based on a phosphonium or an ammonium cation as surfactant were incorporated in an epoxy matrix at 5 wt.%. Dispersion studies were conducted by TEM and showed a non-uniform distribution of the bentonites in the matrix. For both cations, the morphology is a mixture of intercalated and exfoliated areas, and a slightly better dispersion is obtained with the phosphonium bentonite. The flame-retardant properties of these clays were evaluated by various tests. LOI gave information about the flammability of the samples: LOI values remain low for nanocomposites and the differences between the virgin polymer and the nanocomposites are not relevant (Table 4). The flame spread was evaluated by the horizontal burner test (Aerospace standard AITM 2.0003 – FAR 25.853), in which the time required for burning 150 mm of the sample is recorded (Table 4). Therefore, the longer the time, the better the behavior.

The time required for burning the sample is drastically increased by the incorporation of bentonites in the matrix.

Table 4: Flammability characteristics of clay-filled epoxies.

Samples	LOI (%)	Horizontal burner test Time for burning 150mm in horizontal position (s)
Virgin epoxy	18.3	260
Epoxy + ammonium clay (4.7wt.%)	19.7	434
Epoxy + phosphonium clay (4.7wt.%)	19.6	464

Furthermore, contrary to non-filled epoxy, the nanocomposites do not drip. Finally, the fire behavior was studied by cone-calorimetry (Figure 37).

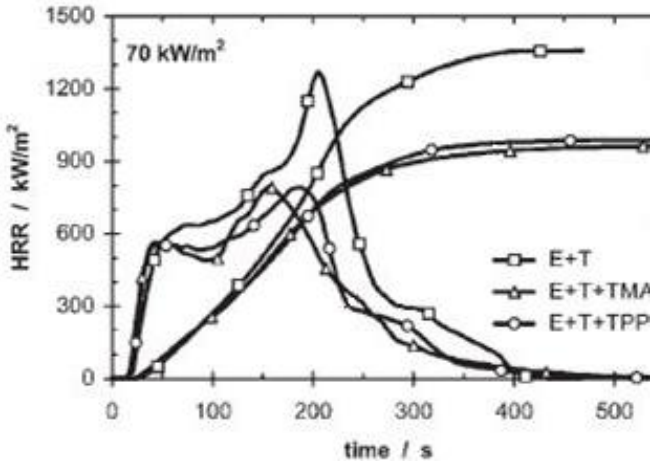

Figure 37: Heat release rate for the different materials versus time applying an external heat flux of 70 kW/m² (E+T= virgin epoxy, E+T+TMA= Epoxy + ammonium clay, E+T+TPP= Epoxy + phosphonium clay)

Different external heat fluxes were used and the influence of the incorporation of nanocomposites depends on the used heat flux. The biggest reductions of the peak of heat release rate (pHRR) are observed for the nanocomposites and are reduced by 1/3 for an external heat flux of 70 kW/m², and no significant difference between the two nanocomposites was observed. The enhancement brought by nanoparticles depends strongly on the heat flux: the reduction of 1/3 at 70 kW/m² is only 1/5 at 30 kW/m². Extrapolating this curve leads to an absence of effect for non-radiant tests such as UL-94 or LOI. Therefore, from this point of view, the results obtained before for the LOI test are consistent with the results for the cone-calorimeter. As a first conclusion, the

authors pointed out the barrier effect of nanoclays in epoxy. However, in this case, the barrier effect is limited.

Schartel et al. [51] also worked on an epoxy system: a bisphenol A diglycidylether-based resin was cured with 4-methyl hexahydrophtalic anhydride (Figure 38), and the reaction was accelerated by 1-methylimidazole.

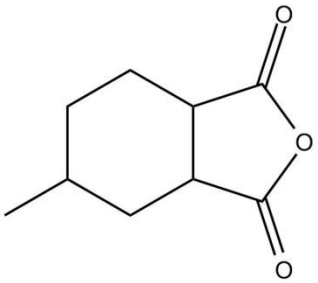

Figure 38: Formula of 4-methyl hexahydroxyphtalic anhydride

Different phosphonium-based clays were incorporated at 5 wt.% in order to study the influence of the morphology and the distribution of clay in this system (different morphologies are obtained by changing the drying conditions). The specific surface (BET) of modified bentonite was determined by nitrogen adsorption and used to evaluate the powder morphology. It varied from 6.7 m^2/g for a commercial ammonium bentonite used for comparison up to 175 m^2/g for the freeze-dried phosphonium bentonite. SEM and TEM showed that the distribution of clay in the matrix is strongly influenced by the characteristics of the clay. It seems that the higher the BET surface of the powder, the better the distribution. Taking into account the results from Hartwig [50], the authors supposed that the incorporation of modified clays alone would not bring sufficient fire properties to the materials. Therefore, they developed mixed systems containing clays and aluminum trihydroxide (ATH). They also used a mixture of unreactive and reactive phosphorus containing flame retardants: triphenylphosphate (unreactive) and Struktol VP3735 (reactive). Struktol VP3735 is the product of the reaction between 9,10-dihydroxy-9-oxa-10-phosphaphenanthrene-10-oxide (DOPO) and an epoxy novolac (no further detail available). LOI investigations showed that a small increase is achieved by incorporating clays in the epoxy matrix and the higher LOI is reached with phosphorus-based flame retardants: 23-23.4 vol.% depending on the phosphonium clay used, instead of 20.9 vol.% for the neat resin and 32.9 vol.% for the phosphorus-based flame retardant. It should be noted that combinations between clays and Struktol or

ATH led to a small antagonistic effect in terms of LOI. The fire behavior was further studied by cone-calorimetry: the pHRR was decreased by incorporating layered silicate, ATH or organo-phosphorus flame retardant. The highest decrease is achieved by the organo-phosphorus flame retardant whereas the smallest is reached with clay. The drying conditions of clay, and therefore the morphology, have an influence on the pHRR. As seen before, the dispersion was strongly linked to the drying conditions of the MMT powder and a better nanodispersion leads to reduced pHRR, up to 51 % at an external heat flux of 70kW/m². Another study by Schartel et al. [52] on similar systems showed a strong relationship between the clay morphology before mixing and the nanocomposite formation, and thus on the reduction in pHRR. The authors concluded that even if the nanocomposite formation in thermosets is less easy to achieve than in thermoplastics, a homogeneous, nano-scaled dispersion of clay is critical for producing a homogeneous residue surface layer during combustion that is able to provide the desired fire retardancy. Therefore, the need for an even dispersion has been confirmed. However, achieving a perfectly exfoliated nanocomposite is not necessary, and an intercalated structure might provide good fire properties, as long as no big inhomogeneities are present in the material. This is consistent with the results from Samyn et al.[49] with modified montmorillonite in polyamide-6: organomodified clays are both nanodispersed and are either exfoliated or have an intermediate dispersion (intercalated/exfoliated). On the contrary, the unmodified clay is microdispersed. The performances in mass-loss calorimetry are affected by the dispersion state: microdispersed clay reduces HRR by 25 % whereas nanodispersed ones provide a 50 % HRR decrease compared to virgin material. It gives therefore evidence that the nanomorphology (tactoids reasonably nanodispersed vs. evenly individual platelets nanodispersed) is not the key factor to get the best flame retardancy properties in terms of pHRR.

More effective systems have been reported by Camino et al. [53] with different organo-modified montmorillonite (OMMT) in epoxy at 10 wt.%. Such a high loading does not allow the formation of a ‘real’ nanocomposite, i.e., microcomposite is probably synthesized. However, differences in the dispersion state, depending on the exchanged cation, can be observed. The authors showed that the composite containing Nanofil 848 (octadecyl ammonium montmorillonite), which has the best dispersion, observed by TEM and Wide Angle X-Ray Diffraction (WXRD), gives good results but not as good as

Cloisite 30B (bis(2-hydroxyethyl) ammonium montmorillonite) (Table 5). On the contrary, Cloisite 25A (dimethyl hydrogenated-tallow(2-ethylhexyl) ammonium montmorillonite) leads to a smaller decrease of pHRR. Such enhancements remain isolated and Zammarano [54] suggested that the particularly high decreases observed for the nanocomposites in this case may be related to different curing conditions between neat resin and the nanocomposites. In fact, 1 wt.% imidazole catalyzed the curing for neat resin whereas it was not considered as necessary for the nanocomposites since clays have been reported to catalyze the epoxy ring opening reaction [55]. But it seems that the use of such catalyst decrease the onset of decomposition temperature. If this phenomenon effectively occurs in this case, the materials containing clays cannot be properly compared with the virgin resin. The virgin resin would be easily degraded and the effect of the incorporation of clay overestimated. This could explain why no similar high decreases of pHRR by clays have been reported in epoxy since then.

Table 5: Cone-calorimeter data of epoxy nanocomposites at 50 kW/m² [53]

Sample	Time to ignition (s)	pHRR (kW/m²)	pHRR decrease (%)
Pure epoxy	34.5	2030	-
Epoxy/Nanofil 848 (10 wt.%)	34.5	1250	48
Epoxy/ Cloisite 30B (10 wt.%)	34.5	650	68
Epoxy/ Cloisite 25A (10 wt.%)	44.0	1570	23

Even if such high effects are isolated for clays in epoxy, it is worth considering that the higher decrease was not brought by the filler with the best exfoliation. This may be linked to the high loadings achieved, which probably do not permit sufficient dispersion of these fillers. The authors also mentioned a possible additional effect of the chemical nature of the surfactant in addition to the physical barrier effect of clay. This effect has not been identified up to now. As a general conclusion, it seems that organoclays do not always show their full potential as flame retardants in epoxies, probably because of the difficulties for controlling their morphology in this matrix. However, their barrier effect could be useful in combination with other flame retardants.

I.2.3.b. Layered Double Hydroxides

Layered double hydroxides (LDHs) are another type of layered crystals and are called anionic clays, by analogy with some lamellar cationic clays. LDHs can either be synthetic or natural (hydrotalcite). Their general formula is $[M^{II}_{1-x}M^{III}_{x}(OH)_2]^{x+}[(Y^{m-})_{x/m}]$, nH_2O, where M^{II} is a divalent metal cation, M^{III} is a trivalent metal cation, and Y stands for *m* valence inorganic or organic acid anions (Figure 39). These anions are variable and a lot of different LDHs have been synthesized, providing a wide range of properties, in particular a high anion-exchange capacity. Hydrotalcites have a octahedral structure similar to brucite ($Mg(OH)_2$) where the partial isomorphic replacement of a bivalent cation with a trivalent cation produces positive charges counterbalanced by hydrated anions.

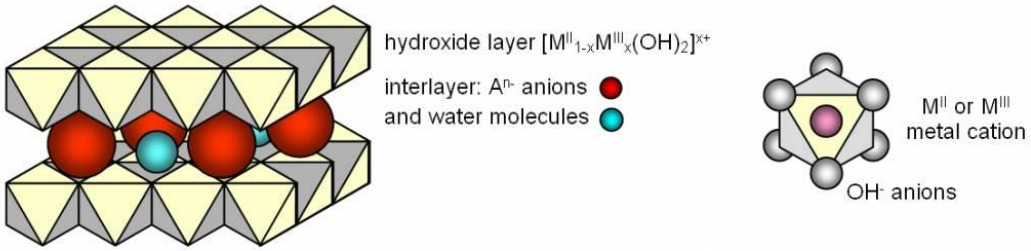

Figure 39: Structure of LDH [56]

Their incorporation into polymer also provides interesting fire retardant properties: they absorb heat during their decomposition and release water and carbon dioxide, which dilutes flammable gases, enhances the heat absorption and reduces the heat release during combustion. Furthermore, a protective ceramic layer is formed on top of the sample, providing a barrier effect [54]. They could be used as a replacement for magnesium hydroxide and aluminium trihydroxide, which are effective, but need to be incorporated at high loadings. Zammarano et al. [57] have noticed the self-extinguishing behavior of epoxy/LDH nanocomposites at the horizontal UL-94 HB test. High reductions of the pHRR during cone-calorimeter experiments have also been observed. For a constant cation mixture (magnesium+aluminum), the reaction to fire depends strongly on the LDH anion: 40 % and 51 % pHRR decrease is reached with 4-toluenesulfonate and 3-aminobenzosulfonate respectively. Samples containing montmorillonite were also tested for comparison: a 27 % pHRR decrease was observed. Finally, samples based on 'traditional flame retardants' such as ammonium polyphosphate (APP) and aluminium

trihydroxide were also tested. Even if LDH provided reduced fire behavior compared to that obtained with APP (80 % decrease of the pHRR), the ignition time was close to that of virgin resin for the LDH-containing samples, whereas it was reduced by the incorporation of APP. Furthermore, LDHs are also likely to enhance mechanical properties and APP degrades them. In fact, in this case, it seems that LDHs act as a nano-intumescent system where the epoxy resin itself is the source of the char, the sulfonate from the LDH is the charring agent, while water and CO_2 are the blowing agents in addition to those of the degrading epoxy. Therefore, the incorporation of modified-LDH in epoxy seems an effective way for providing good fire properties to this polymer.

I.2.3.c. Polyhedral Oligomeric Silsesquioxanes

Among the many particles incorporated in epoxy, Polyhedral Oligomeric Silsesquioxanes (POSS) are one of the most studied in recent years. Their effect on the mechanical and the thermal properties of epoxies as well as their influence on the kinetics of curing has often been reported but the fire properties of the obtained materials have rarely been discussed [58-60]. On the other hand, the interest of POSS as fire-retardant in other polymers has been reported [3, 61, 62]. POSS are structurally well-defined compounds composed of a silicone-oxygen framework having the general formula $(RSiO_{3/2})_n$ (n=6, 8, 10…).The most typical species is the octahedron (n=8) (Figure 40).

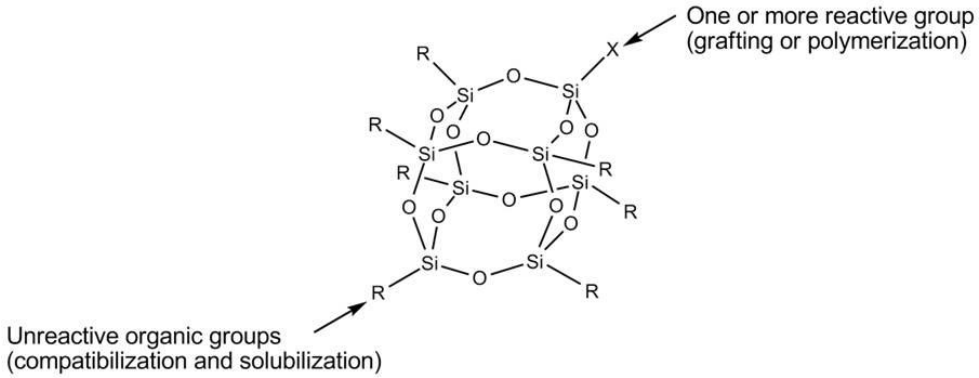

Figure 40: Structure of cage hexahedral silsesquioxane

R can either be hydrogen or any organic group. These molecules are well-defined and their sizes range from 1 to 3nm, which makes them the smallest version of colloidal silica. Depending on the reactivity of the organic group (R), POSS can be classified as non-functional or functional.

Functional POSS are widely studied in epoxies, probably because of the possible reactions occurring between their reactive moieties and the epoxy rings of the resin. An enhancement of LOI has been reported by different authors: 5 wt.% of cyclohexyltrisilanolPOSS leads to a LOI of 32.8 vol.% instead of 22.6 vol.% for the virgin resin used by Lu et al. [63]. Similar trends were observed by Lu et al. [64] for cyclohexyldisilanolPOSS: the LOI increased from 26 vol.% for the virgin resin up to 32 vol.% for a POSS content of 25 wt.%. Another reactive POSS obtained by the reaction between trisilanolisobutylPOSS and triglycidylisocyanurate was incorporated at higher contents (10 wt.%) by Wu et al.[65]. Due to the epoxy ring of the modified POSS, the authors suggested a possible reaction between the hardener and the POSS, leading to a hybrid network. They investigated the reaction to fire using micro-scale calorimetry. The curve corresponding to the hybrid network shows two overlapping peaks instead of one sharp peak and a lower peak of heat release rate compared to the one for virgin resin. Therefore, the peak of heat release rate is decreased by 30 %, showing the interest of the incorporation of reactive POSS in epoxies. Even if such loadings appear high for nanoparticles, the incorporation of POSS in the matrix seems beneficial for the flammability. One question still remains: do these results stem from the presence of the reactive moiety of this POSS, the high loading resulting in significant inorganic content or a combination of these parameters?

Wu et al. [66] studied a DGEBA/phenyltrisilanolPOSS mixture. An aluminum complex was used in order to catalyze the reaction between these two reagents. The morphology of the obtained composites was characterized by SEM (Figure 41).

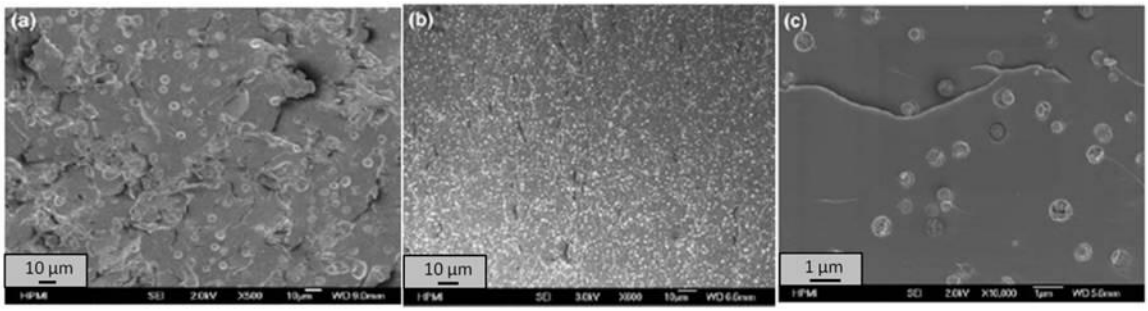

Figure 41: SEM pictures of POSS composites cured with and without aluminum complex. (a) Epoxy/POSS, (b) Epoxy/POSS [Al], (c) higher magnification of b.[66]

The size of POSS particles is decreased when the reaction is catalyzed. In fact, the authors report that the uncured mixture without aluminum complex was clear and

became cloudy during curing, whereas it remained clear for the samples containing aluminum complex. They investigated the effect on the reaction to fire of the resin by cone-calorimetry. All curves are made of two peaks, the first being the highest. The incorporation of POSS in the formulation did not give any significant decrease of the pHRR. The effect was higher for the formulation containing both aluminum complex and POSS: the pHRR was decreased by 33 % and the curve is flattened. The morphology of the residues obtained after burning was characterized by SEM: the combination between POSS and aluminum complex produces a compact, uniform char, whereas holes were observed when POSS are incorporated without Al (Figure 42).

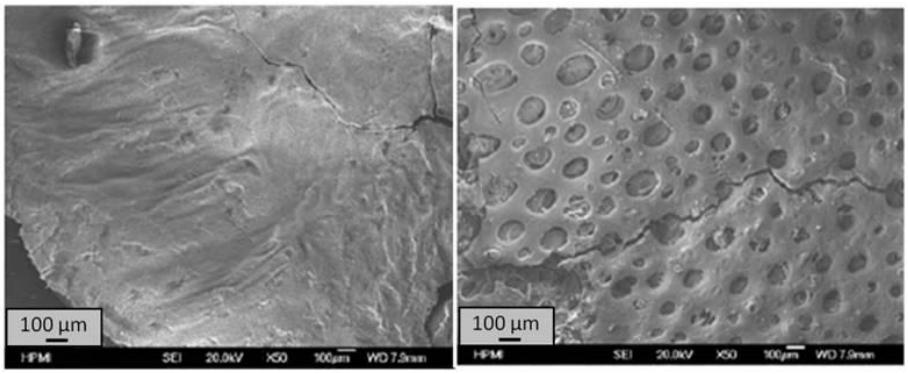

Figure 42: SEM pictures of residues for Epoxy/POSS/aluminum complex (left) and Epoxy/POSS (right)

This difference is probably due to the more even dispersion of POSS when combined with aluminum complex. This is important to point out that in this case, the dispersion is not at the nanoscale. However, the addition of aluminum complex in the formulation led to far more homogeneous dispersion. This is certainly the main reason for the enhanced fire behavior: increasing the interfacial area between the polymer and the nanofiller helps the formation of a protective layer during combustion. This conclusion is similar to that done by Schartel et al. for organoclays [52]. In this case, the authors suggested that the aluminum complex, by favoring the compatibilization reaction between the resin and the reactive moiety of the POSS, leads to the better fire behavior of the system. However, as a general conclusion on reactive POSS, it is not clear if the better reaction to fire observed with reactive POSS is due to the presence of covalent links between the POSS and the resin or simply to the presence of POSS itself. This last study with the aluminum catalyst showed the potential interest in controlling the reaction between the resin and the POSS in order to take full advantage of the POSS properties.

In order to get higher enhancements of the fire properties, combinations between octavinylPOSS and a phosphorus-containing resin have recently been reported by Wang et al. [4]. The phosphorus content in the mixture was kept constant (2 wt.%) and the silicon content varied from 0 to 3 wt.%. (i.e., 0 to 10 wt.% POSS). TEM pictures of the sample containing 3 wt.% POSS showed a homogeneous material and no aggregate could be identified. The reaction to fire was evaluated by means of a micro-scale calorimeter. The curves are made of a single peak, which is sharp for the resin without POSS. Incorporation of POSS in the matrix leads to a decreased pHRR (-44% for the sample containing 3 wt.% silicon) and the shape of the curve is modified, the peak broader. Based on the literature, the authors attributed the positive effect of the incorporation of POSS on the pHRR to the POSS capability for promoting char formation instead of making evolving fuels.

A comparison between reactive and non-reactive POSS was conducted by Franchini et al. [67]. Three different POSS were incorporated in an epoxy matrix: octaphenyl-, glycidoxypropyl-heptaphenyl- and glycidoxypropyl-heptaisobutylPOSS (Figure 43).

This selection lets investigate the effect of the non-reactive ligand type and the presence of reactive moieties on the reaction to fire of the samples. Cone-calorimeter at 35 kW/m² was used in this purpose. For each type of POSS, a decrease of the pHRR was observed at 3.7 wt.% inorganic part (corresponding to 8.3-9.5 wt.% POSS depending on the POSS type). The phenyl-based POSS led to highest decreases: the reduction of the pHRR was -25 %, -34 % and -40 % for glycidoxypropyl-heptaisobutylPOSS, octaphenylPOSS and glycidoxypropyl-heptaphenylPOSS respectively. The cross-section of the residues was observed and revealed that the sample leading to 40 % pHRR reduction has a sponge-like structure. This characteristic was not found in the other samples. Such an observation suggests a better thermal insulation and it would be worth observing the residues into details. UL-94 tests were also conducted and the samples were not classified. However, visual observations show differences between the samples: those containing glycidoxypropyl-heptaphenylPOSS did not release drops during burning, 96 wt.% of the sample remained after burning and it was self-extinguishing. The other samples burnt completely and released incandescent drops. The effect of POSS content was finally investigated: two different POSS content were used i.e., 1.50 wt.% (corresponding to 3.4-3.9 wt% POSS) or 3.70 wt.% of inorganic part.

Small differences were observed and the main conclusion is that the performances obtained with 3.7 wt.% loading can be reached with 1.5 wt.% loading. An influence on the UL-94 test was observed since the final residue was 70 wt.% for 1.5 wt.% POSS instead of 96 wt.% for 3.7 wt.%. These results highlight once more the potential of POSS as efficient flame-retardants in epoxy.

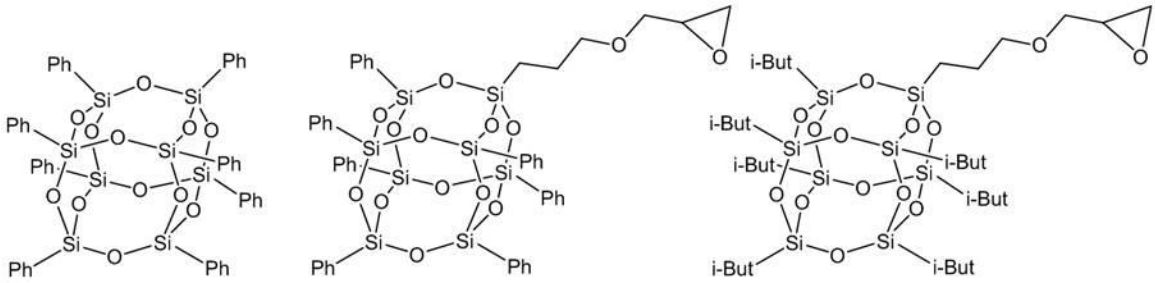

Figure 43: Chemical structures of octaphenylPOSS (left), glycidoxypropyl heptaphenylPOSS (middle) and glycidoxypropylheptaisobutylPOSS (right) (Ph=phenyl, i-But= isobutyl).

I.2.3.d. Carbon nanotubes

Since their discovery by Ijima [68] in 1991, carbon nanotubes (CNTs) have attracted great interest, due to their unique properties, in particular morphology, high mechanical resistance, high thermal conductivity, high electrical conductivity. Carbon nanotubes can be seen as elongated fullerenes: they are graphene sheets rolled up into a hollow cylinder, with each end capped with half of a fullerene molecule [69-71]. There are two major types of carbon nanotubes: single-walled carbon nanotubes (SWNTs) and multi-walled carbon nanotubes (MWNTs) (Figure 44). The first ones are made of a single sheet of graphene, and their diameter lies between 0.3 and 2 nm. Their length is generally more than 200 nm [72]. The second ones are made of several concentric graphene cylinders, where weak Van de Waals forces bind the tubes together. Because of this structure, MWNTs have diameters higher than SWNTs, typically between 10-50 nm. Their length lies between 1-50 µm. Their aspect ratio can be as high as 10 000 [69].

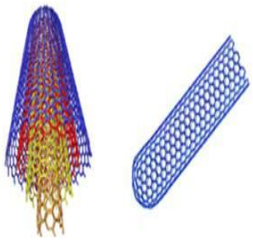

Figure 44: Carbon nanotubes (left : Multiwall Carbon Nanotubes (MWNT), right: Singlewall Carbon Nanotubes (SWNT).

Carbon nanotubes can be synthesized via different methods: arc method, laser method, chemical vapor deposition and even fluidized bed reactors. Due to the synthesis methods, which often require the use of catalysts, carbon nanotubes contain impurities, among them catalyst metals and carbonaceous species [73]. However, treatments like thermal annealing in air or oxygen atmosphere and liquid phase reaction in various acids exist in order to minimize the content of impurities. However, yields are generally low. The goal is now to control the morphology of the synthesized nanotubes and find a way to produce them at big scale (such a result would lower the nanotubes prices and provide bigger batches having the same characteristics). A real problem lies within the reproducibility of the results (even for the synthesis) between different research teams, and even in a single team [74].

Choosing which type of nanotubes to use can be rather hard: SWNTs offer better properties (mechanical properties, thermal conductivities), but their price is higher, whereas MWNTs are cheaper and are easier to process, due to their bigger size. It is necessary to evaluate which properties are needed. Furthermore, researchers define a third type of carbon nanotubes: double-walled carbon nanotubes, whose properties are intermediate between the ones from SWNTs and MWNTs [74]. Mechanical properties of CNTs are striking, because of the strength of the C-C bonds, which are among the strongest in the nature: more than twice the tensile strength of high-strength carbon fibers, with a density lower than that of traditional carbon fibers (1.3 g/dm^3 for CNTs, 1.8-1.9 g/dm^3 for commercial carbon fibers). Carbon nanotubes also combine a high flexibility and strength with a high stiffness. Their thermal conductivity is highly anisotropic: diamond-like over the length of the tube and insulating in the transverse direction. Another particularity of carbon nanotubes is their tendency to aggregate into bundles (diameter: 10-100 nm). This is mainly due to Van der Waals interaction between the different nanotubes. This characteristic is highly detrimental to the composite properties and one of the challenge concerning CNTs is to destroy these aggregates and enhance the dispersion of nanotubes in the matrix [69].

Functionalizing carbon nanotubes

Researchers have tested a lot of different methods in order to improve the dispersion of carbon nanotubes in a polymer matrix. A good dispersion not only makes

more filler surface area available, but also prevents formation of aggregates of the filler acting as stress contractors as well as slippage of nanotube during composites loading. These methods include surfactant-assisted dispersion [75] and covalent functionalization of CNTs. In the case of epoxy composites, amine-functionalized CNTs are mainly found [76-78].

A simple way for dispersing CNTs in a polymer is to use high power dispersion methods, such as ultrasound and high-speed shearing. For example, Sandler et al.[79] dispersed CNTs in epoxy under high speed stirring (2000 rpm) for 1 h and found that intense stirring is an effective process to achieve dispersed CNTs uniformly in epoxy. However the dispersion is not sufficient. Gong et al.[75] used a non-ionic surfactant, polyoxy ethylene-8-lauryl, as a processing aid for epoxy/CNTs composites: the hydrophobic part of the surfactant interacts with the carbon via Van der Waals forces, and the hydrophilic part with the epoxy via hydrogen bonding. The homogeneous dispersion of CNTs in epoxy improves the thermomechanical properties of the composites: with 1 wt.% CNTs, the glass transition temperature is increased from 63 °C to 88 °C and the elastic modulus by over 30 %. It seems that CNTs act as nucleation sites in the matrix and that their inclusion enhances polymer crystallization and increases the melting temperature. However, the incorporation of surfactant in an epoxy system is often detrimental for thermal and fire-retardant properties.

Carbon nanotubes have a rather smooth surface, a property which causes most of the outstanding properties of these materials. However, this “perfection” (defects exists but their density is not high enough) hinders the grafting and reaction of chemicals with the nanotubes. In order to provide active sites, mainly carboxyl and carbonyl groups, different oxidation treatments exist: the most common oxidation system is a 3:1 mixture of sulfuric acid (98 %) and nitric acid (65 %). Liu et al.[80] used this mixture and went further by using subsequently a 4:1 mixture of concentrated sulfuric acid and 30 % aqueous hydrogen peroxide. They considered that the first treatment cut CNTs into about 150 nm in length and opened their ends, and that more functional groups were formed on the CNTs surface due to second treatment. Due to the large spectrum of results obtained by different teams, it seems really important to adjust and control the processing conditions to obtain short CNTs with different length. This point could help to get convergent results between the different teams.

After the oxidation treatment, carboxylic groups on CNTs surface are converted into acid chloride groups by reaction with thionyl chloride. Acid chloride groups are highly reactive and therefore the graft of molecules can be achieved. Acid chloride containing CNTs have been grafted with amines by different research groups. Shen et al.[76] grafted four different amines on MWNTs after thionyl chloride treatment: ethylenediamine, 1,6-hexanediamine, 4,4'-diaminodiphenylmethane and 4,4'-diaminodicyclohexylmethane (Figure 45). The nanotubes were incorporated into an epoxy matrix. SEM images of fracture surface after three-point bending test show that the affinity between functionalized CNTs and the matrix is better than for unmodified CNTs. The impressive number of publications dealing with the incorporation of amine-functionalized CNTs in epoxy reflects the interest for this solution [77, 78].

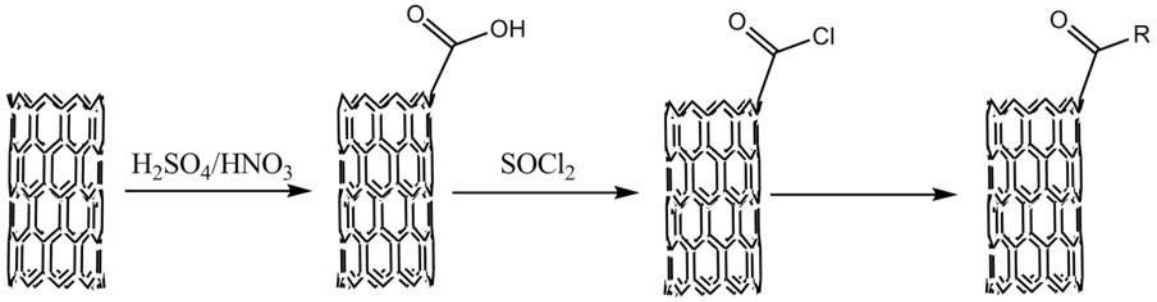

Compound	R
Ethylenediamine	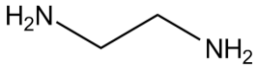
1,6-hexanediamine	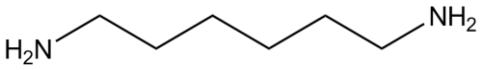
4,4'-diaminodiphenylmethane	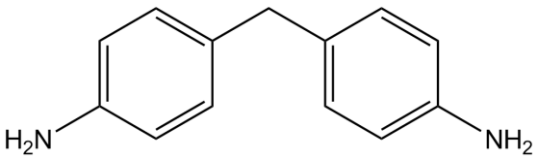
4,4'-diamino-dicyclohexylmethane	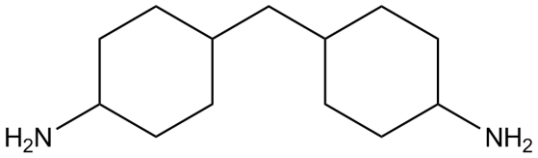

Figure 45: Reaction scheme for the amino-functionalization by Shen et al.[76]

The TGA study permits to observe that the incorporation of raw CNTs in the matrix has slightly no effect, whereas the use of amine-functionalized CNTs has a great effect on the onset decomposition temperature. It seems that because of the strong interactions between the matrix and the functionalized nanotubes, the diffusion of small

molecules is retarded at high temperature. The onset decomposition temperature of samples increases with the CNTs content, but there seems to be an upper limit to the CNTs content because the temperatures decrease when the content reaches 1 wt.%. This phenomenon has been observed by other researchers and it seems that when the CNTs content is too high, the CNTs cannot be properly dispersed and aggregates act as defects in the matrix, quickening the thermal decomposition rate. DSC analyses were also conducted and gave indications on the evolution of the Tg. As for the onset decomposition temperatures, the effect is slightly inexistent with raw CNTs whereas the modifications are bigger with amino-functionalized CNTs. The Tg decreases when the CNTs content increases for 3 amine-functionalized CNTs, and increases before decreasing for the aromatic amine CNTs. This phenomenon is linked with the cure reaction of the matrix and is quite complex.

More recently, the functionalization of CNTs with flame-retardants has been reported by Ma et al.[81]. They covalently grafted a derivative of pentaerythritol biphosphonate (PDSPB) onto MWNTs, until the graft represented 65 wt.% of the final filler. This results in a core-shell structure where MWNTs are the hard core and PDSPB is the soft outer shell. The reaction to fire of the acrylonitrile-butadiene-styrene composite is strongly affected by the presence of CNTs. Only 0.2 wt.% of unmodified CNTs decrease the pHRR by 44 %. The effect is stronger for functionalized CNTs since the decrease reaches 50 %. Increasing the CNTs content up to 1 wt.% reinforces the flame-retardant effect of unmodified CNTs (54 % pHRR decrease), but the influence of the content is less obvious for modified CNTs.

Carbon nanotubes as flame retardants

Carbon nanotubes have been incorporated in various polymers, showing strong fire-retardant effects [62, 82, 83]. Numerous papers deal with the use of raw or functionalized CNTs in epoxy resins and the improvements induced, in particular concerning the mechanical properties and the thermal stability of the prepared materials. However, up to very recently, the effects on the reaction to fire of the resin had never been reported. Kuan et al.[84] functionalized CNTs with vinyltriethoxysilane and incorporated them in an epoxy matrix via sol-gel method. Materials containing up to 9 wt.% CNTs were obtained and tested for their reaction to fire by LOI and vertical UL-

94. LOI gradually increases along with the CNTs content and reaches 29 vol.% for the samples containing 9 wt.% CNTs, instead of 22 vol.% for the virgin polymer. The UL-94 classification is also increased from V-1 for the virgin resin to V-0 for 3 wt.% CNTs in the matrix. The authors linked these results to the strongly modified mechanical properties of the materials. The glass transition of the polymer is affected by the incorporation of CNTs: it increases for CNTs contents higher than 3 wt.%, but no Tg could be recorded for the sample containing 9 wt.%. This result suggests that modified CNTs could be beneficial for the flame retardancy of epoxies. It would however be useful to incorporate unmodified CNTs in the sol-gel system in order to observe their effect on the Tg, since it seems closely related to the enhanced behavior at the UL-94 test. Rahatekar et al. [85] studied the effect of highly-aligned CNTs in epoxy matrix on the peak mass loss rate (PMLR) during gasification (Figure 46). The system used is similar to a cone-calorimeter, with a nitrogen atmosphere instead of air. Therefore, as pointed out by the authors, the condensed phase is studied in the absence of oxidation and there is no feedback from combustion in the gas phase. The results show the mass loss rate as a function of time. A very small amount *i.e.*, 0.0025 wt.% of highly-aligned CNTs resulted in a 45 % reduction of the PMLR and the total time needed for complete mass loss is delayed.

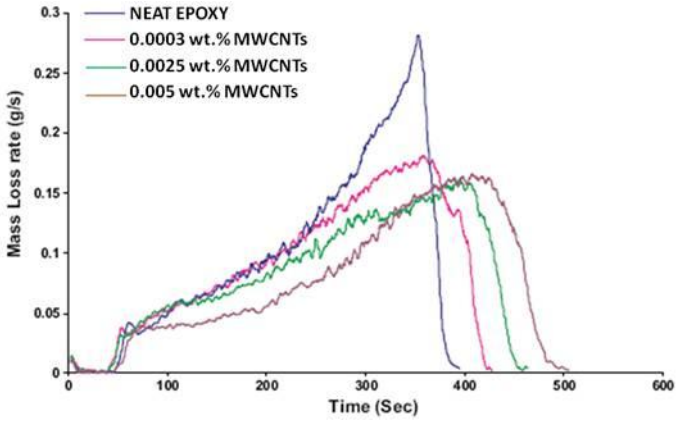

Figure 46: Mass loss rate versus time for different CNT-containing epoxies (Heat flux: 50 kW/m², N_2 atmosphere)[85].

The reduction in PMLR is slightly lower for the 0.005 wt.% CNTs sample. Based on these results and their modeling, the authors suggest that two mechanisms compete. Re-radiation is identified as the main protection mechanism. The nanoadditives form a protective layer on the surface of the sample. As the temperature rises, the thermal

energy reaching the underlying polymer is decreased. At higher loading, this effect is disturbed by the high thermal conductivity brought by CNTs: the heat transfer to the degrading polymer below the charring layer increases. Therefore, the fire-retardant effect is less impressive at higher contents. This study provides helpful data for the comprehension of the reaction to fire of epoxies containing nanoparticles. The exceptional results for CNTs/epoxy composites might also come from the use of highly-aligned carbon nanotubes, which debundle more easily. This is a major advantage compared to 'traditional' carbon nanotubes.

As a conclusion, different nanoparticles have been evaluated in epoxy resins and provide protection against fire. Nanoparticles have already been identified as valuable for the flame retardancy of thermoplastics. One of the involved mechanisms is an increase of the viscosity of the polymer. This effect may be also useful in epoxies since a viscosity drop around 350 °C in epoxy has been identified [86] and could be limited by the incorporation of nanoparticles. However, up to now, the barrier effect is considered as the major effect for protecting this matrix with nanoparticles: an even dispersion of the particles seems essential in order to form a protective barrier on top of the sample. Another parameter is that for some clays, conclusions are different between the authors. This can be attributed to a wider range of morphology achieved with montmorillonite. For example, working with montmorillonite leads to very different fire-retardant effects depending on the used montmorillonite and the composite synthesis method. Carbon nanotubes have not proven a strong fire-retardant effect in epoxy regarding standard methods yet. Layered double hydroxides seem promising, but the current limited range of industrially available ion-exchange limits their potential use at larger scale. Therefore, until the morphology of MMT/epoxy is controlled, one of the best nanoparticles for enhancing the fire properties of epoxy seems to be POSS, even if they are not nanodispersed in the cited studies (probably because of the chosen loadings, which are relatively high).

I.2.4. Phosphorus-based systems

Compounds containing phosphorus have attracted a strong interest for flame-retarding polymers, and especially epoxy resins. They remain cost-efficient, are incorporated at relatively low levels (as low as 5 wt.% in epoxies) and do not release

toxic gases. Furthermore, phosphorus is part of various compounds at different oxidation levels: elementary phosphorus (red phosphorus), inorganic or organic phosphates, phosphinates, phosphonates, phosphines or phosphites (Figure 47).

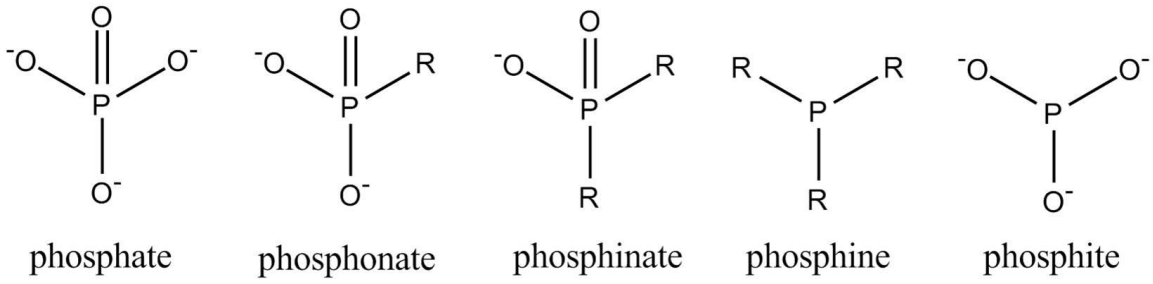

Figure 47: Chemical structure of different phosphorus-based compounds (R=alkyl)

These compounds are generally incorporated to polymers which naturally produce a carbonaceous protective layer (char). They act as char promoter and have therefore in this case a condensed phase action. If the chosen polymer does not naturally lead to the formation of a char, polyols (and especially pentaerythritol) or melamine are incorporated in the system in order to promote intumescence.

Some phosphorus-containing flame retardants also act through a gas-phase mechanism. They volatilize during polymer combustion and release radicals ($PO_2^{\bullet}$ and $PO^{\bullet}$) which can efficiently interact with hydrogen radicals ($H^{\bullet}$) and hydroxyl radicals ($OH^{\bullet}$) from the flame. A study has shown that phosphorus-based flame retardants are respectively five times and ten times more efficient than brominated and chlorinated ones at the same molar concentration [87].

In gas-phase, the mechanisms involved with phosphorus-based flame retardants are similar to that of halogenated compounds. In the special case of $PO^{\bullet}$ radicals, the presence of a third species is necessary (Figure 48).

$$HPO_2 + H^{\bullet} \rightarrow PO^{\bullet} + H_2O$$
$$HPO_2 + H^{\bullet} \rightarrow PO_2^{\bullet} + H_2$$
$$HPO_2 + OH\ PO^{\bullet} \rightarrow PO_2^{\bullet} + H_2O$$
$$PO^{\bullet} + H^{\bullet} + M \rightarrow HPO + M$$
$$PO^{\bullet} + OH^{\bullet} \rightarrow HPO_2 + M$$

Figure 48: Interactions between radicals from the flame and from phosphorus-based flame retardants

The most frequently involved phosphorus-containing radical is $HPO_2^{\bullet}$, followed by $PO^{\bullet}$, $PO_2^{\bullet}$ and $HPO^{\bullet}$.

Because the literature concerning the use of phosphorus as flame retardant in epoxy resins is especially abundant, the next sections will give a representative overview of epoxies having a modified backbone and a special emphasis will be put on intumescent systems. Indeed, the synthesis of polymers with intrinsically enhanced reaction to fire and the use of intumescence are especially valued for epoxy systems.

I.2.4.a. Modifications of the polymer backbone

The use of phosphorus-containing flame-retardant has been significantly developed in various polymers as an alternative to halogen-containing flame-retardants [88-90]. This is also the case for epoxies. Moreover, due to the multiple possibilities for creating phosphorus-based monomers or hardeners, incorporation of phosphorus directly in the backbone of the resin has been intensively studied, as pointed out by Levchik et al.[15, 91, 92] and Jain et al.[93]. The incorporation of the flame retardant directly in the polymer backbone has different advantages, among them avoiding migration of the flame retardant in the polymer before burning. One of the most studied phosphorus reactant is 9,10-dihydro-9-oxa-10-phosphaphenanthrene (DOPO) [91, 94-101]. It is a commercially available compound and is recommended as part of the curing system of epoxies. However, its main drawback is its monofunctionnality, and therefore it cannot be used as curing agent on its own. Numerous references deal with the chemical modification of DOPO, leading to phosphorus containing epoxies and curing agents [91, 102, 103]. Only recent works will be commented in the following part.

Hergenrother et al. [104] synthesized different P-containing hardeners and epoxies. The obtained compounds were used in different formulations. The flammability properties were evaluated by microscale calorimetry, cone calorimetry, Ohio State University (OSU) test and flame resistance (nonstandard test). In the flame resistance test, the time required for self-extinguishing after removal of the flame is recorded. The reference formulation exhibited self-sustained burning in air but formulations containing the P-containing hardener extinguished immediately. P-content above 0.9 wt.% provided a self-extinguishing behavior. In the case of P-containing epoxies, all the samples containing more than 1 wt.% phosphorus extinguished immediately whereas the other burnt between 1 and 2s. Therefore, a minimum P-content in the epoxy or the hardener is required in order to get interesting self-extinguishing behavior. The reaction

to fire was further studied by means of microscale calorimetry. The curves exhibit two peaks, which are shifted to lower temperature when 3 wt.% P is incorporated in the systems compared to reference formulations. Furthermore, the height and area of these peaks are also divided by almost two. The authors suggest that similarly to a catalytic mechanism, phosphorus species reduce both the temperature and activation energy for pyrolysis. The efficiency of phosphorus species in reducing heat release capacity and enhancing char formation seems to be linked to the oxidation state of phosphorus: PO_4>:PO_3≈RPO_3>R_3PO. Similar conclusions have been drawn by Braun et al.[105] on carbon-fiber reinforced composites. Taking advantage of the presence of PO_4 acting through a condensed phase mechanism also limits the amount of phosphorus acting in the gas phase. Therefore, the effects in the gas phase, such as a delayed ignition, are less present. This has to be taken into account depending on the final applicability and therefore the standard to pass. Finally, cone-calorimetry confirmed the presence of intumescence for P-containing samples. For some samples, there was even a complete suppression of heat release rate for 1-2 min after ignition. Therefore, this study showed the interest for phosphorus-based epoxies as low-flammable materials.

Combinations between phosphorus-modified resins and nanoparticles have been studied by different authors. Hussain et al. [94] and Liu et al. [106] have looked for synergistic effects between such resins and nanoclays. However, no positive effect of the presence of nanoclay was recorded. While reviewing the results from Hussain et al., Kiliaris et al. [107] suggested that the lack of synergism between clay and the phosphorus-based resin may be due to the phosphorus moiety hindering the dispersion of clay and leading to a less uniform dispersion. This hypothesis is in accordance with the TEM results and is acceptable.

Toldy et al. [108] also studied combinations between phosphorus reactants and clays in epoxy. Two types of molecules, phloroglucinol and calixresorcinarene, were partially or fully phosphorylated (Figure 49).

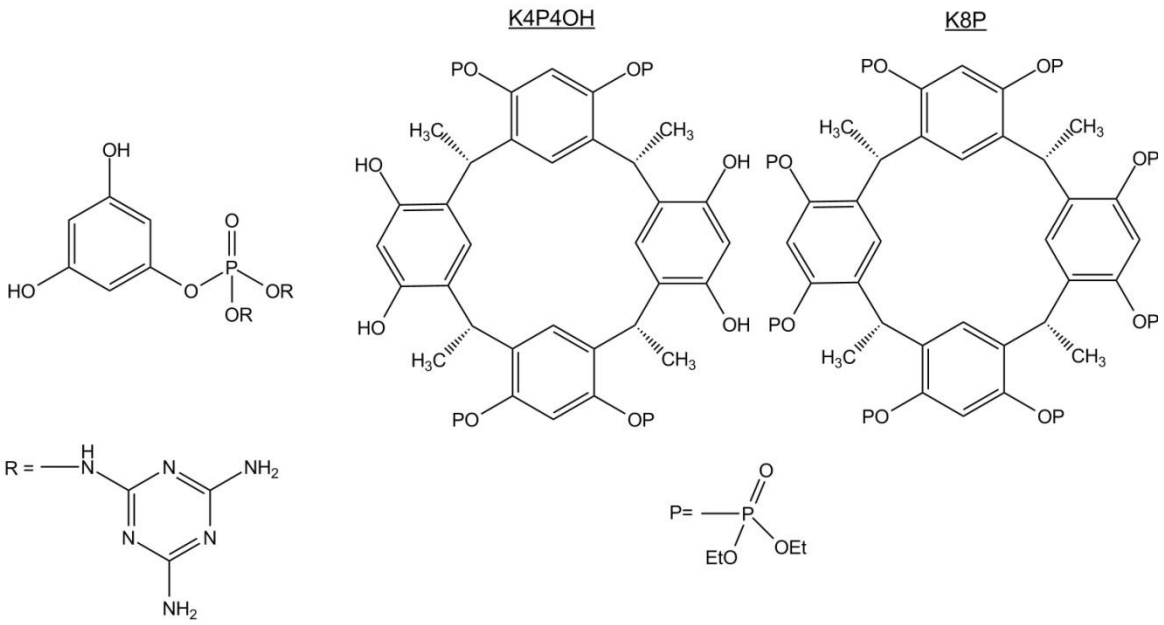

Figure 49:Monophosphorylated phloroglucinol (left), partially (K4P4OH, middle) and fully (K8P, right) phosphorylated C-methylcalix [4] resorcinarene [108].

The best results are obtained with the modified calixresorcinarene. They were identified from the beginning as unable to cure the system and were therefore used as simple additives. Cone-calorimetry revealed that the pHRR is decreased by increasing the quantity of additive. One of the sample corresponding to 2.5% P (named K8P,Figure 49) in the system showed a 61 % pHRR decrease. Another additive (named K4P4OH, Figure 49) also provided a delayed pHRR.

Phosphorus-containing epoxies have therefore widely proven their benefit for flame retarding epoxies. The versatility achieved with such molecules opens a wide range of achievable formulations, depending on the final properties needed. Furthermore, sufficient fire properties are achieved with very low P content. Synergies between organoclays and phosphorus-based epoxies have been examined by different authors. However, in accordance to what has been observed in the first part of this paper, the incorporation of clays sometimes helps to enhance fire properties but can also degrade them.

Mixing phosphorus and silicon containing compounds in epoxy matrices have also been considered, but the contribution of silicon to the flame retardancy of the systems is not often well identified. Hsiue et al. [109] synthesized materials containing phosphorus and silicon via sol-gel method. A phosphorus-based compound bearing epoxide rings (BGPPO) was mixed with DGEBA and TEOS (tetraethylorthosilicate, often

used in sol-gel systems) and cured with DDM. The amounts of BGPPO and TEOS varied. The flammability was evaluated by LOI. First, resins without phosphorus were prepared. The silicon content varied in order to identify the effect of silicon in the system. The reference resin without silicon had a LOI of 26.0 vol.%. It increased gradually along with the silicon content, up to 31.0 vol.% for 8.73 wt.% and 10.20 wt.% Si. BGPPO alone has a LOI of 36.1 vol.% and it is increased for the hybrid material: the LOI reaches 44.5 vol.% for the sample containing 4.35% P and 15.63% Si. Therefore, the use of phosphorus-modified epoxy resins is advantageous, and their flame retardancy may be enhanced by the incorporation of small amounts of silicon.

In summary, combinations between phosphorus and silicon are promising, with phosphorus being the main flame-retardant and silicon acting as synergist.

I.2.4.b. Intumescence

The concept of intumescence is based on the formation of a protective layer which insulates the underlying material from heat and fire. Such intumescent systems require three major components (Table 6: an acid source (generally ammonium polyphosphate), a carbon source (such as char forming polymers or polyols) and a blowing agent (e.g. melamine) [1]. Chemical reactions between these ingredients lead to the formation of the protective intumescent char. A general mechanism has been widely accepted: the acid source decomposes and yields a mineral acid, then it takes part in the dehydration of the carbon source and finally the blowing agent produces gaseous products. These gases are trapped in the char resulting from the carbon source dehydration and make it swell.

Intumescence is therefore a physical protection solution chemically created. The char contains free radicals able to trap those generated during polymer burning. It is also a support for catalytic acidic species that react with oxidized compounds formed during polymer degradation. This also permits to maintain these species in the condensed phase.

Table 6: Main components of intumescent systems

Inorganic acid source	Carbon source
Phosphoric	Starch
Sulfuric	Dextrins
Boric	Sorbitol, mannitol
Ammonium salts	Pentaerythritol, monomer, dimer, trimer
Phosphates, polyphosphates	Phenol-formaldehyde resins
Borates, polyborates	Methylol melamine
Sulfates	Char former polymers (PA-6, PU, PC, …)
Halides	
Phosphates of amine or amide	**Blowing agents**
Products of reaction of urea or guanidyl urea with phosphoric acids	Urea
Melamine phosphate	Urea-formaldehyde resins
Product of reaction of ammonia with P_2O_5	Dicyandiamide
Organophosphorus compounds	Melamine
Tricresylphosphate	Polyamides
Alkyl phosphates	
Haloalkylphosphates	

Intumescent systems have been initially designed as fire protective coatings. The following part is devoted to recent works concerning epoxy resin coatings. Interactions between nanoparticles and intumescent formulations will also be reviewed.

Jimenez et al. [86, 110, 111] widely reported the use of an intumescent protective coating for steel, the formulation optimization and the characterization of its performance. The system is an epoxy-amine system in which two fire retarding agents have been incorporated, separately or combined: a mineral acid (boric acid) and a commercial ammonium polyphosphate. The tests are aimed at linking industrial tests (OTI 95 634) with small-scale lab tests ("Bunsen burner test"). During the industrial test, the sample is heated vertically at high heating rate by a propane burner and the temperature at the backside is recorded. The burning conditions fit as close as possible the ramp of temperature of a hydrocarbon fire heating curve (about 200 °C/min-

UL1709). It was observed that the use of the formulation without fire retardants provides properties close to those of the steel plate only. When APP is added to the formulation, an improvement is observed (time of failure 11.3 min compared to 5 min for uncoated steel). However, the char does not adhere correctly to the steel plate and falls off, causing the failure. Similarly, boric acid yields enhanced fire properties (time of failure 18.2 min), but once more, the char falls off the plate. Finally, a combination between these two fire-retardant additives was incorporated into the system and provides the best properties (time of failure 29.5 min) and the char adheres to the plate. The enhanced behavior was attributed in particular to the combination of phosphates promoting adhesion to steel and of borates which produce a very hard char, resulting in the formation of borophosphates. Experiments using a rheometer were developed and showed that the degradation of the resin at 350 °C leads to a decreased viscosity. The incorporation of boric acid in the formulation limits this decrease by creation of a hard glass (boron oxide), which traps gases and allows a char with good mechanical resistance.

Few publications reported recently coatings based on epoxy resins alone. However, combinations between polyester or acrylates and epoxy resins are found. The influence of the binder in waterborne coatings was studied by Wang et al.[112]. An epoxy emulsion was combined with a self-crosslinked silicone acrylate (SSA) emulsion to get a waterborne intumescent coating. In this system, the well-known APP/pentaerythritol/melamine intumescent system is combined with titanium dioxide, kaolin and expandable graphite. Steel plates were coated by five formulations with epoxy/SSA ratios varying from 39/0 to 27.8/11.2. The samples were tested by recording the temperature on the backside of a heated plate. The shape of temperature profiles is similar for all the coatings. At the beginning of the test, there is almost no difference between them, then, after 20 min, a steady state is reached and its temperature depends on the coating formulation: for epoxy/SSA ratios ranging from 39/0 to 33.4/5.6, the temperature is gradually decreased from 270 °C to 243 °C. When the SSA content increases further, the tendency reverses and the temperature reaches 290 °C. Because the efficiency of an intumescent coating is also linked to the morphology of the char, SEM showed that reasonable amount of SSA in the system led to the formation of dense

foam. Too big amount of SSA gives rise to large cells, therefore decreasing the insulation, as was observed during the fire test.

Polyester or acrylate intumescent coatings enhanced by nanoparticles have been reported. Their study gives clues about the interest for the incorporation of such particles in epoxies. Wang et al.[113-115] reported in a series of three papers the effects of nano-LDH and nano-TiO_2 on intumescent coatings based on mixed acrylate/silicone resins. The aim of the incorporation of these additives was the enhancement of the physical and chemical properties of the char layer, especially adhesion with the substrate. First, a LDH masterbatch was prepared in order to fight the tendency to aggregation of nanoparticles with the aid of dispersant. The dispersion of nanoparticles in the coating was characterized by TEM and compared with the result obtained by the standard procedure. The masterbatch method using dispersant leads to highly enhanced dispersion and was used in the rest of the study. Four coatings containing levels of nano-LDH from 0 up to 3 wt.% were tested for their fire-resistant properties on steel. The temperature on the back-side of the sample was recorded by means of a thermocouple. The sample was heated following ISO-834 curve and the fire-resistant time was defined as the time before reaching 300 °C on the backside of the plate. It can be seen that the incorporation of LDH in the coating up to 1.5 wt.% gradually increased the protection. However, when the LDH content reached 3 wt.%, the tendency reversed. The fire-resistant time of the reference coating is 62 min. Incorporation of 0.5 wt.% LDH leads to a similar result but the time reaches 100 min for the coating containing 1.5 wt.% LDH. When the LDH content is 3 wt.%, the time falls to 48 min. The observation of the residues showed that the intumescence was well-developed for the sample containing 0, 0.5 or 1.5 wt.% LDH (char thickness about 18 mm), but it was nearly absent for the higher LDH content (4.3 mm). Various experiments were conducted in order to elucidate this behavior. The thermal stability of the coatings was then studied by TGA-DTA (Differential Thermal Analysis). The main conclusion is that the incorporation of LDH in this system may enhance the fire protection. Thermal analyses show that the thermal decomposition of LDHs can catalyze the esterification between ammonium polyphosphate and pentaerythritol due to the enhancement of acid activity. XRD showed the presence of aluminium and magnesium oxides. The char containing these oxides seems more resistant and effective than a simple char. LDHs have to be

incorporated at a specific content (1.5 %): an increase of the LDH content leads to an increased reticulation density, and thus, to a decreased mass loss, but a too high LDH content hinders intumescence. Indeed, incorporation of too much LDH probably increases the viscosity of the system and the formation of the protective layer is more problematic. Furthermore, Castrovinci et al.[116] identified an antagonistic effect between ammonium polyphosphate (APP) and aluminium trihydroxide (ATH). APP and ATH reacted together, decreasing the APP amount available for the formation of the intumescent layer. A similar phenomenon could occur for the acrylate intumescent coating since LDH is an organo-modified magnesium-aluminum mixed hydroxide. A further study was conducted on a similar intumescent system containing LDHs (0.9 wt.%) and nano-TiO_2 particles (0.9 wt.%). They found that the incorporation of TiO_2 mechanically reinforced the char by reacting with ammonium polyphosphate or phosphoric acid and forming TiP_2O_7. Finally, coatings containing TiO_2 and no LDH were reported and showed that 1.6 wt.% nano-TiO_2 in an intumescent system already containing micrometric TiO_2 improves slightly the fire-resistant time from 81 min to 96 min. In this case, nanoparticles are not used as the main ingredients bringing fire properties, since it is incorporated in an intumescent coating. However, they prove their efficiency for enhancing the existing acrylate system when used at an appropriate content. Therefore, it would be interesting to see if such particles bring also interesting properties to epoxy coatings.

As a conclusion, even if fire-resistant coatings are mainly based on ‘classical’ intumescent systems, research in this field is very active and many parameters in the formulation can increase the fire retardancy. Mixing resins, acrylate, silicon or epoxy, opens a new range of available properties. The incorporation of nanoparticles in acrylate systems have shown their potential interest and their transposition to epoxy may be useful. Therefore, depending on the substrate and the use, tailored epoxy coatings can be developed for fire retardancy.

I.3. CONCLUSION

In this chapter, the main components of epoxy systems have been described, as well as the reactions involved in the preparation of samples. The thermal decomposition of

epoxy networks has also been reviewed. Then, the mechanisms involved in the burning of polymers have been detailed. Different solutions for fire-retarding them have then been described. The use of flame-retardants is still the major method for improving the reaction to fire of materials. Conventional flame-retardants include halogenated compounds, metallic hydroxides, incorporation of boron, silicon or phosphorus in the system. Indeed, phosphorus-based materials are widely used in the flame retardancy of epoxy resins. The potential of nanofillers in epoxy resins has also been investigated. Even though they have proven their flame retardant effect in different thermoplastics, their interest in thermosets is still to be proved. Finally, the use of intumescent systems for protecting polymer has been considered.

The work described in this thesis is dedicated to the better understanding of the potential of two different types of nanofillers (POSS and CNTs) as flame retardants in epoxies, since few systems are reported in the literature. A second approach will be the study of the interactions between some of these nanofillers and a traditional phosphorus-based flame retardant.

Chapter II - Experimental techniques

This chapter is first devoted to the preparation of epoxy samples and to the functionalization of carbon nanotubes which are incorporated in this epoxy matrix. Then, the characterization methods for these modified CNTs will be exposed. Evaluation of the general properties of epoxy resins will be described thereafter, and the techniques used for assessment of the reaction to fire and the elucidation of the protection mechanisms will finally be presented.

II.1. MATERIALS PREPARATION

This section summarizes the method used for grafting organic moieties on the surface of CNTs, the formulations of the different epoxy samples and finally, the conditions of the preparation of epoxy resins.

II.1.1. Carbon nanotubes functionalization

Two synthesis paths lead to the production of CNTs grafted with flame-retardant moieties. The different steps are described below.

Unless otherwise stated, all materials were obtained from commercial suppliers and used without further purification. Carbon nanotubes were supplied by Nanocyl (Nanocyl-7000 at 90 % purity). They are multi-wall carbon nanotubes. Sulfuric acid (97 wt.%),nitric acid (65 wt.%), thionyl chloride ($\geq$ 99 %) and ammonia solution (28 %) were supplied by VWR. Chloroform (analysis grade) and thionyl chloride were supplied by Merck. Cyanuric chloride (99 %) and ethylenediamine (99 %) were supplied by Acros Organics.

The synthesis was first developed for the functionalization with melamine and then adapted for the functionalization with POSS. The first part is common to both syntheses.

Oxidation of CNTs by acid treatment was carried out by sonication for 30min (100 W, 50 kHz) of a suspension of 1 g of CNTs in 250 mL of sulfuric acid /nitric acid (3/1). The CNTs suspension was diluted with water (5/1, v/v).The oxidized CNTs were washed with water then filtered through 0.45 µm Millipore membrane until the pH was neutral. The oxidized CNTs were dried at 80 °C for 20 h under atmospheric pressure. A suspension of 1 g of oxidized CNTs in 250 mL of thionyl chloride was refluxed with stirring for 18 h then unreacted thionyl chloride was removed by distillation and the activated CNTs (CNT-COCl) were dried under reduced pressure.

The second part of the modification process of CNTs is different for the two products. During the synthesis, all reactions involving air- or moisture-sensitive compounds were performed in a nitrogen atmosphere.

- *Synthesis of 6-chloro-2,4-diamino-1,3,5-triazine:* The sample of 6-chloro-2,4-diamino-1,3,5-triazine was obtained by the reaction of 2 g of 2,3,6-trichloro-1,3,5-triazine (0.011 mol) with 1.47 mL of aqueous ammonia solution (28 %) in a mixture of 50 mL H_2O and 50 mL acetone at 45 °C overnight (this reaction is well-known and can be found in textbooks about triazines [117, 118]). The precipitate was washed with water, filtered and dried at atmospheric pressure at ambient temperature leading to 0.4 g of 6-chloro-2,4-diamino-1,3,5-triazine (0.0027 mol, yield 25 %).

  ^{13}C-RMN (DMSO-d_6): 157 ppm (C-NH_2), 150 ppm (C-Cl)
- *Functionalization of CNTs by melamine:* To a cold suspension of 2 g of CNT-COCl in 200 mL of chloroform were added dropwise 2 mL of ethylenediamine ; when no more acidic vapor evolved, the suspension was refluxed with stirring for 18 h. The ethylene diamine functionalized CNTs were washed with water, filtered and dried at 80 °C under atmospheric pressure. A suspension of 1 g of ethylene diamine functionalized CNTs with an excess of 1 g of 6-chloro-2,4-diamino-1,3,5-triazine in 200 mL of water was refluxed for 18 h. The melamine-functionalized CNTs were washed, filtered and dried under reduced pressure before use.
- *Functionalization of CNTs by POSS:* To a cold suspension of 1 g of CNT-COCl in 200 mL of dried chloroform were added 13 g of aminopropylisobutylPOSS ; when no more acidic vapor evolved, the suspension was refluxed with stirring for 72 h. The POSS-functionalized CNTs were washed, filtered and dried under reduced pressure before use.

II.1.2. Epoxy samples

This section describes the different commercial fillers incorporated in the epoxy matrix and the preparation of the samples. AminopropylisobutylPOSS, trisilanolphenylPOSS, FirequenchPOSS (FQ-POSS) and octamethylPOSS (OMPOSS) were supplied by Hybrid Plastics (respectively AM0265, SO1458, Firequench 1286 and

MS0830) (Figure 50). Ammonium polyphosphate (AP422) was supplied by Clariant, Germany (Exolit AP series).

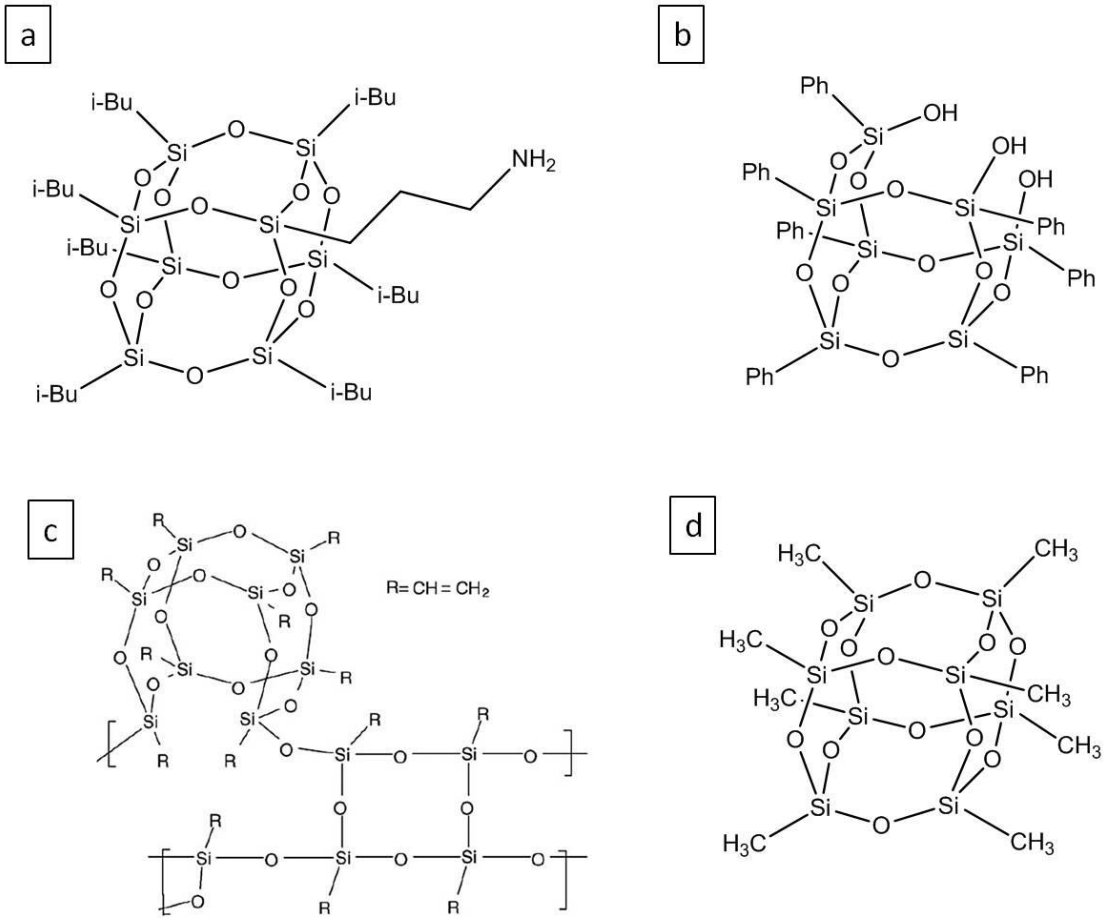

Figure 50: Scheme of POSS. a: aminopropylisobutylPOSS, b: trisilanolphenylPOSS, c: Firequench 1286, d: octamethylPOSS

Epoxy prepolymer (Bisphenol-A diglycidylether, EEW=172-176) and the hardener diethylenetriamine (DETA, 99 %) were supplied by Sigma-Aldrich (Figure 51).

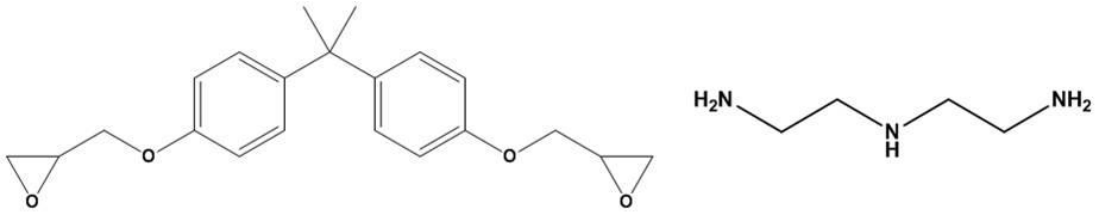

Figure 51: Epoxy prepolymer (left) and hardener (right)

Epoxy prepolymer was put in an oven at 50 °C overnight in order to avoid crystallization. Fillers were mechanically mixed with 80 g epoxy at 1600 rpm for 20 min. The mixture was then sonicated for 1 h (100 W, 50 kHz). After cooling down at room temperature, the amine hardener was mechanically incorporated in the mixture at

200 rpm for 5 min. The mixture was then put into aluminum molds coated with a silicon-based demolding agent and degassed at room temperature. The samples were then cured in a ventilated oven according to the following schedule: 30 min at 30 °C, 30 min at 40 °C and 1 h at 50 °C.

Table 7 summarizes the different fillers incorporated in the epoxy resin, as well as their loading.

Table 7: Epoxy formulations

Sample name	Filler 1	Loading (wt.%)	Filler 2	Loading (wt.%)
Virgin epoxy	-	-	-	-
Epoxy _CNT-0.5	CNTs	0.5	-	-
Epoxy_CNT-COOH-0.5	CNT-COOH	0.5	-	-
Epoxy_CNT-amine-0.5	CNT-amine	0.5	-	-
Epoxy_CNT-melamine-0.5	CNT-melamine	0.5	-	-
Epoxy_CNT-POSS-0.5	CNT-POSS	0.5	-	-
Epoxy_OMPOSS-5	OctamethylPOSS	5	-	-
Epoxy_trisilanolphenylPOSS-5	TrisilanolphenylPOSS	5	-	-
Epoxy_aminopropylisobutylPOSS-5	AminopropylisobutylPOSS	5	-	-
Epoxy_FQ-POSS- 5	Firequench 1286	5	-	-
Epoxy_APP-5	APP	5	-	-
Epoxy_APP-4.5_CNT-0.5	APP	4.5	CNTs	0.5
Epoxy_APP-4_OMPOSS-1	APP	4	OMPOSS	1

II.2. CARBON NANOTUBES CHARACTERIZATION

In this section, the different techniques used for checking the existence of covalent links between CNTs and the organic functions are presented.

II.2.1. Infrared spectroscopy

FTIR spectra were recorded between 500 and 4000 cm^{-1} on Nicolet impact 400D spectrometer in KBr pellets. The final spectra resulted from 64 scans and were processed by OMNIC software with a resolution of 4 cm^{-1}.

II.2.2. Liquid-state Nuclear Magnetic Resonance

^{1}H and ^{13}C NMR spectra were recorded on an Avance 300 Bruker with deuterated $CDCl_3$ (≥ 99.8 %, Eurisotop) as solvent. 64 scans were necessary for achieving of a correct signal/noise ratio. Because of the limited solubility of CNTs, ^{1}H spectra for CNT-COOH and CNT-POSS were obtained from a suspension in CDCl3 and the number of scans was increased up to 512.

In order to assign the numerous peaks obtained by monodimensional ^{1}H NMR on POSS, monodimensional ^{13}C and bidimensional ^{1}H-^{13}C sequences were used. The monodimensional sequences were Attached Proton Test (APT) and Distortionless Enhancement by Polarization Transfer (DEPT) whereas the bidimensional sequence was Heteronuclear Multiple Quantum Coherence (HMQC, 32 scans).

II.2.3. X-ray photoelectron spectroscopy

The XPS experiments were carried out in an ultra-high vacuum KRATOS Axis Ultra spectrometer using the monochromatized Al Kα (1486.6 eV) source. A constant analyzer pass energy of 40 eV was used. Pressure was in the 10^{-10} Torr range during the analyses. Simulation of the experimental peaks was carried out using the Gaussian-Lorentzian mixture from CasaXPS software. Quantification took into account a linear background subtraction.

II.2.4. Thermogravimetric analysis

Thermogravimetric analyses (TGA) were carried out at a heating rate of 10 °C/min in synthetic air (flow rate: 50 mL/min, Air Liquide grade), using a Setaram TG 92 microbalance. The samples (5 mg) were placed in open vitreous silica pans. The precision of the temperature measurements was 1.5 °C over the whole range of temperature (20-800 °C).

II.3. EPOXY MORPHOLOGY AND GENERAL PROPERTIES

The previous chapter has shown that the general properties of epoxy resins have an effect on their reaction to fire. This section details the different techniques used for assessing morphology of filled resins as well as some of their general properties.

II.3.1. Scanning electron microscopy

Electron microscopy permits to observe very small objects thanks to a high energy electron beam. In the case of scanning electron microscopy (SEM), a thin electron beam scans the sample. The electrons interact with the atoms that make up the sample and produce signals that contain information about the sample surface topography and composition. Side resolutions of 3 to 10 nm and magnifications from 10 to 500 000 times are available with this type of microscope.

In this thesis, samples were analyzed with a Hitachi S4700 microscope. All samples were ultra microtomed at room temperature for surfacing. Secondary electron SEM images of composites were obtained at 6 kV, 10 µA .

II.3.2. Transmission electron microscopy

Another type of microscopy is transmission electron microscopy (TEM). In this technique, a beam of electrons is transmitted through an ultra-thin specimen, interacting with the specimen as it passes through. An image is formed from the interaction of the electrons transmitted through the specimen; the image is magnified and focused onto an imaging device, such as a fluorescent screen, on a layer of photographic film, or to be detected by a sensor such as a CCD camera.

The samples studied in this thesis were ultra microtomed with a diamond knife on a Leica ultracut UCT microtome, at room temperature, to give sections with nominal thickness of 70 nm. Sections were transferred to Cu grids of 400 meshes. Bright-field TEM images of composites were obtained at 200 kV under low dose conditions with a FEI TECNAI 62 20 electron microscope, using a Gatan CCD camera. Low magnification images were taken at 17 000x and high-magnification images were taken at 80 000x.

II.3.3. Glass transition temperature

Differential scanning calorimetry is widely used for the characterization of polymers. It lets investigate different properties such as glass transition, crystallinity or melting temperatures. In order to investigate the influence of fillers on the glass transition temperature of the studied epoxy samples, a Q100 DSC from TA Instruments was used. The analysis was divided in 2 cycles: the first one removes the thermal history of the material and the second one is aimed at measuring the glass transition temperature (Figure 52). The samples were heated between -50 °C and 200 °C at 20 °C/min under a 50 mL/min nitrogen flow. The thermal program is detailed in Figure 52. The samples (5 mg) are enclosed in aluminum pans. The error margins for calculated glass transition temperatures lie around 4 °C.

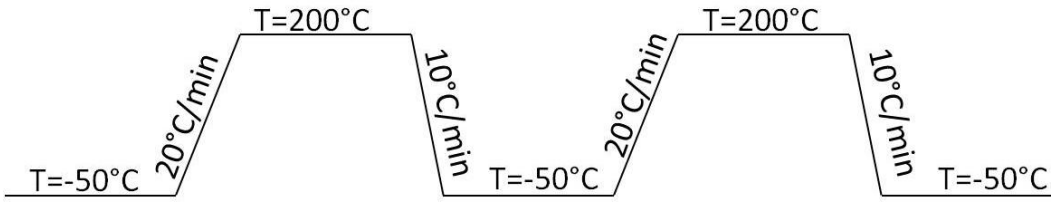

Figure 52: Thermal cycle for DSC analysis

II.3.4. Infrared spectroscopy

Infrared spectra were recorded between 500 and 4000 cm^{-1} on a Nicolet 400D spectrometer equipped with an mono-reflexion ATR unit (Dura SamplIR II, SensIR, diamond crystal). In order to minimize the signal/background ratio, spectra result from 32 scans with a 4 cm^{-1} resolution. Omnic software was used for the processing of the interferograms and the spectra. For the study of kinetics of curing, the aforementioned spectrometer was equipped with a heating ATR unit (GladiATR, Pike Technologies).

II.3.5. Thermal conductivity

The thermal conductivity of nanocomposites was measured by a Hot Disk thermal analyzer (TPS2500, Sweden), which was based upon the transient plane source method. This apparatus was equipped with a heating furnace controlled by the Hot Disk software (Figure 53). The dimension of bulk specimens is 20 x15 ×4 mm^3 with the sensor placed between two similar plates of materials. The sensor supplied a heat pulse between

0.01 W and 0.04 W for 40 to 160 s to the sample (depending on the sample) and recorded relevant temperature.

Figure 53: Furnace (left) and sample holder (right) of TPS2500

II.3.6. Thermal stability

Thermogravimetric analyses (TGA) were carried out at a heating rate of 10 °C/min in synthetic air (flow rate: 50 mL/min, Air Liquide grade), using a Setaram TG 92 microbalance. The samples were ground in liquid nitrogen in an ultra-centrifuge mill to produce a powder (500 µm as average particle size). The samples (10 mg) were placed in open vitreous silica pans (covered with gold in order to avoid reactions between pans and APP and/or its degradation products). The precision of the temperature measurements was 1.5 °C over the whole range of temperature (20-800 °C).

Interactions between the compounds of a formulation can be revealed by comparing the experimental TG curve with a "calculated" TG curve (W_{calc}) obtained by linear combination of the TG curves of the formulation ingredients weighted by their contents.

where x_i is the content of compound i and *Wi* is TG curve of the compound *i.*

The ΔW curve is calculated by subtracting the calculated curve from the experimental curve. Every positive interaction (stabilization of the system compared to the theoretical value) is then shown by a positive value of the curve (ΔW>0) and every negative interaction (destabilization) by a negative value of the curve (ΔW<0).

II.4. REACTION TO FIRE AND THERMAL DEGRADATION

II.4.1. Reaction to fire

II.4.1.a. Mass-loss calorimetry

The Fire Testing Technology Mass Loss Calorimeter was used to perform measurements (reaction to fire) on samples following the procedure defined in ASTM E 906. A schematic representation of the mass loss calorimeter is given in Figure 54. Our procedure involved exposing specimens having a disk shape with a 77 mm diameter and a 5 mm or 2.5 mm thickness in horizontal orientation. Specimens were wrapped in aluminum foil leaving the upper surface exposed to the heater and placed on a ceramic backing board at a distance of 25 mm from cone base (or 35 mm when the expansion is measured). External heat flux of 35 or 50 kW/m² was used for running the experiments. This flux corresponds to common heat flux in a mild fire scenario. Heat release rate (HRR) is measured as a function of time and it is reproducible to within 10 %. Minimum three tests were carried out on each material.

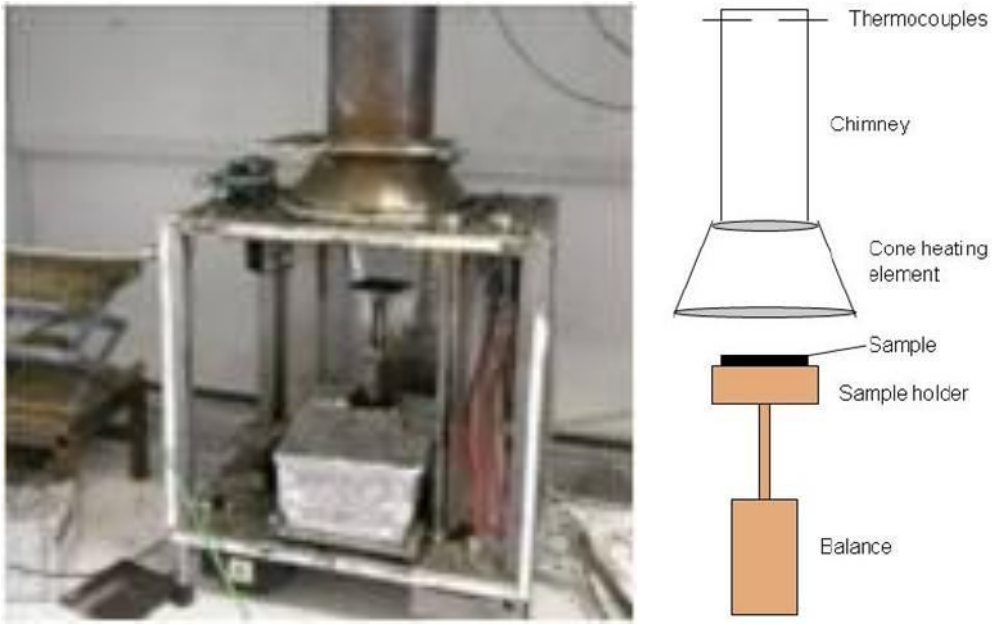

Figure 54: Mass-loss calorimeter picture

II.4.1.b. Pyrolysis Flow Combustion Calorimetry

The fire-retardant capability for limiting the release of combustible products was evaluated with a pyrolysis combustion flow calorimeter (PCFC) supplied by Fire Testing

Technology Ltd. Samples about 5mg were placed in open alumina pans and were degraded in a nitrogen atmosphere at a heating rate of 1 °C/s and a nitrogen flow of 80 cc/min. The decomposition gases were then burnt in a nitrogen/oxygen mixture (80 cc/min and 20 cc/min respectively) and the heat release rate was recorded as a function of temperature. No measurement of the mass as a function of time is available with this device. Nevertheless, pans were weighted before and after the experiment on a separate microscale. However, the weights were so small (less than 1 mg) that the differences were not considered as relevant.

II.4.2. Thermal degradation

II.4.2.a. Thermogravimetric analysis

TGA were carried out at 10 °C/min under synthetic air (flow rate: 50 mL/min, Air Liquide grade), using a Setaram TG 92 microbalance. The composite samples were ground in liquid nitrogen in an ultra-centrifuge mill to produce a powder (500 µm). The samples were placed in open vitreous silica pans. The precision of the temperature measurements was 1.5 °C over the whole range of temperature (20-800°C).

II.4.2.b. Viscosity measurement

Visco-elastic measurements were carried out in order to evaluate the rheological behavior of the system when the temperature increases. The formation of an effective char occurs via a semi-liquid phase, which coincides with gas formation and expansion of the surface. Gases released from the degradation of the intumescent material, and in particular of the blowing agent, have to be trapped and to diffuse slowly in the highly viscous melt degraded material in order to create a layer with appropriate morphological properties as shown in Figure 55.

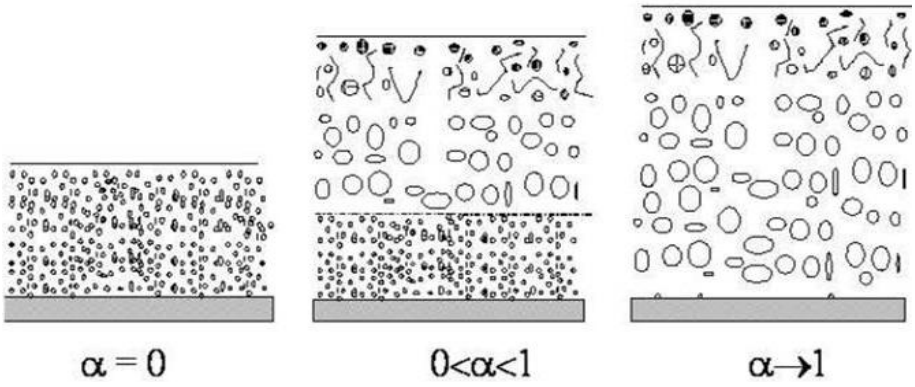

Figure 55: Development of intumescence (α= conversion degree)

If the degraded matrix has too low a viscosity, easy diffusion of gases takes place and the gases will not be trapped but rather escape to feed the flame. If the viscosity is too high, there can be formation of some cracks which allow the oxygen to diffuse into the char and thus decrease the efficiency of the protective layer. The viscosity of the degraded matrix in the blowing phase is, as a consequence, a critical factor [119, 120].

The rheological studies are based on the use of Thermal Scanning rheometer TSR Rheometric Scientific ARES-20A, in a parallel plate configuration. This apparatus allows an original approach of the study of the physical behavior of an intumescent coating as both the apparent viscosity and the swelling can be simultaneously measured as a function of temperature and/or time.

In order to measure the viscosity and the expansion, sample pellets (thickness = 1 mm) are positioned between the two plates (Figure 56).

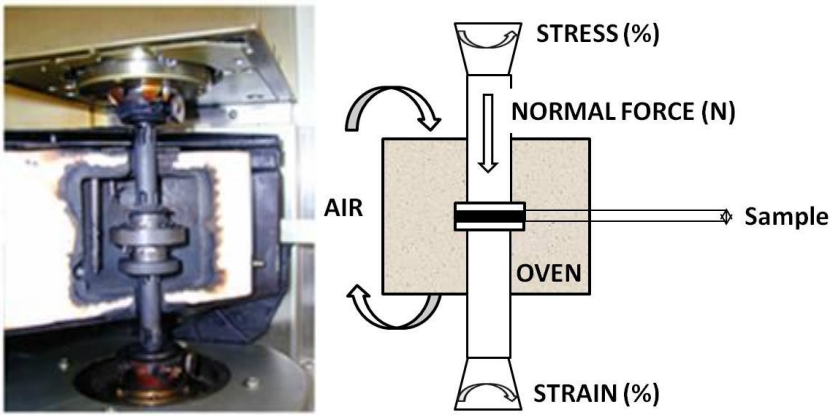

Figure 56 : Dynamic visco-elastic measurements in a parallel-plate rheometer (left: picture, right: schematic)

Testing is carried out using a "Dynamic Temperature Ramp Test" with a heating rate of 10 °C/min in the range 25-500 °C, a strain of 1 % and a constant normal force of 100 N (200 Pa). This test leads to the apparent complex viscosity values (used as measurements about the abilities of the systems to expand). It is important to point out that only an apparent viscosity measurement is carried out (depending on the testing conditions) and that these results should be used only for comparison between the samples.

II.4.2.c. Solid-state NMR

Solid-state NMR is a powerful tool for determining the configuration of given nuclei. Because of the low-abundance of some nuclei, the radiofrequency pulse is poorly absorbed in some cases. In order to overcome this limitation, protons of the sample can be excited and a dedicated sequence called "cross-polarization" permits to transfer this energy to atoms of lower abundance.

Cross-polarization (CP) leads to a large enhancement of the excitation of the nuclei. However, the large number of protons in the sample interferes with the decay of the isolated nuclei due to weak interactions of the spins. This results in a broadening of the signal. This drawback can be ignored by the use of a "^{1}H-dipolar decoupling": a strong radio frequency signal holds the protons in a highly resonating state so that they are not able the absorb resonance from the nuclei.

Finally, in solid-state, existence of chemical shift anisotropy has a strong effect on the spectra: peaks are broadened. Through a tensoral analysis of the magnetic moments in a molecule, it is possible to demonstrate that a "Magic angle" exists. When spinning at this angle, there is minimization of the broadening.

^{31}P NMR analyses are carried out on a Bruker Avance II 400 spectrometer with a 4mm probe. The Larmor frequency is 40.5 MHz (9.4 T). Measurements are performed with ^{1}H dipolar decoupling at 10 kHz in MAS (Magic Angle Spinning) conditions. Between the scans, a 120 s delay was used: this value is a compromise between the time needed for relaxing nuclei and the reasonable duration of the test. Phosphoric acid (H_3PO_4) in aqueous solution (85 %) was used as a reference.

^{29}Si NMR analyses are carried out on the same spectrometer equipped with a 7 mm probe. Measurements are performed with cross-polarization and ^{1}H dipolar decoupling

at 5 kHz in MAS conditions. Contact time was set at 6s and the delay between scans was 5 s. Tetramethylsilane ($Si(CH_3)_4$) was used as a reference.

^{13}C NMR analyses are carried out on the same spectrometer as above and equipped with a 4 mm probe. Measurements are performed with cross-polarization and ^{1}H dipolar decoupling at 10 kHz or 12.5 kHz in MAS conditions. Contact time was set at 1 s and the delay between scans was 5 s. Tetramethylsilane ($Si(CH_3)_4$) was used as a reference.

II.4.2.d. X-ray diffraction

XRD spectra were recorded in the 10°–80° 2θ range using a Bruker AXS D8 diffractometer ($\lambda_{(Cu\ K\alpha)}$ = 1,5418 Å, 40 keV, 25 mA) in configuration 2θ/θ. The acquisition parameters were as follows: a step of 0.02°, a step time of 2 s. The data are analyzed using the diffraction patterns of inorganic crystal structure database (ICSD)[121].

II.4.2.e. Temperature measurement

Intumescent samples are characterized by the formation of an insulating layer that forms on top of the sample during their burning. During mass-loss calorimeter experiments, K-type thermocouples were inserted in the samples at three different locations (Figure 57). This setting permits to evaluate the temperature gradients in the burning polymer.

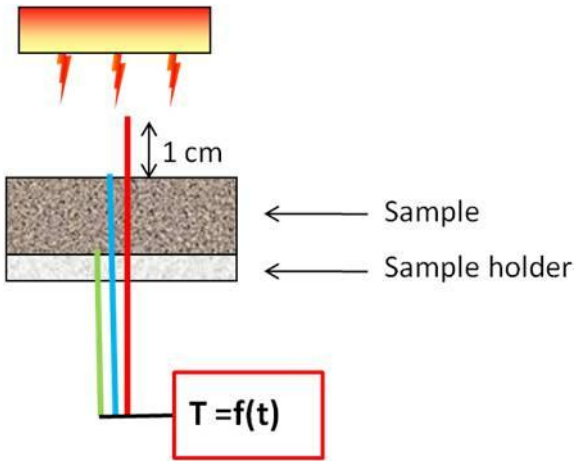

Figure 57: Temperature measurement setting

II.4.2.f. Swelling

In order to measure the swelling of intumescent samples during mass-loss calorimetry and link it to other parameters, the development of the char was monitored

by an infrared camera (Figure 58). The obtained imaged were then processed via an image analysis software and the relative swelling was calculated.

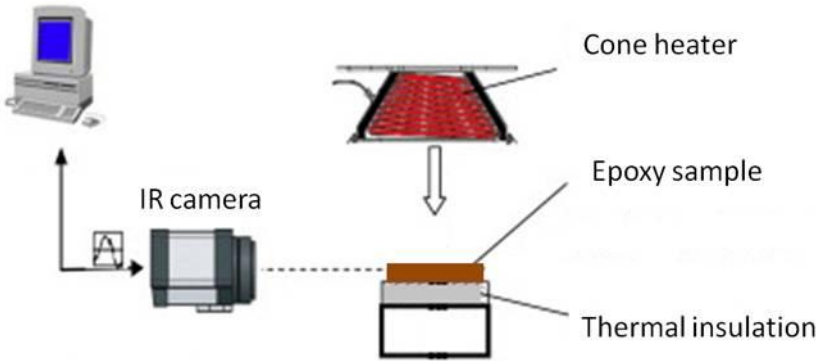

Figure 58 : Experimental set-up for measuring the swelling during a mass loss experiment using infrared camera

Although no information about temperature will be investigated (the surface emissivity of the sample during burning is not known), the use of infrared camera provides some benefits. Indeed the infrared camera allows to get clear images with a greater contrast to make image analysis than traditional camera. Typical infrared images at the beginning of the experiment, when ignition occurs, and at the maximum of expansion of the intumescent sample are shown in Figure 59.

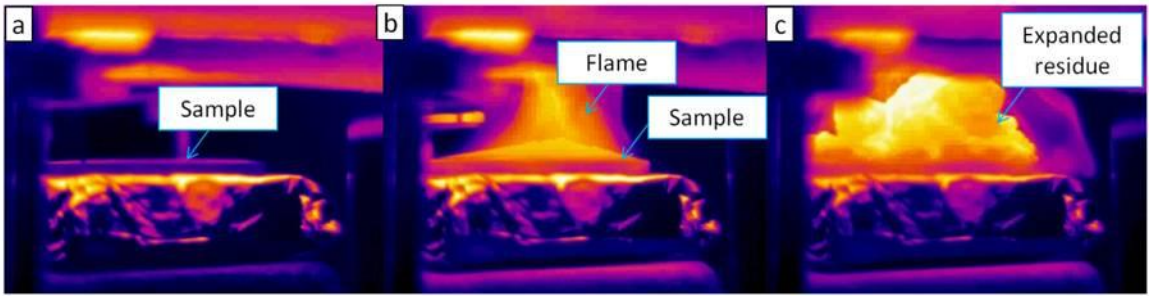

Figure 59 : IR images of an intumescent epoxy before ignition (a), at $t_{ignition}$ (b) and at the maximum of expansion (c)

II.4.2.g. Electron probe micro-analysis

Electron probe microanalysis (EPMA) is an analytical technique that is used to establish the composition of small areas on specimens. EPMA is one of several particle-beam techniques. A beam of accelerated electrons is focused on the surface of a specimen using a series of electromagnetic lenses, and these energetic electrons produce characteristic X-rays within a small volume (typically 1 to 9 cubic microns) of the specimen. The characteristic X-rays are detected at particular wavelengths, and their

intensities are measured to determine concentrations. All elements (except H, He, and Li) can be detected because each element has a specific set of X-rays that it emits. This analytical technique has a high spatial resolution and sensitivity. Additionally, the electron microprobe be used as a scanning electron microscope and obtain highly magnified secondary- and backscattered-electron images of a sample.

In this thesis, the samples were characterized with a Cameca SX100 electron probe micro analyzer with four wavelength dispersive X-ray spectrometers (WDS), which allows the performance of microscopic and elemental analyses.

Previously to the EPMA study, the sample was carbon coated with a Bal-Tec SCD005 sputter coater. Back scattered electrons (BSE) images were obtained at 15 kV, 10 nA. Si X-ray profile was carried out at 15 kV, 15 nA. A TAP (Thallium acid phthalate, $C_8H_5O_4Tl$) crystal was used to detect the Si Kα X-ray.

II.4.2.h. Digital microscopy

Digital microscopes are a variation of a traditional optical microscope that uses optics and a charge-coupled device (CCD) camera to output a digital image to a monitor. In our case, the microscope enables to get a clear view of residues obtained after burning thanks to the high depth of field. Images of chars were taken with a VHX-1000 microscope (Keyence) at 30x magnifications and stitch together in order to get a clear image of the whole char.

II.5. CONCLUSION

In this chapter, experimental techniques used in the preparation and the characterization of the reaction to fire of flame-retarded epoxy resins were described. Details about the methodologies developed in the next chapters for understanding the mechanisms of the modified reaction to fire of some resins were also given.

The synthesis of modified carbon nanotubes as well as the preparation methods for epoxy bulk materials was described. The techniques used for the characterization of these materials are then presented. Practical description of the evaluation of flame retardancy was conducted and the various methods used for the elucidation of the fire protection mechanisms were detailed. The next chapter investigates the potential of different nanoparticles as flame-retardants in a model epoxy resin.

Chapter III - How nanoparticles modify the reaction to fire of epoxies

The first chapter of this thesis has established the wide range of nanoparticles which have shown a flame retardant effect in various polymers. It was should also be noticed that only few references concerned epoxy matrices. However, promising results published by Franchini et al. [67] have shown that POSS may enhance the performances of epoxy tested by cone-calorimetry. They evaluated three types of POSS: octaphenylPOSS, glycidoxypropylheptaphenylPOSS and glycidoxypropylheptaisobutyl-POSS (Chapter I, p.76). Although epoxy groups of the two last POSS may react with the amine hardener during sample preparation and have therefore a stronger interaction with the matrix, the fire performances were not greatly affected by this parameter. On the contrary, the best results were obtained with POSS bearing phenyl groups, which are considered as char promoter. Furthermore, the interest of CNTs as flame retardant has been proven in thermoplastics [83, 122-124] but the occurrences in epoxy resins are associated to non-conventional cases: modification of CNTs and incorporation in the matrix via sol-gel method [84] or cone-calorimetry testing in an inert atmosphere [85]. All these results suggested investigating more precisely the potential of POSS and CNTs as flame retardants in epoxy resins.

This chapter is divided into two main sections: the evaluation of commercial nanofillers as flame retardants will be followed by that of functionalized carbon nanotubes. First, CNTs and different POSS will be incorporated in an epoxy resin and the reaction to fire of the obtained materials will be tested by mass-loss calorimetry. Then, in order to further enhance the fire performances, CNTs will be functionalized by two different potentially flame-retardant moieties. The first one contains a melamine cycle whereas the second one is based on a POSS moiety. The characterization of the functionalization will be carried out by means of various analytical techniques (TGA, FTIR, XPS and NMR). Then, the reaction to fire of the filled resin will be assessed. In each case, the morphology of the resin and the dispersion state of the fillers will be characterized. Finally, conclusions on the potential of the studied nanoparticles as flame-retardant in epoxies as single fillers will be drawn.

III.1. EPOXY FILLED WITH COMMERCIAL NANOPARTICLES

In this part, different commercial nanoparticles will be incorporated in the epoxy resin. Four types of POSS have been selected in order to investigate the effects of the nature of organic moieties at their corners. AminopropylisobutylPOSS and trisilanolphenylPOSS (Chapter II, p.97) may react with epoxy groups of the prepolymer before curing and would therefore reinforce the interaction between the fillers and the matrix. This could also favor a better dispersion of these particles in the epoxy. Since a sufficient level of dispersion can be needed in order to fully develop flame-retardant properties, this possibility has been especially valued. OctamethylPOSS (OMPOSS) have also been incorporated in our epoxy system. Contrary to the two previously selected POSS, these POSS should not react with the matrix during curing. Furthermore, Vannier et al.[3] have established their positive effect on the reaction to fire of polyethylene terephtalate. FQ-POSS (poly(vinylsilsesquioxane))have also been tested and consist of an incomplete POSS cage. Incorporation of 10 wt.% FQ-POSS in thermoplastic polyurethane has revealed a strong reduction of the peak of heat release rate (-80 %) [125]. Considering that the flame retardancy of epoxy containing CNTs is not widely described in the literature, unmodified CNTs were also incorporated in this matrix.

Once identified which particles to use in our epoxy, the loading issue has been addressed. Indeed, one of the aims of the incorporation of nanoparticles in polymers is the reduction of the total amount of fillers (more details p. 64). In order to choose the best loading, results from the literature were analyzed. Zammarano et al.[57] incorporated layered double hydroxides at 5 wt.% in epoxy. Epoxy/POSS samples from Franchini et al.[67] contained 3.4-3.9 wt.% POSS up to 8.3-9.5 wt.% (corresponding respectively to 1.5 wt.% or 3.7 wt.% inorganic content depending on the POSS). Therefore, based on these literature results, the different POSS were incorporated at 5 wt.% in the epoxy. The loading is much lower for CNTs, as they dramatically enhance the viscosity of the uncured resin and therefore, its processability. Reports concerning epoxy/CNT composites generally consider contents below 1.5 wt.% [76, 126-128]. In this study, epoxy containing 0.5 wt.% CNTs will be tested.

Before the evaluation of the reaction to fire of epoxies filled with nanoparticles, the morphology as well as the thermal properties will be characterized, since they might influence the flammability of the composites.

III.1.1. Composites morphology and thermal properties

III.1.1.a. Dispersion state of nanoparticles

Before any investigation of the fire performances, the general aspect and the dispersion state of the formulations should be investigated [49]. Figure 60 shows the macroscopical aspect of the samples before burning. Whereas Virgin epoxy is completely transparent with small bubbles (Figure 61a), aminopropylisobutylPOSS, FQ-POSS and OMPOSS lead to opaque white epoxy samples. On the contrary, the sample containing trisilanolphenylPOSS is almost transparent, with only small white aggregates (Figure 61c). Therefore, the dispersion state seems better for this last POSS. Indeed, the presence of several reactive silanol moieties could enhance the compatibility between the particles and the matrix. It can also be attributed to the presence of phenyl groups, which should have good affinity for the benzene-rings of the DGEBA resin. Finally, the incorporation of only 0.5 wt.% CNTs produces a black sample.

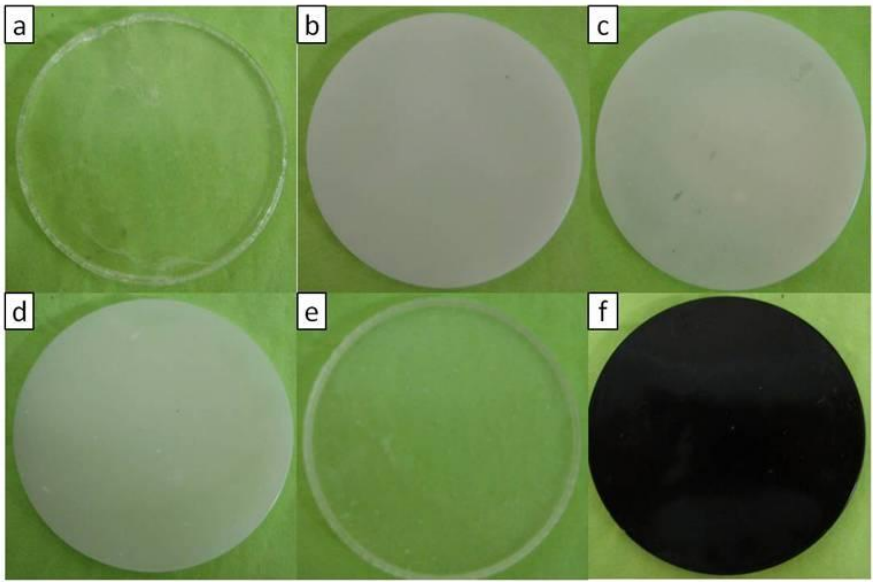

Figure 60: Pictures of epoxy formulations before test (a: Virgin epoxy, b: Epoxy_aminopropylisobutylPOSS-5, c: Epoxy_FQ-POSS-5, d: Epoxy_OMPOSS-5, e:, Epoxy_trisilanolphenylPOSS-5 f: Epoxy _CNT-0.5)

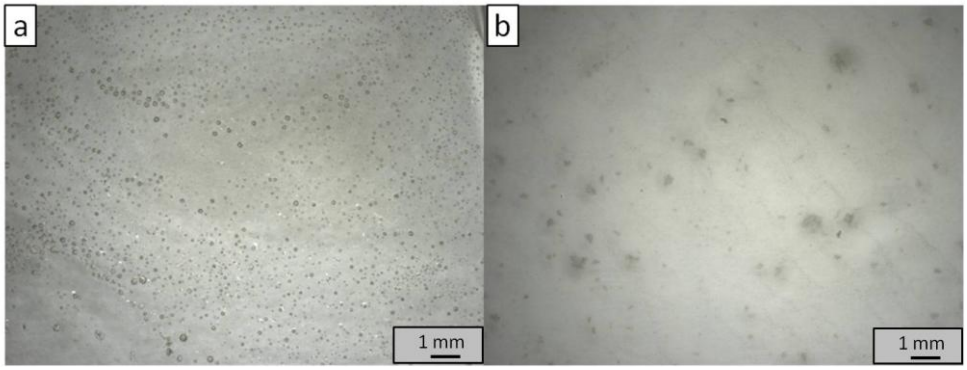

Figure 61: Optical microscopy images of Virgin epoxy (a) and Epoxy_trisilanolphenylPOSS-5 (b)

A closer look into the dispersion of nanoparticles in the epoxy matrix was achieved by SEM and TEM.

SEM reveals that aminopropylisobutylPOSS is very inhomogeneously dispersed in the matrix (Figure 62). Furthermore, the size of agglomerates as high as 20 µm reinforces the conclusion that this kind of POSS is not correctly dispersed.

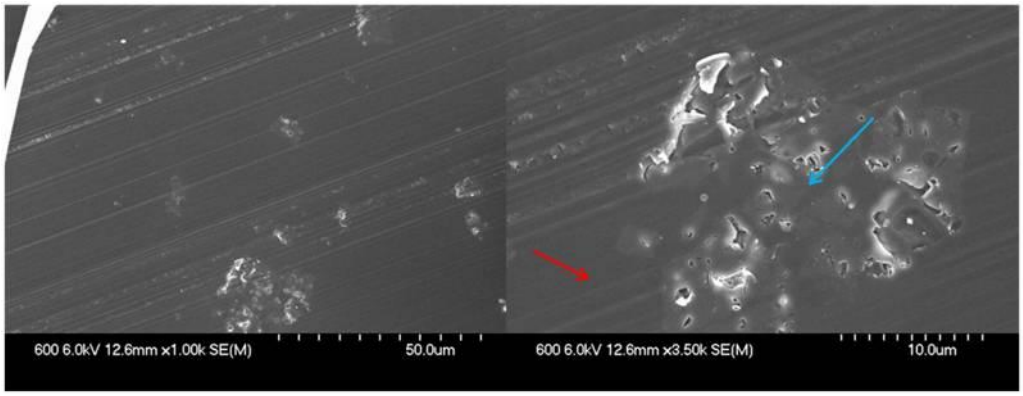

Figure 62: SEM pictures of Epoxy_aminopropylisobutylPOSS-5

The areas identified on Figure 62 (blue and red arrows) were analyzed by Electron-Probe Micro-Analysis in order to clear any doubt on the nature of these aggregates. It was confirmed that they are made of POSS (Figure 63a). Carbon, oxygen and silicon are detected in the aggregates whereas only carbon and oxygen are present in the neighbor matrix (Figure 63b).

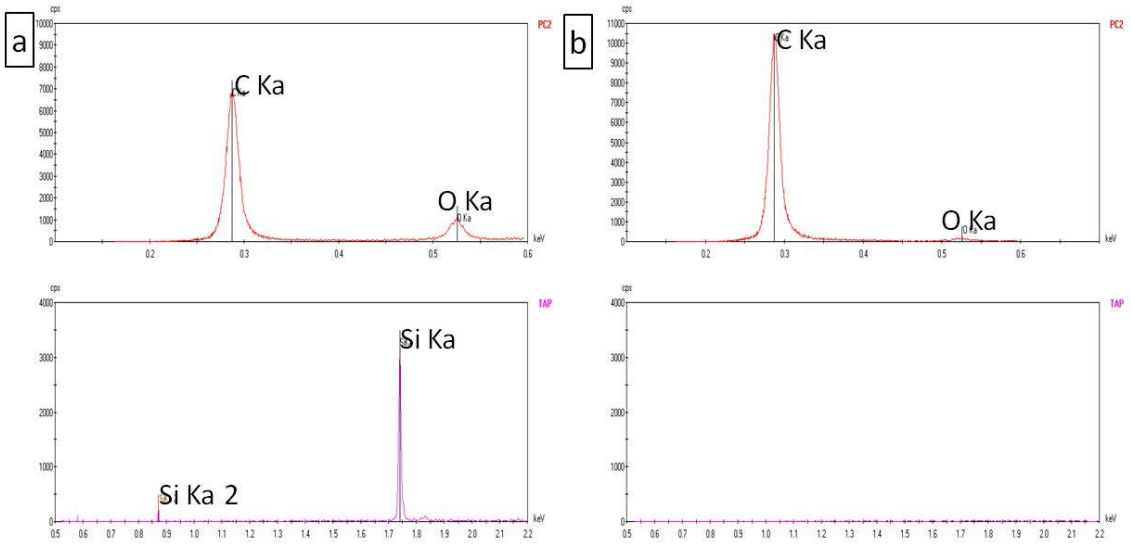

Figure 63: C, O and Si spectra of aggregates (a) and matrix (b) in Epoxy_aminopropylisobutylPOSS-5. The analyzed areas are shown on Figure 62.

Then, Epoxy_trisilanolphenylPOSS-5 formulation was studied (Figure 64). This type of POSS appears as very small black dots regularly dispersed in the epoxy matrix. These POSS are therefore well-distributed in the matrix.

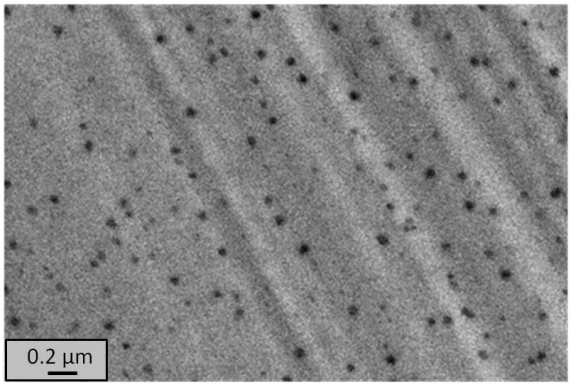

Figure 64: TEM pictures of Epoxy_trisilanolphenylPOSS-5

FQ-POSS do not provide such a good dispersion (Figure 65). In fact, big aggregates are observed in some areas and other areas are totally empty. A closer look to these structures shows tightly entangled round-shaped particles.

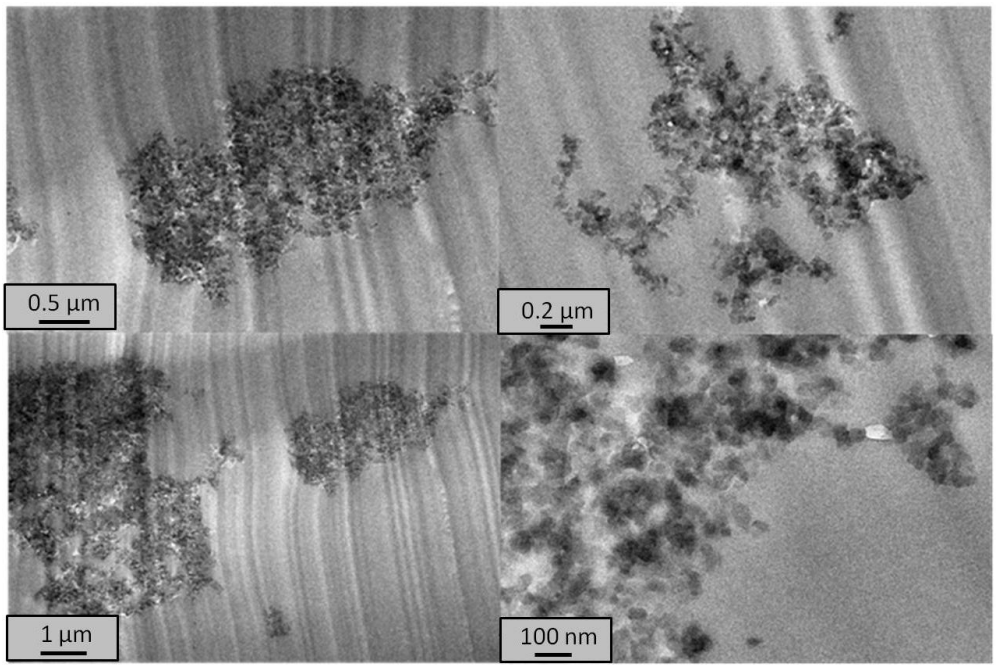

Figure 65: TEM pictures of Epoxy_FQ-POSS-5

The sample containing 5 wt.% OMPOSS reveals that POSS appear as small rods, some of them being individualized (Figure 66). However, the quantity of POSS observed by TEM seems low compared to the theoretical content. It is because of the existence of big aggregates by SEM giving a vision of the whole sample (Figure 67).

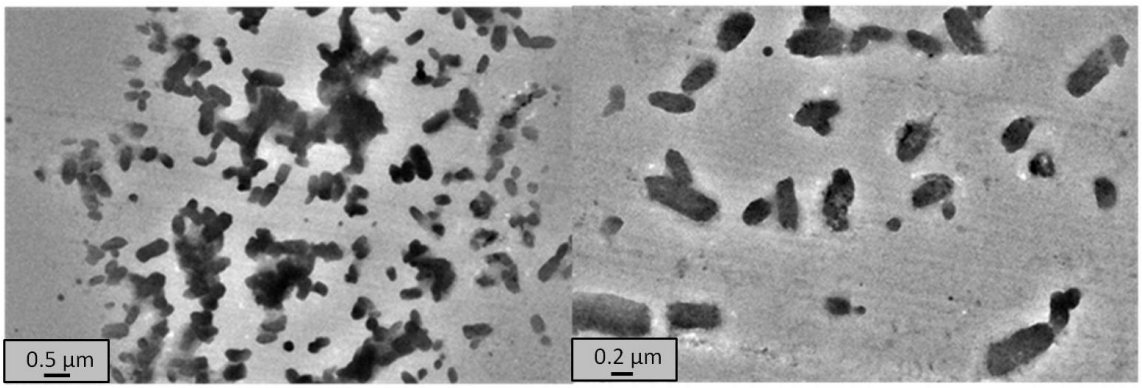

Figure 66: TEM pictures of Epoxy_OMPOSS-5

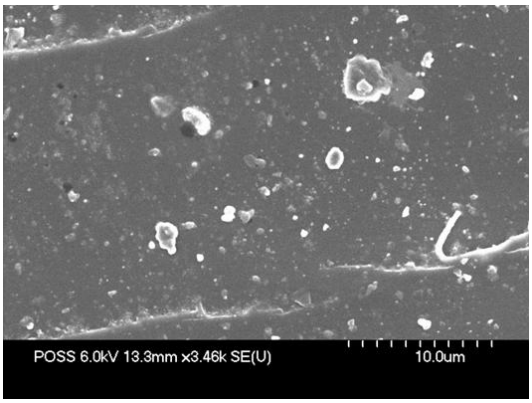

Figure 67: SEM picture of Epoxy_OMPOSS-5

Finally, the dispersion of CNTs in the epoxy matrix was evaluated by TEM (Figure 68). Even if CNTs are not as tightly entangled as some examples in the literature, the dispersion is not homogeneous. Figure 68a shows an area with a high CNTs density, whereas Figure 68c comprises individualized CNTs, but in low quantity. An intermediate concentration is present on Figure 68b. Finally, Figure 68d reveals the presence of big CNTs aggregates.

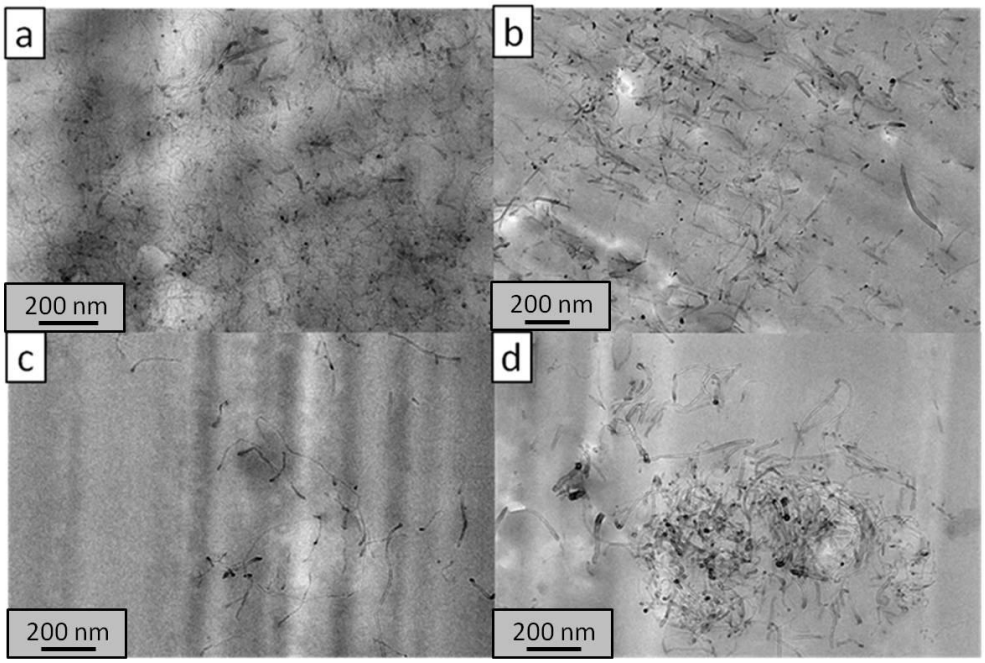

Figure 68: TEM pictures of Epoxy _CNT-0.5

A first conclusion on the dispersion state of particles in the epoxy matrix can be drawn. The dispersion level differs between samples, a constant fact being the absence of a homogeneous dispersion. Most samples are divided into areas having a high nanoparticles concentration and others with fewer particles. This suggests a limited

compatibility between the matrix and the fillers. This problem may be overcome by optimization of dispersion process. This issue is frequently repeated in the literature [74, 129]. However, in the frame of the LAYSA project, it was required to keep a simple process since three functionalities should be combined in the end, each of them with its specificities. The current section therefore evaluates the potential of the different nanofillers as flame retardants and does not optimize their utilization.

III.1.1.b. Determination of glass transition temperatures

Incorporation of fillers, and especially nanoparticles, often induce changes in the glass transition temperature (T_g). Indeed, the T_g of an epoxy network is linked to the crosslinking density ( ) through Di Benedetto's equation [130, 131] (Equation 1):

Equation 1: Di Benedetto's equation

where Tg_0 is the *Tg* of the system at the initial time , Tg_∞ is the *Tg* of the fully crosslinked network and λ is Tg_0/Tg. Any important variation of the crosslinking degree of the samples, and therefore the Tg, is to be known, as the reaction to fire may be modified [15].

The glass transition temperatures measured by DSC (Table 8) present small variations, but they remain limited. This is in accordance with the results of Ni et al. [132] and Liu et al. [133]. They have studied different Epoxy/POSS composites and showed that for contents below 40 wt.%, the Tg is close to that of Virgin epoxy. Concerning CNT-containing samples, different results coexist in the literature. Some references report an increase of the T_g, whereas others do not show any significant effect of CNTs on the T_g of the epoxy [134]. In fact, Allaoui et al. [135] analyzed these various results and concluded that MWNT should more likely increase the T_g or leave it unmodified. In our case, CNTs do not induce modifications on this parameter.

Table 8: Glass transition temperatures (T_g) of Epoxy/nanoparticles formulations

Formulation	T_g (°C)
Virgin epoxy	132
Epoxy_aminopropylisobutylPOSS-5	130
Epoxy_trisilanolphenylPOSS-5	131
Epoxy_FQ-POSS-5	131
Epoxy_OMPOSS-5	132
Epoxy _CNT-0.5	132

III.1.1.c. Crosslinking density

The extent of curing was further monitored by Fourier Transform Infrared Spectroscopy (FTIR). A characteristic spectrum is shown on Figure 69.

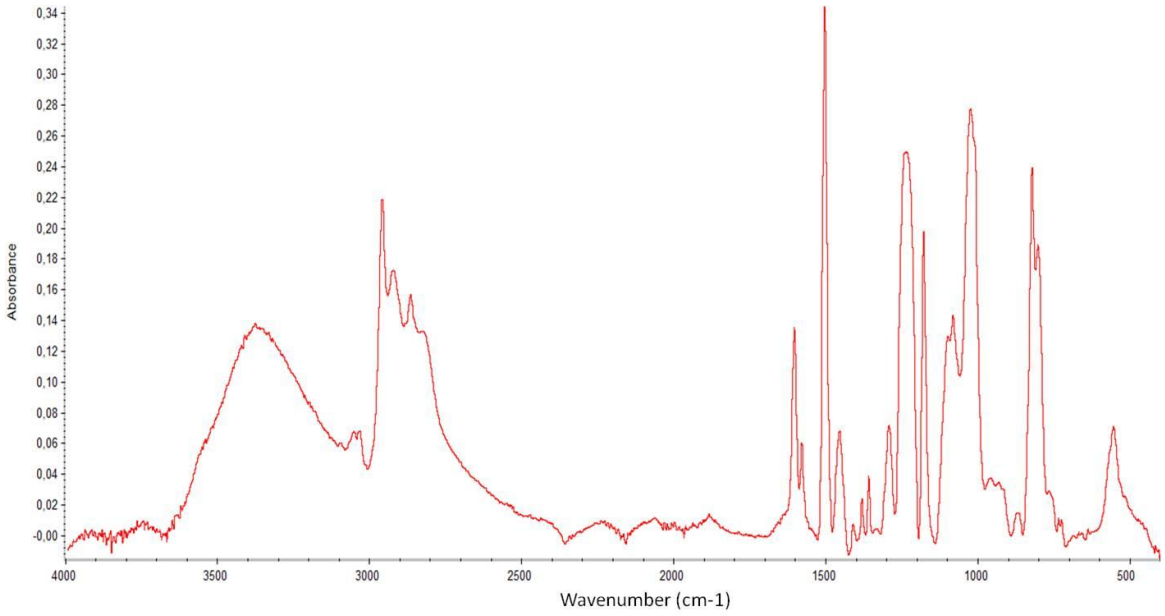

Figure 69: Infrared spectrum of Virgin epoxy

First, the unreacted mixture between the prepolymer and its hardener, as well as the final unfilled material, have been studied by Attenuated Total Reflectance (ATR) IR spectroscopy (Table 9).The peaks have been attributed according to literature [136, 137]. Bands between 3200 and 3400 cm^{-1} result from the stretching of amines. Then, bending of aliphatic carbons is observed between 2800 and 3100 cm^{-1}. The presence of aromatic rings is revealed by three bands between 1500 and 1610 cm^{-1}. Secondary alcohols resulting from the curing reaction are seen at 1257 cm^{-1}. Finally, 914 cm^{-1} is the characteristic resonance of unreacted epoxide ring.

Table 9: Infrared spectroscopy bands of epoxy systems (δ=bending ,ν= stretching, m=medium absorption, s= strong absorption)

Moiety	Prepolymer (cm^{-1})	Hardener (cm-1)	Cured resin (cm-1)
ν N-H (primary, then secondary amine after curing)		3352	3371
ν N-H (primary amine)		3275	
ν Csp2-H	3052		
ν Csp3-H	2964		2960
ν Csp3-H	2926	2923	2917
ν Csp3-H	2869		2856
ν Csp3-H		2847,2809	
ν Csp2- Csp2 (C=C aromatic ring)	1606		1605
δ N-H (primary amine)		1594	
ν Csp2- Csp2 (C=C aromatic ring)	1578		1580
ν Csp2- Csp2 (C=C aromatic ring)	1506 (s)		1506 (s)
δ Csp3-H	1454	1454	1457
δO-H (secondary alcohol)			1257 (s)
νC-O (aromatic ether Ph-O-)	1182		1179
νC-O(secondary alcohol)	1082		1083
valence C-C	1031 (s)		1018
δCsp2-H	970		
Epoxide ring	914 (m)		
δCsp2-H aromatic para-di-substituted	827(s)		820(s)

The spectra before and after curing were compared for different formulations in order to get the crosslinking density. The number of epoxide rings decreases during the curing and so does their absorption band. Bands remaining invariable during the curing, corresponding to linkages not taking part in the reaction, are used as quantitative reference in the analysis, here the C=C vibration in the benzene ring at 1506 cm^{-1} [138]. The variation in the absorbance of one of the reactive bands allows to quantify the progress of the reaction, having defined the conversion degree as in Equation 2.

$$\alpha=1-(A^*_t/A^*_0)$$

Equation 2: Conversion degree

where A^*_t is the reduced absorbance after some time and A^*_0 is the absorbance at the beginning of the curing process. These two values are corrected using a reference band. The method consists in dividing the absorbance of the reactive band by the

absorbance of an invariant band. This correction also avoids the effects of the variations in mass and thickness of the sample. The final relative error margins are estimated to 10 %.

Crosslinking densities of epoxy formulations are presented in Table 10. However, it could not be determined for some formulations (Epoxy_aminopropylisobutylPOSS-5 and Epoxy_trisilanolphenylPOSS-5), as there is overlapping between peaks of the resins and those of the filler. The other formulations have very similar crosslinking densities, which range from 72 % for Epoxy _CNT-0.5 to 83 % for Epoxy_OMPOSS-5. Taking into account that there are variations inside the samples itself (the curing process is initiated at the centre of the sample), the crosslinking densities are considered as similar for all these formulations.

Table 10: Crosslinking density of Epoxy/nanoparticles formulations

Formulation	Crosslinking density (%)
Virgin epoxy	81
Epoxy_aminopropylisobutylPOSS-5	-
Epoxy_trisilanolphenylPOSS-5	-
Epoxy_FQ-POSS 5	82
Epoxy_OMPOSS 5	83
Epoxy _CNT	72

III.1.1.d. Thermal stability

Assessing the thermal stability of polymers is useful for understanding the fire behavior of polymers even if the reaction to fire cannot simply be reduced to a better thermal behavior. Indeed, the thermal stability of materials has an influence on the reaction to fire of polymeric materials since they release fuels during their thermal degradation. If these combustible compounds are produced in suitable conditions, they may contribute to the fire development. Figure 70 and Table 11 show therefore the Thermogravimetric analysis results of epoxy formulations containing nanoparticles in thermo-oxidative conditions. Virgin epoxy degrades in two main apparent steps. A first one ranges from 200 to 430 °C with an transient residue of 40 wt.%, whereas the second one between 430 and 610 °C leads to the complete degradation of the resin (no residue is left). Regarding the samples containing different POSS, they all begin to degrade in the

same way, but their transient residues are completely different. All POSS-containing samples degrade faster than neat resin in the low temperature range (T<250 °C). Some of them have thereafter a slower decomposition with higher transient residue. The temperature at the maximum degradation rate is very similar for Virgin epoxy and Epoxy/aminopropylisobutylPOSS (343-345 °C). It is shifted towards higher temperature for Epoxy_FQ-POSS-5 (355 °C), Epoxy_trisilanolphenylPOSS-5 (377 °C) and Epoxy_OMPOSS-5 (390 °C). Concerning transient residues, the presence of aminopropylisobutylPOSS and FQ-POSS lead to residues of 56 and 50 wt.% respectively after the first degradation step. On the contrary, trisilanolphenylPOSS reach this transient residue (lower amount) at slightly higher temperatures, with a residue of 30 wt.%. Finally, OMPOSS has the lowest intermediate residue (24 wt.%). The second degradation step has the same shape for all POSS-containing formulations. Differences lie within the maximum degradation temperature associated to this step. Virgin epoxy, epoxy_aminopropylisobutylPOSS-5 and Epoxy_OMPOSS-5 degrade at similar temperatures (508-510 °C), whereas Epoxy_trisilanolphenylPOSS-5 and Epoxy_FQ-POSS-5 are stable at higher temperatures (540 °C). Finally, the sample containing CNTs presents a different behavior. The first degradation occurs at temperature similar to Virgin epoxy (338 °C), but the degradation is slower, leading to a much higher intermediate residue (65 wt.%). The last degradation temperature is similar to that of Virgin epoxy (508 °C). The final residues for all formulations are very similar, ranging from 1 to 5 wt.%. The higher residues are obtained with trisilanolphenylPOSS (3 wt.%) and FQ-POSS (5 wt.%).

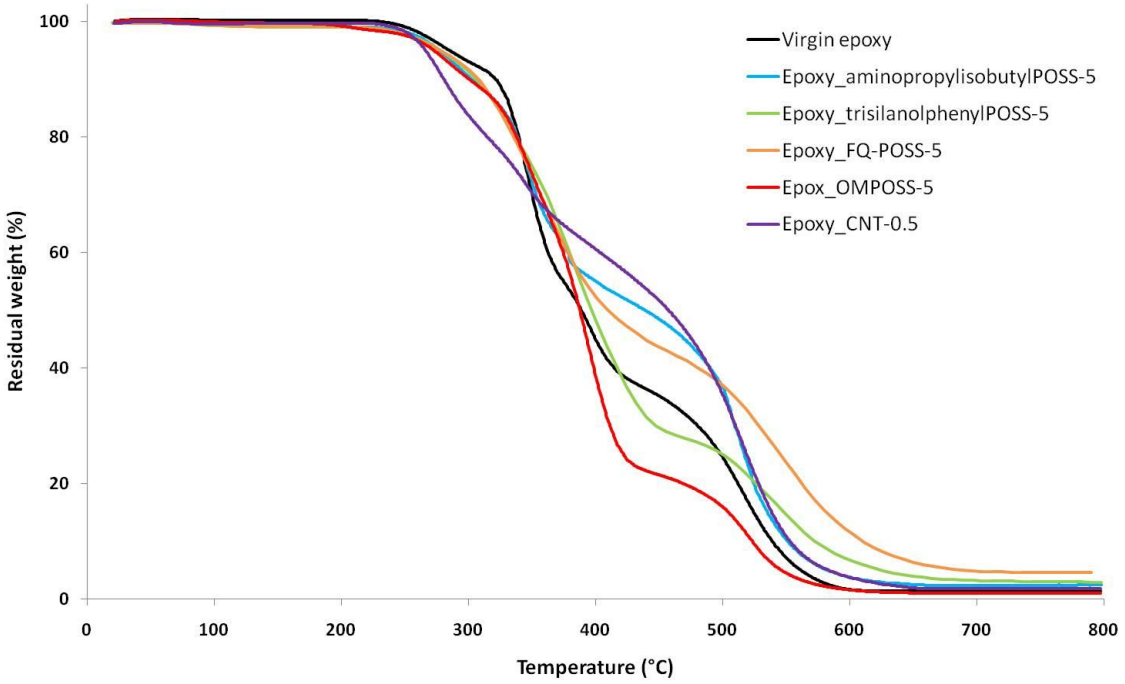

Figure 70: TGA curves of epoxy formulations containing nanoparticles in thermo-oxidative atmosphere (Air, 10°C/min)

Table 11: Main steps of the thermo-oxidative degradation of Epoxy/nanoparticles formulations

Formulation	Step 1 (°C)	Transient residue (wt.%)	Step 2 (°C)	Residue (wt.%)
Virgin epoxy	343	40	510	1
Epoxy_aminopropylisobutylPOSS-5	345	56	509	2
Epoxy_trisilanolphenylPOSS-5	377	30	540	3
Epoxy_FQ-POSS-5	355	50	540	5
Epoxy_OMPOSS-5	390	24	512	1
Epoxy _CNT-0.5	338	65	508	2

Figure 71 shows the weight difference curves of the different epoxy formulations containing nanoparticles (Chapter II, p.102), obtained by subtracting the calculated curve from the experimental one. With aminopropylisobutylPOSS, FQ-POSS and CNTs, there is a destabilization area beginning at 240-260 °C and ending at 350 °C, followed by a large stabilization. The maximum stabilization occurs around 415 °C for aminopropylisobutylPOSS and CNTs, corresponding to the end of the first degradation step, whereas it is shifted towards higher temperatures for FQ-POSS (530 °C). It seems therefore that a kind of highly stable residue is created between FQ-POSS and the epoxy

during the first degradation step. Concerning CNTs, the stabilization effect is counterbalanced by the destabilization at lower temperatures, which results in an earlier decomposition. TrisilanolphenylPOSS behaves slightly differently. Indeed, two stabilization areas (350-400 °C and 512-620 °C) coexist with two destabilizations areas (280-350 °C and 400-515 °C). Considering the temperatures at which they occur, it seems that at the beginning of each degradation step (300 and 500 °C respectively), the degradation is accelerated by the presence of POSS, but it results in a more stable structure, leading to the stabilization areas. Taking into account that the crosslinking degree is not different for this formulation compared to the other ones, we can suggest that the trisilanol moieties did not react with epoxide rings during curing. Therefore, during the thermal decomposition of the sample, silanols can still react with the degradation products of the resin and modify the thermal degradation. Finally, the sample containing OMPOSS is stabilized between 260 °C and 390 °C, corresponding to the beginning of the first degradation step. A large destabilization is recorded thereafter (390-600 °C).

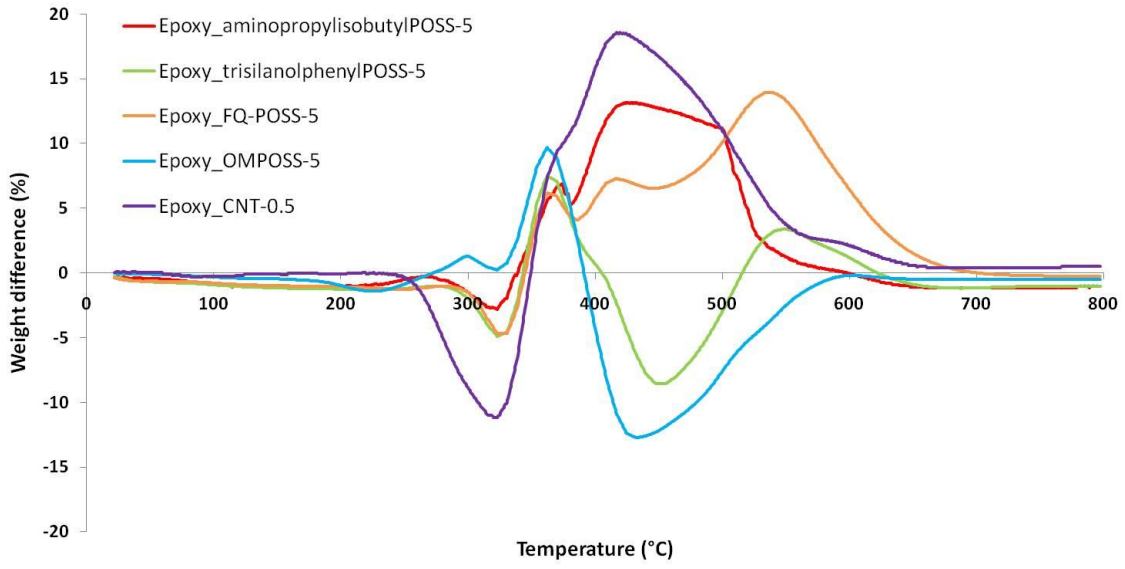

Figure 71: Weight difference curves of Epoxy/nanoparticle formulations (experimental-calculated)

The thermal stability of the composite containing POSS or CNTs has been characterized, as well as interactions between the fillers and the matrix. The presence of POSS in the polymer does not induce a reduction of thermal stability. Decomposition temperatures are similar, and differences lie in the intermediate residues. Weight difference curves show that the stabilization/destabilization interactions depend on the

type of POSS. Concerning CNTs, the onset of decomposition is slightly moved towards lower temperatures, but this leads to a higher intermediate residue.

III.1.2. Reaction to fire

The reaction to fire of the filled resins was assessed by mass-loss calorimetry (Figure 72 and Table 12).

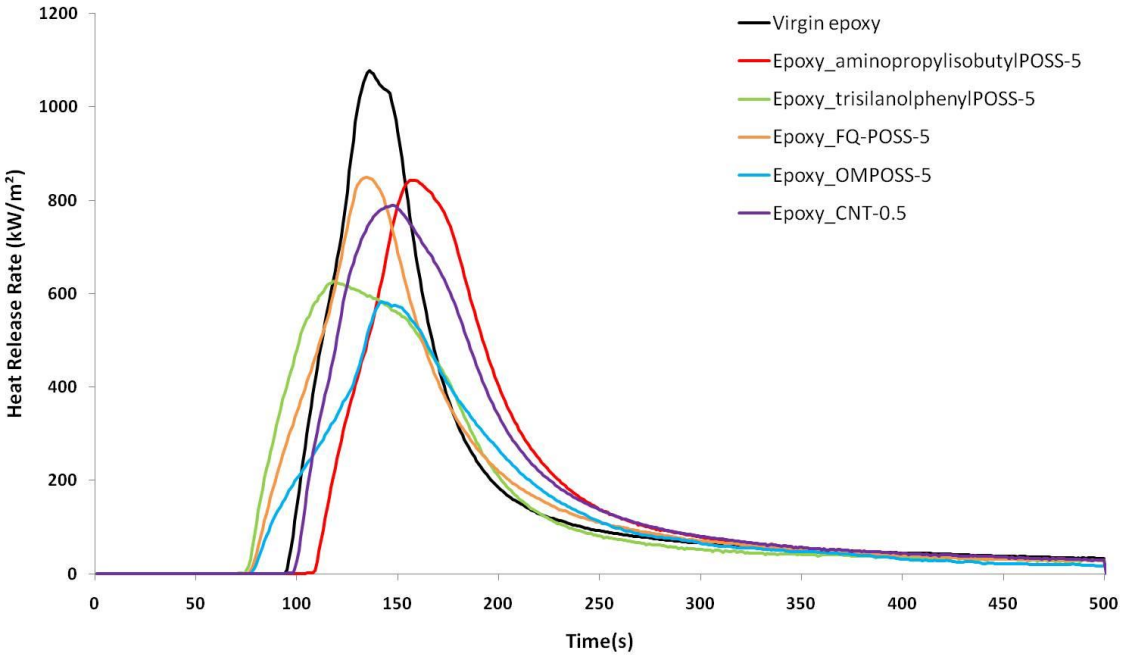

Figure 72: Heat release rate versus time for epoxy formulations containing nanoparticles (Heat flux: 35 kW/m², thickness: 5 mm, distance: 25 mm)

The different POSS tested have been chosen in order to evaluate the influence of different properties: presence of reactive groups (amine or silanol) or aromatic substituents (phenyl). Apart from the POSS bearing an amine group, all POSS decrease the time to ignition by 20-30 %. The thermal stability is not directly linked to the faster ignition. Another possibility is that because the materials are inhomogeneous, fillers act as defects. Indeed, inhomogeneities in the material induce mechanical stress that limits the resistance of the material under the heat flux. The sample containing CNTs ignites similarly to Virgin epoxy. The effects on the peak of Heat Release Rate (pHRR) are also studied. First, incorporation of the amine-bearing POSS at 5 wt.% decreases the pHRR by 22 %. In this case, the use of a reactive group does seem beneficial. The effect is stronger with trisilanolphenylPOSS, as the pHRR is decreased by 42 %. However, it is not clear if this advantage is due to the silanol moiety reacting with the epoxy ring or to the

phenyl groups at the corners of the POSS, which could promote charring. The conclusions by Franchini et al.[67] suggest that the latter is more probable. They obtained the strongest pHRR reduction with a POSS having an epoxide ring and phenyl groups at its corners. They also had an important reduction with octaphenylPOSS. On the contrary, they observed that the presence of an epoxide ring alone on the last POSS did not greatly reduce the pHRR. The fire-retardant effect of FQ-POSS is also limited (-21%). The best effect on pHRR is provided by OMPOSS (-46 %). The temperature corresponding to the maximum degradation rate in TGA seems to be linked to reduction of pHRR (coefficient of determination=0.94). Even if the first step is initiated at lower temperatures when POSS are used, the degradation rate during the first step has therefore an effect on the reduction of pHRR. On the contrary, the amount of intermediate residue and the characteristics of the second degradation step are not directly linked to the reaction to fire.

Concerning the incorporation of CNTs, a decrease of the pHRR is observed (-27 %), whereas the time to ignition remains almost unchanged. CNTs have therefore a flame-retardant effect in epoxy resins.

Table 12: Mass-loss calorimeter main parameters for Epoxy/nanoparticles formulations. The differences compared to virgin material are % set into brackets. (Heat flux: 35 kW/m², thickness: 5 mm, distance: 25 mm)

Formulation	t_{ign} (s) (% decrease)	pHRR (kW/m²) (% decrease)	THR (MJ/m²) (% decrease)
Virgin epoxy	94	1078	79
Epoxy_aminopropylisobutylPOSS-5	104 (+11)	843 (-22)	78 (-1)
Epoxy_trisilanolphenylPOSS-5	70 (-26)	627 (-42)	73 (-8)
Epoxy_FQ-POSS-5	74 (-21)	849 (-21)	78 (-1)
Epoxy_OMPOSS-5	67 (-29)	582 (-46)	63 (-20)
Epoxy _CNT-0.5	95 (+1)	789 (-27)	82 (+4)

The total heat released (THR) during a mass-loss calorimetry experiment is also an important parameter: it evaluates the amount of heat produced during the combustion of the sample. Figure 73 shows the total heat released as a function of time for epoxy formulations containing nanoparticles.

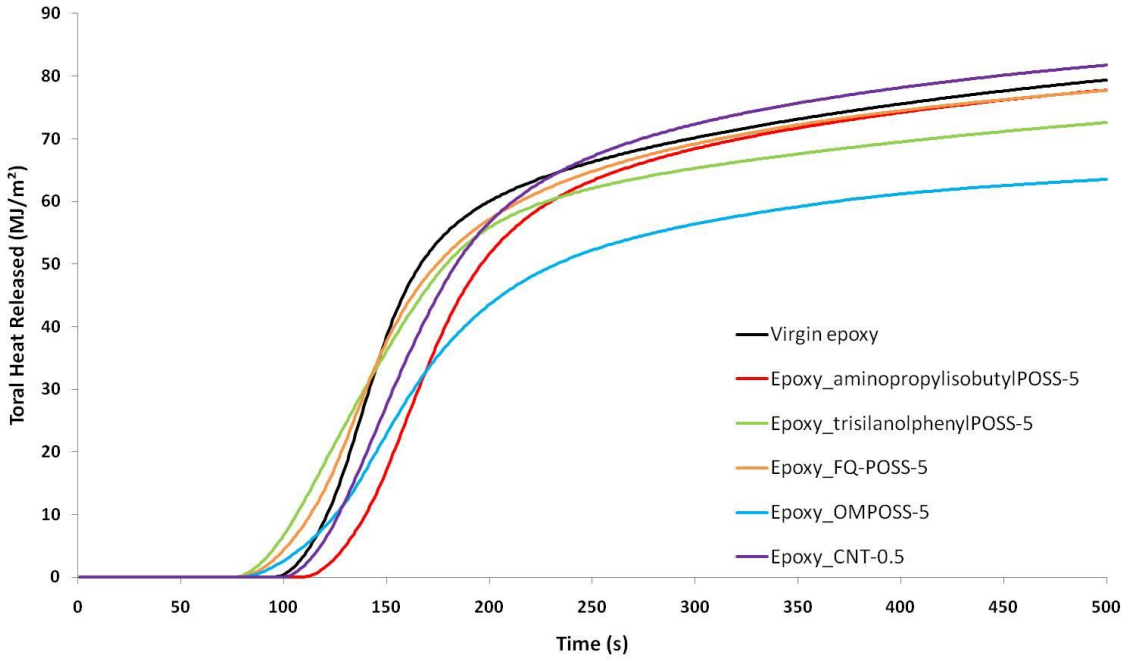

Figure 73: Total Heat Released as a function of time for epoxy containing nanoparticles (Heat flux: 35 kW/m², thickness: 5 mm, distance: 25 mm)

The final THRs for FQ-POSS, CNTs or aminopropylisobutylPOSS are similar to that of Virgin epoxy. The initial increase for Epoxy/aminopropylisobutylPOSS occurs later than for the two others because of the higher time to ignition. The formulation containing trisilanolphenylPOSS has a beginning similar to that of FQ-POSS, but the final plateau is set at a lower value (THR decreased by 9 % compared to Virgin epoxy). The effect is stronger with OMPOSS: the THR is decreased by 20 %. Epoxy _CNT-0.5 composite does not behave similarly. The heat release begins slightly later than for Virgin epoxy but the final result lies in the same range. Materials containing trisilanolphenylPOSS and OMPOSS degrade at the beginning but they create a protective layer on top of the sample (Figure 75). Then the remaining material is protected and does not degrade so quickly, leading to a THR decrease. Other samples are apparently not able to create such an efficient thermal barrier.

In order to choose the best nanoparticle for flame-retarding the epoxy resin, a summary of the properties of the different materials is presented in Figure 74. For each formulation, the THR, i.e. the tendency for globally releasing heat, is plotted as a function of FIGRA ($pHRR/t_{pHRR}$) [50, 139, 140], which represents the capability of the flame retardant for delaying the time where the fire is at its maximum. This plot gives a

compact overview of the flame retardant behavior of materials and classifies them: the best results are obtained when the formulation lies in the bottom-left corner of the figure, whereas it is the worst in the upper-right corner.

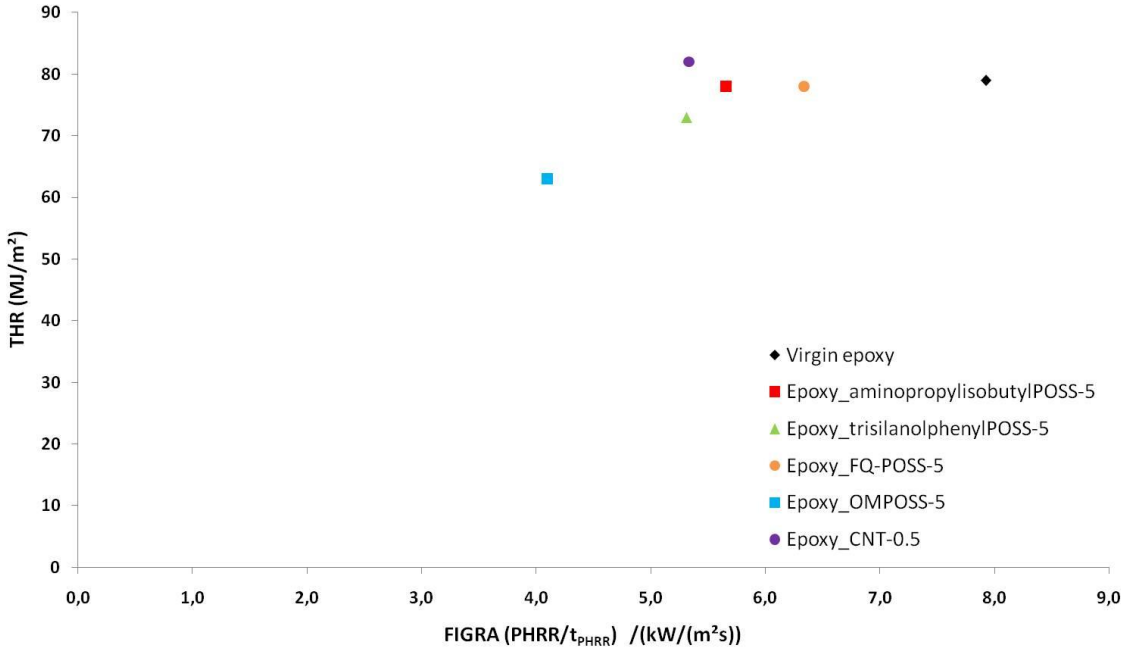

Figure 74 : Efficiency assessment (THR as a function of FIGRA) of different POSS in epoxy (Heat flux: 35 kW/m², thickness: 5 mm, distance: 25 mm)

First, it is clear that the differences in terms of THR are low between most of the filled resins and the Virgin one. The only significant enhancement of the THR is brought by the incorporation of OMPOSS (20 %). Concerning the FIGRA, it is once more obvious that the best results are obtained with OMPOSS (-48 % compared to Virgin epoxy). Limited enhancements are gained by using FQ-POSS (FIGRA decreased by 20 %). The three last formulations (Epoxy_aminopropylisobutylPOSS-5, Epoxy_trisilanolphenylPOSS-5 and Epoxy _CNT-0.5) have an intermediate and similar behavior (FIGRA decreased by 29-33 %).

The residues obtained after burning are shown on Figure 75.

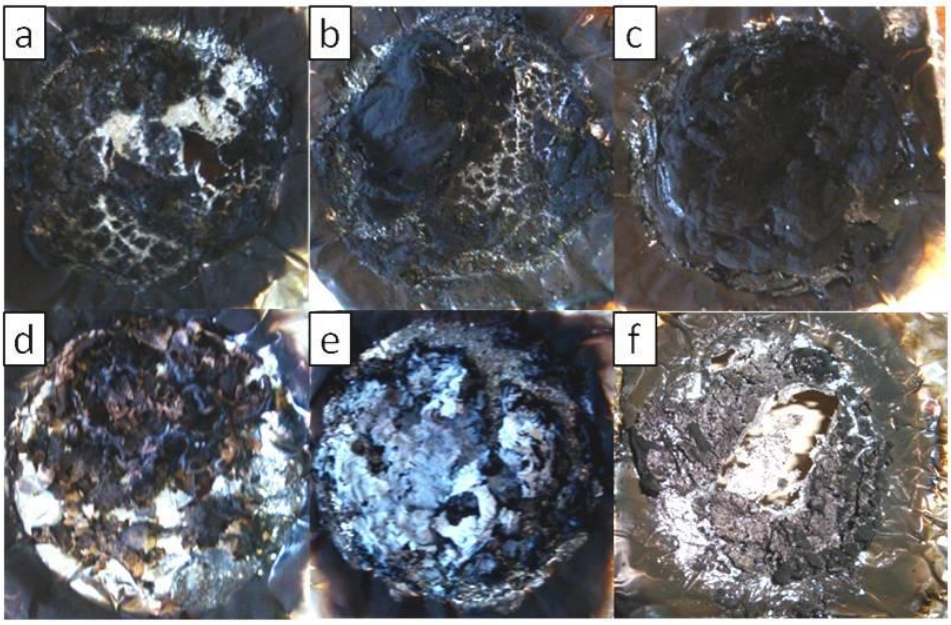

Figure 75: Pictures of residues after burning of different POSS-containing epoxy resins (topview). a: Virgin epoxy, b: Epoxy_aminopropylisobutylPOSS-5, c: Epoxy_trisilanolphenylPOSS-5, d: Epoxy_FQ-POSS-5, e: Epoxy_OMPOSS-5, f: Epoxy _CNT-0.5 (Heat flux: 35 kW/m², thickness: 5 mm, distance: 25 mm)

There is almost no residue after the burning of Virgin epoxy: only a blackened powder is observed and the aluminium foil used for maintaining the sample is partially destroyed (Figure 75a). Incorporation of aminopropylisobutylPOSS leads to a different structure: islands subsist with a partially swollen black residue, but there are voids in many areas (Figure 75b). The conclusions are quite similar for trisilanolphenylPOSS, with a more homogeneous island distribution (Figure 75c). Higher amount of residue may result from the tendency of phenyl groups for promoting char. The sample containing FQ-POSS leaves a black and reddish residue in some areas but the material is burnt down to the aluminium foil in many others (Figure 75d). The use of OMPOSS produces thin gray-white layers on the whole surface of the sample (Figure 75e). Finally, CNTs leads to a residue similar to that of Virgin epoxy (Figure 75f). As a first conclusion, the samples with the best fire properties are those having a protection on the whole sample surface at the end of the experiment. The less important performance of other samples may originate in the absence of protection in some areas of the sample. In fact, the way of action of nanoparticles in other polymers has been identified mainly as the creation of a protective barrier on top of the sample. Even if these observations only reflects the state of the sample after burning and not during it, it can be suggested that there is no

significant protection through barrier mechanism because of a lack of residue in some areas, resulting in limited flame-retardant properties. The only exception is the sample containing OMPOSS, which gives the best fire behavior. This conclusion has to be qualified, since the morphology of the samples during burning may differ from that at the end of the experiment.

Therefore, the fire performances are affected by the organic moieties at the corners of POSS. It is highly interesting that the best dispersion, obtained with trisilanolphenylPOSS, does not lead to the best fire properties. Indeed, a good dispersion is frequently described as a key parameter in the flame retardancy of nanocomposites [51, 124]. Other particles such as CNTs are not homogeneously dispersed in the epoxy and provide little enhancement of fire properties. However, Bourbigot et al.[124] have proven the benefits of using CNTs functionalized with flame retardant moieties instead of unmodified ones in a thermoplastic matrix. Therefore, it was decided to improve the dispersion of CNTs in the epoxy by grafting them with two different fire-retardant moieties.

III.2. CARBON NANOTUBES GRAFTING AND CHARACTERIZATION

In this section, two different moieties have been grafted on carbon nanotubes for their potential effect as flame retardants. The first one is melamine, a very well-known flame retardant [34]. Melamine has already been grafted on CNTs and the resulting filler has been incorporated in poly(lactic acid) [124]. The reaction to fire is enhanced with functionalized CNTs, whereas it is unchanged with as-received CNTs. The dispersion observed by TEM is also greatly enhanced. In this study, the fire performances were therefore linked to the filler dispersion in the matrix. Using such filler in an epoxy could also enhance its dispersion and then the reaction to fire of the epoxy formulation.

POSS have been identified in the literature as beneficial for the thermal stability and the reaction to fire of epoxies [67]. In the previous part, it was also proven that CNTs and POSS had a flame-retardant effect on the studied epoxy, even if limited in most of the cases. The second moiety grafted on carbon nanotubes is therefore aminopropylisobutylPOSS, since it can be covalently linked to CNTs thanks to the

reactivity of the amine group. Based on all these results, it was worth combining the properties of CNTs and POSS as single filler for epoxy matrix. Therefore, CNTs functionalized with aminopropylisobutylPOSS were synthesized and incorporated into the epoxy.

III.2.1. Functionalization

The first part of the synthesis of functionalized carbon nanotubes is common to both melamine- and POSS-grafted nanotubes. The synthesis pathway of these two compounds is described in Figure 76. The first step is an oxidation in a strong acidic media, in order to create reactive carboxylic acid groups at the surface of the nanotubes. It has been shown by various authors that this reaction in sulfonitric acid has different effects: the oxidation provides mainly carboxylic acid moieties, as expected, but also alcohols [141]. Furthermore, the combination between oxidation and sonication promotes the cutting of CNTs into smaller rods. Therefore, the first step of this synthesis is a balance between the formation of required acidic groups and the partial destructuration of CNTs. The obtained acidic groups are then activated with thionyl chloride before grafting the reactive amine: aminopropylisobutylPOSS or ethylenediamine, depending on the final CNTs type. After this step, CNT-POSS are obtained. The synthesis of melamine-grafted CNTs requires further steps. Ammonia is reacted with cyanuric chloride in a water/acetone media at 50 °C overnight in order to product 6-chloro-2,4-diamino-1,3,5-triazine. This molecule, close to melamine, reacts with the modified carbon nanotubes, leading to CNT-melamine.

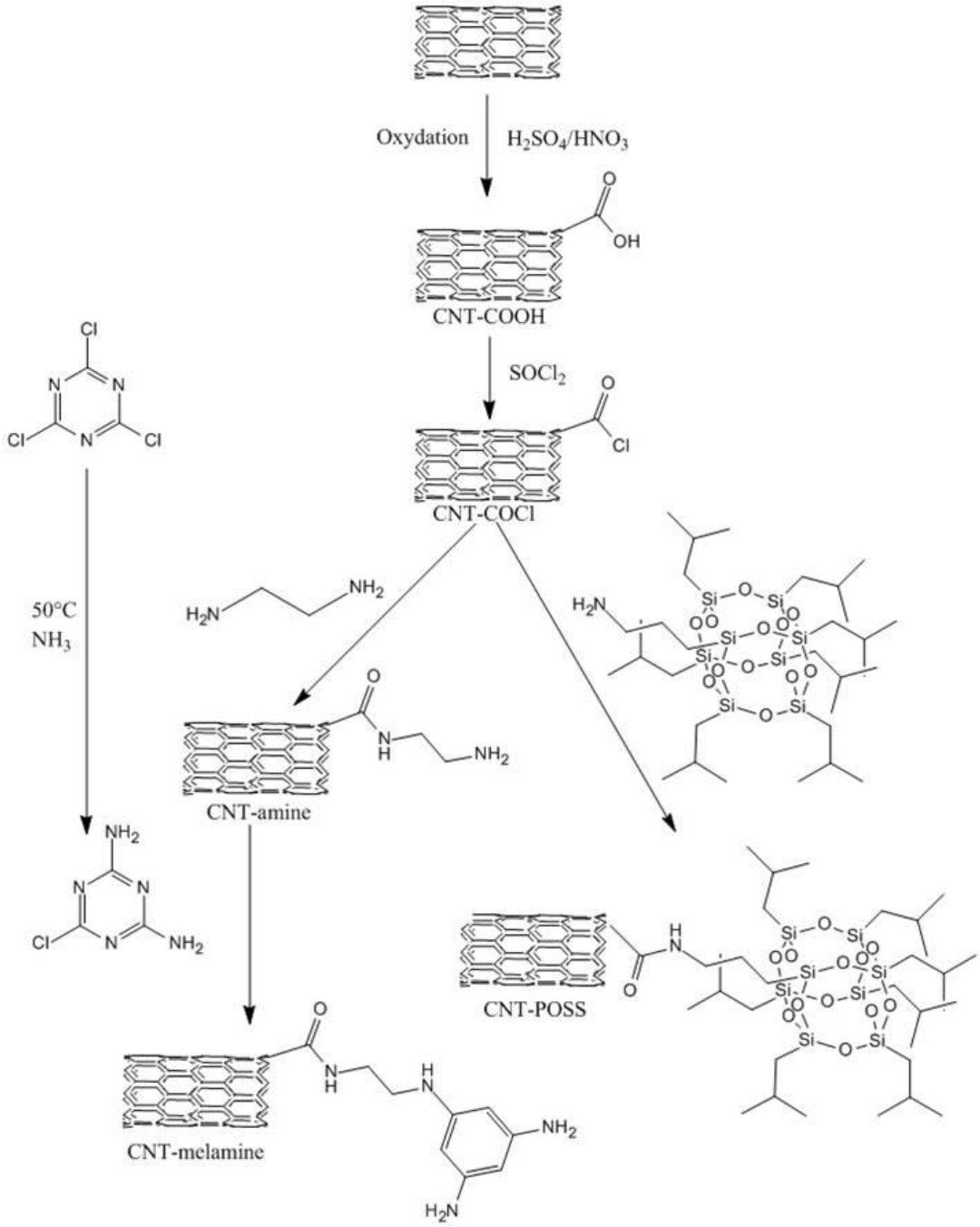

Figure 76: Synthesis scheme of grafted carbon nanotubes

III.2.2. Characterization

One of the main challenges when covalently grafting carbon nanotubes is to prove the existence of an effective covalent linkage formation between the CNTs and the graft and to quantify the graft molar fraction. Different methods are reported in the literature, each of them with its own advantages and drawbacks. Therefore, no consensus on the better method has been reached yet and only one or two methods are

used in each paper. In this part, the characterization of melamine- and POSS-grafted nanotubes has been conducted by infrared spectroscopy, liquid-state NMR, X-ray photoelectron spectroscopy and thermogravimetric analysis. Each method will be used for assessing the covalent grafting of CNTs and its advantages and drawbacks will be clearly stated. Finally, clear conclusions about the grafting will be given.

III.2.2.a. Thermal stability

Thermogravimetric analyses were conducted on grafted carbon nanotubes in two purposes. First, evaluation of their thermal stability before their incorporation in the epoxy matrix is essential. The grafting involved the creation of organic moieties, which degrade at lower temperatures than virgin carbon nanotubes. Therefore, the polymer containing modified carbon nanotubes could degrade at lower temperatures than that containing as-supplied CNTs. Second, modifications of the degradation steps and mass losses were identified as further clues of the grafting efficiency. The nanotubes were first degraded in an air atmosphere (Figure 77).

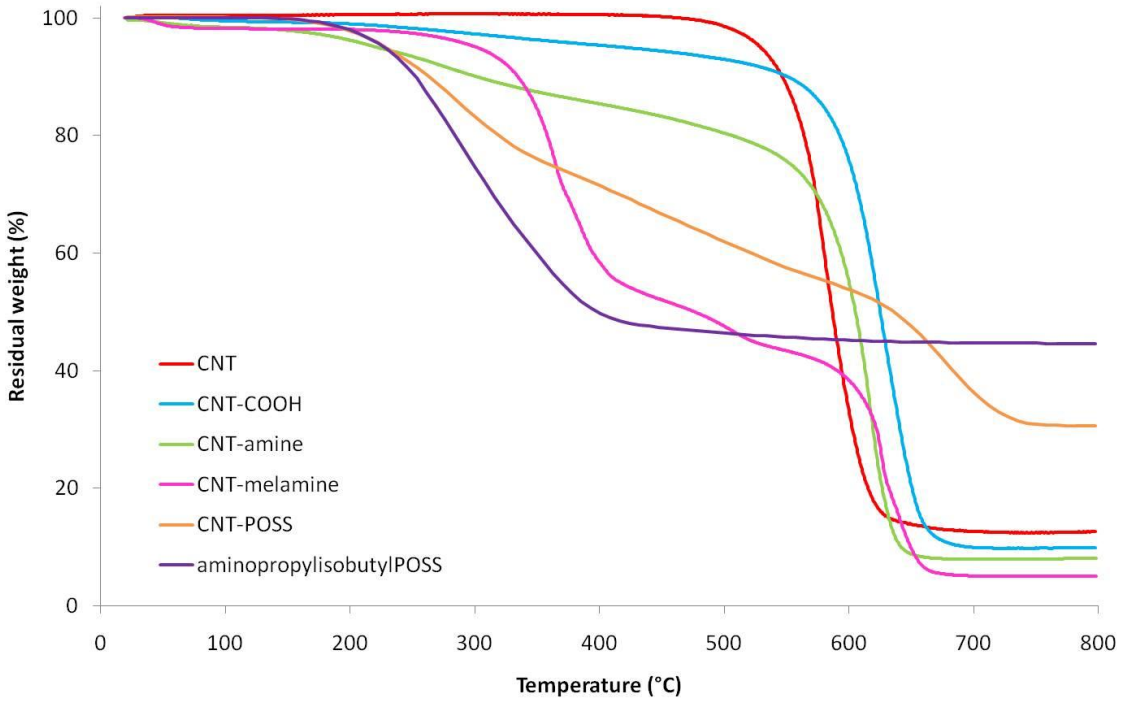

Figure 77: TGA curves of grafted carbon nanotubes in thermo-oxidative atmosphere (Air, 10°C/min).

As-supplied carbon nanotubes degrade in a single-step at relatively high temperature (581 °C), thanks to the good thermal stability of graphene sheets

constituting the CNTs. Once the CNTs are oxidized (CNT-COOH), a first degradation occurs at low temperature: 10 wt.% are lost between 195 °C and 626 °C. It is attributed to the carboxylic acid moieties leaving the CNTs in the range 150-350 °C, and then to the elimination of hydroxyl functionalities attached to the CNTs walls between 350 °C and 500 °C. Finally, the degradation at temperatures higher than 500 °C is attributed to the thermal oxidation of the remaining disordered carbon [142]. The main degradation step of CNT-COOH occurs at slightly higher temperature than for unmodified CNTs (626 °C instead of 581 °C for pristine CNTs). Therefore, the intermediate residue after the first degradation of CNT-COOH is more stable than unmodified CNTs (probably because impurities are removed during the oxidation step). The amine-modified CNTs have a completely different behavior. They degrade in two main apparent steps. The first one begins around 130 °C and ends up at 500 °C, with a mass loss of 20 wt.%. This step can be attributed to the loss of ethylene diamine grafted on the CNTs. The last step is similar to that of CNT-COOH, with a maximum degradation rate at 621 °C. CNT-melamine degrades in three distinct steps. A first one between 260 °C and 400 °C can be attributed to the partial loss of the grafted functions. The second one may result from successive condensation of melamine. The last one (631 °C) is due to the CNTs degradation. Finally, there are two degradation steps for CNT-POSS. The first one at 289 °C corresponds to the POSS degradation (free POSS degrade at 289 °C), whereas the other at 682 °C is the sign of the degradation of CNTs themselves. These steps, as well as the final residue, are compiled in Table 13. The residue reaches 13 wt.% for pristine CNTs. It is reduced for all the functionalized CNTs, except for CNT-POSS. The lower residue for CNT-COOH, CNT-amine and CNT-melamine can be attributed to the combination of the loss of organic moieties during thermal degradation with the purification step during oxidation: this eliminates impurities that are still present in as-received CNTs. The residue is much higher (31 wt.%) for CNT-POSS. We can suspect the grafting of POSS molecules on CNTs or else the trapping of POSS molecules inside CNTs bundles during synthesis: POSS would degrade into silica at high temperature and contribute to a higher residue formation.

Table 13 : Thermal degradation steps of modified CNTs (Air, 10 °C/min)

Formulation	Step 1 (°C)	Step 2 (°C)	Step 3 (°C)	Residue (wt.%)
CNTs			581	13
CNT-COOH			626	10
CNT-amine	267		621	8
CNT-melamine	366	510	631	5
CNT-POSS	289		682	31
aminopropylisobutylPOSS	289			45

The carbon nanotubes were then degraded under pyrolysis conditions (Figure 78). Pristine CNTs are stable up to 570 °C and they degrade slowly afterwards. This degradation is however limited, as the final residue is 96 wt.%. Once oxidized, CNT-COOH degrade in two steps. The first one is initiated at very low temperatures (from 100 °C) experiment and suggests a loss of water. In fact, Datsyuk et al. [142] have attributed a similar weight loss to water adsorbed on highly hydrophilic acid-treated CNTs. Furthermore, the presence of endohedral water in CNTs has been studied by various groups [143-145] and it may be that in our case residual water is trapped inside CNTs bundles and is release during the heating at high temperatures. The mass loss during this step is however limited as the intermediate residue amounts 90 wt.%. A second step begins at 564 °C and the weight loss continues slowly until the highest temperature is reached. The final residue reaches 79 wt.%. CNT-amine show similar trends, with higher weight losses: the first degradation step begins at 180 °C and ends at 581 °C (21 wt.% weight loss) and the last degradation follows immediately with a continuous volatilization up to 800 °C. The more intense first step can be attributed to the loss of amine. CNT-melamine shows a better stability in the lower temperature range as the degradation begins only around 250 °C. In this case, the thermogram clearly shows three step: the first one between 250 °C and 400 °C corresponds to the major degradation (42 wt.% loss). The second one between 400 °C and 541 °C shows a slower volatilization (13 wt.% loss). The last degradation rate is similar and this third step begins at 587 °C and lasts to 800 °C. The final residue reaches 27 wt.%. The initial degradation step can be attributed to the decomposition of melamine which results in the release of ammonia and the condensation of melamine into larger aromatic species. These species are stable up to 600 °C where they degrade at the same time as CNTs. Finally, POSS

degrade in a single step between 200 and 400 °C, where they lose 97 wt.%. CNT-POSS degrade in two steps. The first one occurs between 200 and 400 °C and corresponds to the release of most of the grafted POSS (55 wt.% loss). The last step is less important and only 3 wt.% are lost during it. The cause of the absence of continuous mass loss at higher temperatures for CNT-POSS can be considered. It is possible that a silica residue is produced by the degradation of POSS and that it relatively protects CNTs against further degradation. These results are summarized in Table 14.

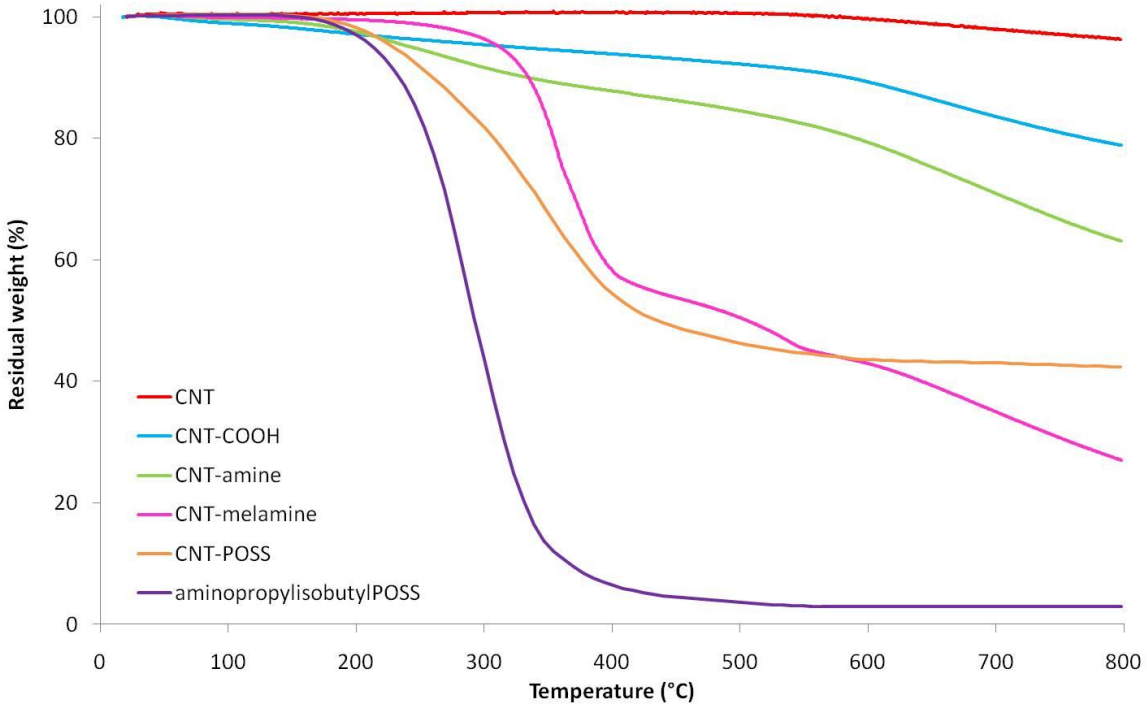

Figure 78: TGA curves of modified carbon nanotubes in pyrolysis conditions (N_2, 10°C/min).

Table 14: Thermal degradation steps of modified CNTs (N_2, 10°C/min)

Formulation	Step 1 (°C)	Step 2 (°C)	Step 3 (°C)	Residue (wt.%)
CNTs		656		96
CNT-COOH		647		79
CNT-amine	243	666		63
CNT-melamine	353	526	700	27
aminopropylisobutylPOSS	284			3
CNT-POSS	360	650		42

Even if this method cannot assure that covalent links are created between CNTs and their grafts, modifications of the thermal degradation suggest at least that strong interactions between them have been created.

III.2.2.b. Infrared spectroscopy

Infrared spectroscopy is a quick and simple method for the identification of bonds in a molecule. It is therefore often used for a first characterization of grafted CNTs [146]. Fourier Transform Infrared (FTIR) spectroscopy was used in order to detect changes in CNTs molecules along the different functionalization steps. The resulting spectra are compiled in Figure 79.

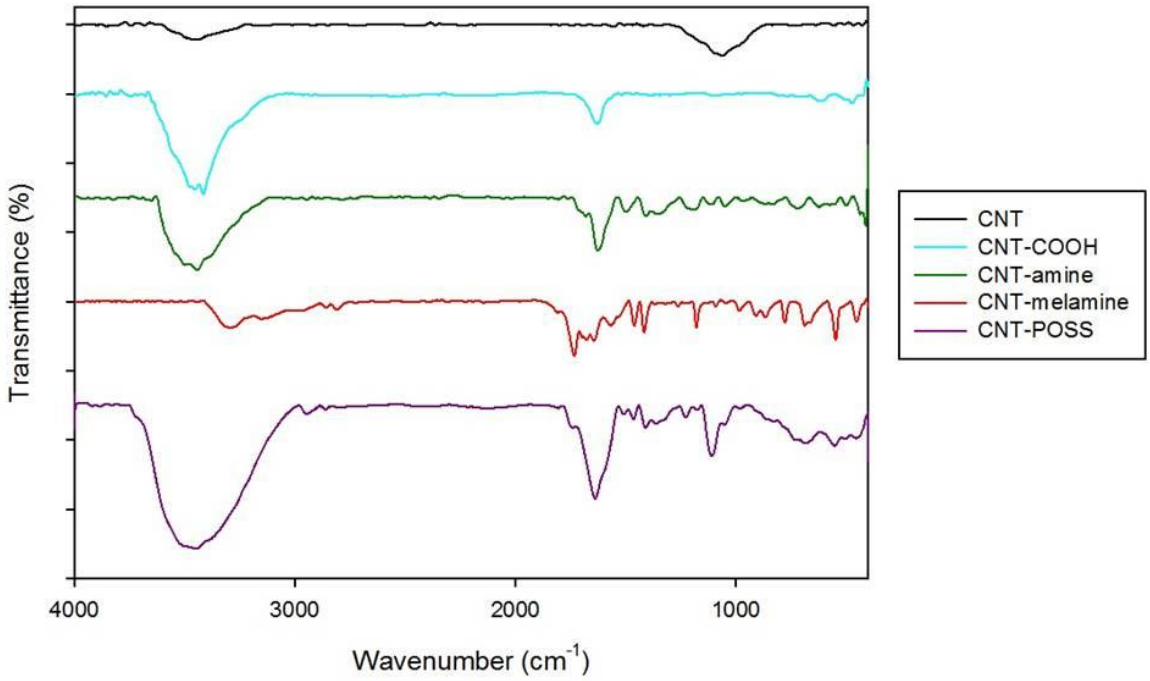

Figure 79: FTIR spectra of carbon nanotubes during grafting

As-received CNTs show two broad bands centered at 3446 and 1062 cm^{-1}. They are attributed respectively to –OH and C=O stretching at the open ends and defects of the MWNT [77]. After oxidation, the spectrum exhibits a broad and intense band centered at 3430 cm^{-1}, attributed to –OH stretching and a sharper peak at 1634 cm^{-1} due to a carbonyl bonding [147]. It is also worth noticing the disappearance of the peak due to the impurities in as-received CNTs (1062 cm^{-1}). Therefore, carboxylic acid is produced at the surface of CNTs during the oxidation/purification step. The next step of the synthesis of CNT-melamine consists in the grafting of a molecule of ethylenediamine, leading to the formation of an amide bond. The broad band between 3100 and 3700 cm^{-1} is enlarged and results from the stretching of the primary amine and the secondary amide (N-H stretching vibrations)[147]. A strong absorption can be distinguished at 1624 cm^{-1}.

This is the evidence of the amide linkage (C=O stretching at 1624 cm^{-1}). The additional peak at 1499 cm^{-1} is attributed to C-N stretching in the amide function. Additional bands are recorded in the spectrum of the final CNT-melamine and are brought by the aromatic species.

The spectra for CNT-POSS give similar results. A strong band appears at 1638 cm^{-1} (C=O stretching), along with a second one at 1512 cm^{-1} (C-N stretching). The strong absorption at 1109 cm^{-1} is due to the Si-O-Si network. Similar signals were recorded by Chen et al.[146] when analyzing CNTs grafted by aminopropylisooctylPOSS. They attributed a band at 1706 cm^{-1} to the stretching vibration of the C=O group of the amide, whereas a broad and less intense band at 1555 cm^{-1} was assigned to the combination of the bending vibration of the N-H group and the stretching vibration of the C-N bond of the amide group. The stretching of Si-O-Si also gave a peak at 1111 cm^{-1}.

FTIR has therefore evidenced that each kind of moiety is effectively grafted on CNTs. However, even this technique is fast and simple to implement, it is not the most precise one, in particular because overlaps can occur. Furthermore, no quantification of the grafting is available.

III.2.2.c. Liquid-state NMR

In the last paragraph, we have established the formation of covalent links during the functionalization of CNTs. However, a single FTIR band was shifted by functionalization and it was necessary to confirm the grafting by another method. Liquid-state Nuclear Magnetic Resonance (NMR) was used for this purpose: this is a quick method and we supposed that if covalent links were created between CNTs and their graft, different signals would be modified on the NMR spectra.

Different authors have investigated the effectiveness of CNTs functionalization by NMR. Some of them have used ^{13}C solid-state NMR in order to study the structure of CNTs, either functionalized or not [148-150]. However, in our case, the paramagnetic nature of CNTs hindered the correct setting of the experiment and only carbons from the core of the CNTs could be observed. Based on this observation and other references [151-154], it was decided to disperse functionalized CNTs in a suitable solvent and perform liquid-state ^{1}H NMR.

1D and 2D NMR (HMQC experiment) were used in order to assign the signals from aminopropylisobutylPOSS. A typical 2D spectrum is shown on Figure 80.

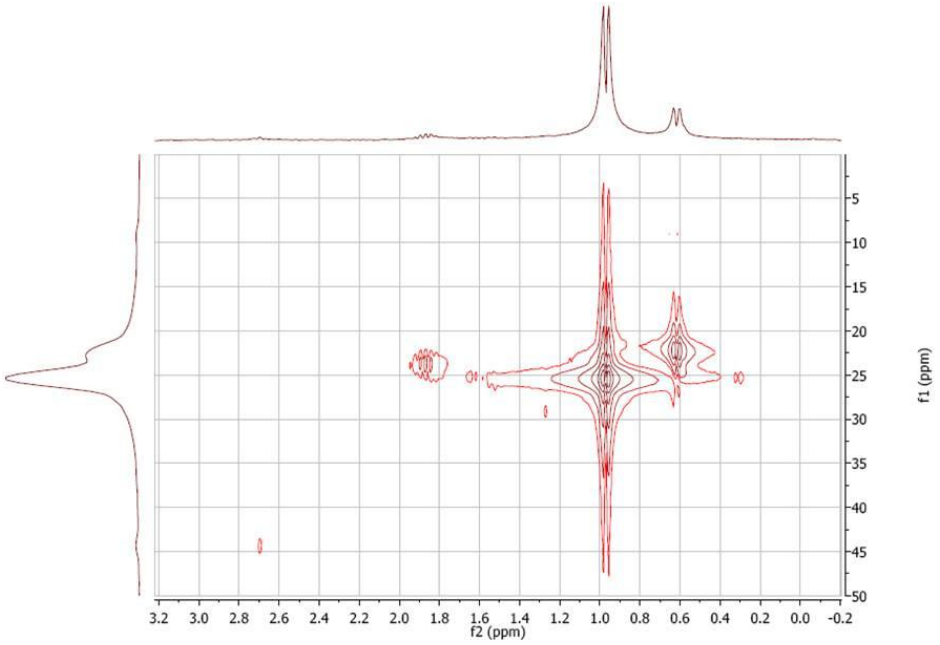

Figure 80: 2D NMR experiment of aminopropylisobutylPOSS

Then, proton NMR experiment was conducted on the grafted nanotubes. Figure 81 shows a comparison between the ^{1}H NMR spectra of aminopropylisobutylPOSS and CNT-POSS. The NH_2 signal of aminopropylisobutylPOSS appears at 2.38 ppm (star) and shifts to 8.24 ppm in CNT-POSS due to the formation of the amide bond The CH_2NH_2 signal of POSS observed at 2.67 ppm (dot), does not appear in CNT-COOH spectrum and it shifts to 2.94 ppm in CNT-POSS spectrum because of CH_2NHCO.

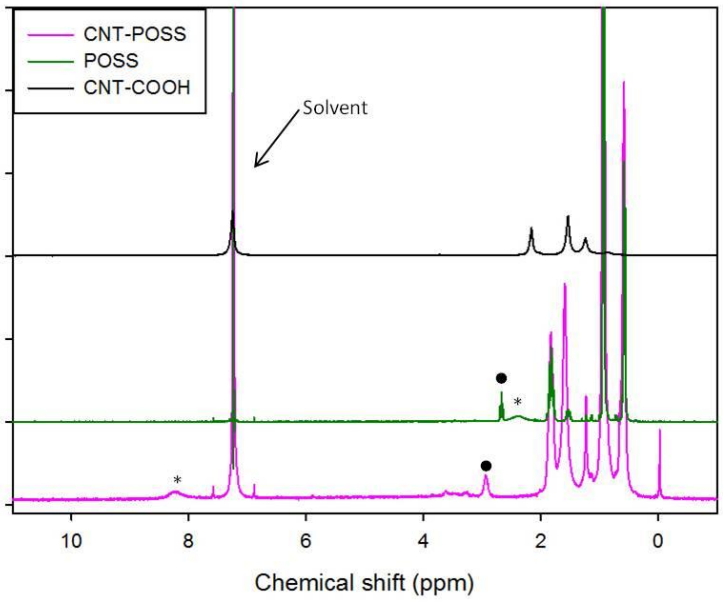

Figure 81: ^{1}H NMR spectra of CNT-COOH, POSS and CNT-POSS in $CDCl_3$

Similar experiments were conducted with CNT-amine and CNT-melamine. However, because the graft is in these cases less specific than POSS, the signals cannot be isolated and no conclusion on the effectiveness of the grafting can be drawn from this technique.

As a conclusion, liquid-state NMR allows to assess the grafting of CNTs quite rapidly: a one-hour acquisition is sufficient for recording the shifting of two signals corresponding to the amine becoming an amide and to the CH_2 group next to it in the case of CNT-POSS. This technique is therefore valuable for this purpose, but cannot be used in each case (overlaps occurred in the case of CNT-melamine).

III.2.2.d. X-ray photoelectron spectroscopy

The XPS C1s and O1s spectra of the CNT-COOH are presented on Figure 82. The XPS C1s spectrum shows an asymmetric peak with a long tail in the higher energy region. Its deconvolution shows a main peak at 284.0 eV, attributed to the C-C bonds in a graphitic structure in agreement with the literature, and six more contributions centered at 284.9, 285.7, 286.6, 287.9, 289.2 and 290.6 eV. According to the literature, the peak centered at 284.9 eV can be attributed either to defects on the nanotubes structure [142] or to sp^3-hybridized carbon atoms as in diamond-like carbon [155]. Contributions at higher binding energies at 285.7, 286.6, 287.9 and 289.2 eV correspond to carbon atoms attached to different oxygen atoms. They are assigned to the following bounds C-O,

C=O, O=C-O and carbonates-like species, respectively. Finally, the O-O* transition loss peak is observed at 290.6 eV.

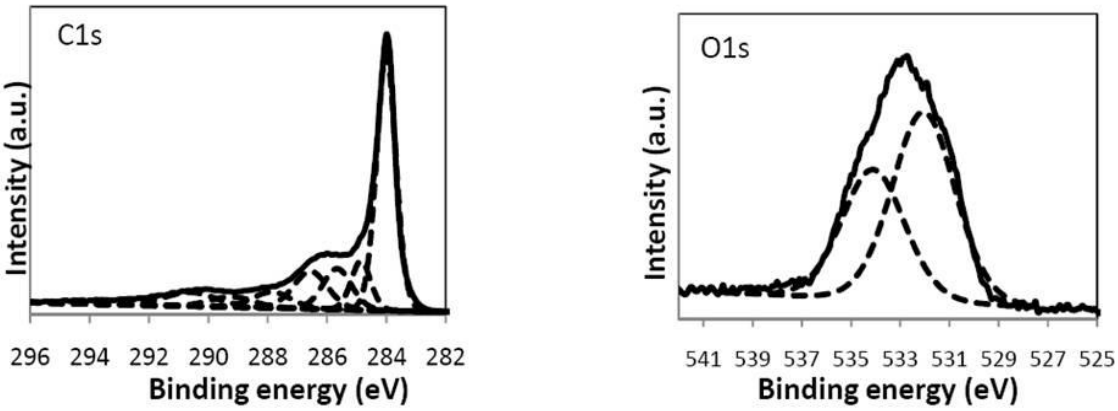

Figure 82: XPS C1s and O1s spectra of the CNT-COOH

Moreover, Table 15 shows the relative intensity of each component of the C1s spectrum. We can then observe that the C-O and C=O functions have equal contributions (12 %) as expected because of –COOH on the CNT. Concurrently the O1s spectrum clearly shows two components centered at 532.1 and 534.1 eV assigned to hydroxyl (O-C, O-H) (59 %) and carboxylic (O=C-O) (41 %) groups on the CNT surface, respectively.

Table 15: XPS C 1s spectrum decomposition of CNT-COOH

	sp^2 C=C (%)	sp^3 C-C, C-H (%)	C-O (%)	C=O (%)	O=C-O (%)	Carbonates (%)	π- π* transitions
CNT-COOH	49	10	12	12	6	4	7

Finally, the total amount of carbon and oxygen on the CNT samples is also summarized in Table 16. We can observe that the O atomic concentration is quite similar in the CNT-COOH, CNT-amine and CNT-melamine.

Table 16: XPS quantification results of CNTs

Sample	Element	Peak position (eV)	Full Width at Half Maximum (eV)	Atomic concentration (%)
CNT-COOH	C 1s	284.0	0.8	93.4
	O 1s	534.1-532.1	3.0	6.6
CNT-amine	C 1s	284.4	0.9	91.2
	O 1s	533.7-531.9	2.1	6.3
	N 1s	401.7-399.7	1.9	2.5

CNT-melamine	C 1s	284.4	0.9	92.1
	O 1s	534.7-532.4	2.4	6.7
	N 1s	402.1-400.1	2.2	1.2
CNT-POSS	C 1s	284.4	1.1	83.7
	O 1s	533.9-532.3	1.5	11.3
	N 1s	402.1-400.0	2.0	0.7
	Si 2p	102.7	1.5	4.3

In Figure 83, the C1s, O1s and N1s spectra of the CNT-amine are presented. The N1s spectrum clearly shows two components centered at 401.7 and 399.7 eV due to the presence of carbon (N-C) and hydrogen (N-Hx) atoms bound to nitrogen, respectively. Moreover, the CNT-amine C1s spectrum reveals trends similar to those observed for the CNT-COOH C1s spectrum. However, we can observe an increase of the component around 286 eV while that around 287 eV decreases. This is due to the presence of –NHx functions bound to carbon atoms. Unfortunately, it is not possible to simulate this contribution because the values of the C-N and C-O bounds binding energies are quite similar.

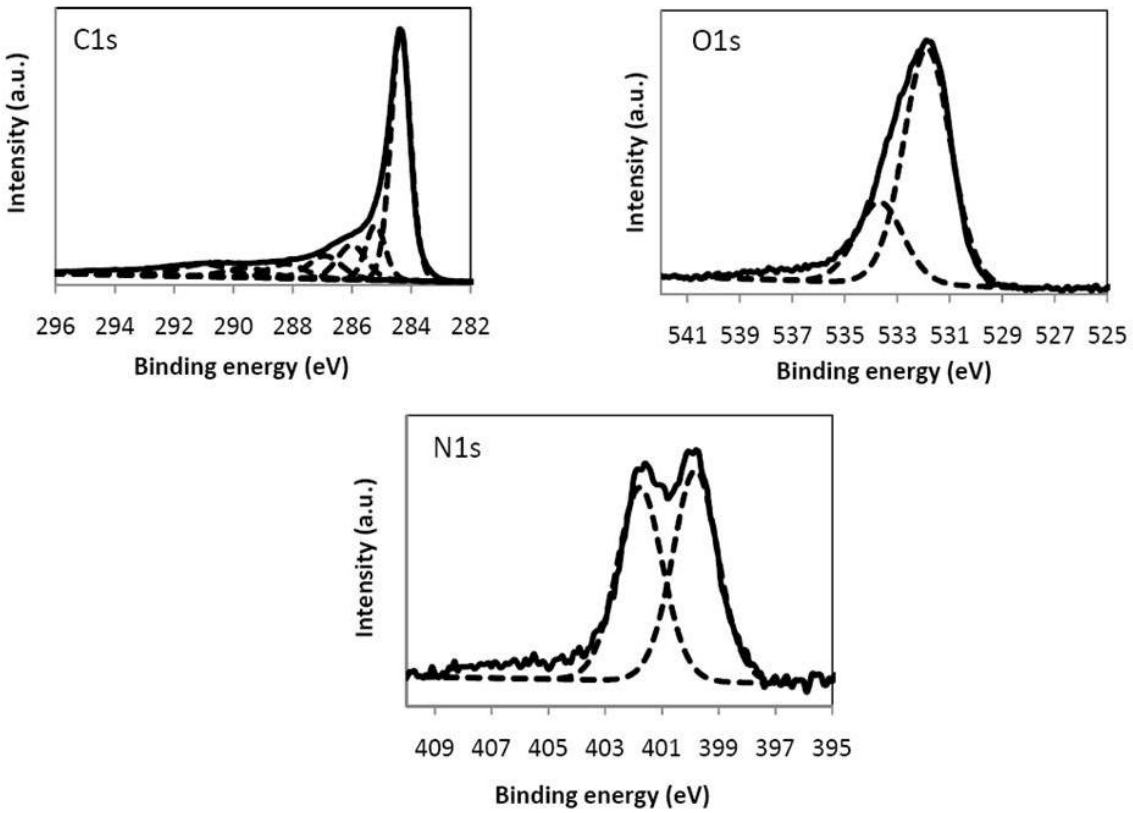

Figure 83: XPS C1s, O1s and N1s spectra of the CNT-amine

In Figure 84 and Figure 85, the C1s, O1s and N1s spectra of CNT-melamine and CNT-POSS and also Si2p spectrum of CNT-POSS are presented. The C1s, O1s and N1s spectra reveal similar trends to those observed for the CNT-amine. However, we can observe in the N1s spectrum, the formation of a weak contribution around 406 eV which can be assigned to the presence of oxidic nitrogen species. Finally, in the Si2p region, we observe a peak centered at 102.7 eV, characteristic of the presence of Si-O and Si-N bounds. Unfortunately, as previously, it is not possible to simulate both components.

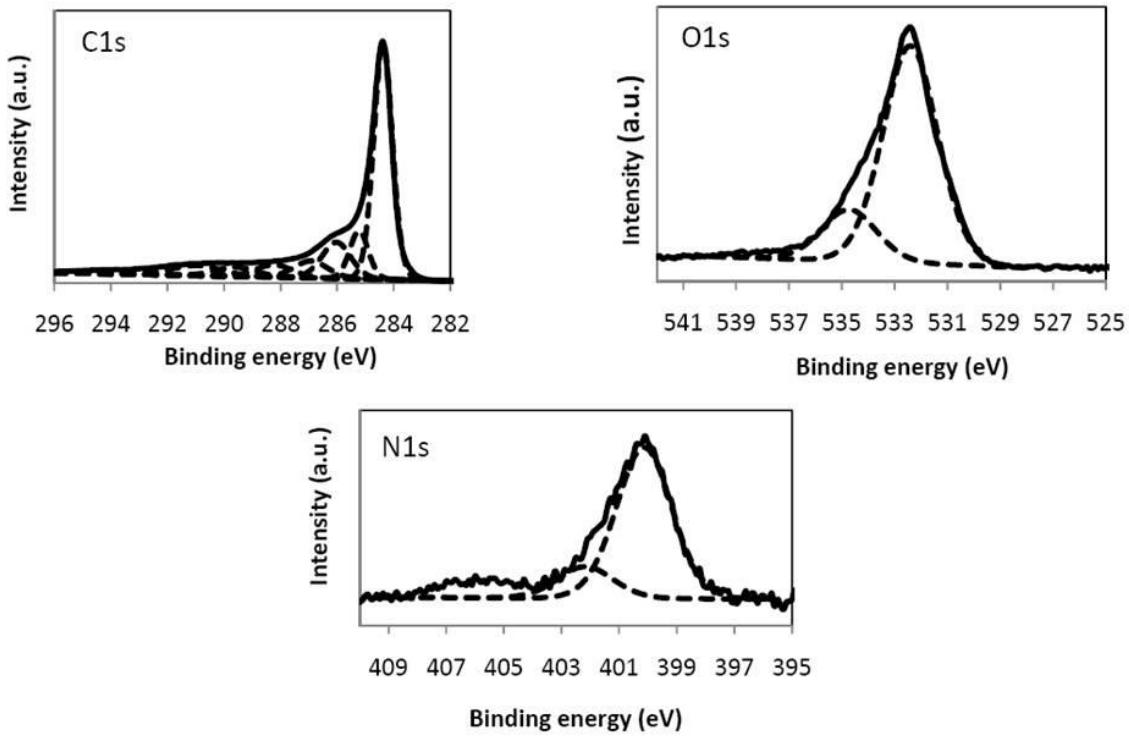

Figure 84: XPS C1s, O1s and N1s spectra of the CNT-melamine

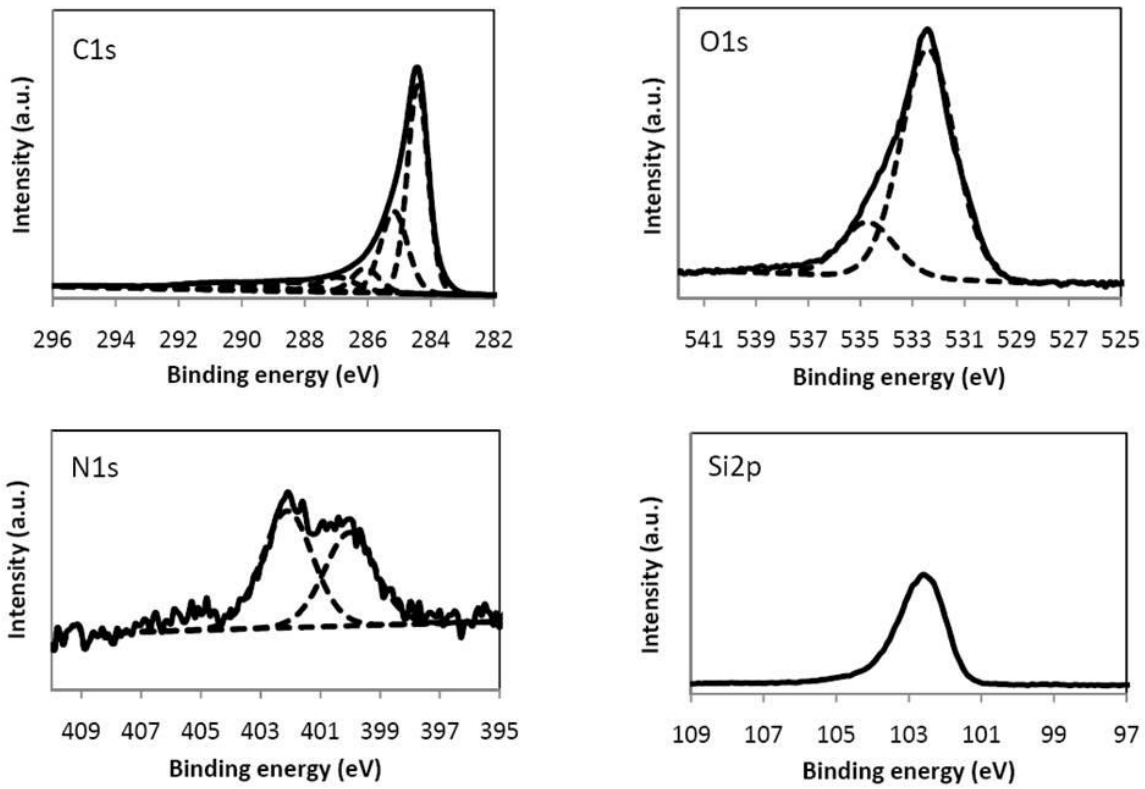

Figure 85: XPS C1s, O1s, N1s and Si2p spectra of the CNT-POSS

All these results prove that the grafting has been successfully conducted and give a first approximation of the graft amount (variations between entangled CNTs and batches do not permit to be more definitive): 6 % of carbon atoms from CNT-COOH are part of carboxylic acids. CNT-amine, CNT-melamine and CNT-POSS contain respectively 2.5, 1.2 and 0.7 % nitrogen and the presence of oxidic nitrogen species has been observed in CNT-POSS.

III.2.2.e. Conclusion on functionalization

In this part, different techniques have been used in order to check the covalent functionalization of CNTs. Thermogravimetric analyses have emphasized modifications of the thermal stability of CNTs once grafted, which are a first hint of the creation of an interaction between CNTs and organic moieties. However, since the purification of CNTs is mixed (removal of impurities in acidic media) with its functionalization, it is not easy to conclude on the grafting effectiveness. Then, infrared spectroscopy has evidenced the grafting via the shifting of characteristic bands in modified CNTs. Liquid-state NMR has also proven the grafting, even more precisely than infrared spectroscopy, but it could

not be used for CNT-melamine. Then, XPS appears as the most complete method, since it evaluates the efficiency of grafting and gave quantifications. Furthermore, thermogravimetric analyses also suggest that even if the thermal stability of CNTs is affected by the functionalization, the obtained materials are sufficiently stable for being incorporated in the epoxy matrix. The main conclusion of this section is therefore that flame-retardant moieties have been successfully grafted on the surface of CNTs. In the following section, these modified CNTs are incorporated in an epoxy resin and the properties of the resulting materials will be characterized.

III.2.3. Properties of epoxy containing modified-CNT

III.2.3.a. Dispersion state of nanoparticles

One of the reasons for functionalizing CNTs was the enhancement of the dispersion of CNTs in the epoxy. Therefore, the homogeneity as well as the extent of the dispersion was evaluated by TEM. Figure 86 shows how CNT-COOH is dispersed in the matrix. Even if individualized CNTs can be observed, most of them remain in tight bundles. This is consistent with the presence of hydrophilic carboxylic acid moieties: their affinity for the aromatic epoxy matrix is limited.

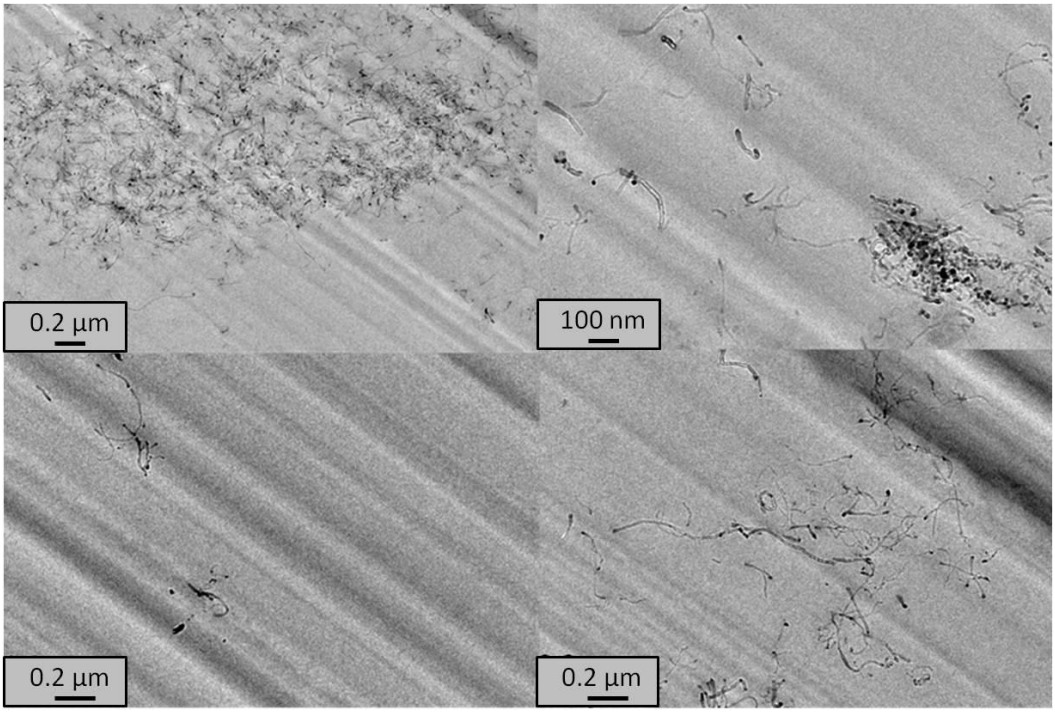

Figure 86: TEM pictures of Epoxy _CNT-COOH-0.5 composite

The dispersion of CNT-amine is then shown in Figure 87. CNTs are mainly localized in big agglomerates. There are however some individualized CNTs. Such CNTs have already been used for reinforcing an epoxy resin [147]. However, the samples have only been observed by SEM after flexural tests. The interaction between the matrix and the modified CNTs was improved compared to pristine CNTs, but the extent of the dispersion has not been assessed. In our case, it seems that the functionalization does not help the dispersion of CNTs in the matrix. This could be due to an insufficient interaction between the matrix and its filler. Zhu et al. [156] have worked on diamine-functionalized SWNT. One of their hypotheses was that diamines could create bridges between CNTs during functionalization. This also may explain why CNTs remain together.

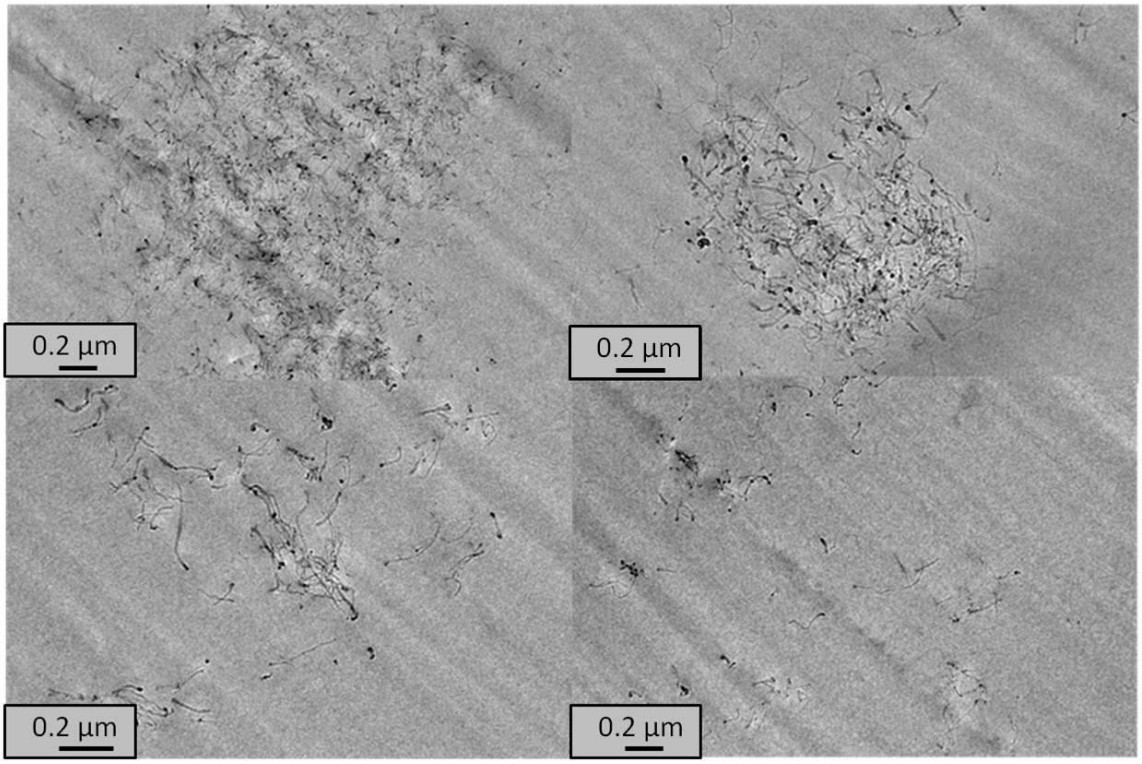

Figure 87: TEM pictures of Epoxy _CNT-amine-0.5 composite

CNT-melamine appears better dispersed (Figure 88a). CNTs seem to create a network in the matrix. The dispersion is more homogeneous, even if areas without nanotubes are still observed. However, bigger bundles (Figure 88b) suggest that part of the CNTs are held together and coated by melamine. In fact, non-covalent functionalization of CNTs give similar structures: Ma et al. [81] have functionalized CNTs

with a flame-retardant containing phosphorus and aromatic cycles. Their modified CNTs seem coated by the flame-retardant.

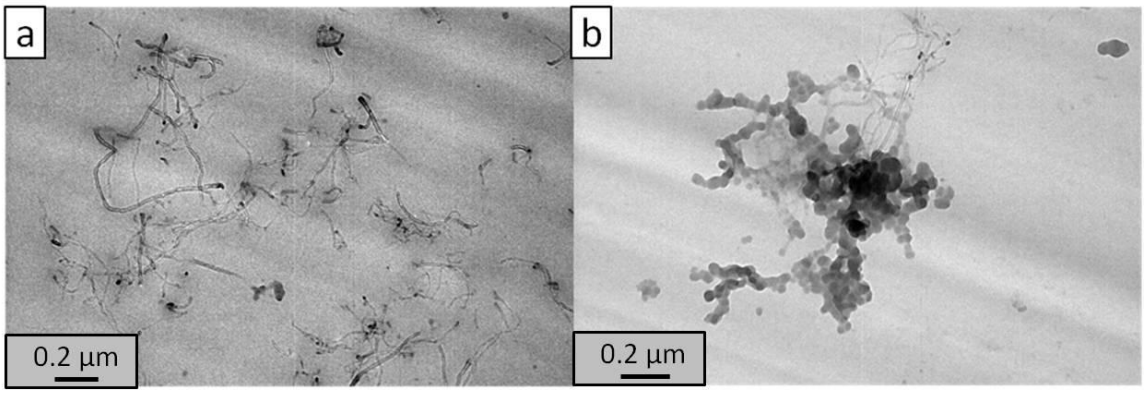

Figure 88: TEM pictures of Epoxy _CNT-melamine-0.5 composite

Finally, CNT-POSS were incorporated in the matrix. Figure 89a and Figure 89b reveals the presence of individualized CNTs. Free POSS that could not be removed during the washing of functionalized CNTs also subsist in the matrix (Figure 89c). Figure 89d shows that very different areas can be identified in this sample: the left of the picture is full of individualized CNTs and the right area is full of POSS and no CNT can be seen. Between them, an empty area is observed. Because few CNTs have been identified, bigger aggregates are certainly present elsewhere. However, the observation of CNT composite is tricky since they cannot be effectively identified by SEM whereas only small areas can be analyzed by TEM.

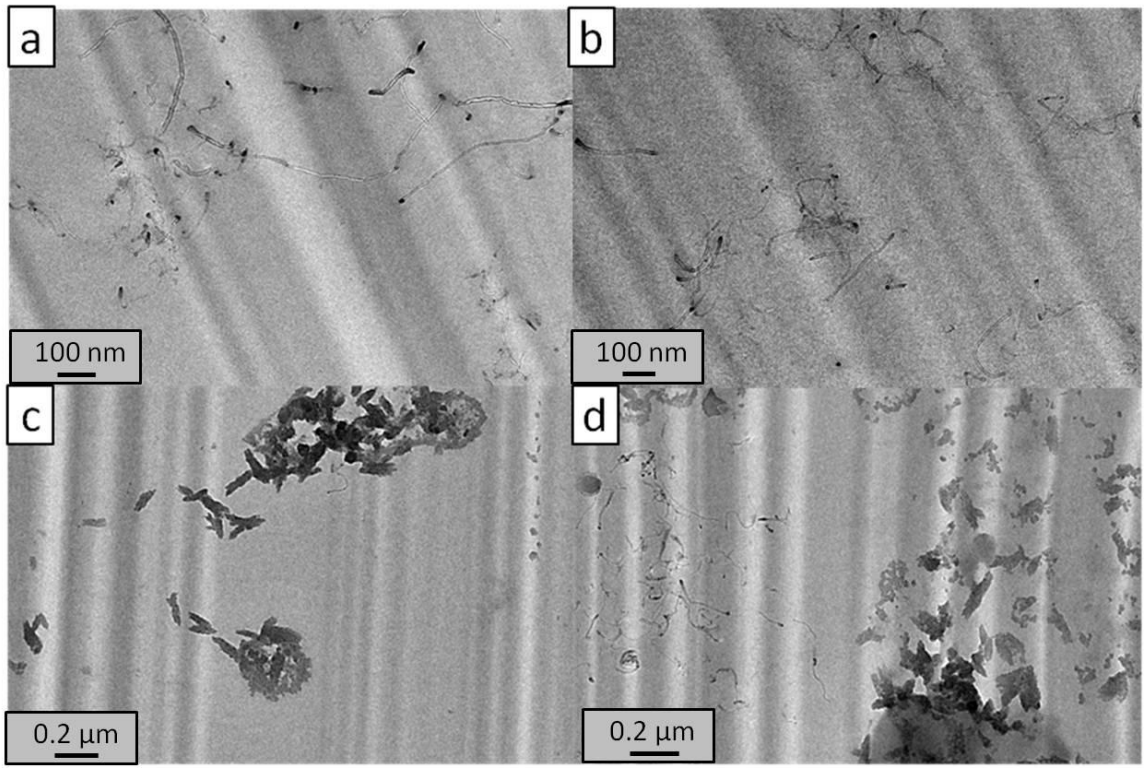

Figure 89: TEM pictures of Epoxy _CNT-POSS-0.5 composite

The main conclusion of this section is that the modification of CNTs does not significantly enhance their dispersion in this matrix. However, the dispersion of functionalized CNTs in the epoxy matrix has been fully characterized and this parameter is often important for discussing the reaction to fire of polymers.

III.2.3.b. Crosslinking density

As in the first part of this chapter, the crosslinking density of the formulations was calculated by means of FTIR in order compare the properties of the final material (Table 17). Unfortunately, the spectra could not be systematically used for the calculations, since there are overlapping between the signals of the fillers and the resin. When available, the calculated crosslinking densities lie between 72 and 77%. These samples have therefore similar crosslinking densities.

Table 17: Crosslinking density of Epoxy /CNT formulations

Formulation	Crosslinking density (%)
Virgin epoxy	77
Epoxy _CNT-0.5	72
Epoxy _CNT-COOH-0.5	-
Epoxy _CNT-amine-0.5	75
Epoxy _CNT-melamine-0.5	-
Epoxy _CNT-POSS-0.5	-

III.2.3.c. Thermal stability

The thermal stability of epoxy containing modified CNTs is presented in Figure 90 and Table 18. The thermal behavior of Virgin epoxy and epoxy containing pristine CNTs have already been commented before in this chapter (p.123). However, the previous experiments were conducted with gold foils in the pans, since they were parts of a series of experiments involving phosphorus-containing species (Chapter IV, p.172). Indeed, silica from the pan is able to react with phosphorus compounds when heating, therefore creating phosphosilicates. The use of a gold foil avoids this problem but since it cannot be perfectly adapted to the sides of the pan, its presence slightly modifies the amount of residue during TGA. The following results should not be compared to others in this thesis in terms of residue (note that the residues remain in the same order anyway and that the same conclusions may apply).

Except for CNT-POSS, all the functionalized CNTs modify the thermogram in the same way as pristine CNTs. The first degradation step occurs at similar temperatures, but with a higher degradation rate (calculation based on the derivative curves and not shown). The second degradation step is similar to that of Virgin epoxy. On the contrary, Epoxy _CNT-POSS-0.5 degrades similarly to Virgin epoxy during the first step and is less stable during the second one.

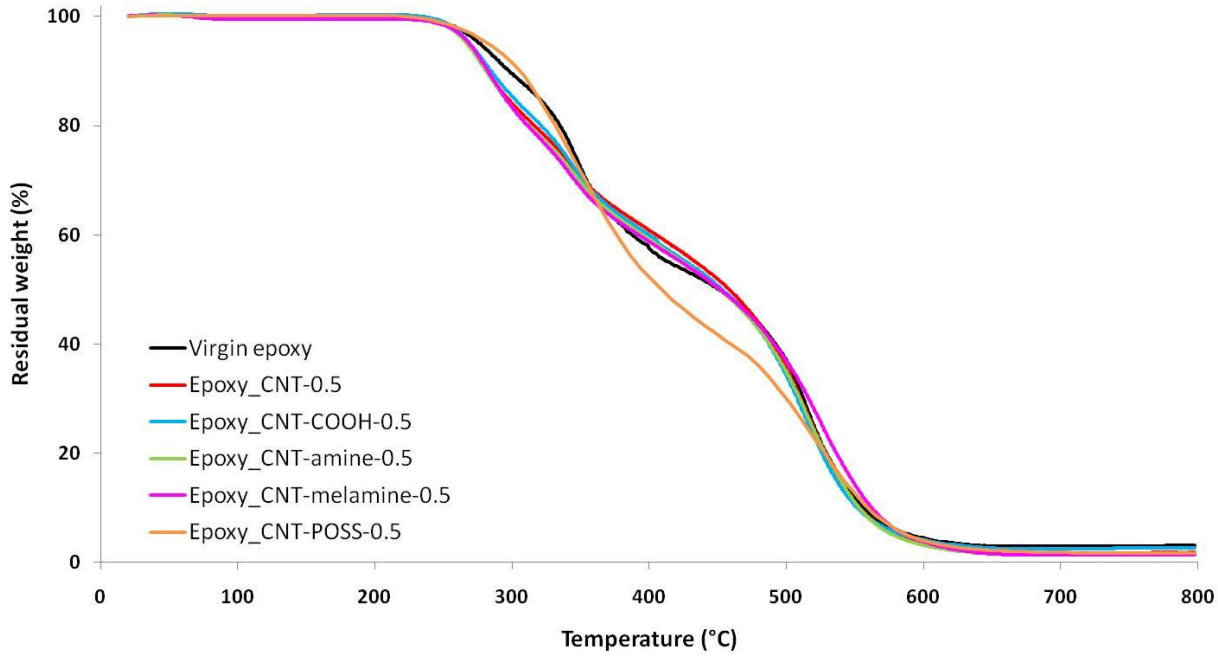

Figure 90: TGA curves of epoxy resins containing modified CNTs in thermo-oxidative atmosphere (Air, 10°C/min)

Table 18: TGA main parameters of epoxy containing modified CNTs (Air, 10°C/min)

Formulation	Step 1 (°C)	Step 2 (°C)	Residue (wt.%)
Virgin epoxy	344	511	3
Epoxy _CNT-0.5	340	507	2
Epoxy _CNT-COOH-0.5	340	507	3
Epoxy _CNT-amine-0.5	340	510	2
Epoxy _CNT-melamine-0.5	338	519	1
Epoxy _CNT-POSS-0.5	342	511	2

Figure 91 shows the difference weight curves of epoxy containing functionalized CNTs. Except for CNT-POSS, they modify the degradation of Virgin epoxy in the same way: destabilization occurs between 220 and 390 °C. Interactions above 400 °C are lower than 3 wt.% and therefore considered as negligible. CNT-POSS interact in an opposite way with epoxy. Between 215 and 340 °C, the system is not destabilized as with other CNTs, but a destabilization occurs between 340 °C and 560 °C

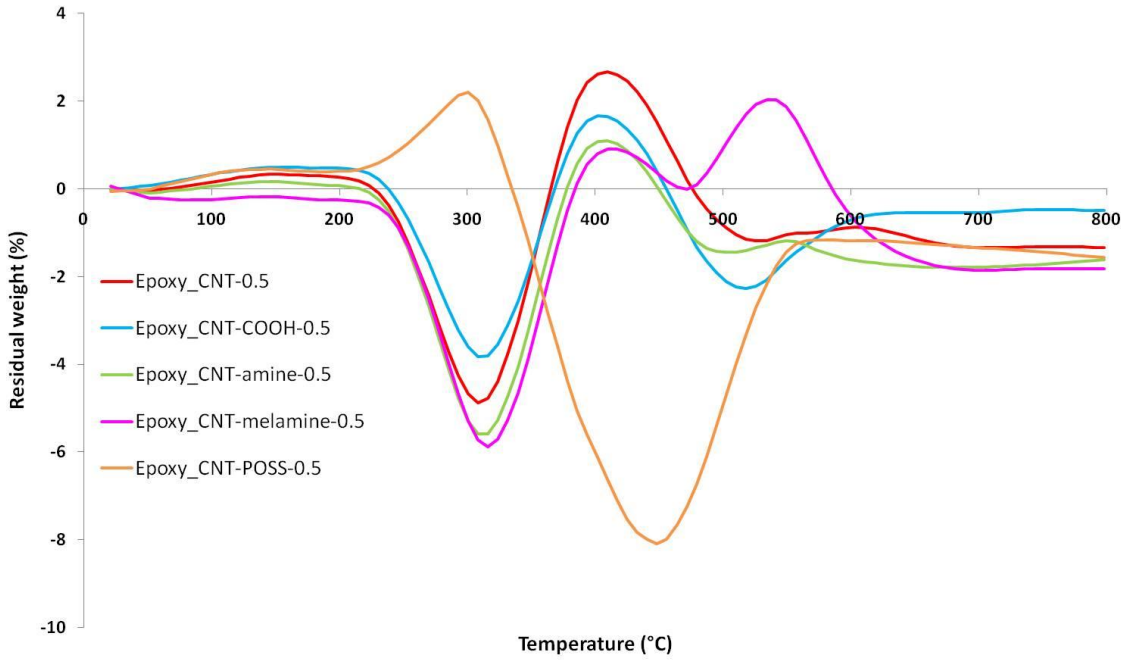

Figure 91: Weight differences curve of epoxy containing functionalized CNTs

III.2.3.d. Thermal conductivity

The thermal conductivity (k) of Virgin epoxy and Epoxy _CNT-0.5 has then been evaluated by Hot Disk method. Indeed, there are many reports of the enhancement of electrical conductivity by incorporation of CNTs in polymer matrices and other also report similar phenomena for thermal conductivity. Figure 92 and Figure 93 show respectively the thermal conductivity and thermal diffusivity of Virgin epoxy and Epoxy _CNT-0.5 up to 200 °C. Different phenomena are highlighted. Below the T_g, the two formulations have similar thermal conductivity. It is then increased for Virgin epoxy whereas it remains at the same level for Epoxy _CNT-0.5. Furthermore, the thermal diffusivity of Epoxy _CNT-0.5 is always below that of Virgin epoxy. Han et al.[157] have very recently reviewed results on the thermal conductivity of polymeric CNT/composite. They emphasized different facts: large discrepancies are found in the literature, since CNTs are reported to increase the thermal conductivity of polymers in some cases whereas it lowers it in other cases. Furthermore, many factors such as diameter or length may affect CNTs capability for modifying the thermal conductivity. Interestingly, they reminded that one difficulty for increasing k is phonon mismatch at interfaces, which causes a high interfacial thermal resistance. Indeed, when CNTs do not form a

network in the polymer, phonons cannot propagate properly and the heat conductivity decreases. This is certainly the case in the presence of CNTs bundles (observed in our Epoxy_CNT-0.5 samples).

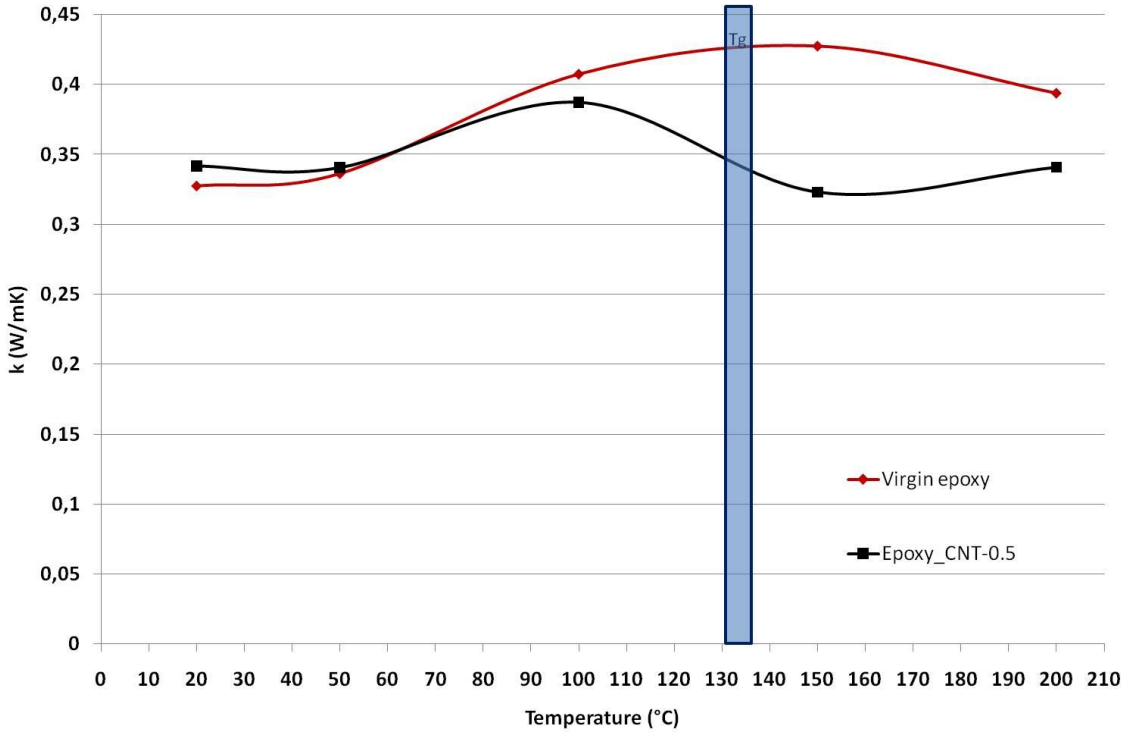

Figure 92: Thermal conductivity as a function of temperature for Virgin epoxy and Epoxy _CNT-0.5

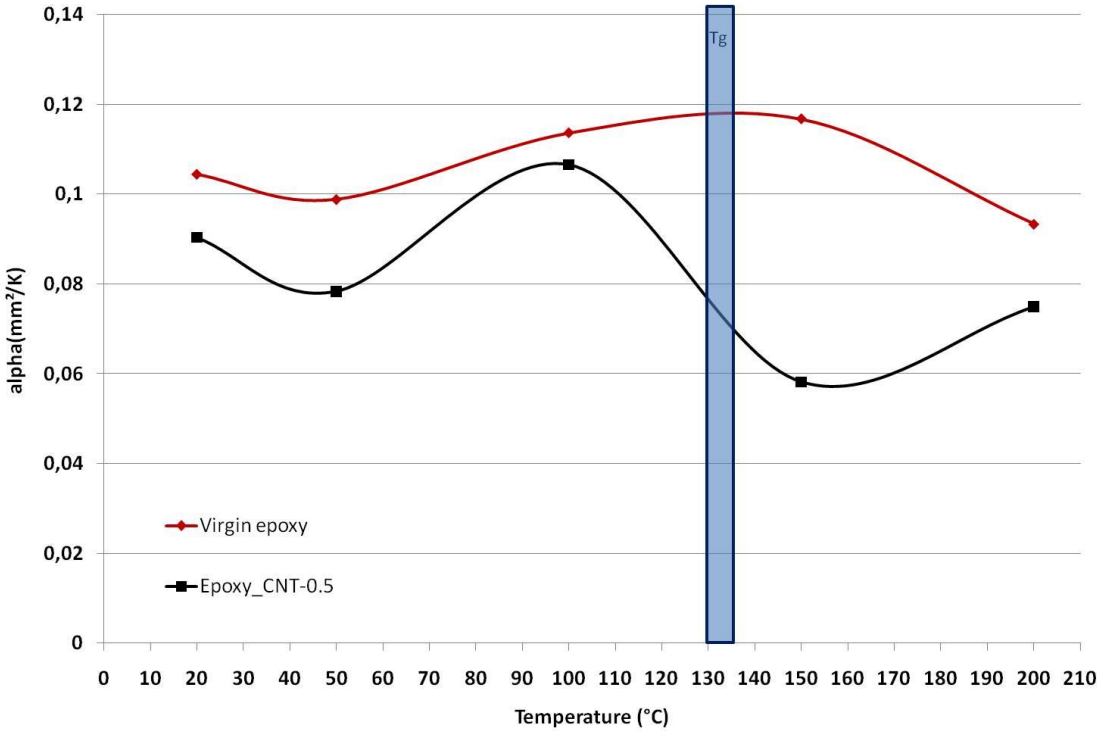

Figure 93: Thermal diffusivity as a function of temperature for Virgin epoxy and Epoxy _CNT-0.5

III.2.3.e. Reaction to fire

The reaction to fire of epoxy containing functionalized CNTs is shown in Figure 94 and Table 19.

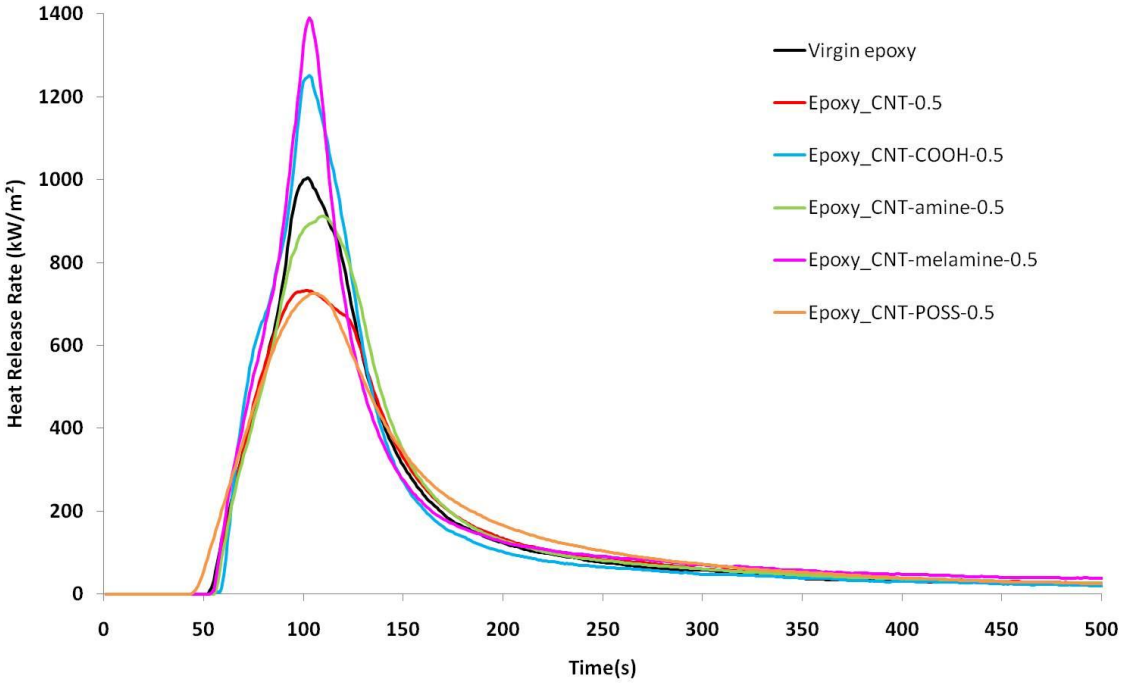

Figure 94: Heat release rate versus time for epoxy containing functionalized CNTs (Heat flux: 35 kW/m², thickness: 5 mm, distance: 25 mm)

Table 19: Mass-loss calorimeter main parameters for Epoxy/CNTs formulations. The differences compared to virgin material are % set into brackets (Heat flux: 35 kW/m², thickness: 5 mm, distance: 25 mm)

Formulation	t_{ign} (s)	pHRR (kW/m²)	THR (MJ/m²)
Virgin epoxy	52	1004	81
Epoxy _CNT-0.5	54 (+4)	733 (-27)	77 (-5)
Epoxy _CNT-COOH-0.5	54 (+4)	1252 (+25)	85 (+5)
Epoxy _CNT-amine-0.5	52 (+0)	912 (-9)	83 (+2)
Epoxy _CNT-melamine-0.5	54 (+4)	1391 (+39)	91 (+12)
Epoxy _CNT-POSS-0.5	43 (-17)	725 (-28)	81 (+0)

Incorporation of pristine CNTs in the epoxy matrix decreases the peak of heat release rate by 27 %. This performance is similar to that obtained with the same material at 35 kW/m². Surprisingly, CNT-COOH and CNT-melamine increase strongly the pHRR,

respectively by 25 and 39 %. As for CNT-amine, there is almost no effect on the pHRR (-9 %). POSS-grafted CNT decrease the pHRR in the same range as pristine CNTs (-27 %).

The Total Heat Released (THR) was calculated from the mass-loss calorimeter test results (Figure 95).

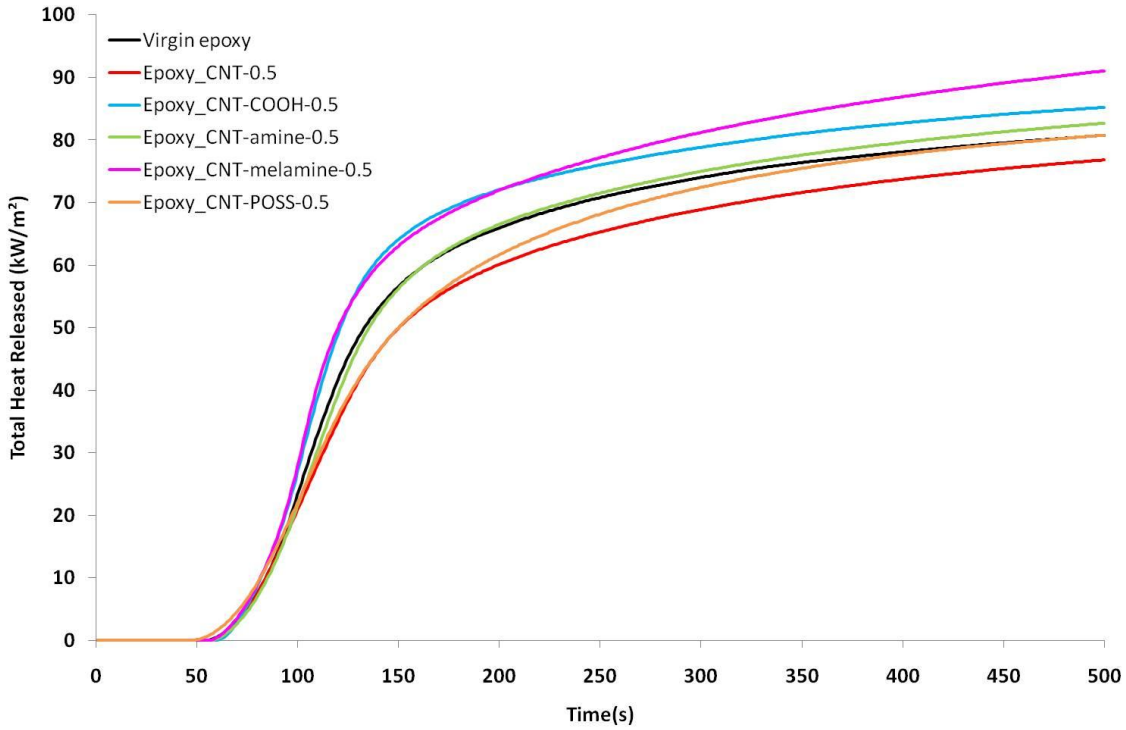

Figure 95: Total Heat Released versus time for epoxy containing functionalized CNTs (Heat flux: 35 kW/m², thickness: 5 mm, distance: 25 mm)

The variations of the THR depending on the CNTs functionalization remain small: apart from the melamine-grafted CNTs, which increase the THR by 12%, the final differences are lower than 5 %.

The generally accepted mode of action of CNTs in polymers seems also confirmed [122]. At the beginning, a layer is formed, but it is not efficient enough for limiting the degradation of the underlying polymer. Once the layer is degraded (or not well-formed), there is no other phenomenon limiting the fire propagation and the polymer burns strongly. Different CNTs grafts do not lead to the same performances of filled materials. However, the use of functionalized CNTs has not proven its superiority compared to unmodified CNTs.

As a first conclusion, the incorporation of carbon nanotubes in epoxy, either functionalized or not, has not proven its interest for enhancing the flame retardancy of

epoxy resins. This conclusion is confirmed by Figure 96, where the THR is plotted as a function of FIGRA. Similarly to the previous study on commercial nanoparticles, this plot permits to classify the different materials very quickly in terms of reaction to fire. The general tendency is confirmed as the most interesting formulation is provided by untreated CNTs and the worst is CNT-melamine. However, it should be pointed out that none of these formulations is greatly promising, as the best one has performances close to that of Virgin epoxy and our approach should be then improved.

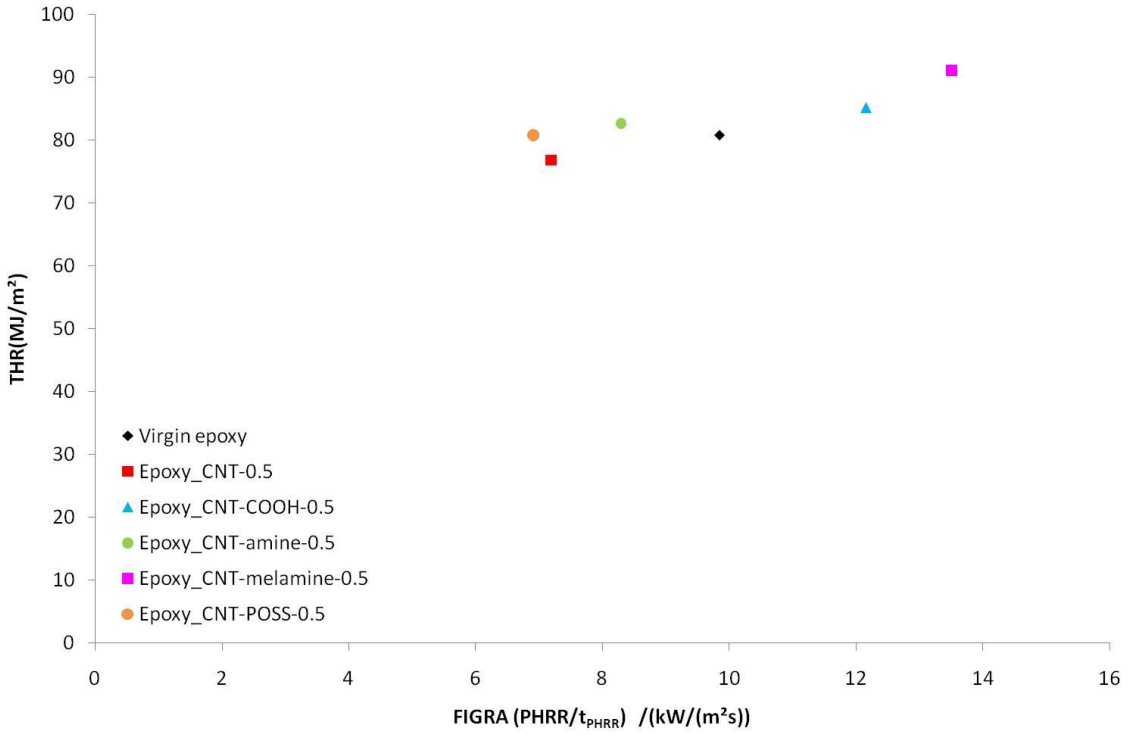

Figure 96: Efficiency assessment (THR versus FIGRA) for the different functionalized CNTs (Heat flux: 35 kW/m², thickness: 5 mm, distance: 25 mm)

III.3. CONCLUSION

Two different types of nanoparticles have been studied in this chapter as potential flame retardants for epoxy resins. On the one hand, four different types of POSS have been chosen. Some of them were able to react with the epoxy prepolymer, other had aromatic moieties on their corners, which are supposed to enhance the interactions between the filler and the matrix, and also should help char formation. TrisilanolphenylPOSS, which has the best dispersion, does not lead to the best fire properties. Indeed, the best behavior is observed with OMPOSS, which is aggregated.

On the other hand, CNTs were incorporated in the epoxy matrix. In order to further enhance their dispersion in the matrix and to improve the reaction to fire of the composite, they were covalently functionalized with two fire-retardant-like moieties. The intermediate compounds of synthesis were subsequently incorporated in the resin. However, the reaction to fire of the obtained materials is not greatly enhanced. Furthermore, in some cases strong negative effects are encountered with no apparent link to the dispersion or thermal stability as we observed with POSS.

Nanoparticles have not proven that they can effectively flame-retard epoxies when used alone. However, since they have been effectively used in combination with traditional flame retardants in different cases, the next chapter will investigate the possible interactions between two nanoparticles and a traditional filler.

Chapter IV - Combination between traditional FR and nanoparticles

The previous chapter has shown that limited enhancement could be obtained by the use of nanoparticles alone in the epoxy system. However, many of their applications, such as electronic printing wire-boards or public transportation require high levels of flame retardancy [92]. Among the solutions usually available, intumescent systems offer good fire performances. Furthermore, the wide range of formulations available permits to get tailor-made properties [158]. Jimenez et al. [86] have proven the efficiency of ammonium polyphosphate (APP) for increasing the resistance to fire of epoxy resins used as paints for protecting steel. On the contrary to this latter work, when bulk materials are flame-retarded in order to limit their contribution to the fire growth, the loadings achieved are low compared to many systems. Indeed, Zammarano et al.[57] have reported the efficiency of APP in an epoxy system at only 5 wt.% loading whereas suppliers recommend incorporation from 10 to 20 wt.% [56]. Based on these observations, the materials studied in this chapter contain 5wt.% flame-retardant. Considering the potential of some nanoparticles studied in the last chapter and also the existence of synergies between nanoparticles and traditional flame retardants in other polymers [3, 5], systems containing both ammonium polyphosphate and carbon nanotubes or octamethylPOSS will be studied. Similarly to what has been conducted in the previous chapter, the formulations will be characterized before mass-loss calorimetry experiment in terms of glass transition temperature, crosslinking density, dispersion, thermal conductivity and thermal stability. Fire performance in mass-loss calorimetry and pyrolysis combustion flow calorimetry will then be assessed.

IV.1. EPOXY CHARACTERIZATION

Before the evaluation of the reaction to fire of the materials, the study of their morphology seems of prime importance. In fact, the incorporation of fillers in epoxy resins can affect the final properties in different ways. Subsequently, the new material generally behaves differently towards fire. Similarly to thermoplastics, fillers may shift the glass transition temperature[159], among other mechanical properties. Another modification lies in the processing of thermosets. Fillers are added to the prepolymer (or hardener in some cases) before the final tridimensional network is created so that the curing kinetics and final crosslinking density could be modified. Therefore, the first part

is dedicated to the determination of the crosslinking density of the different formulations and their glass transition temperature. Modifications of the curing kinetics induced by the incorporation of fillers will also be discussed. Then, the morphology of the obtained composites will be studied, as well as their thermal conductivity and their thermal stability.

IV.1.1. Crosslinking density

Similarly to the characterization conducted in Chapter III, FTIR was used on the filled resins in order to evaluate the crosslinking density of materials and the results are presented in Table 20. Considering the possible inhomogeneities in the epoxy resins and the method's accuracy (10 % error margins), the crosslinking density is similar between all formulations and lie between 78 and 83 %, which is relatively high.

Table 20: Crosslinking densities of the different formulations.

Formulation	Crosslinking density (%)
Virgin epoxy	81
Epoxy_OMPOSS-5	83
Epoxy_APP-5	82
Epoxy_APP-4.5_CNT-0.5	80
Epoxy_APP-4_OMPOSS-1	78

Differential Scanning Calorimetry (DSC) was also used for the evaluation of the glass transition temperature (T_g) (Table 21). It shows that the T_g is not greatly affected by the incorporation of the fillers. Indeed, it varies between 130 and 136 °C, with error margins lying around 3 °C.

Table 21: Glass transition temperature (Tg) of the different formulations

Formulation	T_g (°C)
Virgin epoxy	132
Epoxy_OMPOSS-5	132
Epoxy_APP-5	136
Epoxy_APP-4.5_CNT-0.5	130
Epoxy_APP- 4_OMPOSS-1	133

IV.1.2. Kinetics of curing

In order to further study the possible modifications of the epoxy matrix induced by the incorporation of fillers, the curing kinetics was assessed by using a heating ATR-IR spectrometer.

Figure 97 shows the crosslinking degree as a function of time for the five epoxy formulations. During the first curing step at 30 °C, all formulations begin to cure and Virgin epoxy, Epoxy_APP-5 and Epoxy_APP-4_OMPOSS-1 presents the same rate of curing. It seems therefore that APP does not affect the curing rate of epoxy. It is lower for the sample containing OMPOSS alone. The sample containing both APP and CNTs also has a lower curing rate at shorter times. At the end, the crosslinking degrees are very similar for Virgin epoxy, Epoxy_OMPOSS-5 and Epoxy_APP-4_OMPOSS-1. They are slightly lower for Epoxy_APP-5 and Epoxy_APP-4.5_CNT-0.5. Therefore, the curing rate is lower for Epoxy_OMPOSS-5 at the beginning, but the effect is reduced thereafter and the final crosslinking degree is close to that of virgin epoxy. On the contrary, Epoxy_APP-5 behaves like virgin epoxy at the beginning and has a lower final crosslinking degree. Finally, Epoxy_APP-4.5_CNT-0.5 is less reactive during the whole experiment.

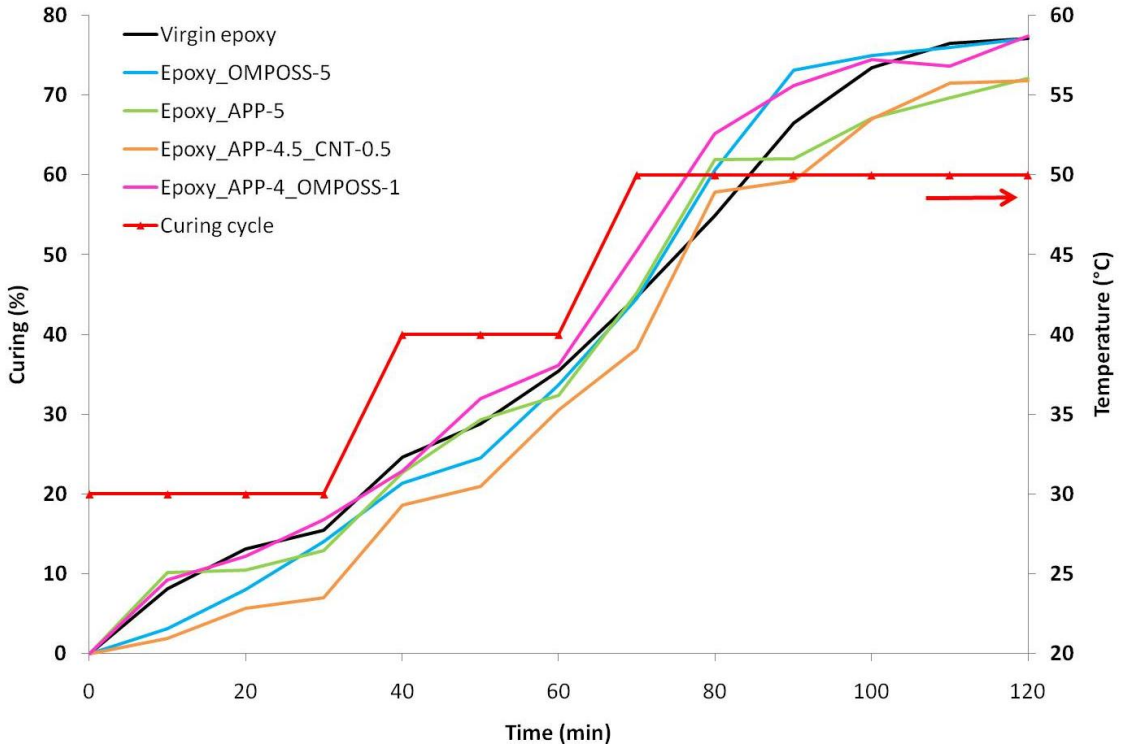

Figure 97: Crosslinking degree as a function of time measured by infrared spectroscopy

These results are consistent with the literature, even if no reference was found on the reactivity of epoxy containing APP. There are however many reports on the effects of nanoparticles on the curing process of epoxies. In our case, POSS incorporated alone in the matrix slows down the curing during the step at 30 °C. Zhang et al. [160] have also observed a lower curing rate at the beginning of the curing of epoxy containing 10 wt.% octaaminopropylPOSS. Concerning CNTs, our results suggest a retardation of the curing during the whole experiment. Allaoui et al. [135] have reviewed literature on Epoxy _CNT: although accelerated cure in the early stage is reported in many cases, no effect or even retardation occur in another one. The presence of residual catalysts in CNTs is frequently identified as the main parameter accelerating the curing. In our case, it can be suggested that the high viscosity of the uncured mixture in the presence of CNTs may hinder the homogenization of the system and that areas rich in hardener are next to others with low hardener content. In this case, some areas, with low hardener content, would be cured less quickly than others, with high hardener content.

IV.1.3. Morphology of the composites

Before investigating the dispersion of fillers in the matrix, the general aspect of samples has been assessed as we did in the previous chapter (Figure 98). Virgin epoxy is completely transparent (Figure 98a). Incorporation of OMPOSS alone in the matrix produces a white material, almost opaque, and small aggregates can be distinguished (Figure 98b, blue circles). The sample containing APP alone is translucent with a creamy color (Figure 98c). The combination between APP and CNTs leads to a black material (Figure 98d). Finally, combining OMPOSS and APP in the matrix still gives a translucent material, but qualitatively less than for APP alone, and similarly to OMPOSS alone, there are inhomogeneities (Figure 98e, blue circles).

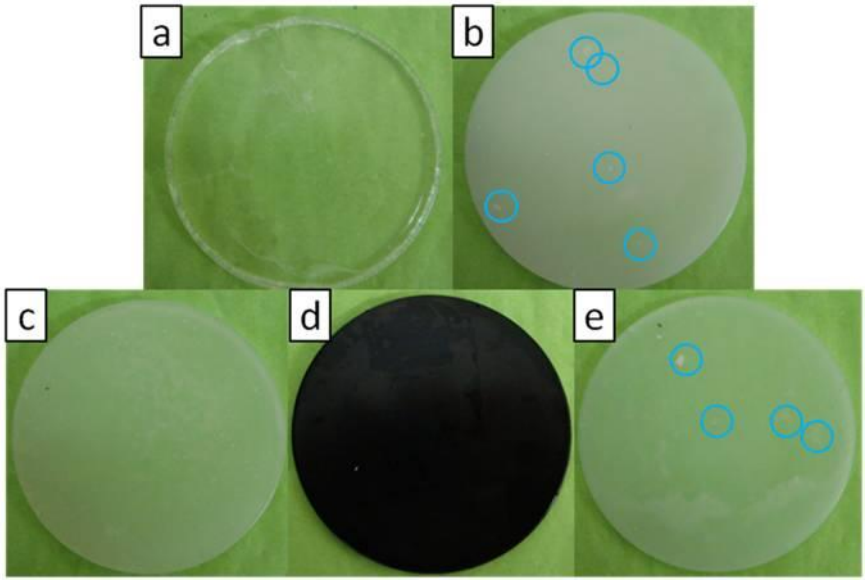

Figure 98: Pictures of epoxy formulations. a: Virgin epoxy, b: Epoxy_OMPOSS-5, c: Epoxy_APP-5, d: Epoxy_APP-4.5_CNT-0.5, e: Epoxy_APP-4_OMPOSS-1 (blue circles: aggregates)

It has been shown in the literature that the dispersion of fillers in a polymer matrix has a strong influence on the reaction to fire of thermoplastics. On the contrary, Chapter III has evidenced that in our case, it does not seem to be a critical parameter. However, since knowing the dispersion of fillers in a matrix might be helpful for understanding many phenomena, epoxy samples were observed by electronic microscopies.

Depending on the filler size, the five formulations were studied by Scanning Electron Microscopy (SEM) and some of them by Transmission Electron Microscopy (TEM). In fact, APP is a micrometric-sized filler with an average diameter of 15 µm [56]. Therefore, SEM is the best method for the observation of this filler in the matrix. On the contrary, nanofillers such as POSS and carbon nanotubes should be observed by TEM. Two parameters were particularly observed: the homogeneity of the dispersion in the whole matrix and the size of aggregates if present.

Figure 99 presents the unfilled resin, observed in order to study the texture of the resin itself. It reveals that there is no specific appearance of the resin. Small particles are distinguished at the surface of the specimen, but they are likely resin shards produced during the preparation of the sample or dust particles.

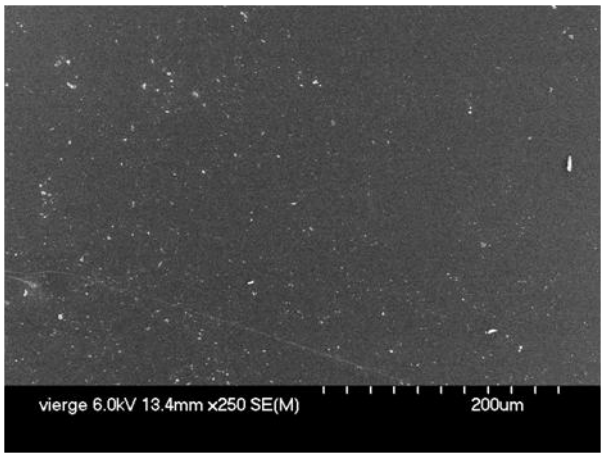

Figure 99: SEM image of Virgin epoxy

The dispersion of APP was then evaluated (Figure 100). SEM pictures show that APP is homogeneously dispersed in the matrix. The particles are also individualized, as their size lie around 20 µm (mean particle size of APP is about 15-20 µm). The white lines are attributed to micro-fractures occurring during the preparation of the samples and initiated by APP agglomerates which act as stress concentration centers.

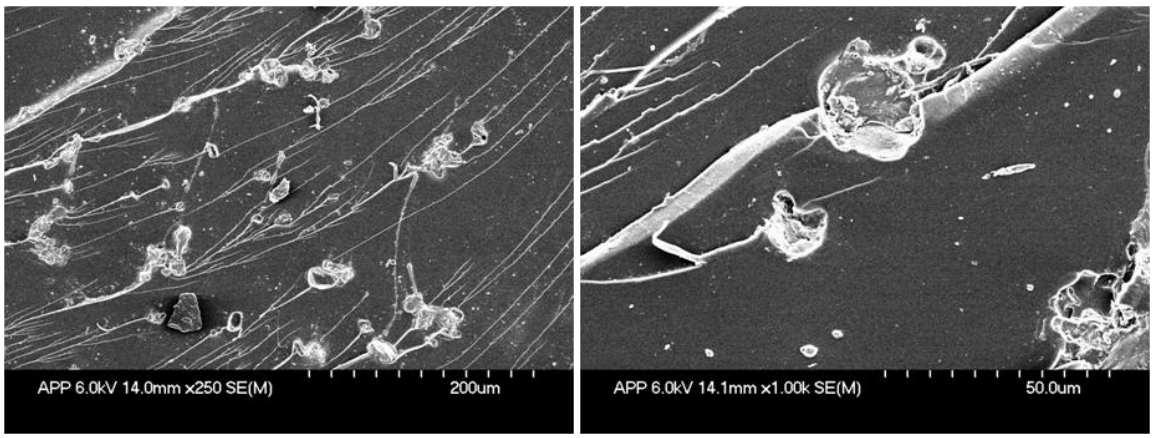

Figure 100: SEM images of Epoxy_APP-5

Combinations between micro- and nanofillers were then studied. First, the sample containing APP and OMPOSS was observed (Figure 101). In this case, SEM is used to evaluate the homogeneity of the dispersion. We can therefore see that the dispersion of APP in epoxy in the presence of POSS is very similar to that of APP alone. Very small particles with diameter of a few microns are evenly dispersed in the matrix. A closer look on this sample by TEM shows that they are POSS or grinded APP particles (Figure 102). Indeed, the morphology of the sample containing POSS alone has already been studied and discussed in Chapter III and the hypothesis that the aggregates observed on Figure

102 is supported by these previous observations of Epoxy_OMPOSS-5. The dispersion of POSS in the APP_OMPOSS-5 formulation is similar to that of OMPOSS alone. Small agglomerates (mean diameter: 0.5-1 µm) are evenly distributed in the whole sample.

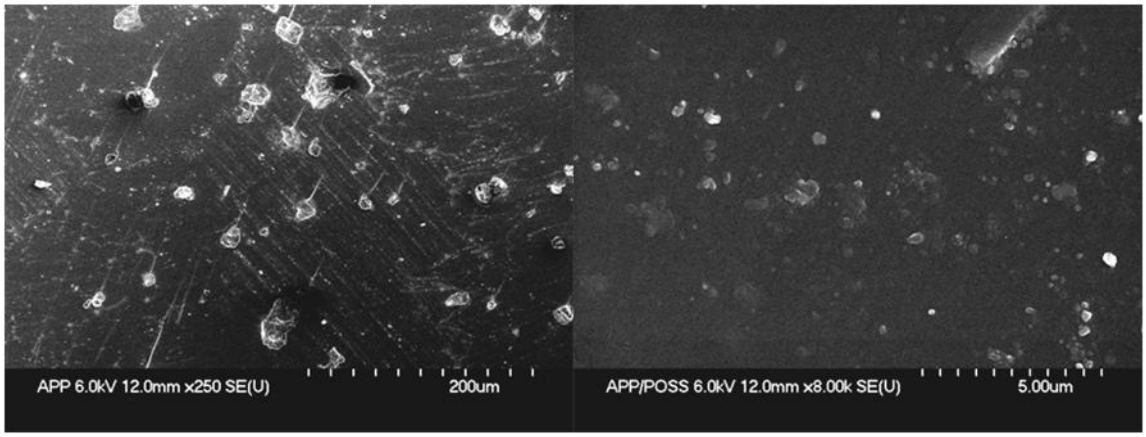

Figure 101: SEM image of Epoxy_APP-4_OMPOSS-1

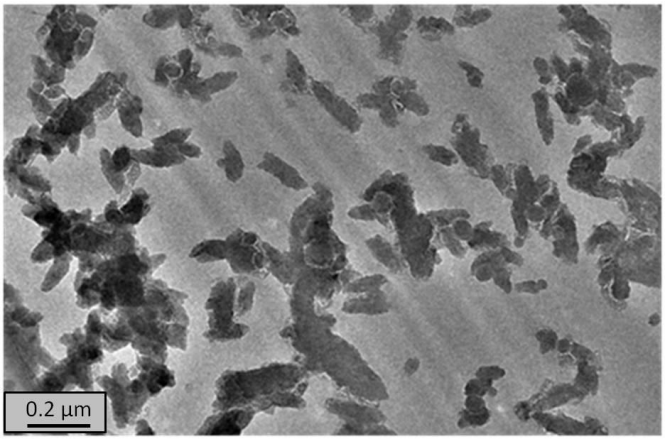

Figure 102: TEM image of Epoxy_APP-4_OMPOSS-1

Finally, the morphology of samples containing APP and CNTs was characterized. SEM pictures show that APP is homogeneously dispersed in the matrix, similarly to the sample containing APP alone (Figure 103). Areas with different texture (red arrows) are identified as CNT-rich areas (from the experience of the lab), as shown by larger magnifications. CNTs are not well dispersed in the matrix: some areas are completely free of them. Furthermore, holes in the matrix can be seen. They are likely due to the increase of viscosity of the uncured material (due to the presence of CNTs), which does not permit the easy release of gases produced during curing (blue circles).

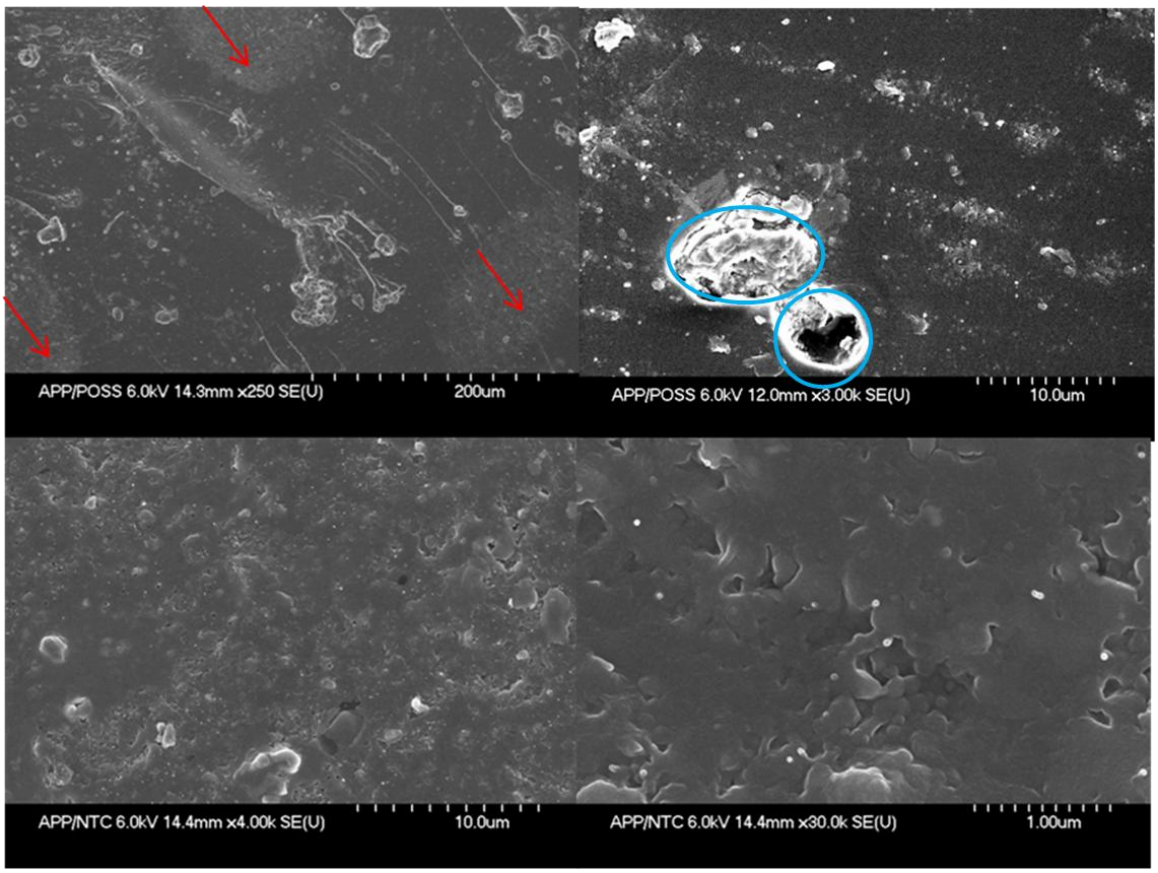

Figure 103: SEM images of Epoxy_APP-4.5_CNT-0.5 (red arrows: CNT-rich area, blue circles: holes)

A closer look on the dispersion of CNTs in the matrix is given by TEM (Figure 104). Apart from areas where no CNT is found, CNTs are packed in bundles and tightly entangled.

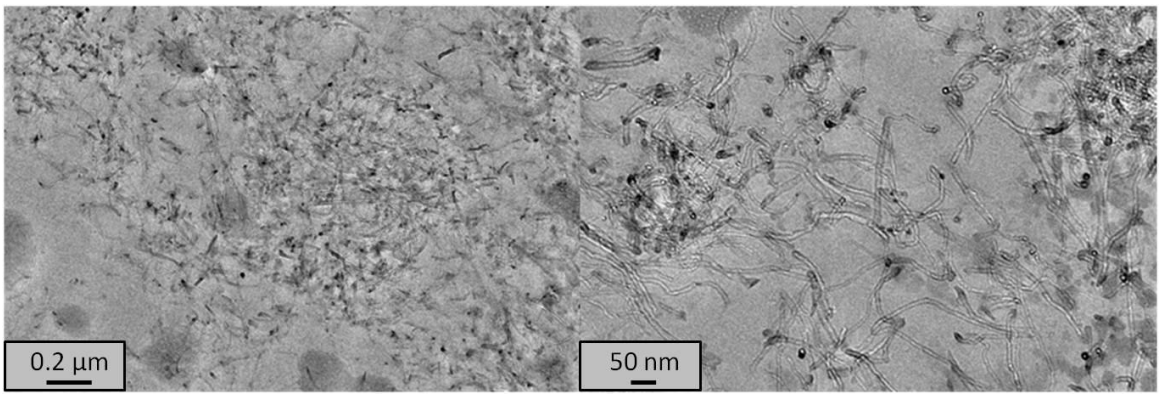

Figure 104: TEM images of Epoxy_APP-4.5_CNT-0.5

As a conclusion on the dispersion of fillers in the matrix, APP is rather homogeneously dispersed in epoxy, either alone or in combination with nanofillers. Furthermore, the size of APP particles corresponds to the specifications from the supplier, suggesting that the dispersion is good. Nanoparticles do not lead to similar

conclusions. The incorporation of OMPOSS in the matrix, either alone or not, produces a material with POSS everywhere in the matrix. Visual observation of the material shows that there are aggregates. Finally, the dispersion of CNTs in epoxy containing APP is inhomogeneous. Big areas containing no CNTs are easily found and CNTs bundles lie in the whole material. Furthermore, small holes can be found in the matrix. They may result from the increased viscosity of the uncured resin once CNTs are incorporated in it. During the curing, gases cannot be easily evacuated and could create holes in the final material.

IV.1.4. Thermal conductivity

Similarly to the analysis conducted in Chapter III, the thermal conductivity of the different formulations between 20 and 200 °C has been evaluated (Figure 105). The behaviors of Virgin epoxy and Epoxy _CNT-0.5 have already been commented in Chapter III, but are reminded here for comparison purpose. Below Tg, the thermal conductivity of virgin epoxy increases along with the temperature. Once the Tg is reached, it stabilizes and then begins to decreases at 200 °C, probably because of the onset of the degradation of the polymer: breaking of network certainly decrease phonon mobility causing the decrease of the thermal conductivity. Epoxy_APP-5 has a constantly increasing thermal conductivity, but it slows down above Tg. The higher conductivity values recorded for this sample may be linked to the crystallinity of APP. Indeed, phonons are better transmitted in geometrically regular and strong bonds. As an example, heat conductivity is higher in crystalline regions of polymers than in amorphous ones [157]. Therefore, phonons can be accelerated in APP particles, which would explain the higher thermal conductivity observed for Epoxy_APP-5. It should be noticed that the thermal conductivity still increases after the Tg for Epoxy_APP-5 whereas there is a stagnation for Virgin epoxy.

It has been shown in Chapter III that the thermal conductivity of Epoxy _CNT-0.5 slightly increases below the Tg, and is reduced thereafter. A recent publication reports the modification of the thermal conductivity by incorporation of CNTs in an epoxy matrix [161]. They observed a decrease of the thermal conductivity for a 1.6 vol.% content, and attributed it to the formation of CNTs bundles which limits phonon transfers at the

interface between the matrix and CNTs. Epoxy_APP-4.5_CNT-0.5 behaves closely to that of virgin epoxy and Epoxy _CNT-0.5. The presence of CNTs hides the effect of APP and the final composite behaves like Epoxy_CNT-0.5. The thermal conductivity is almost constant below Tg, it is higher at 150 °C, but a decrease similar as virgin epoxy follows. Concerning Epoxy_OMPOSS-5, the thermal conductivity increases constantly between 20 and 200 °C. It is close to Epoxy_APP-5 and Epoxy_APP-4.5_CNT-0.5 at 20 °C and has an intermediate behavior at 200 °C. Finally, the thermal conductivity of Epoxy_APP-4_OMPOSS-1 slightly increases between 20 °C and 50 °C and is constant thereafter.

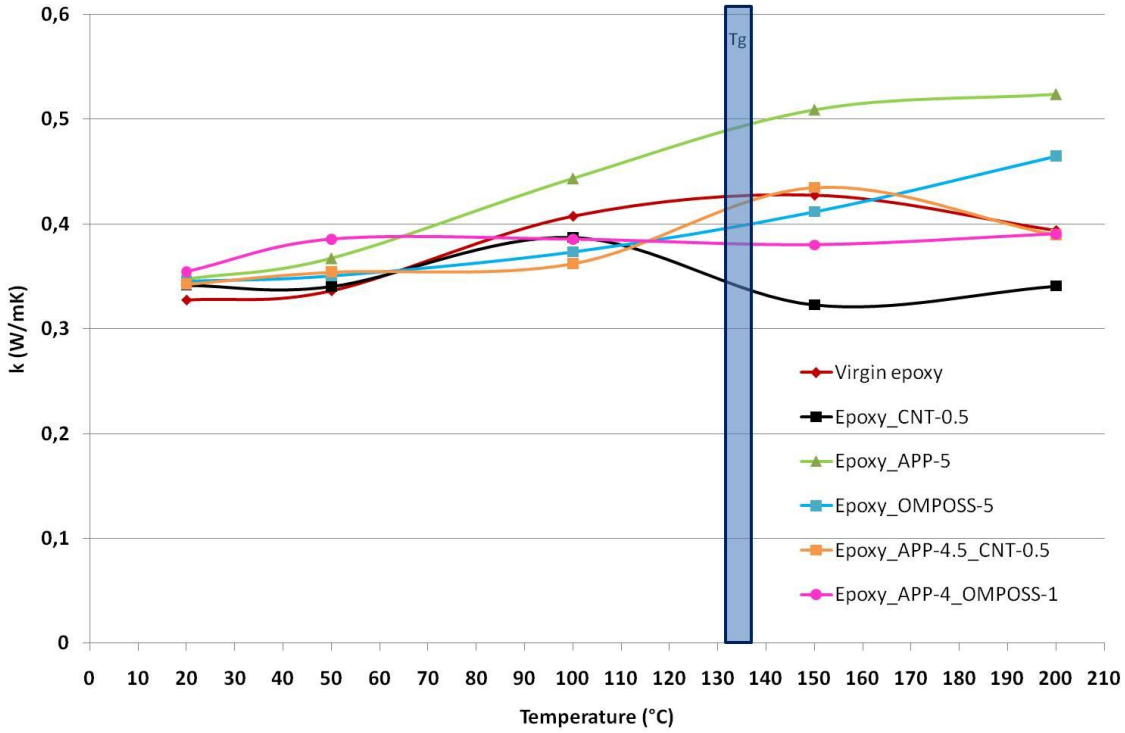

Figure 105: Thermal conductivity of epoxy formulations

Figure 106 shows the thermal diffusivity of the five epoxy formulations between 20 °C and 200 °C. It remains almost constant for virgin epoxy. Chapter III has shown that Epoxy _CNT-0.5 has a lower diffusivity, whatever the temperature. On the contrary, the thermal diffusivity of Epoxy_APP-5 is 2.5 to 3 times higher than that of virgin epoxy below the Tg, and almost twice as high above the Tg. The thermal diffusivity of Epoxy_APP-4.5_CNT-0.5 appears as a linear combination of those of Epoxy_APP-5 and Epoxy _CNT-0.5. However, the contribution of CNTs seems to hide that of APP. The thermal diffusivity of Epoxy_OMPOSS-5 remains almost constant up to 150 °C and

increases at 200 °C. Finally, Epoxy_APP-4_OMPOSS-1 has an intermediate behavior below the Tg, but the thermal diffusivity is closer to that of virgin epoxy at 200 °C.

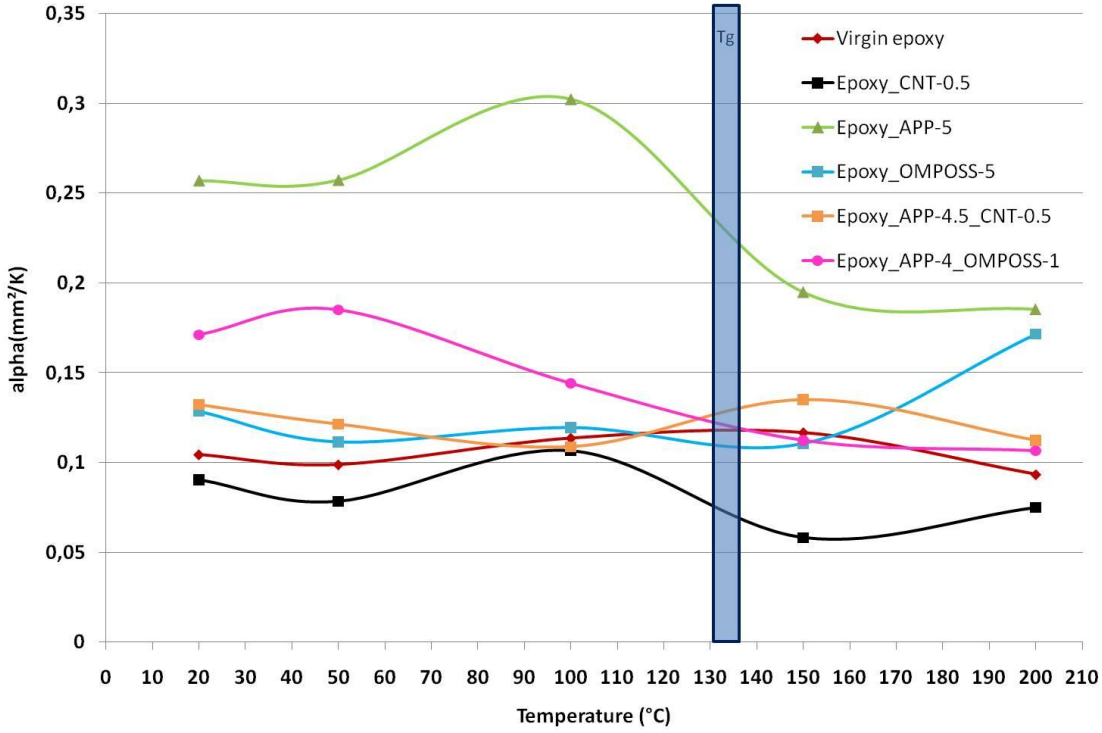

Figure 106: Thermal diffusivity of epoxy formulations

IV.1.5. Thermal stability

Figure 107 shows the TG curves in air of the different epoxy resin formulations. The weight loss of virgin epoxy occurs in two main apparent steps: a first one between 200 °C and 430 °C corresponding to a 60 % weight loss and a second one between 430 °C and 610 °C leading to the total weight loss of the resin. According to literature [162], the first step corresponds to the decomposition of the epoxy network which results in a transient char. This char is then oxidized and leads to a further weight loss corresponding to the second weight loss step. The incorporation of OMPOSS alone in this system slightly modifies this degradation path. The main weight loss step begins at lower temperatures (160 °C) and the intermediate residue is 20 wt.% lower than that of virgin epoxy. The maximum weight loss rate is however slightly shifted toward higher temperatures (from 355 °C for Virgin epoxy to 385 °C for Epoxy_OMPOSS-5). The thermal degradation of OMPOSS has been studied by Fina et al. [163] and Vannier et al. [61] and they have shown that this weight loss occurs in a single step between 200 and

350 °C and produces silica. Furthermore, an incomplete sublimation was also noticed. The residual weight is thus lower than that of Virgin epoxy after the first weight loss step. A second step similar to that of virgin epoxy occurs between 500 °C and 600 °C leading to the complete polymer weight loss.

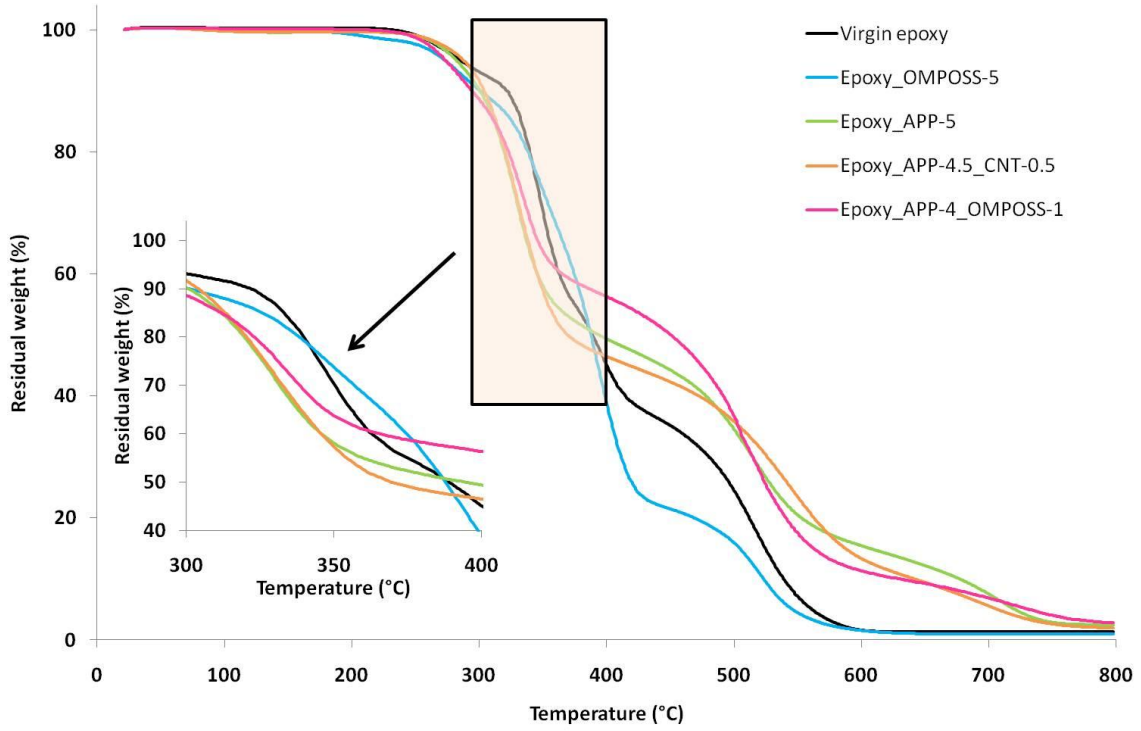

Figure 107: Experimental TGA curves under air of epoxy formulations (10°C/min)

When APP is incorporated into the resin, the main weight loss occurs at lower temperatures compared to the virgin epoxy: the maximum weight loss rate temperature is shifted down from 347 °C to 329 °C and the intermediate residue is 10 % higher than that of virgin epoxy. The weight loss between 460 °C and 600 °C remains but it does not lead to the complete weight loss of the resin. A more stable char (20 wt.% residue) is produced and an additional third step takes place between 580 and 750 °C. This step corresponds to the final weight loss of the char. The modifications of the thermal degradation of the Epoxy_APP 5 system due to the addition of CNTs or OMPOSS are also observed. Incorporation of CNTs does not have an important effect on the first weight loss step of Epoxy_APP 5, except that the intermediate residue is 5 % lower. The second weight loss step occurs at slightly higher temperatures and the residues during the last step are lower than that of Epoxy_APP 5. Concerning the incorporation of OMPOSS, the first weight loss step leads to a 10 % higher intermediate residue. The second weight

loss step occurs in the same temperature range as Epoxy_APP 5 and the residues are lower during the last degradation step.

Figure 108 shows the differences between the experimental TG curve and the calculated one for each filled epoxy.

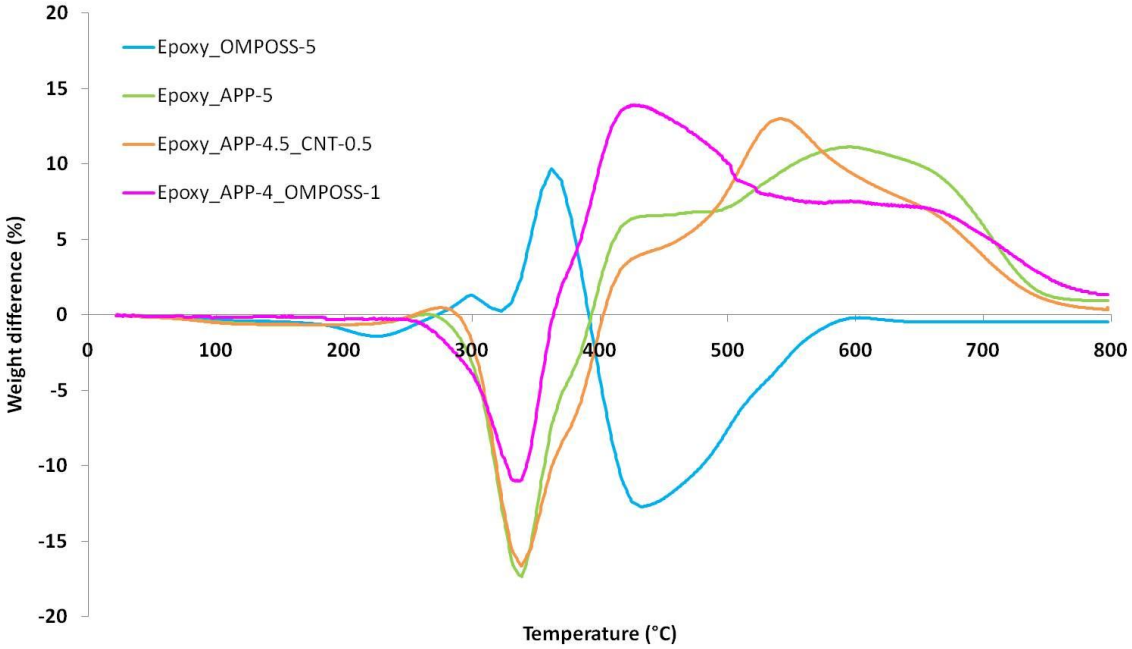

Figure 108: Difference weight curves between experimental and calculated TGA for epoxy formulations

When the filler is OMPOSS alone, the most important stabilization effect (10 %) occurs between 300 and 400 °C: the main weight loss step of the epoxy is limited by the presence of silica after decomposition of OMPOSS. However, this is a temporary effect the weight loss is faster than that of virgin epoxy between 400 and 600 °C. The incorporation of APP alone leads to different interactions. First, an important destabilization occurs between 250 and 400 °C. APP decomposes into phosphoric acid, which catalyzes the char formation [164]. Supporting this mechanism is the immediate two-step stabilization afterwards, between 400 and 700 °C. When CNTs are added to the Epoxy_APP-5 composite, the weight difference curve follows similar trends as for Epoxy_APP-5. The initial destabilization between 280 °C and 400 °C is the same but the following stabilization is slightly delayed. Therefore, it seems that CNTs disturb the char formation. Finally, incorporation of OMPOSS to Epoxy_APP-5 reveals a lower initial destabilization than for APP alone. Both this destabilization and the following stabilization are shifted towards lower temperatures: the destabilization is shifted respectively from 270 °C for Virgin Epoxy to 250 °C for Epoxy_APP-4_OMPOSS-1, and the

stabilization is shifted from 400 to 390 °C. Furthermore, the first stabilization step for Epoxy_APP 4_OMPOSS-1 is higher than the second one whereas it is the contrary for the two other intumescent formulations.

The thermal degradation of epoxy formulations was then studied under nitrogen (Figure 109). Indeed, during combustion phenomena, oxygen depletion occurs after a few moments. The study of the degradation of materials under pyrolysis is therefore useful. All samples degrade in a single main step. After it, the residual weight is not completely stabilized and a continuous mass loss occurs until the experiment ends at 800 °C. The main degradation for virgin epoxy is set at 353 °C, and the residue after this step reaches 35 wt.% (at 430 °C). However, a slower degradation occurs and only 14 wt.% remain at 800 °C. Epoxy_OMPOSS-5 degrades similarly. The maximum degradation is observed at 355 °C and the intermediate residue is lower than that for virgin epoxy (25 wt.% at 480 °C). On the contrary, the final residue is slightly higher (17 wt.%). The curves corresponding to intumescent systems are very similar. The main degradation occurs at 336 °C, 337 °C and 339 °C for Epoxy_APP-5, Epoxy_APP-4.5_CNT-0.5 and Epoxy_APP-4_OMPOSS-1 respectively and the intermediate residue lie between 20 and 24 wt.%.

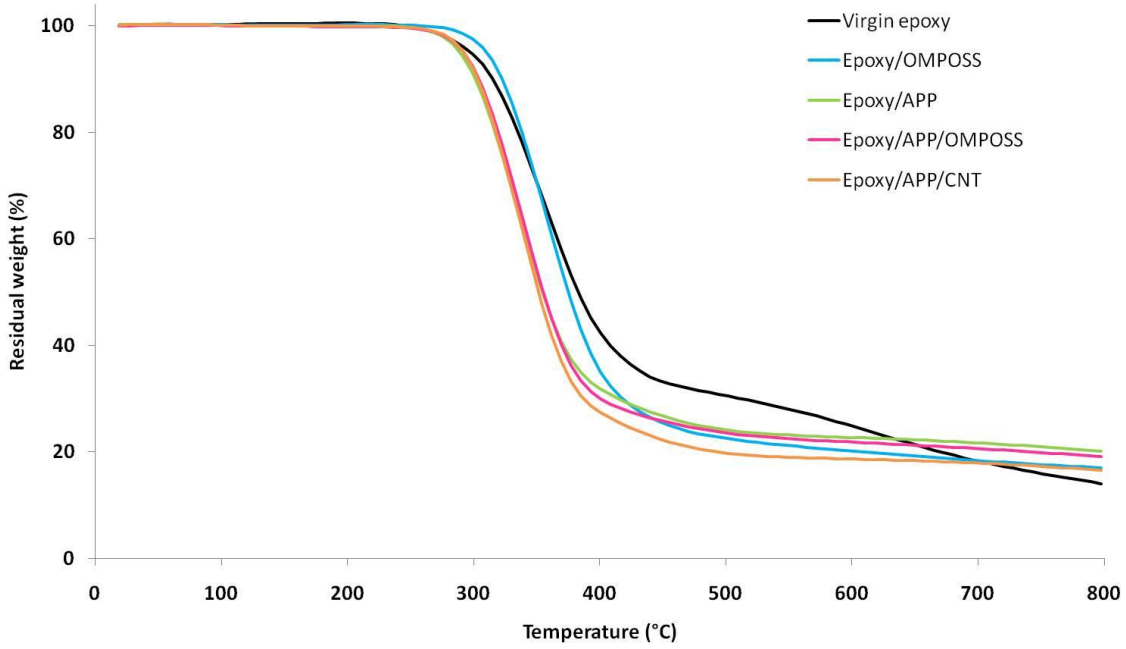

Figure 109: Experimental TGA curves under N_2 of epoxy formulations (10°C/min)

IV.2. REACTION TO FIRE

The previous part has established that there are differences in the thermal degradation of samples under air. Less difference are observed under nitrogen. The thermal conductivity and diffusivity are also affected by the presence of fillers. In this part, the reaction to fire will be assessed by mass-loss calorimetry on samples having two different thicknesses (2.5 and 5 mm, more details p.180) and by pyrolysis-flow combustion calorimetry.

IV.2.1. Mass-loss calorimetry

IV.2.1.a. Mass-loss calorimetry with thick samples

First, the reaction to fire of the different formulations was tested by mass-loss calorimetry. HRR as a function of time of virgin epoxy and of the fire-retardant formulations are presented in Figure 110 and Table 22. The incorporation of 5 wt.% APP in epoxy leads to a 50 % decrease of pHRR. OMPOSS at 5 wt.% exhibits a pHRR decreased by 46 % compared to virgin epoxy. When combining APP and OMPOSS, a synergistic effect providing a 68 % decrease of pHRR is shown. HRR does not go back to zero for this samples, since a stable intumescent sample is produced and blocks the chimney (as a result, there is accumulation of heat in the chimney and the thermocouples giving HRR measurements are not cooled down). On the contrary, the combination between APP and CNTs leads to an antagonism since only a 28 % pHRR decrease is observed (pHRR is higher than that of Epoxy_APP-5 and close to that of Epoxy_CNT-0.5).

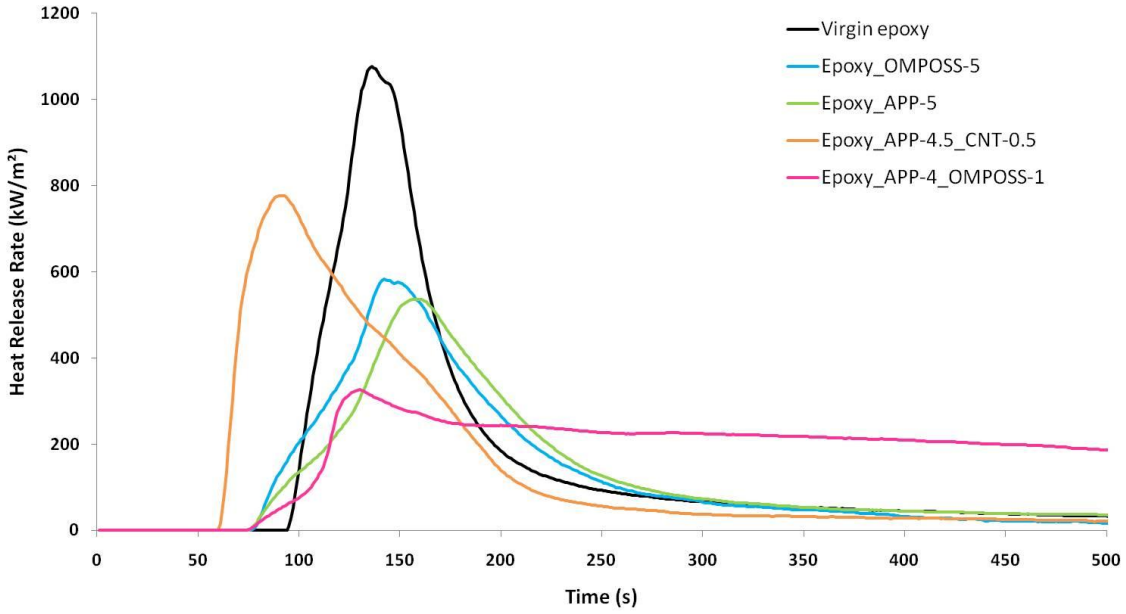

Figure 110: Heat release rate versus time for epoxy formulations (Heat flux: 35 kW/m², thickness: 5 mm, distance: 25 mm)

The time to ignition is also affected by the incorporation of flame retardants: compared to virgin epoxy (94 s), the ignition occurs earlier for each filled formulation. It is similar for Epoxy_APP-5 and Epoxy_APP-4_OMPOSS-1 (75 s compared to 94 s for virgin epoxy) and slightly shorter for Epoxy_OMPOSS-5 (67 s). The time to ignition is drastically shortened (55 s) for Epoxy_APP-4.5_CNT-0.5 compared to virgin epoxy. It is noteworthy that in the particular case of polymers containing CNTs, this behavior has already been commented [83]. The black color of the sample containing CNTs (higher absorption compared to the others) suggests the possibility of an increased absorption of the radiant heat at the beginning of the mass-loss calorimeter experiment (the other samples are either white or translucent before blackening). Therefore, the sample containing CNTs can absorb more quickly the radiant heat, leading to accumulation of heat at the surface and then to a faster ignition because the sample reaches its temperature to ignition faster. This is in accordance with the conclusions drawn with the observations on thermal diffusivity in the first part of this chapter. The presence of CNTs bundles limits the circulation of phonons that are blocked in the bundles, leading to a located heat rise. These areas act as defects: they degrade and release fuels early.

Table 22: Mass-loss calorimeter main parameters for epoxy formulations (Heat flux: 35 kW/m², thickness: 5 mm, distance: 25 mm)(*unavailable because of excessive foaming)

Formulation	t_{ign} (s)	pHRR (kW/m²) (% reduction)	THR (MJ/m²) (% reduction)	Residual weight (wt.%)
Virgin epoxy	94	1077	79	0
Epoxy_OMPOSS-5	67	582 (-46)	63 (-20)	0
Epoxy_APP-5	75	536 (-50)	63 (-20)	19
Epoxy_APP-4.5_CNT-0.5	55	776 (-28)	76 (-4)	8
Epoxy_APP-4_OMPOSS-1	75	326 (-68)	90 (*)	21

Regarding the total heat release (THR) (Table 22), it is decreased by 20 % when APP or OMPOSS are incorporated alone in the resin. The combination between APP and CNTs leaves the THR almost unmodified compared to virgin epoxy (-4 %), confirming the antagonism observed on the pHRR. Finally, the value for Epoxy_APP-4_OMPOSS-1 formulation cannot be used: this sample produces a very stable and intumescent char that hinders the ventilation in the mass-loss chimney and causes a heat accumulation in the system (HRR values cannot come back to zero avoiding the calculation of THR).

The morphology of the residues after mass-loss experiment should give indications on the fire retardant behavior (Figure 111).

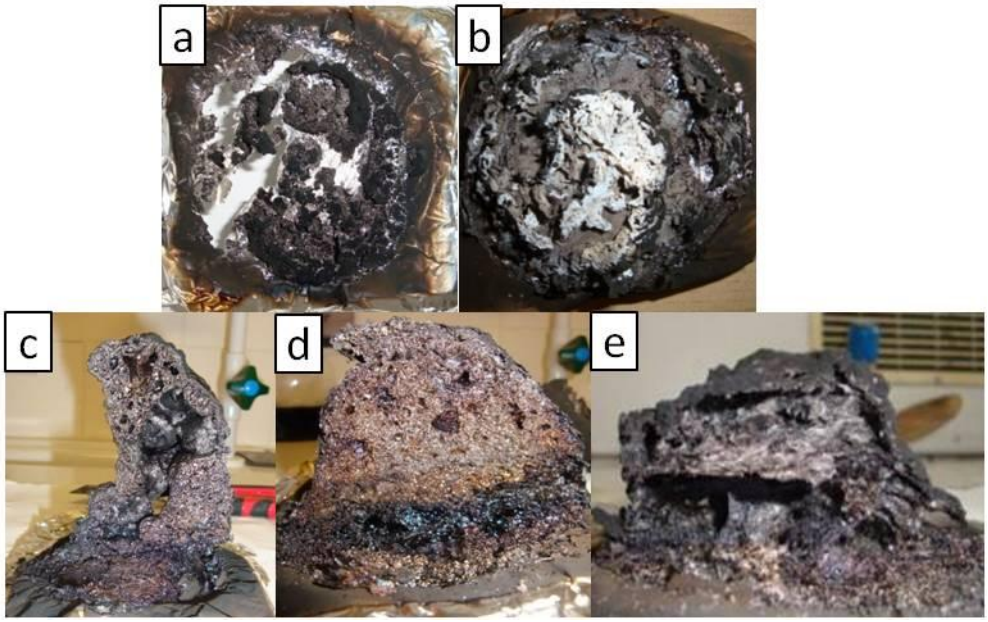

Figure 111: Pictures of the chars obtained after mass-loss calorimeter test - a: virgin (top view), b: Epoxy_ OMPOSS-5 (top view), c: Epoxy_APP-5 (cross-section), d: Epoxy_APP-4_OMPOSS-1 (cross-section), e: Epoxy_APP-4.5_CNT-0.5 (cross-section) (Heat flux: 35 kW/m², thickness: 5 mm, distance: 25 mm)

While virgin epoxy leaves almost no residue (the white in the background is part of the insulating sample holder), incorporation of 5 wt.% OMPOSS produces a fragile residue made of very thin gray-white layers (probably constituted of silica coming from the degradation of POSS [163]). APP-based formulations provide an intumescent phenomenon (formation of an expanded char). However, the addition of OMPOSS or CNTs in combination with APP drastically changes the final residue. The sample containing 5 wt.% APP produces a high char (height = 63 mm compared to 5 mm before the experiment, i.e. 1160 % expansion), with important voids inside. In this case, the char structure is not resistant enough: cracks at different locations are formed probably because of the evolving gas flow. When APP is partly substituted by OMPOSS, the residue is smaller (height = 41 mm i.e. 720 % expansion). In this case, the char seems to be more resistant and only small cracks can be distinguished in the middle of small bubbles distribution. Furthermore, two areas are easily distinguished: the lower area is black whereas the upper one is filled with bubbles and has a metallic appearance. In the particular case of hydrogen-POSS and OMPOSS, Fina et al. have shown that sublimation occurs during thermal degradation in addition to the formation of the silica layer [163]. It suggests that POSS sublimates during the polymer burning and it is trapped and condensed in the residue. This phenomenon would explain the presence of the upper area full of bubbles and the black area probably constituted of residual polymer. The formation of metallic carbon during carbonization has already been observed [165] and may be the cause of the metallic glints of the upper area. During the carbonization process, radical carbons are created in important quantities and this could make the char conductive. Finally, when CNTs partly substitute APP, the residue is slightly smaller (height = 35 mm i.e. 600 % expansion). Very large and easily breakable cells are created. Furthermore, very small holes can be distinguished at the top surface of the specimen.

Weight loss of the samples was also recorded during the mass-loss experiments (Figure 112 and Table 22).

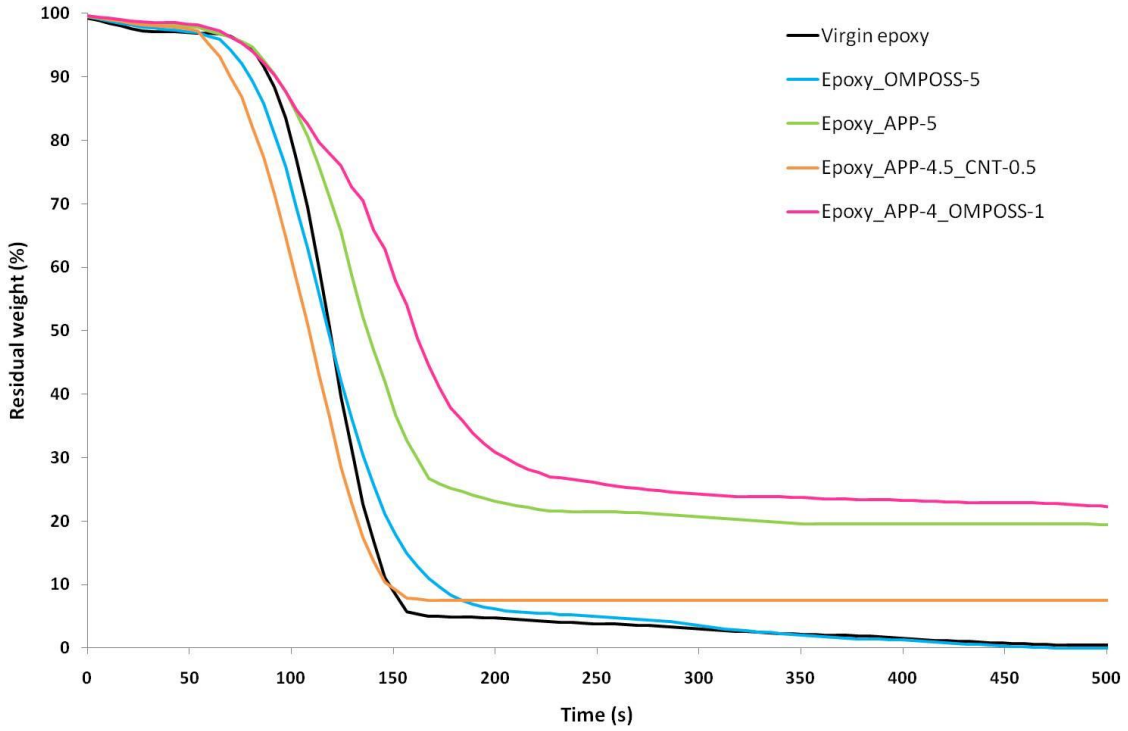

Figure 112: Residual weight versus time for epoxy formulations ((Heat flux: 35 kW/m², thickness: 5 mm, distance: 25 mm)

Virgin epoxy degrades in a fast single step. The sample containing 5 wt.% OMPOSS degrades quicker than virgin epoxy between 60 and 130 s and the degradation rate is decreased thereafter until 200 s. This is consistent with the generally accepted way of action of POSS: during the burning of the sample, a ceramic layer is formed which protects the material from further degradation [63, 65, 67, 163]. In the case of epoxy containing OMPOSS, this layer does not seem to be efficient enough since the degradation continues until the end of the experiment at lower rate. The incorporation of APP (5 wt.%) in epoxy clearly increases the residual weight. The initial mass loss (before 60 s) is similar for all specimens but it is reduced thereafter for Epoxy_APP-5 and Epoxy_APP-4_OMPOSS-1. The mass of the final residue is relatively high (19 wt.%) for Epoxy_APP-5, showing further that the produced intumescent char is able to limit the polymer degradation and subsequently its weight loss. Similar observations can be done for the combination between APP and POSS. However, it is noteworthy that the main degradation step is delayed compared to APP alone (25 s shifting towards higher times). On the contrary, the results obtained for the combination between APP and CNTs confirm the negative interaction between these two particles. The degradation begins

earlier compared to virgin epoxy. This result supports the aforementioned hypothesis concerning the possibly modified heat absorption for samples containing CNTs. The final residue is higher than for non-filled epoxy (7.5 wt.%), but it consists mainly of a hollow structure providing limited protection.

IV.2.1.b. Mass-loss calorimeter with thin samples

In order to further test the efficiency of the better protection provided by the combination between APP and OMPOSS and to avoid the blocking of the chimney by the char produced, the same experiments were conducted with thinner samples. Instead of samples 5 mm thick, the additional ones are 2.5 mm thick. The Heat Release Rate as well as the residual weight were recorded as a function of time. Figure 113 and Table 23 show the fire-retardant performances of the different epoxy formulations. All formulations are characterized by a single peak of HRR. It reaches 813 kW/m² for virgin epoxy. The incorporation of 5 wt.% OMPOSS in the matrix has a very limited effect since the pHRR is only decreased by 10 %. Since this value lies within the error margins, OMPOSS does not have a significant fire retardant effect on the epoxy for thin samples.

Concerning intumescent systems, epoxy containing 5 wt.% APP exhibits a pHRR decreased by 31 % compared to virgin epoxy. The reduced flame-retardant performance compared to that shown in thick samples (i.e. -50 %) can be explained by the same phenomenon as above. In order to insulate the underlying polymer, the protective layer needs to be thick enough. Because of this, less polymer is protected in thin samples and the flame-retardant effects are not so strong. Combinations between APP and nanoparticles were also evaluated. Mixing CNTs and APP still leads to an antagonism (28 % pHRR decrease), although it is limited compared to thick samples. On the contrary, Epoxy_APP 4_OMPOSS 1 provides interesting properties since the pHRR is decreased by 50 % compared to virgin epoxy, therefore showing the best results.

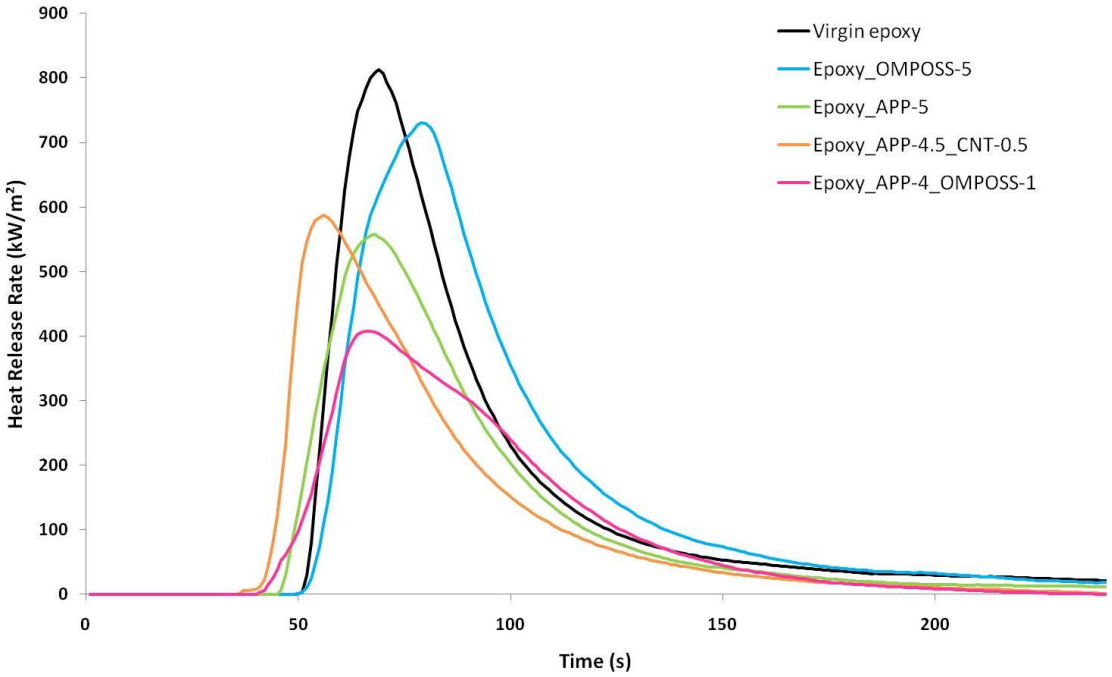

Figure 113: Heat release rate as a function of time for thin epoxy formulations (Heat flux: 35 kW/m², thickness: 2.5 mm, distance: 25 mm)

The time to ignition is also influenced by the incorporation of flame retardants in the epoxy (Figure 113 and Table 23). Virgin epoxy ignites after 49 s. TTI for samples containing APP or OMPOSS alone lies in the same range (46 and 50 s) respectively. On the contrary, it is significantly reduced for the combinations between APP and nanoparticles. The presence of CNTs leads to the fastest ignition (37 s), followed by APP/OMPOSS (41 s).

Table 23: Mass-loss calorimeter main parameters for thin epoxy formulations (Heat flux: 35 kW/m², thickness: 2.5 mm, distance: 25 mm)

Formulation	tign (s)	pHRR (kW/m²) (% reduction)	THR (MJ/m²) (% reduction)	Residual weight (wt.%)
Virgin epoxy	49	813	33	4
Epoxy_OMPOSS-5	50	731 (-10)	36 (+9)	3
Epoxy_APP-5	46	557 (-31)	26 (-21)	12
Epoxy_APP-4.5_CNT-0.5	37	587 (-28)	25 (-24)	8
Epoxy_APP-4_OMPOSS-1	41	408 (-50)	23 (-30)	15

Figure 114 and Table 23 shows the Total Heat Released (THR) as a function of time for thin epoxy formulations. Thanks to lower amount of polymer with thin samples, no blocking of the extracting chimney occurred and the calculation of THR was therefore

possible. The THR for virgin epoxy reaches 33 MJ/m². Confirming its limited interest for the flame retardancy of thin samples, incorporation of OMPOSS alone increases this value up to 36 MJ/m² (+9 %). Intumescent systems lower it. Indeed, APP and APP/CNTs give similar results with 26 and 24 MJ/m² respectively (21 and 24 % decrease) and APP/OMPOSS further decrease it by 30 %.

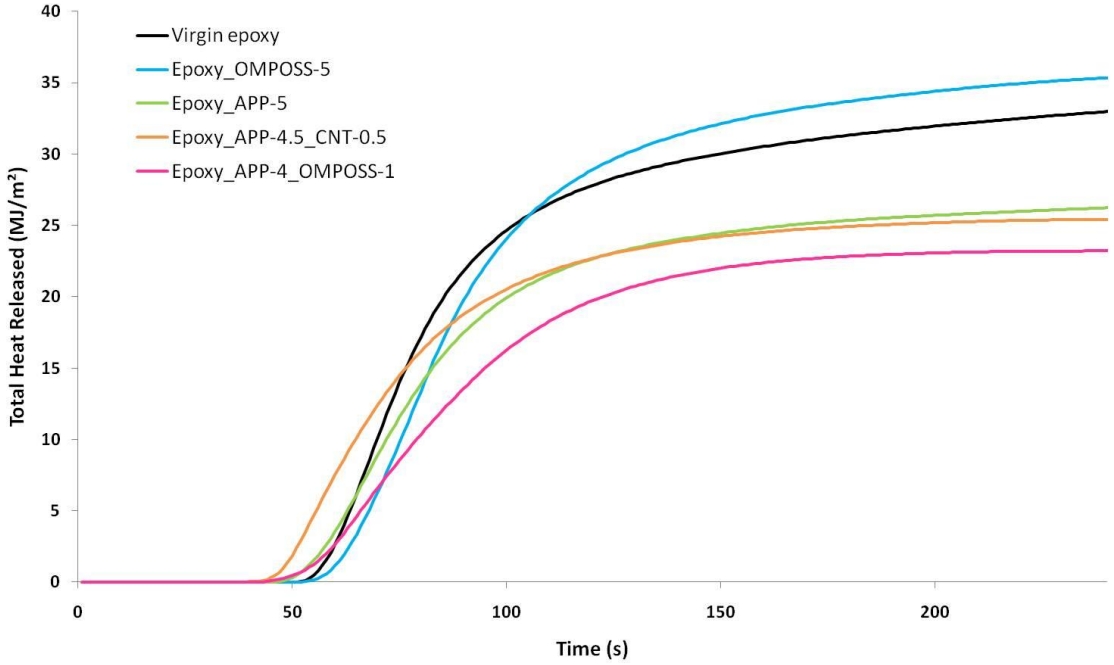

Figure 114: Total Heat Released as a function of time for thin epoxy formulations (Heat flux: 35 kW/m², thickness: 2.5 mm, distance: 25 mm)

Finally, the residual weight was recorded as a function of time (Figure 115 and Table 23). All samples degrade in a single step. Before ignition (i.e. before 49 s), virgin epoxy keeps more than 95 wt.% of its initial weight. Then, burning leads to the very quick degradation of the resin, and between 50 s and 80 s, 87 wt.% of the sample are lost. The remaining and non-cohesive residue is then slowly degraded. The final residue amounts to 4 wt.%. The sample containing OMPOSS has a similar behavior. 95 wt.% of the sample are intact before ignition, which occurs at 50 s. At 90 s, only 8 wt.% of the sample remains. Therefore, the main weight loss is extended to a slightly longer period, but the final residue is very similar (3 wt.%). This further shows the limited interest of OMPOSS alone as a flame-retardant for thin epoxy samples.

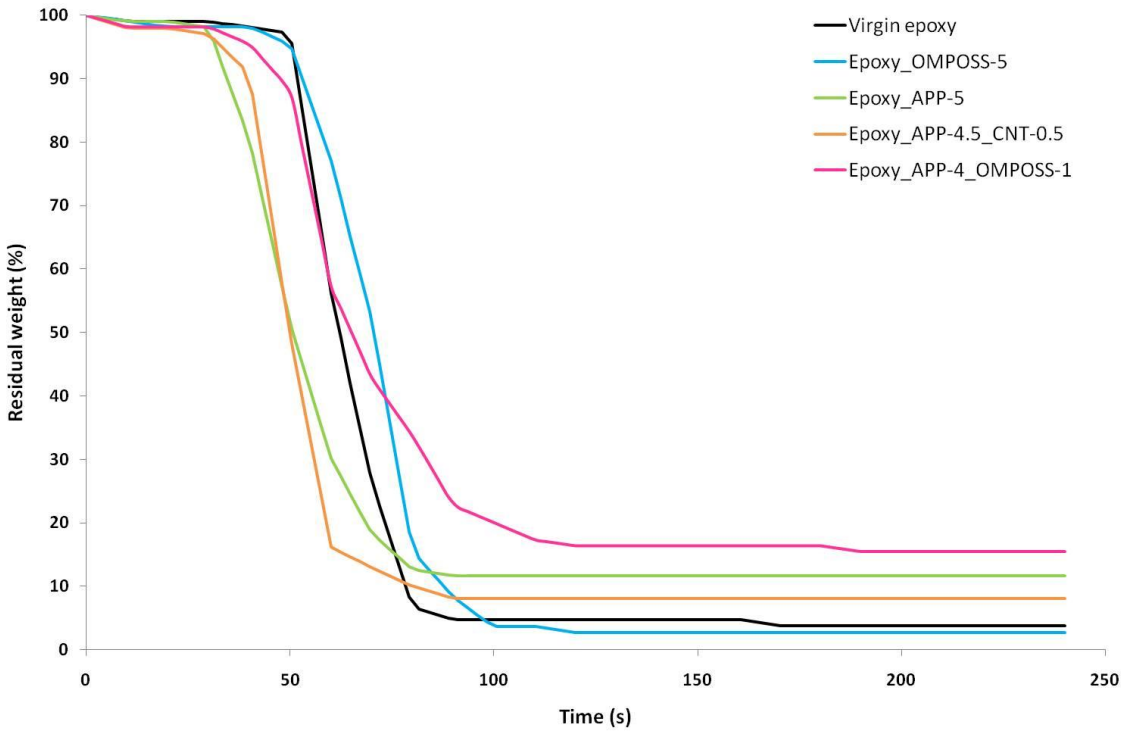

Figure 115: Residual weight versus time for thin epoxy formulations (Heat flux: 35 kW/m², thickness: 2.5 mm, distance: 25 mm)

Intumescent systems begin to degrade earlier, but they do so as to stabilize the system at the end. The sample containing APP alone begins to lose weight before ignition: 90 wt.% of the specimen remain at 35 s, but the ignition occurs only at 46 s (ammonia is released during the degradation of APP and is not flammable). At this time, the sample keeps only 64 wt.% of its initial weight. Shortly after 50 s, the system stabilizes, the weight loss slows down and the final residue reaches 12 wt.%. The curve corresponding to APP/CNTs is very similar, except that the ignition (37 s) and the beginning of the degradation occur simultaneously. From that point of view, this system behaves similarly to virgin epoxy or Epoxy_OMPOSS 5. However, the final residue is higher (8 wt.%). This is another evidence of disturbances induced by CNTs in the intumescent system.

Finally, the sample containing both APP and OMPOSS loses its weight later. It ignites at 41 s, when 95 wt.% of the sample remains. Then, the weight is lost very slowly: at 90 s, when the other samples lie between 5 and 12 wt.%, APP/OMPOSS still has 22 wt.% left. The final residue is also higher (15 wt.%). This fact further shows the interest of the incorporation of OMPOSS in Epoxy_APP 5.

As a first conclusion on the fire properties of the epoxy formulations, the use of OMPOSS alone seems beneficial when samples are thick, but the interest is much more limited for thin samples. This can be linked to the efficiency of the protective silica layer created on top of the specimen during burning. It has to be thick enough and in the case of thin samples, this can only be achieved when an important part of the polymer has already burnt. Intumescent systems give promising results. Their flame-retardant effect is reduced when thin samples are tested instead of thicker ones, but they still provide interesting properties. Combinations between APP and nanoparticles show how important the nature of the nanofiller is. CNTs lead to an antagonism, whereas OMPOSS provides a synergy.

IV.2.2. Pyrolysis Combustion Flow Calorimetry (PCFC)

The heat released by the burning of combustible compounds and the temperatures at which they are released can be evaluated by PCFC. In our case, this is very helpful for determining if a flame retardant modifies the degradation pathway towards less flammable species or acts through a condensed phase mechanism. As an example, it cannot be used for assessing the reaction to fire of intumescent systems, since the sample size does not allow the formation of a protective layer (samples are grinded and weight around 5 mg). Only one main step is observed for all samples in the conditions of the experiment (high heating rate compared to TGA) (Figure 116 and Table 24).

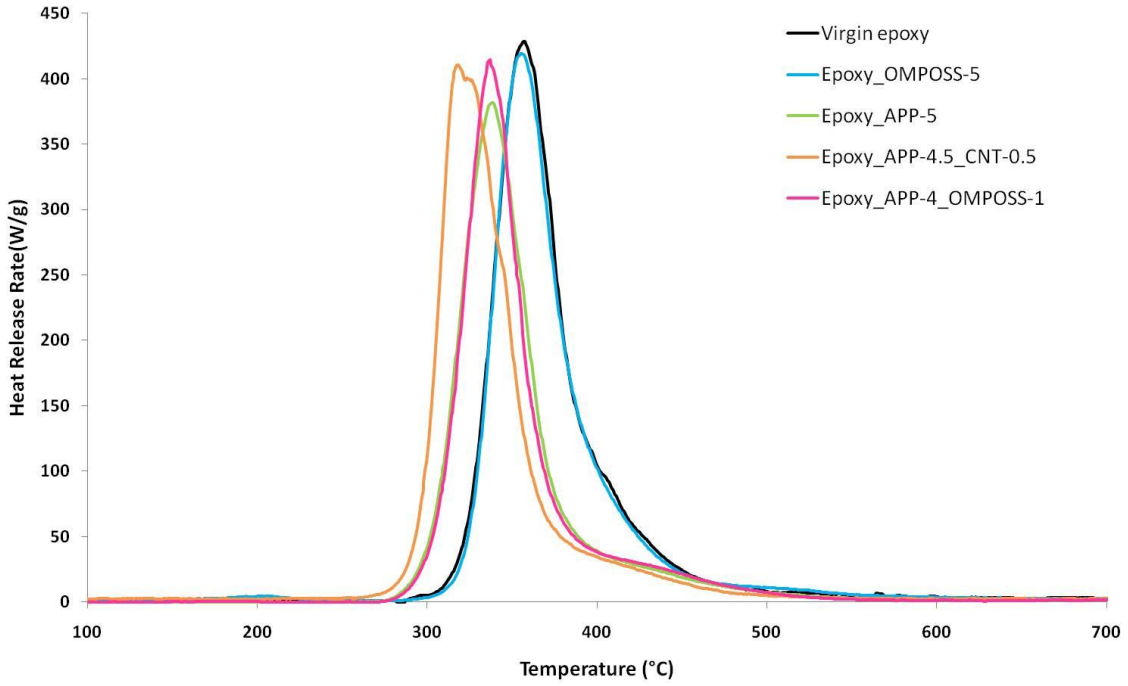

Figure 116: PCFC Heat Release Rate as a function of temperature (Heating rate: 1°C/s)

The curves are very similar for virgin epoxy and Epoxy_OMPOSS-5. The pHRR occurs at 357 °C and 355 °C and reaches respectively 428 and 419 W/g. Incorporation of APP alone slightly reduces the pHRR (381 W/g, -11 %), and the degradation occurs at lower temperatures (337 °C) (Table 24). The combination between APP and POSS does not improve the reduction observed with APP alone, and moreover, the pHRR reaches 414 W/g for APP/POSS (3 % reduction compared to virgin epoxy) at the same temperature as APP alone. Finally, the negative aspects of the partial substitution of APP by CNTs are once more observed: the pHRR reaches 410 W/g (-4 %) and occurs at the lowest temperature among all samples: 318 °C.

Table 24: PCFC main parameters for epoxy formulations (Heating rate: 1°C/s)

Formulation	pHRR (W/g) (% reduction)	Temp.@pHRR (°C)
Virgin Epoxy	428	357
Epoxy_OMPOSS-5	419 (-2)	355
Epoxy _APP-5	381 (-11)	337
Epoxy_APP-4.5_CNT-0.5	410 (-4)	318
Epoxy_APP-4_OMPOSS-5	414 (-3)	337

Therefore, the heat released during these experiments is slightly reduced when APP is incorporated in virgin epoxy. The partial substitution of APP by OMPOSS, which exhibit

an important positive effect in mass-loss calorimetry, does not lead to such results with the PCFC. The pHRR is higher with Epoxy_APP-4_OMPOSS-1 than with Epoxy_APP-5, but it is released at the same temperature range. Indeed, methyl groups at the corners of POSS can contribute to the heat release since they are organic. The pHRR for Epoxy_APP-4.5_CNT-0.5, which showed an antagonism with APP by mass-loss calorimetry, is also higher than for Epoxy_APP-5. Furthermore, it occurs at lower temperature for the material containing CNTs and APP than for others. Therefore, there is no relationship between the behavior of these materials in both fire tests [166]. This has already been established by various authors. Such results are supporting the hypothesis that the main action mechanism of the different systems takes place in the condensed phase. On the contrary, the results reported by Wang et al. [4] showed a synergism between a phosphorus-modified resin and octavinylPOSS measured by PCFC. In that case, the octavinylPOSS more likely reinforces the established gas-phase action of the phosphorus modifier and so, it explains why HRR measured by PCFC is reduced (less fuel to burn) [103].

IV.3. CONCLUSION

Formulations containing micro and nanofillers, either alone or in combination have been tested in terms of reaction to fire. Mass-loss calorimetry reveals that OMPOSS alone is efficient when the samples are thick enough, but are less interesting otherwise. APP is also affected by the geometry of the sample, but it is still a good fire-retardant for our thin formulations. Combining this microfiller with CNTs does not provide any improvement, whereas the use of APP/OMPOSS is highly beneficial to the system. These results are not correlated to those obtained by pyrolysis flow combustion calorimetry. The morphology of the samples was characterized before ignition in terms of dispersion, curing degree and glass transition temperature. These analyses, associated to the assessment of the thermal stability, do not provide answers on the origins of the observed reaction to fire. Why are this synergy between APP and OMPOSS , and the antagonism between APP and CNTs created ? The next chapter investigates these phenomena by analyzing the composition of the system at different key moments and also by studying how the protection is developed.

Chapter V - Protection mechanisms involved in the reaction to fire

Chapter IV has evidenced that combining micro- and nanofillers in an epoxy resin has different effects on the enhancement of the reaction to fire of these materials depending on the nanoparticle type. In particular, APP is an efficient flame-retardant which acts through an intumescent mechanism and its combination with CNTs or OMPOSS drastically changes the reaction to fire of epoxy. In the presence of APP and OMPOSS, an impressive intumescent structure is created and a synergy is observed in terms of mass-loss calorimetry. On the contrary, the incorporation of CNTs together with APP in the epoxy provides a residue that is less-structured than that of Epoxy_APP-5. The mass-loss calorimetry performance is subsequently deteriorated. The use of thermogravimetric analyses in thermo-oxidative and pyrolytic conditions may help to understand the interactions between the fillers. In the case of the studied formulations, few differences have been observed in nitrogen, whereas more important interactions have been evidenced under air. In particular, the amount of transient residue is different for Epoxy_APP-5, Epoxy_APP-4.5_CNT-0.5 and Epoxy_APP-4_OMPOSS-1. These observations are not sufficient for understanding the whole protection mechanisms. Therefore, this chapter is devoted to an in-depth study of different parameters that influence the development of intumescence. First, since this protection acts through a condensed phase mechanism, the aspect of the residues will be observed at different times of mass-loss calorimetry experiment. Since the thermogravimetric analyses in thermo-oxidative conditions were different depending on the formulation, the composition of the system will be assessed by solid-state NMR on residues in order to detect the creation of any additional species. Then, another side of intumescent systems will then be evaluated. Indeed, developing an efficient protective structure is also a matter of good synchronization between different phenomena. Therefore, in the second part of this chapter, parameters such as apparent viscosity as a function of temperature or swelling capability and temperatures inside the samples during fire testing will be recorded. A general overview for all of these results for each formulation will be given. Finally, mechanisms of action will be proposed.

V.1. COMPOSITION AND ASPECT OF FORMULATIONS ALONG TIME: SNAPSHOTS

In this part, mass-loss calorimetry experiments were stopped at characteristic times of the HRR curve. The chosen times are “just before ignition”, “at pHRR” and “at 500 s”, corresponding to the end of the experiment. For intumescent specimens, experiments were also stopped “during swelling”. First, the general aspect of these residues will be described. Further analyses will be conducted by digital microscopy and electron-probe microanalysis in order to compare the repartition of voids and phosphorus in the final intumescent residues. Then, the composition of these residues will be characterized by solid-state NMR. Finally, a conclusion on the analysis of these residues will be drawn.

Establishing the absence of gas-phase action is useful: intumescence is a well-known condensed-phase phenomenon but the developed systems are completely new. Therefore, in order to eliminate any doubt on the possibility of a gas-phase action, gases evolved during the thermal degradation of epoxy formulations were analyzed by FTIR but no difference was observed between the formulations by this method (results not shown). In the following section, only condensed-phase phenomena will therefore be considered.

V.1.1. Residues aspect

Samples removed from the heat source just before ignition are blackened but inhomogeneously deteriorated (Figure 117). No further description and no NMR analysis were therefore carried out on them.

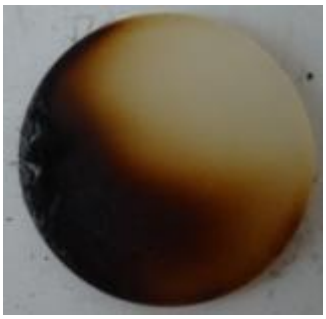

Figure 117: Epoxy_APP-5 sample before ignition

Virgin epoxy

Pictures of the residues of Virgin epoxy at pHRR and 500 s are shown in Figure 118. At pHRR, as a char-forming polymer, part of the epoxy is swollen into a black and cohesive residue. However, an important area of the material has been completely degraded, and the underlying aluminium foil is even destroyed. The residue after 500 s shows the foil only partially covered by a thin black powder.

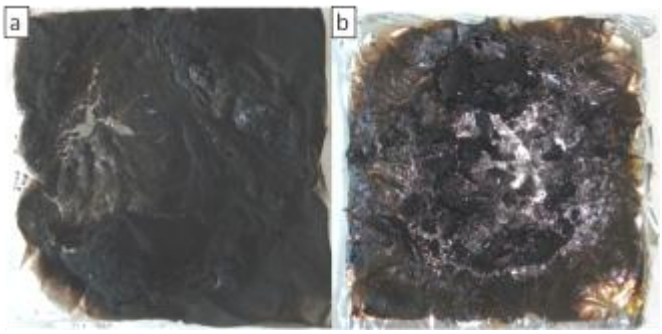

Figure 118: Virgin epoxy residues during mass-loss calorimeter experiments (a: at pHRR, b: 500 s)

Epoxy/OMPOSS

The morphology of Epoxy_OMPOSS-5 residue at pHRR and at 500 s is shown in Figure 119. At pHRR, the residue is well-structured. The whole surface of the initial sample is covered by a black and smooth residue (Figure 119a). Examination of the cross-section reveals that the inside consists of big cells (Figure 119b). The drawback of this residue is its excessive stiffness resulting in fragility. In fact, at 500s, only a collapsed black and white material similar to ashes is recovered (Figure 119c and d). Therefore, a protective structure is created during burning thanks to the presence of OMPOSS. However, it does not resist long enough. The white regions at the end of the experiment are ascribed to silica produced during combustion [163].

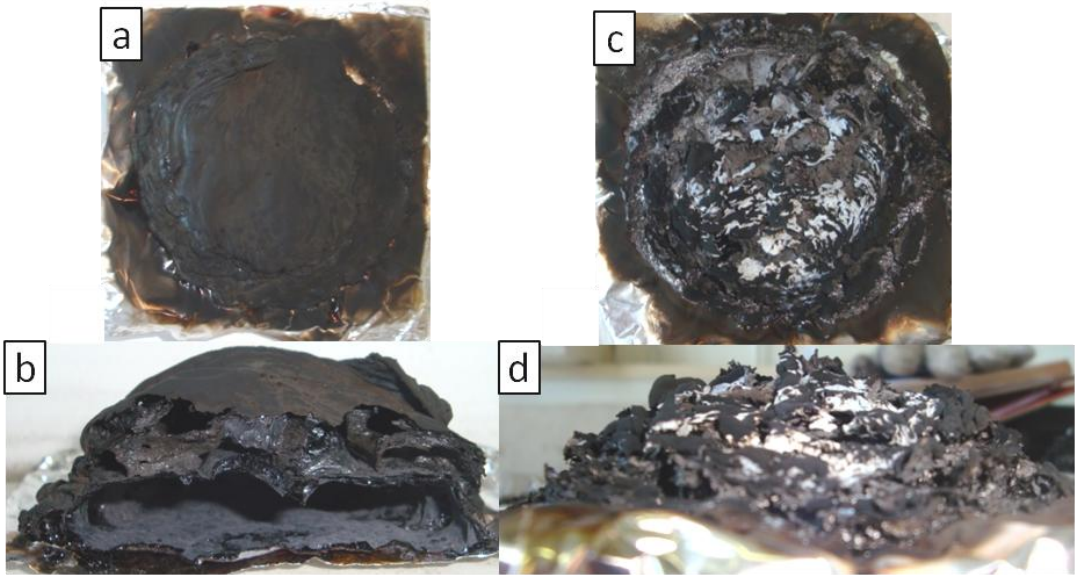

Figure 119: Epoxy_OMPOSS-5 residues during mass-loss calorimeter experiments. At pHRR (a: topview, b: cross-section) and at 500 s (c: topview, d: cross-section)

Epoxy/APP

Stopping mass-loss calorimeter experiments at different times permits to observe the development of the intumescent structure in Epoxy_APP-5. Once the swelling has begun, the material begins to expand (Figure 120b). The whole surface of the initial sample is covered by a black crust (Figure 120a). Large cells are created in the structure (Figure 120b). However, it is noteworthy that these cells are empty and that the residue does not contain any foam at this point. Then, at pHRR, a vitreous residue is observed at the bottom of the sample (Figure 120c). The initial material is therefore sufficiently preserved so that there is still epoxy at the bottom of the sample. Figure 120d shows that the material is fully expanded into a very high structure with foam in it. Finally, at 500 s, the expanded char remains (Figure 120e) but a brief look into the sample (Figure 120f) reveals that there are big voids inside it.

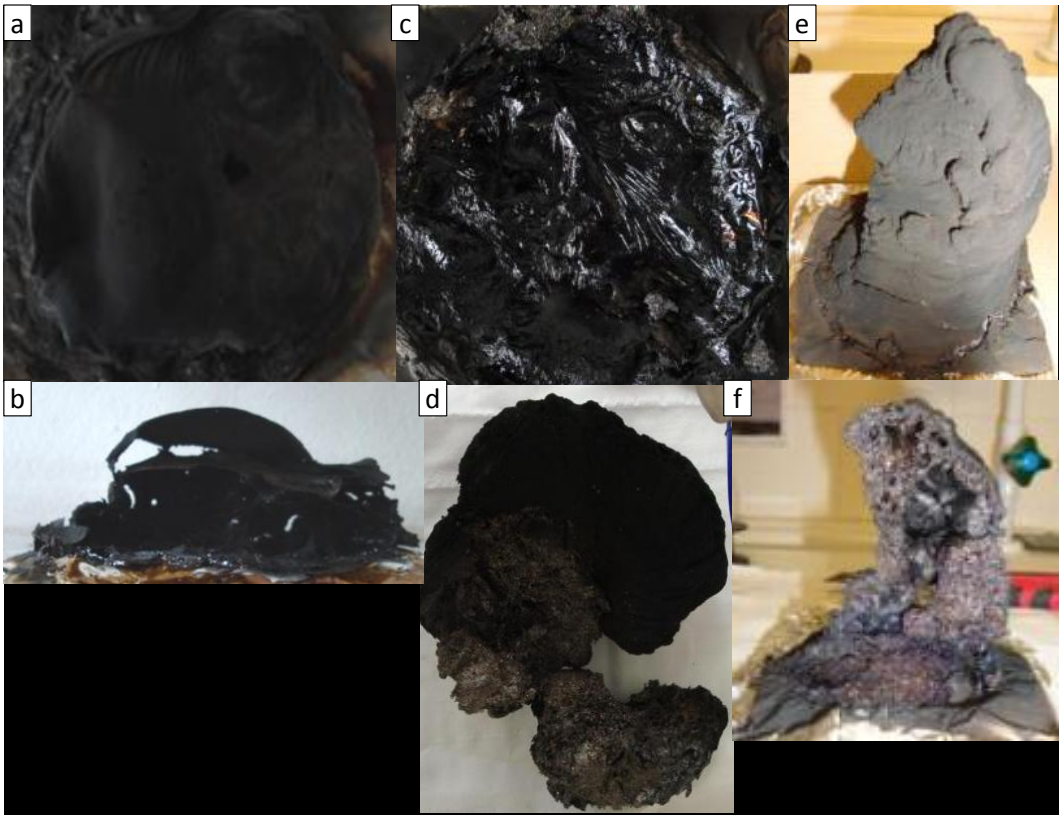

Figure 120: Epoxy_APP-5 residues during mass-loss calorimeter experiments. During swelling (a: top view and b: cross-section), at pHRR (c: bottom of the residue and d: char), 500 s (e: top view and f: cross-section).

Epoxy/APP/CNTs

Incorporation of CNTs in the Epoxy_APP-5 system induces important differences in the morphology of the residues along the testing. During swelling, there is an underlying polymer layer covered by a thin crust of carbonized material (Figure 121a). However, this protection layer is very fragile and easily breakable. Figure 121b shows that the residue obtained at pHRR covers the whole initial sample, but that small holes appear at its surface. Furthermore, the inner part of the sample is simply made of large cells (Figure 121c), whereas there is an important foaming in epoxy containing APP alone. The morphology does not significantly change between pHRR and 500 s, as shown in Figure 121d and Figure 121e.

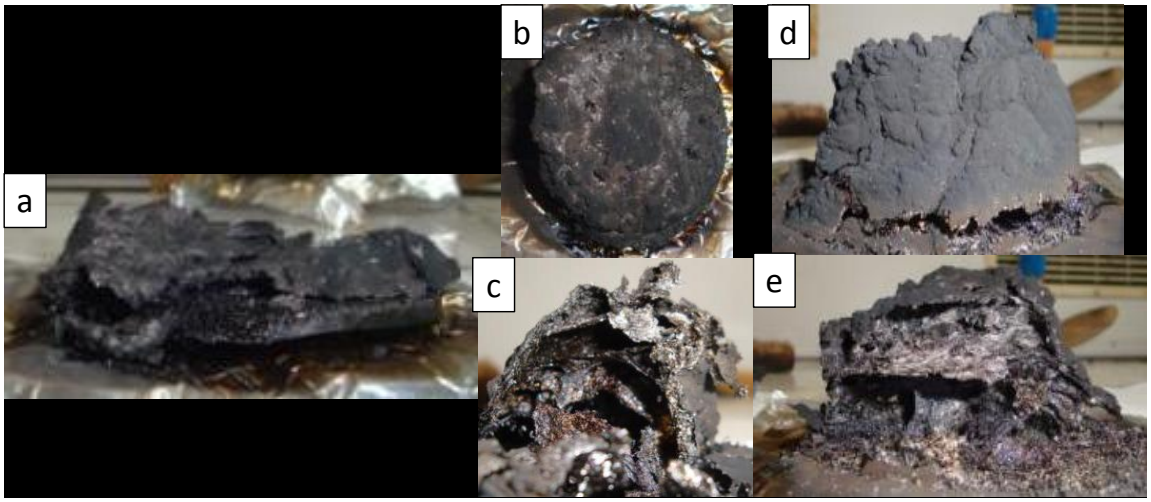

Figure 121: Epoxy_APP-4.5_CNT-0.5 residues during mass-loss calorimeter experiments. During swelling (a: side view), at pHRR (b: top view and c: cross-section), 500 s (e: side view and f: cross-section).

Epoxy/APP/OMPOSS

Epoxy_APP-4_OMPOSS-1 sample removed from the heat source during swelling is already high compared to other formulations (Figure 122a). Furthermore, foaming has occurred in the inside of the material (Figure 122b), whereas Epoxy_APP-5 has only a hollow structure at the same time. Similarly to Epoxy_APP-5, the bottom of the sample at pHRR is black, solid and very dense, suggesting the presence of almost intact polymer at the bottom of the sample (Figure 122c). A big char is created on top of it (Figure 122d). Finally, at the end of the experiment, the structure is similar to the previous one (Figure 122e and Figure 122f). The char is well-structured with numerous voids inside. Interestingly, the upper part has a metallic appearance, whereas the lower one is black. This suggests that the material is not homogeneously deteriorated and that the upper part may protect the lower one.

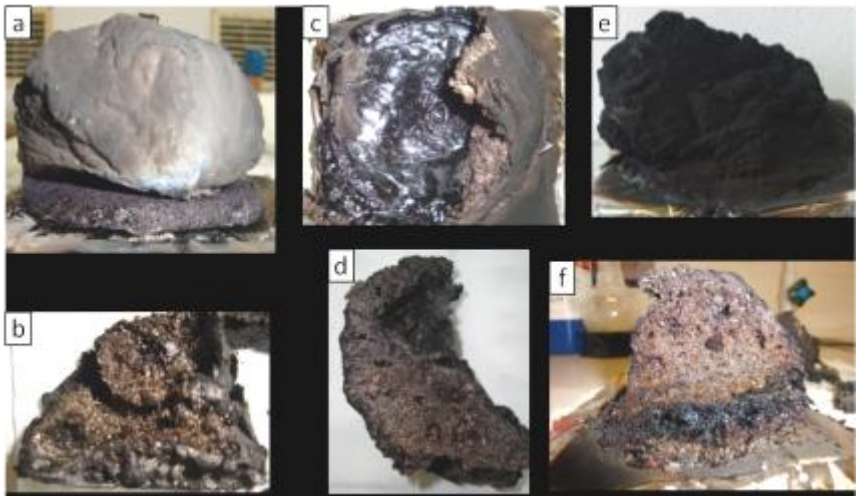

Figure 122: Epoxy_APP-4_OMPOSS-1 residues during mass-loss calorimeter experiments. During swelling (a: side view and b: cross-section), at pHRR (b: top view and c: cross-section), 500 s (e: side view and f: cross-section).

Comparison of the intumescent residues

The morphology of the residues after burning explains why a better behavior is observed with Epoxy_APP-4_OMPOSS-1 than with Epoxy_APP-5. Figure 123 shows vertical sections of the residues for Epoxy containing APP alone or combined with OMPOSS. These pictures let us appreciate the extent of the foaming inside the samples. Areas containing big bubbles (Figure 123, red circles) are next to areas where small bubbles are mostly found (Figure 123, blue rectangles). When APP is incorporated into epoxy alone, foaming occurs. Large bubbles are present in the whole samples. On the contrary, the combination between APP and OMPOSS leads to two different morphologies. Big bubbles are still produced, but mostly in the lower part of the sample. A large area with thinner ones is located on top of the residue. An evaluation of the size of the bubbles in the red circles reveals that the mean diameter lies about 1mm in both cases. The size of the big bubbles is therefore similar in the two formulations. On the contrary, the percentage corresponding to the area with almost only thin bubbles compared to the whole sample is 25 % for Epoxy_APP-5 and 70 % for Epoxy_APP-4_OMPOSS-1. Therefore, when the matrix does not resist to the internal pressure (presence of gases), big bubbles are created in both cases. However, these bubbles are mostly located at the bottom of the sample in the case of Epoxy_APP-4_OMPOSS-1 whereas they are found everywhere in Epoxy_APP-5. Subsequently, the percentage of the whole surface corresponding to denser areas (thin

bubbles, blue rectangles), which are supposed to provide a better protection against heat, is lower in the case of Epoxy_APP-5. Finally, because of the excess brittleness of the residue for APP/CNTs, it was not possible to analyze it.

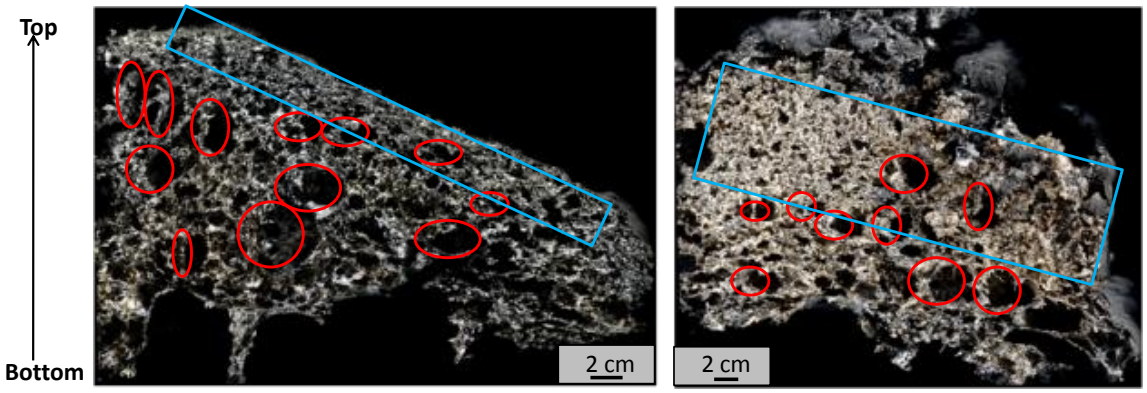

Figure 123: Cross-sections of the whole residues from Epoxy_APP-5 (left) and Epoxy_APP-4_OMPOSS-1 (right).

A deeper insight into these bubbles is given by Figure 124. Bubbles are linked together and they create a kind of network in both cases. However, the walls are thin in the case of Epoxy_APP-5 whereas the incorporation of OMPOSS in this system seems to partly fill the cavities and thicken the walls. Furthermore, during the cutting of the sample, Epoxy_APP-5 is brittle, whereas Epoxy_APP-4_OMPOSS-1 is much more resistant. It seems therefore that OMPOSS reinforces the structure of the char (at least mechanically).

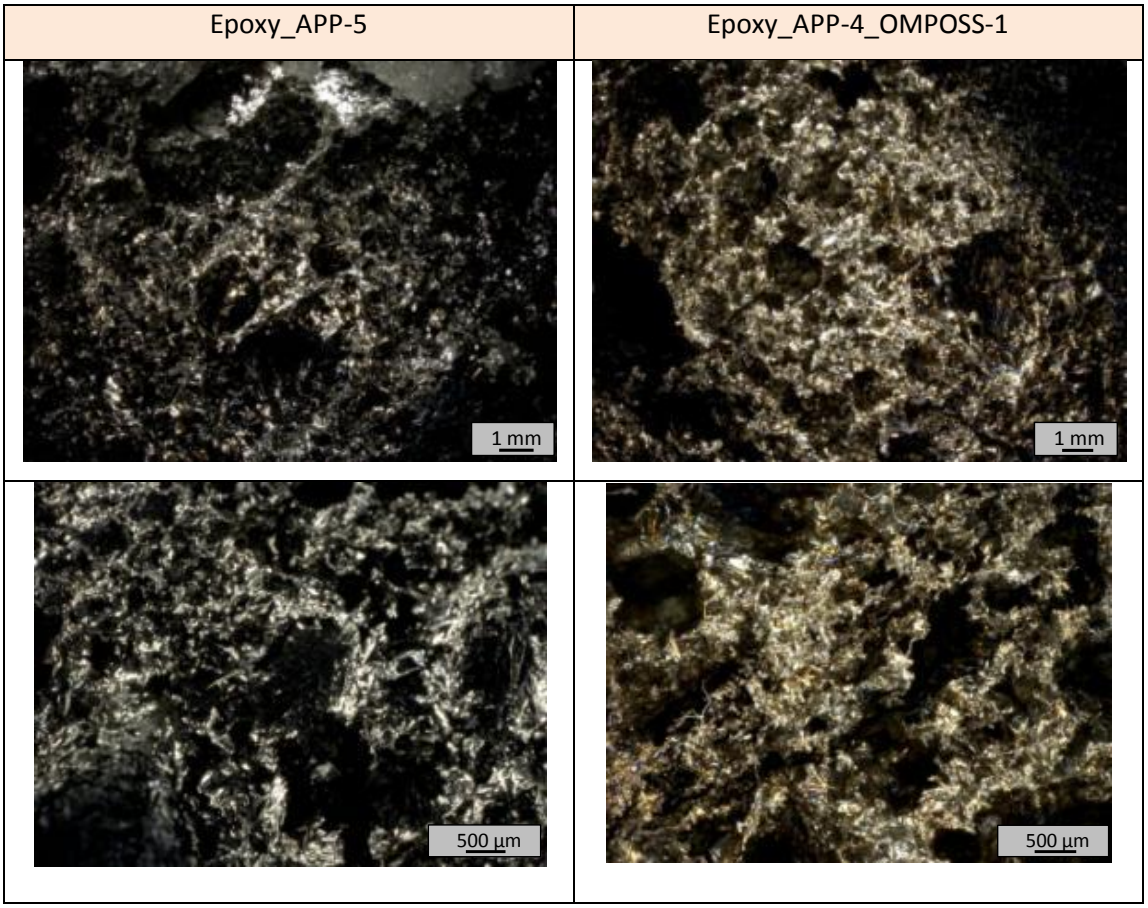

Figure 124: Close-view of the bubbles in the char of Epoxy_APP-5 (left) and Epoxy_APP-4_OMPOSS-1 (right)

Taking into account the different morphology of the char when OMPOSS is incorporated in the Epoxy_APP-5 system, it was decided to analyze the distribution of phosphorus in the residues (the silicon concentrations were too low for being detected). The residues were studied by electron-probe microanalysis (EPMA) (Figure 125). In order to get a better detection of phosphorus in the sample, the results were obtained on samples containing 10 wt.% filler instead of 5 wt.% in the normal case. For both Epoxy_APP-5 and Epoxy_APP-4_OMPOSS-1, high levels of phosphorus are mostly located at the bottom of the samples. Moreover, the comparison of both formulations on top or at the bottom of the samples suggests that in the presence of OMPOSS, phosphorus is more evenly distributed in the residues. This is consistent with digital microscopy observations, which have shown that Epoxy_APP-4_OMPOSS-1 contained more thin bubbles than Epoxy_APP-5, i.e. that matter is more evenly distributed in the residue in the case of Epoxy_APP-4_OMPOSS-1. Since phosphorus is located in the walls

surrounding the bubbles, the presence of small bubbles contributes to its even distribution.

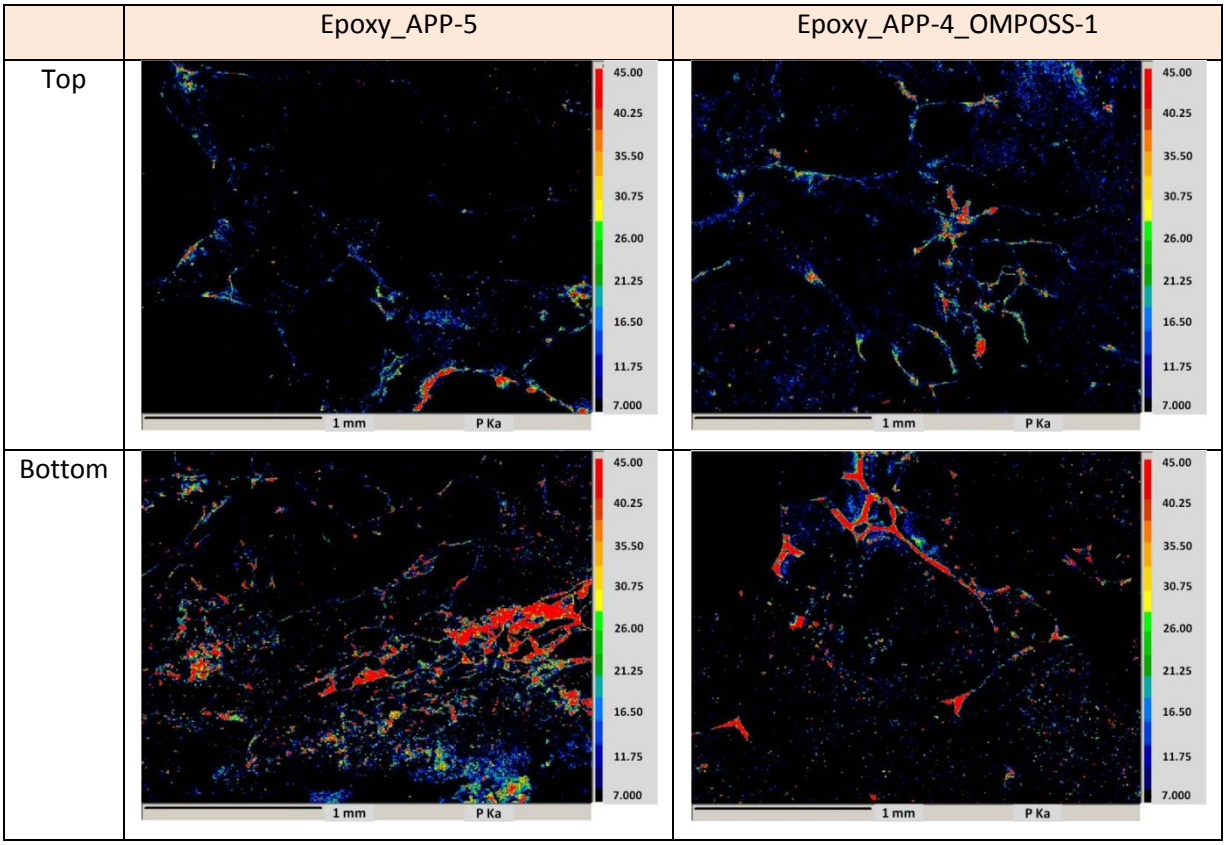

Figure 125: EPMA mappings of phosphorus in the upper and lower parts of the char for Epoxy_APP-5 and Epoxy_APP-4_OMPOSS-1 (10 wt.% loading)

V.1.2. Residues composition

The residues described in the previous section have been analyzed by solid-state NMR in order to check if the differences in the morphologies obtained over time for all formulations could result from the creation of different species.

Virgin Epoxy

Even though the degradation of epoxy resins has been widely described in the literature [15], virgin epoxy residues have been analyzed by solid-state NMR for later comparison with fire-retarded formulations. Figure 126 shows the spectra of virgin epoxy residues at different times. The study of a non-degraded DGEBA cured with triethylenetetramine by Tavares et al. [167] has been used for assigning peaks of virgin DGEBA/DETA.

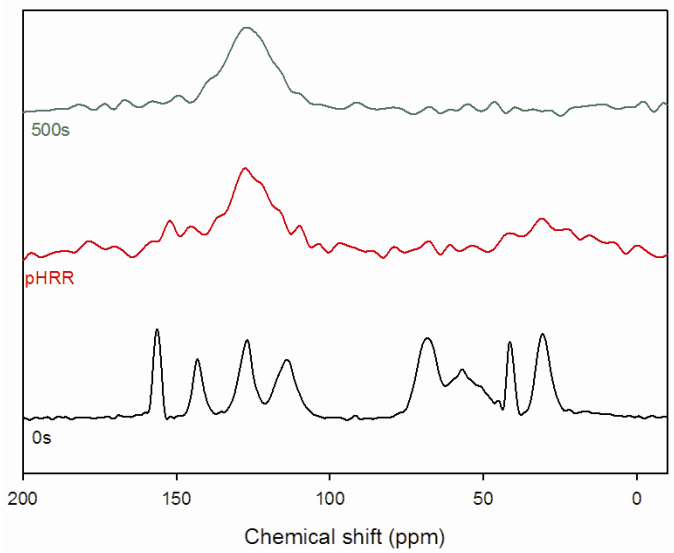

Figure 126: ^{13}C CP-DD-MAS NMR spectra of the residues of Virgin epoxy at different mass-loss experiment times

Nine wide peaks can be distinguished before degradation. The four peaks above 100 ppm correspond to the aromatic carbons of the DGEBA cycles. They are respectively assigned to C_4 (156 ppm, see Figure 127), C_7 (143 ppm), C_6 (127 ppm) and C_5 (114 ppm). Carbons next to oxygen atoms in aliphatic ethers or alcohols give the peak at 69 ppm (C_3, C_{10} and C_{11}). The peak at 56 ppm comes from the C_{12}-N group resulting from the opening of epoxide ring during the curing of the resin. Unreacted epoxide rings can be identified at 41 ppm and 51 ppm (C_1 and C_2 respectively). The carbon linking the two aromatic rings also contributes to the peak at 41 ppm (C_8). Finally, the peak at 30 ppm comes from the CH_3 groups of the bisphenol A units (C_9).

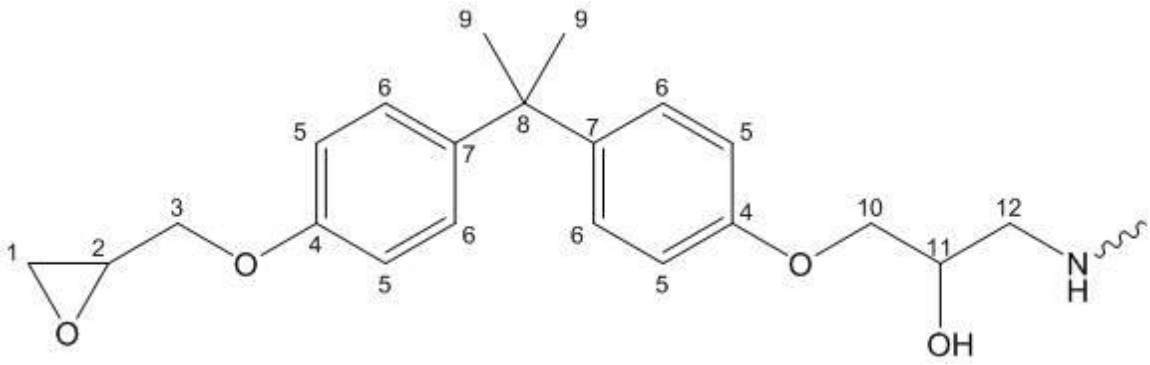

Figure 127: Base structure of DGEBA/DETA epoxy resin

The two other spectra correspond to further steps in the burning of the material: at pHRR and at 500 s. However, these spectra are very similar, showing that once the burning is initiated, the sample is very quickly deteriorated. A broad band is observed at

127 ppm. The broadness of the band shows that there are non-magnetically equivalent carbons. According to the literature, it is due to the carbonization of the material resulting in a condensed aromatic structure made of aromatic and polyaromatic species that are partially oxidized [1, 110]. A band with low-resolution between 14 and 40 ppm is ascribed to the aliphatic degradation products of the resin. In fact, Rose et al. studied by ^{13}C solid-state NMR the degradation of an epoxy cured with diphenyldiaminosulfone [24]. They observed in particular a peak at 20 ppm attributed to methyl groups linked to aromatic species and another one at 14 ppm attributed to alkyl moieties, without further precision. This observation is consistent with the results for our resin. Then, once the material starts to burn, the degradation is very quick, as observed by the measurement of residual weight during mass-loss calorimetry (Chapter IV). Epoxy polymer degrades, as evidenced by the NMR spectra showing the complete disappearance of the undegraded epoxy. The carbonization process takes place at pHRR.

Epoxy/OMPOSS

After the observation and characterization of the residues of the reference resin, the decomposition of the resin containing OMPOSS alone was studied. The residues of the non-intumescent OMPOSS formulation were analyzed by ^{13}C and ^{29}Si solid-state NMR, due to the presence of OMPOSS. ^{13}C NMR spectra are shown on Figure 128. Before degradation, the spectrum exhibits almost the same peaks as virgin epoxy. An additional peak at -5 ppm is due to the methyl groups of OMPOSS. At pHRR, these peaks are still observed. Interestingly, OMPOSS and/or part of its degradation products remain in the structure (-5 ppm), although its specific band exhibits a lower resolution. Its peak enlargement is probably due to the loss of crystallinity when the sample is heated, as suggested by Vannier et al.[61]. Furthermore, this can also be ascribed to the breaking of some bonds in the POSS. Different structures coexist, but are still sufficiently close to each other for giving signals in the same chemical shift range [61]. A band appears in the aliphatic carbon range (10-30 ppm) and is assigned to the aliphatic degradation products of the polymer. Another important feature is the broadening of the peak at 127 ppm, which results in a unique band at the end of the combustion. This is the only one band observed at 500 s, and is assigned to the carbons of the char.

Therefore, the incorporation of OMPOSS in the resin does not change significantly the structure of the initial material. The interest of OMPOSS as flame-retardant is the preservation of epoxy resin at pHRR. It is not completely degraded and could explain the reduction by 46 % of pHRR compared to the virgin epoxy. Since the carbonization process has begun, peaks are less defined, but the initial species are still present. However, this protection does not extend to the end of the experiment, since only carbons from the char are distinguished at 500 s.

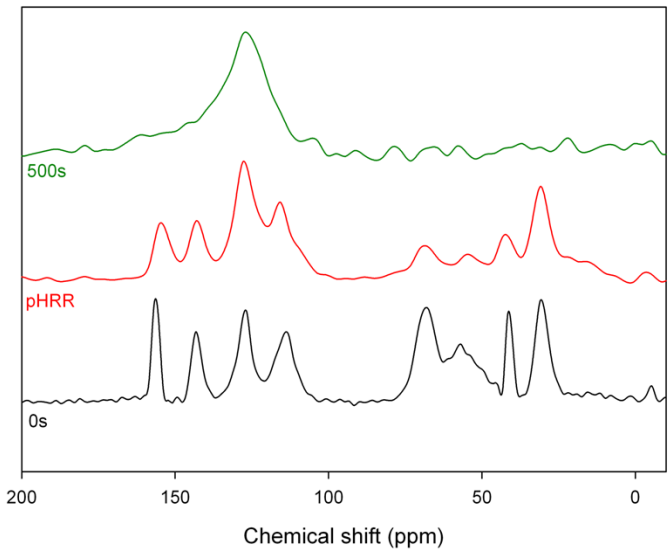

Figure 128: ^{13}C CP-DD-MAS NMR spectra of the residues of Epoxy_OMPOSS-5 at different mass-loss experiment times

The previous paragraph has shown that the epoxy resin was partially preserved until the pHRR is reached. The current one shows the ^{29}Si spectra and is aimed at identifying how long OMPOSS are present in the matrix (Figure 131). Before commenting these results, the M, D, T and Q nomenclature on silicon species is reminded on Figure 129. This classification is based on the nature of the groups surrounding silicon atoms. Depending on the number of alkyl group linked to the silicon atoms, they will be referred to as M (3 alkyl groups), D (2 groups), T (1 group) or Q (no alkyl group).

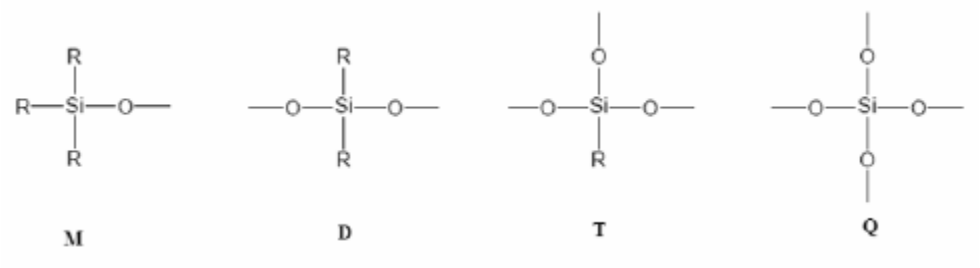

Figure 129: M, D, T, Q nomenclature on silicon species

This classification is further specialized depending on the number of –O-Si- groups attached to the studied silicon atom. The nomenclature for T silicon atoms is described in Figure 130. The *i* exponent is added to the previous classification to this end.

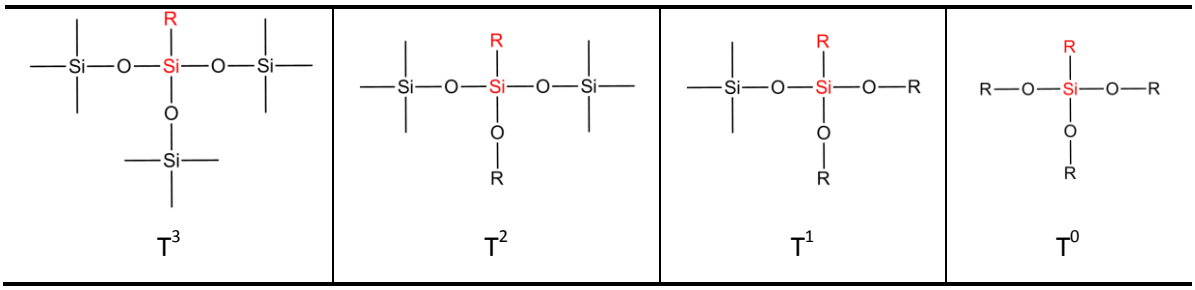

Figure 130: T nomenclature for silicon atoms

OMPOSS are characterized by a double peak at -66 ppm and -67 ppm in the non-degraded material (Figure 131). Vannier et al. [61] have attributed them to silicon atoms T^3 linked to methyl groups on one side, and to three O-Si moieties on the other side. The presence of two peaks instead of a single one is probably due to the distortion of POSS cages in the powder, which results in different binding angles. At pHRR, these peaks are broadened and only a peak centered at -66 ppm is distinguished. Similarly to what has been observed for ^{13}C NMR, the breaking of POSS into smaller species associated to crystallinity loss is certainly the major cause of this phenomenon. At the end of the experiment, this peak is still observed, but an additional broad band lying between -100 and -120 ppm appears. According to Vannier et al. [61], the links between silicon atoms and methyl groups remain during the burning (-66 ppm). A larger silicon network is also created during the partial POSS decomposition, leading to the broad peak between -98 and -110 ppm attributed to silica [61].

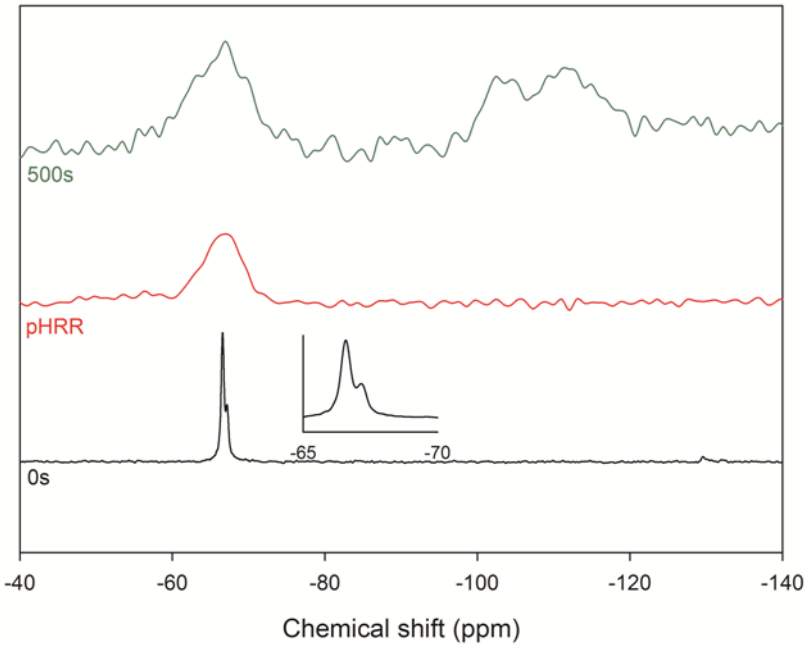

Figure 131: ^{29}Si NMR spectra of the mass-loss calorimeter residues of Epoxy_OMPOSS-5

Solid-state NMR reveals that the initial structure of the resin is preserved longer than for virgin epoxy, and that OMPOSS degrades in a mixture of broken cages and silica in the condensed phase.

Epoxy/APP

The degradation of intumescent systems has then been investigated. First, the reference intumescent epoxy, Epoxy_APP 5, has been studied. In this case both ^{13}C and ^{31}P NMR experiments were carried out on the residues. As shown by ^{13}C NMR (Figure 132), the material before combustion is similar to virgin epoxy. During the swelling, two different layers have been identified (Figure 120, p.193). The bottom layer is made of almost intact resin, with peaks at 156, 143, 127, 114, 41 and 30 ppm. The upper one, on the contrary, is already carbonized, as shown by the single peak at 127 ppm. The spectra corresponding to the same layers at pHRR are similar to the previous ones. The bottom layer shows characteristic peak of the epoxy resins. However, the peaks at 69 ppm (C-O) and 56 ppm (C-N) are broadened with low resolution and the band corresponding to CH_3 from the degradation products in the aliphatic carbon area is recorded. This is the sign of the decomposition of the resin, C-N and C-O bonds being one of the weakest points of the epoxy network [168]. The upper layer still shows only carbonized material. Finally, at 500 s, the bottom is also degraded and the spectra at the top and at the bottom are

identical (only one of them is shown here). Once more, only aromatic carbons from the char are identified at 127 ppm.

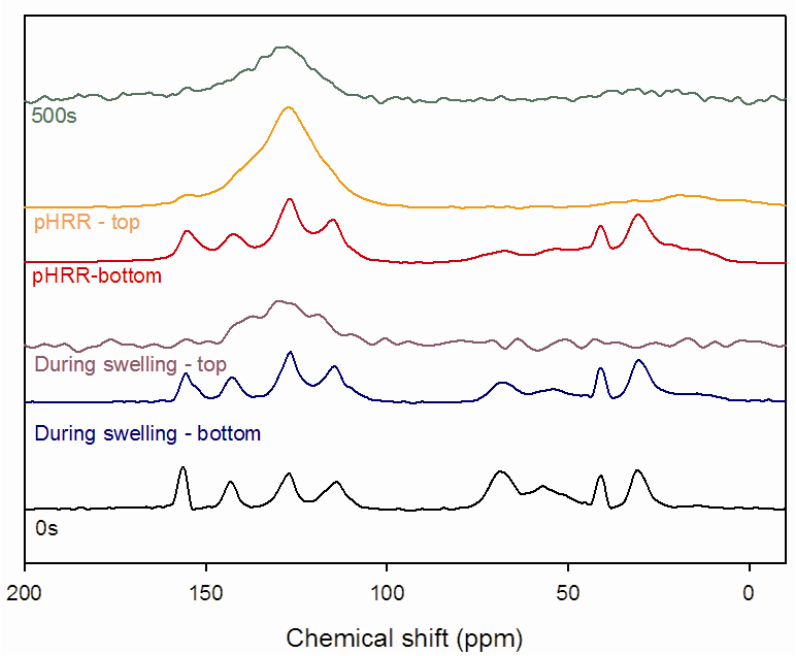

Figure 132: ^{13}C CP-DD-MAS NMR spectra of the mass-loss calorimeter residues of Epoxy_APP-5

Similarly to what has been done for Epoxy_OMPOSS 5, suitable nuclei were tracked in order to study how flame-retardants work. In this case, ^{31}P NMR spectra are shown in Figure 133. Before degradation, APP exhibits a single band at -22 ppm (P-O-P links, here in polyphosphates). During the swelling, APP degrades (the spectra corresponding to the two different layers are similar and only one of them is shown). The peak at -11 ppm is attributed to the formation of orthophosphates linked to aromatic species and/or pyrophosphates [169]. The presence of phosphoric acid is revealed by the thin peak at 0 ppm. This is in accordance with the aforementioned mechanism of action of APP, which begins to degrade into ammonia and phosphoric acid. Furthermore, a well-defined peak at 30 ppm is attributed to phosphonic acid. Its presence will be discussed below. At pHRR, the vitreous bottom consists of three main bands centered at 0, -11 and -22 ppm. They are respectively attributed to phosphoric acid, orthophosphates linked to aromatic species and/or pyrophosphates, and P-O-P links of condensed phosphates [170]. An additional band is recorded at 16 ppm, and corresponds to phosphonate esters. These latter species, as well as phosphonic acid, are rather unexpected, since the initial flame-retardant is a phosphate. Their presence suggests therefore that a reductive

phenomenon occurs during the burning. Karrasch et al. [171] have encountered a similar phenomenon while thermally treating a polycarbonate containing bisphenol A bis(diphenyl-phosphate). They attributed the formation of phosphonate esters to the graphitic structure of the char which could act as a possible reduction agent. In fact, the reduction of phosphates by graphite is used for the production of elemental phosphorus [172]. Even if no other mention of such a phenomenon in the residues of polymeric materials was found, this explanation seems suitable: after ignition, reductive conditions are fulfilled near the flame. Furthermore, ^{13}C NMR has shown that carbonization has occurred on top of the sample, probably creating a pre-graphitic structure, as established by Raman spectroscopy by Bourbigot et al. [173].

The analysis of the char at pHRR shows similar peaks for the bottom and the top parts, with better defined ones on top. Phosphoric acid and orthophosphate linked to aromatic species or pyrophosphate are displayed by the peaks at 0 and -11 ppm. A large band centered at -23 ppm is recorded in the bottom spectrum and is attributed to condensed phosphates [110]. At the end of the experiment, peaks at 0, -11 and 23 ppm are present at the bottom of the sample and have the same attributions as before. On top of the sample, the only peak is that of phosphoric acid.

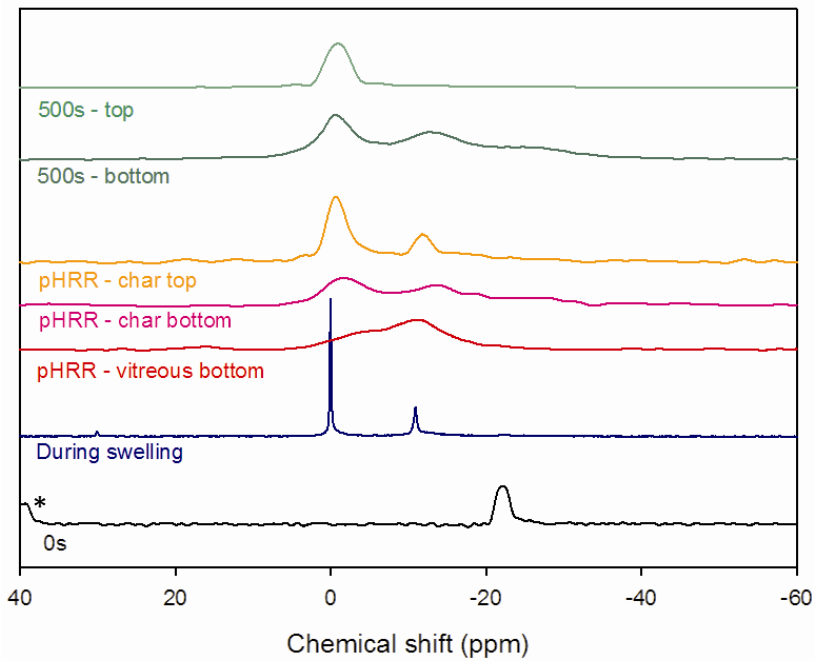

Figure 133: ^{31}P NMR spectra of the mass-loss calorimeter residues of Epoxy_APP-5 (*= spinning sideband)

Therefore, the species produced during the burning of Epoxy_APP 5 and identified in ^{13}C and ^{31}P NMR are well-correlated with the mode of action of APP reported in the literature. An intumescent char is formed on top of residual material and protects it from a quick degradation.

Epoxy/APP/CNTs

After studying the degradation of Epoxy_APP-5 during mass-loss calorimetry experiment, the effect of the incorporation of nanoparticles in this system was assessed. In this part, the degradation of the epoxy matrix containing both APP and CNTs will be studied.

Figure 134 depicts the ^{13}C NMR spectra of the residues of Epoxy_APP-4.5_CNT-0.5. Before degradation, the spectrum is similar to that of virgin epoxy. During the swelling, the spectrum still shows the presence of residual polymer and also shows aliphatic product degradation. However, when pHRR is reached, there is only the characteristic peak at 127 ppm, showing that all carbons of the condensed phase contributed to the formation of the char. Therefore, contrarily to what happens with Epoxy_OMPOSS 5 or Epoxy_APP 5, there is no residual polymer in the material at pHRR. At 500 s, the peak at 127 ppm is the only one remaining.

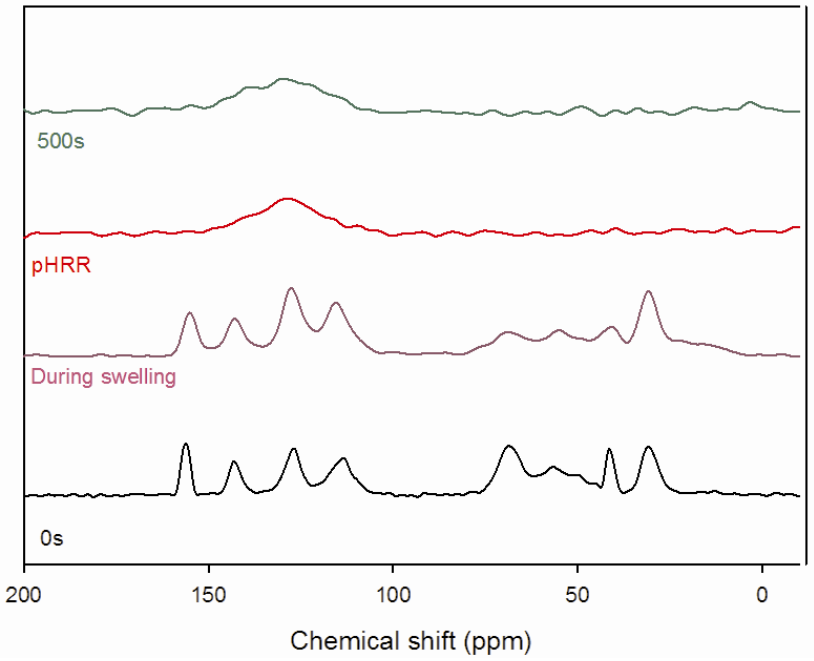

Figure 134: ^{13}C CP-DD-MAS NMR spectra of the mass-loss calorimeter residues of Epoxy_APP-4.5_CNT-0.5

Figure 135 shows the ^{31}P NMR spectra obtained during the decomposition of Epoxy_APP 4.5_CNT 0.5. Before decomposition, the only peak (-22 ppm) is due to the presence of unreacted APP. During swelling, phosphoric acid (0 ppm) and pyrophosphates and/or orthophosphates linked to aromatic cycles (-11 ppm) are detected in the upper part of the sample. At its bottom, a broad band is observed between 0 and -22 ppm. Deconvolution reveals that it is made of three peaks corresponding to APP (-22 ppm), pyrophosphates and/or orthophosphates linked to aromatic cycles (-11 ppm) and orthophosphate linked to aliphatic carbons (-4 ppm). Therefore, APP is already well degraded on top of the polymer, whereas the decomposition has just begun inside the sample. At pHRR, two broad bands at 0 ppm and -11 ppm correspond respectively to phosphoric acid and pyrophosphates. A less visible one at -23 ppm is assigned to P-O-P links in condensed phosphates. At the end of the experiment, only phosphoric acid subsists.

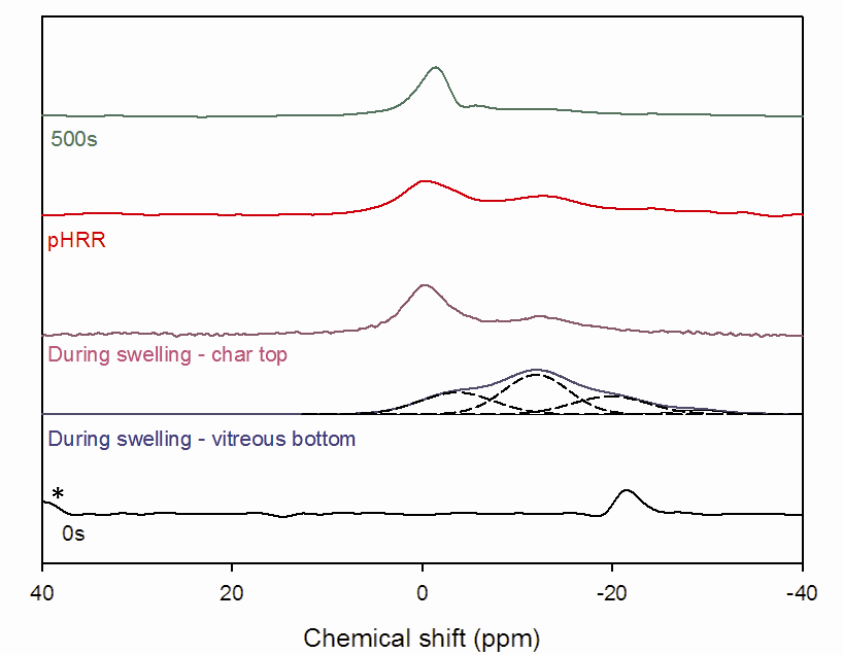

Figure 135: ^{31}P NMR spectra of the mass-loss calorimeter residues of Epoxy_APP-4.5_CNT-0.5 (*=spinning sideband)

The less effective morphology of the char created by Epoxy_APP-4.5_CNT-0.5, compared to Epoxy_APP-5, does not seem to come from additional created species. The only difference observed by solid-state NMR is that different layers can be identified in Epoxy_APP-5 whereas Epoxy_APP-4.5_CNT-0.5 is generally uniformly degraded. Furthermore, the peaks from the initial epoxy resin have completely disappeared at

pHRR according to ^{13}C NMR spectrum of Epoxy_APP-4.5_CNT-0.5 and there is still residual polymer in Epoxy_APP-5.

Epoxy/APP/OMPOSS

The last studied formulation is Epoxy_APP-4_OMPOSS-1. Similarly to previous samples, the morphology of the residues and the species created during the burning are characterized.

The ^{13}C NMR spectra corresponding to Epoxy_APP-4_OMPOSS-1 (Figure 136) are very similar to those of Epoxy_APP-5. Before degradation, peaks from the aromatic part of the resin are recorded at 156, 143, 127 and 114 ppm. Ether groups (CH-O and CH_2-O) have a contribution at 69 ppm. The chemical shifts of carbon linked to nitrogen atoms (CH_2-N and CH-N) appear at 56 and 50 ppm respectively. The peak at 41 ppm is due to unreacted epoxy rings. Finally, CH_3 from the bisphenol-A unit are recorded at 30 ppm. The peak due to the methyl groups of OMPOSS is can also be distinguished at -5 ppm. During the swelling, whereas the same peaks are broadened at the bottom of the sample, aromatic carbons from the char appear on the upper part. The band due to aliphatic degradation products around 19 ppm appears and is still observed at pHRR. Furthermore, peaks from the polymer at 155, 142, 127, 115, 69, 56, 41 and 30 ppm remain at the bottom of the sample when pHRR is reached. However, at the end of the experiment, only carbonized material remains.

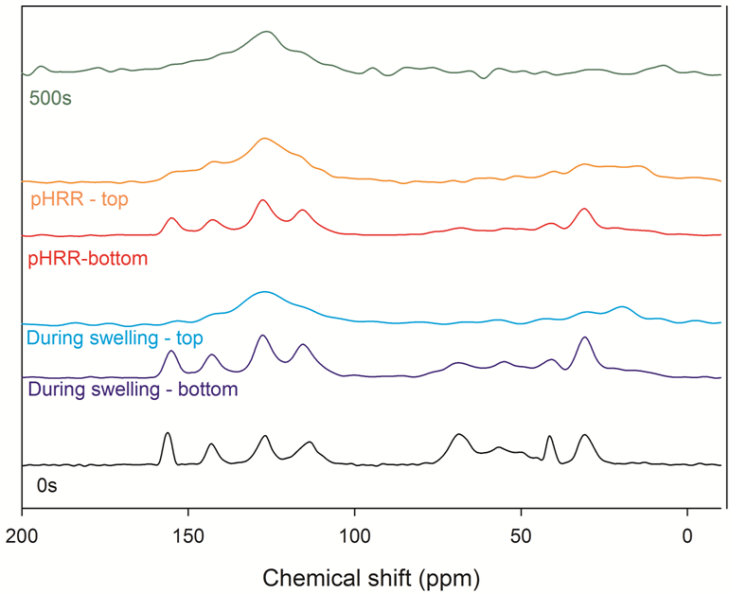

Figure 136: ^{13}C CP-DD-MAS NMR spectra of the mass-loss calorimeter residues of Epoxy_APP-4_OMPOSS-1

The phosphorus-containing species encountered during the combustion of Epoxy_APP-4_OMPOSS-1 (Figure 137) are close to that of Epoxy_APP-5. Before burning, unreacted APP leads to a peak at -22 ppm. During the swelling, analysis of the bottom reveals the presence of phosphoric acid (0 ppm), pyrophosphates and/or orthophosphates linked to aromatic cycles (-11 ppm) and phosphonate esters (17 ppm). On top of the sample, signals at 0 ppm and -11 ppm are assigned to phosphoric acid and pyrophosphates and/or orthophosphates linked to aromatic cycles. Phosphonic acid is detected at 33 ppm. The presence of P_4O_{10} is also revealed by resonances at -45 and -53 ppm [174]. This species results from the decomposition of APP. Since it is identified on top of the sample, where the most violent burning takes place (highest temperature), its early formation is not surprising. The presence of reduced species can be explained by the same phenomenon as in Epoxy_APP-5 (graphitic species acting as reduction component). At pHRR, the vitreous bottom still contains phosphoric acid, pyrophosphates and/or orthophosphates linked to aromatic cycles and phosphonate esters. The bottom of the char contains the two first species and condensed phosphates (P-O-P, -22 ppm), whereas only phosphoric acid is identified in the top layer. Finally, at the end of the experiment, the bottom part contains phosphoric acid, pyrophosphate and/or orthophosphates linked to aromatic cycles and condensed phosphates. In the middle, phosphoric acid, orthophosphates linked to aliphatic carbons and pyrophosphates are present. On top of the sample, only the two first species are identified. Therefore, in the case of Epoxy_APP-4_OMPOSS-1, no additional phosphorus-containing species is identified compared to Epoxy_APP-5.

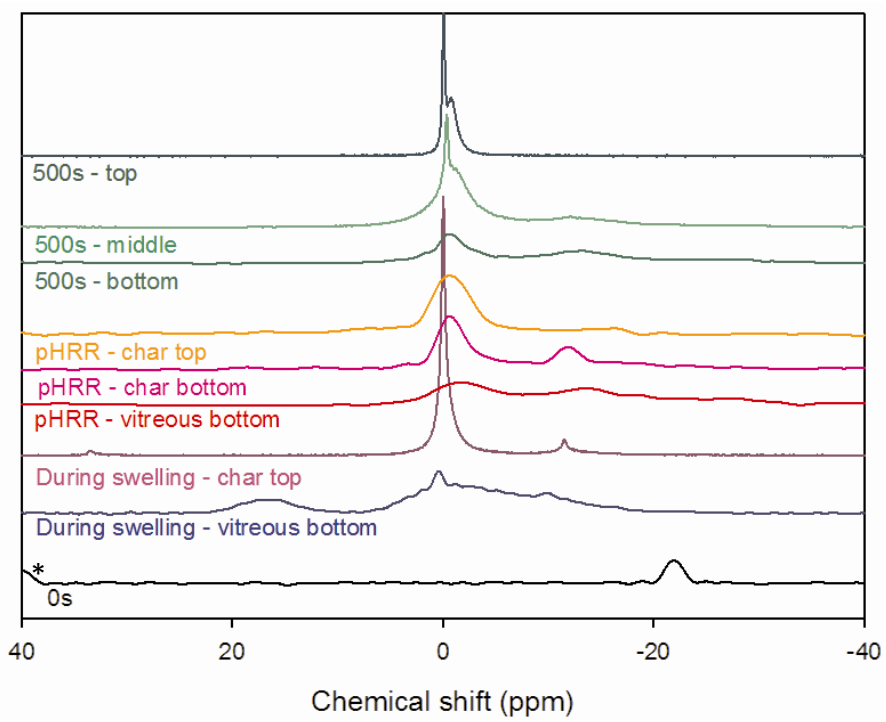

Figure 137: ^{31}P NMR spectra of the mass-loss calorimeter residues of Epoxy_APP-4_OMPOSS-1 (*=spinning sideband)

The ^{29}Si spectrum before degradation shows only the thin peak of OMPOSS at -66 ppm (Figure 138). During the swelling, the peak is broadened and is hard to detect. On the other samples, no silicon peak could be detected. The best hypothesis about this phenomenon is that the combination between the low silicon content in the matrix and the impressive expansion of the sample dilutes the silicon too strongly. Therefore, the contents are so low that nothing can be detected. This also explains why the signal is already difficult to detect during the swelling. Because of this, it was decided to thermally degrade the mixture of APP and OMPOSS without matrix, in order increase the silicon content and try to detect any potential chemical reaction between the two fillers.

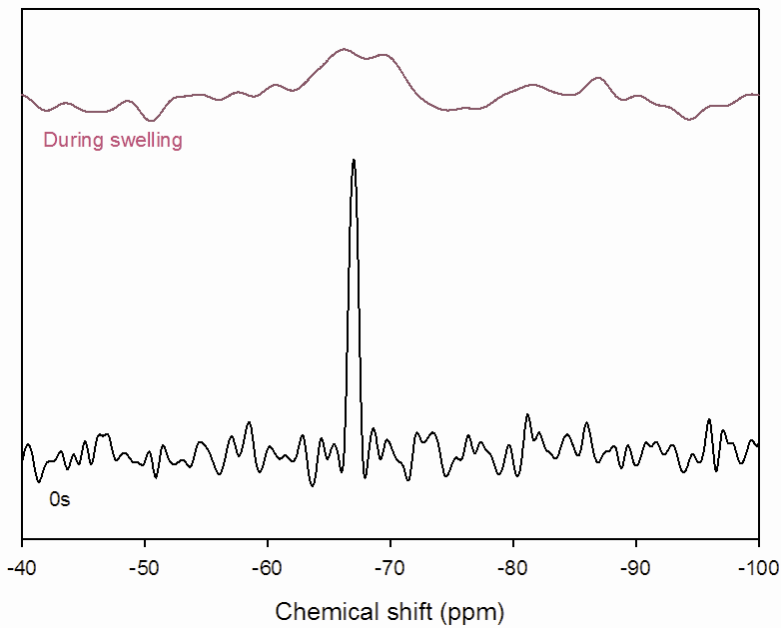

Figure 138: ^{29}Si NMR spectra of the mass-loss calorimeter residues of Epoxy_APP-4_OMPOSS-1

APP/OMPOSS

As explained above, the APP/OMPOSS filler mixture was degraded under air in an oven and the residues were analyzed in order to detect any reaction between APP and OMPOSS. The temperatures were chosen in accordance to TGA experiment (Figure 139). The mixture degrades in two main steps at 250 °C and 620 °C. When comparing the experimental curve to the calculated one, the first step occurs at temperatures lower than calculated one (30 °C shift). It seems that the presence of APP might promote the degradation/sublimation of OMPOSS. There is no such modification for the last degradation step. However, the final residue is higher than expected (13 wt.% instead of 5 wt.%). It can be suggested that the APP residue partially traps and/or react with OMPOSS, therefore limiting the total weight loss.

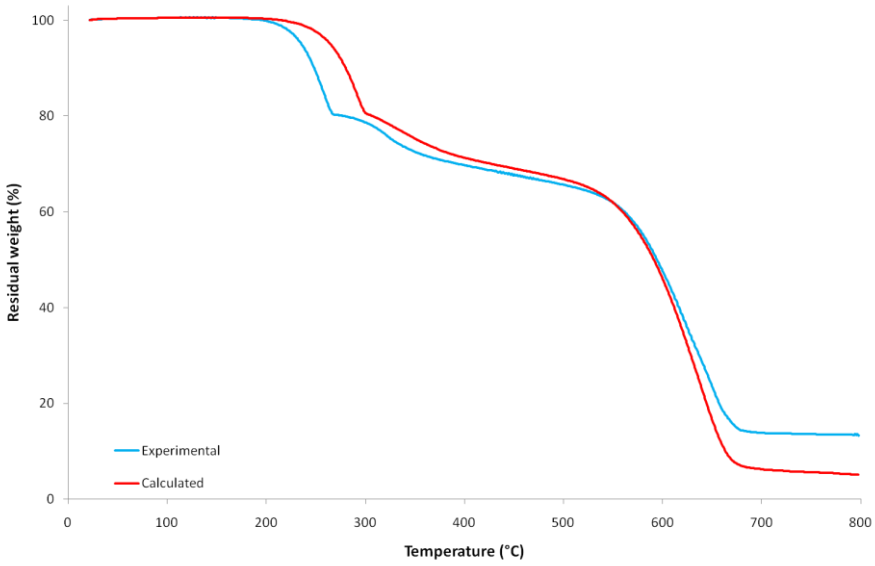

Figure 139: Experimental and calculated TGA curves of the APP/OMPOSS mixture

Considering the results from the TGA, it was decided to thermally degrade the samples at different temperatures in an oven and analyze the solid residues by NMR. Three different samples were considered. Two of them were heated up to 250 °C and 700 °C with a ramp set a 10 °C/min and the samples were directly removed from the oven at the end. The third sample was heated in the same conditions up to 250 °C and then left 3 hours in the oven in order to let slow reactions taking place.

After a simple heating at 250 °C, the ^{31}P spectrum shows the characteristic peak of ammonium polyphosphate at -22 ppm (Figure 140). When the APP/OMPOSS mixture goes up to 250 °C with a final three-hour isotherm, APP has begun to degrade and peaks are recorded at 0 ppm (phosphoric acid), -11 ppm (pyrophosphate) and -22 ppm (ammonium polyphosphate). Indeed, the residue is white, suggesting that no carbonization has occurred and therefore leading us toward pyrophosphate at -11 ppm instead of orthophosphate linked to carbons.

Finally, at 700 °C, apart from phosphoric acid (0 ppm), peaks at -45 and -53 ppm reveal the presence of P_4O_{10} [174]. This latter species is the result of the decomposition of APP into phosphoric acid, which is dehydrated at high temperature.

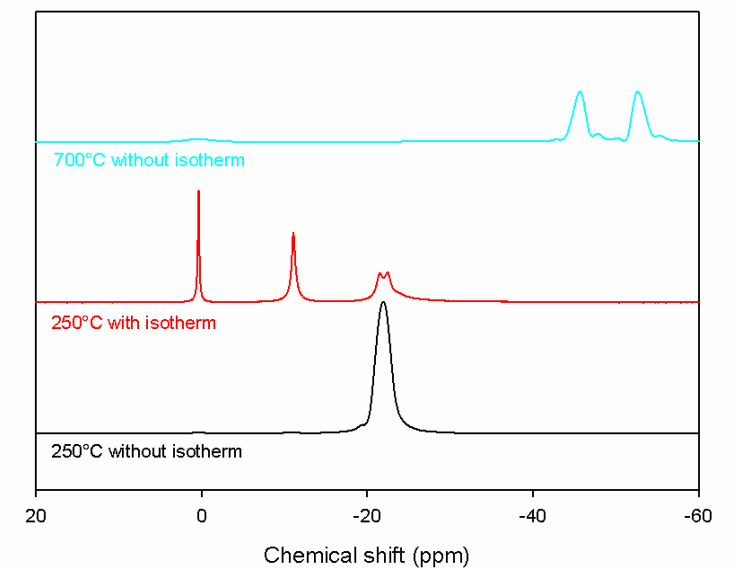

Figure 140: ^{31}P NMR spectra of the thermal residues of APP+OMPOSS

^{29}Si NMR experiments were also carried out on these samples. Unfortunately, the experiments had to be stopped and no result is available by ^{29}Si NMR. Indeed, these experiments are quite long and during them, the sample is heated because of high speed spinning. This resulted in the production of phosphoric acid, which went into the NMR probe.

The gases evolved during TGA were also analyzed by FTIR. First, the FTIR spectra of the thermal degradation products of APP alone (Figure 141) were analyzed. The two peaks at 928 and 968 cm^{-1}, which correspond to ammonia released by APP during its thermal decomposition are slightly shown at 237 °C. The maximum intensity for these peaks is reached at 272 °C. Then, it is reduced till the end of the experiment.

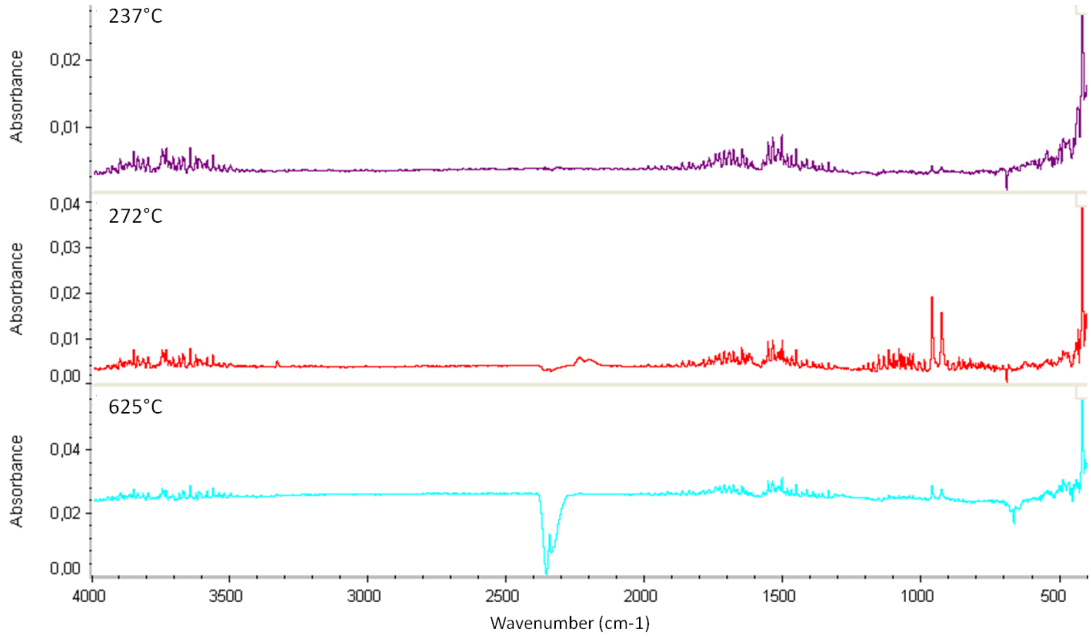

Figure 141: FTIR spectra of APP thermal degradation products (Air, 10°C/min)

Then, the same experiment was carried out on the mixture of APP and OMPOSS (Figure 142). At 221 °C, a peak at 1130 cm^{-1} is attributed to a degraded POSS cage: the spectrum of intact OMPOSS has a strong absorption between 900 and 1200 cm^{-1}. Then, at 305 °C, the peaks of ammonia from APP are recorded at 928 and 968 cm^{-1}. The experiment could not be carried out at higher temperatures since the high amount of gases and sublimed products partly solidified in the apparatus and could not be correctly evacuated. However, this analysis shows that the peaks corresponding to the ammonia from APP and to the degraded POSS cage are seen separately, and that no other species is observed in the gas phase below 305 °C.

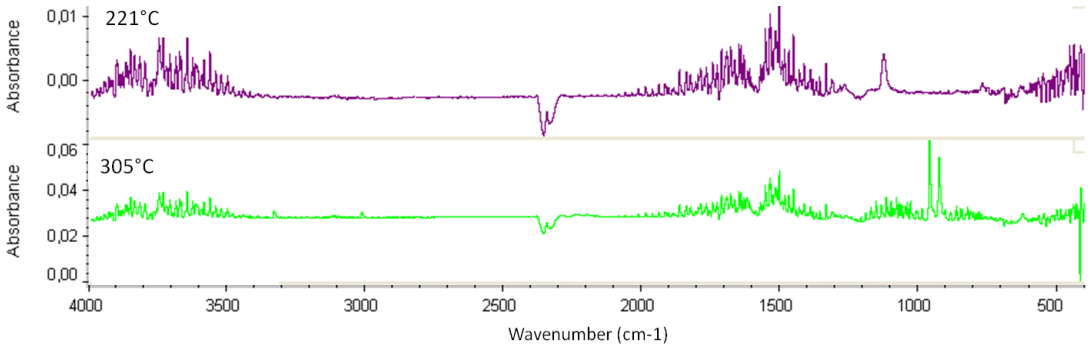

Figure 142: FTIR spectra of APP/OMPOSS thermal degradation products (Air, 10 °C/min)

XRD analysis was carried out on the APP/POSS mixture previously heated at 700 °C. Figure 143 reveals the presence of a crystalline phase identified as SiP_2O_7.

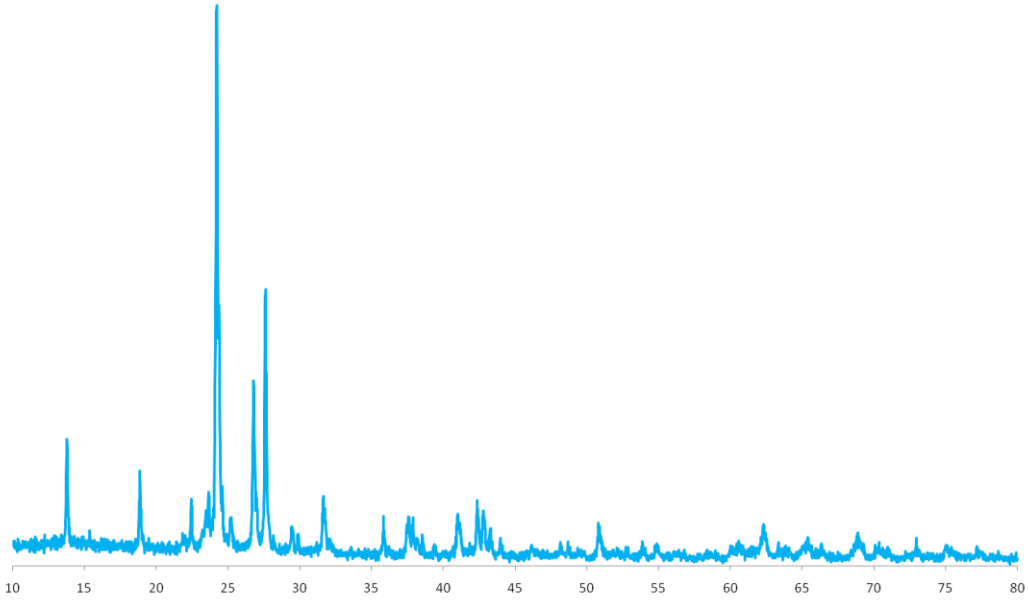

Figure 143: XRD analysis of APP/POSS residue at 700°C

These experiments have therefore shown that it is possible to get silicophosphates by heating APP and OMPOSS together. However, they are not detected by solid-state NMR. Therefore, if the reaction really occurs in Epoxy_APP 4_OMPOSS 1 during combustion, the amount of silicophosphate is very low. Indeed, if the additional residue at the end of the TG curve (at 800 °C) is made of SiP_2O_7, this corresponds only to 13 % of the silicon atoms introduced by the OMPOSS at the beginning. Silicophosphates can reinforce the char structure but are not the major reason explaining the synergy.

V.1.3. Conclusion on the aspect and composition of the systems

Observations of the aspect of the residues over time for each formulation, combined to the analysis helps to understand the mechanisms involved in the reaction to fire of these formulations. Virgin epoxy degrades quickly into a non-cohesive char and no residual peak from the polymer can be seen in solid-state NMR. Incorporation of OMPOSS in it slows down the degradation of the polymer, since its peaks can still be detected at pHRR. The decomposition of OMPOSS produces a mixture of silica and degraded cages containing silicon. Furthermore, a structured residue is obtained at

pHRR but it does not resist until the end of the test and collapses. APP alone in the epoxy resin degrades into ammonia, phosphoric acid and pyrophosphate. Links between the aromatic part of the resin and phosphorus-containing moieties can also be created, and reinforce the char. Indeed, an important intumescence occurs on top of this sample. The incorporation of CNTs in the Epoxy_APP-5 system does not modify the chemical species produced during its burning. However, the visual appearance of the residues suggests that the char does not develop so easily and it seems that a less effective protection is created. Then, Epoxy_APP-4_OMPOSS-1 also produces the same species as Epoxy_APP-5 upon thermal degradation. The difference between these two systems seems once more to lie in the structure of their char. During the swelling, a well-developed char exhibiting a foamed structure is observed with Epoxy_APP-4_OMPOSS-1, whereas the intumescent char is almost empty (large voids) with Epoxy_APP-5. Promotion of the degradation of OMPOSS by APP has been evidenced but no additional species explains this phenomenon. Therefore, it has been established that the antagonism and synergy phenomena do not lie in the creation of additional species. Because the observation of the residues suggests that physical parameters are modified, intumescence in dynamic conditions will then be studied in the next part.

V.2.DYNAMIC EVOLUTION

The previous paragraphs have established that no reaction explaining the synergy in mass-loss calorimetry occurs between APP and OMPOSS. Similarly, the analysis of the sample containing both APP and CNTs, which displays an antagonistic behavior, did not show anything particular. Furthermore, the observation of the residues at the end of the experiment and during it revealed that the structure of the char obtained is completely different. Indeed, it has been shown by Jimenez et al.[86] that the efficiency of an intumescent system results from the right synchronization between the degradation of the resin and the release of gases. On the other hand, if the viscosity of the material is too low when gases are released, they cannot be trapped in the structure and the intumescence does not occur properly. On the contrary, if the viscosity is too high, the materials cracks and gases are not correctly trapped either. Therefore, the next part is

dedicated to the understanding of the formation of the char and the characterization of the protection provided. First, the viscosity of the different formulations will be recorded during thermal degradation. Then, the efficiency of the systems in terms of thermal protection will be assessed. The expansion of samples during mass-loss calorimetry experiments will also be evaluated. Finally, these parameters will be compared in order to propose a mechanism of action for these formulations.

V.2.1. Viscosity measurement

The influence of nanofillers on the viscosity of epoxy resins has been widely discussed for processing issues [175]. Jimenez et al. [86] have shown that during the thermal degradation of an epoxy resin, a viscosity drop occurs. They have also observed that efficient flame-retardants limit this drop. Since the viscosity of the formulation is known for having an influence on the efficiency of intumescent systems (p.104), complex viscosity measurements were conducted between 25 °C and 500 °C on intumescent samples and virgin resin for comparison.

Figure 144 shows the complex viscosity of virgin epoxy and intumescent formulations between 25 and 500 °C. Before the degradation of the materials, thermosets remain solid and the parallel plate viscosity measurements do not mean anything. On the contrary, when the materials degrade, they change into a viscous paste and viscosity data are available. TG curves (see Chapter IV) have therefore been superposed to the viscosity measurements in order to detect relevant temperature ranges.

For each formulation, the viscosity is very similar for Epoxy_APP-5 and Epoxy_APP-4_OMPOSS-1 ($5.6x10^4$ Pa.s) and lower for Virgin epoxy and Epoxy_APP-4.5_CNT-0.5 ($1.5x10^4$ Pa.s) up to 320-350 °C. Then when the resin degrades, a viscosity drop is observed in all cases. The viscosity of Virgin epoxy decreases rapidly after 350 °C and it then increases quite rapidly after 370 °C, because of carbonization process. When APP alone is incorporated in the matrix, the viscosity decreases at lower temperatures (330 °C). Unfortunately, this formulation went over the edges of the sample holder during swelling and the final viscosity increase could not be properly recorded. However, it is noteworthy that the minimum viscosity lies in the same range

as that of Virgin epoxy. The viscosity of Epoxy_APP-4.5_CNT-0.5 drops at 330 °C and its increases after 350 °C. The temperature range with a low viscosity is shifted towards lower temperatures compared to Virgin epoxy. The viscosity drop at lower temperatures for Epoxy_APP-5 and Epoxy_APP-4.5_CNT-0.5 compared to Virgin epoxy is due to the release of liquid phosphoric acid by APP during its thermal decomposition combined to the catalytic properties of this acid on the decomposition of the epoxy network, as observed by TGA. Finally, in the case of Epoxy_APP-4_OMPOSS-1, the viscosity drop is shifted towards higher temperatures compared to APP alone (340 °C instead of 330 °C) and the minimum viscosity is shifted towards higher temperatures, even higher than for Virgin epoxy (380 °C). Furthermore, the minimum viscosity of Epoxy_APP-4_OMPOSS-1 (1616 Pa.s) is higher than that of Virgin epoxy (500 Pa.s) and Epoxy_APP-4.5_CNT-0.5 (825 Pa.s). TG curves show that the degradation of Epoxy_APP-4_OMPOSS-1 begins at temperatures similar to other intumescent systems but that it is stabilized thereafter (higher transient residue and maximum degradation rate temperature). This is consistent with the viscosity drop observed at higher temperatures and with a higher viscosity. Therefore it seems that the presence of OMPOSS in the Epoxy_APP-5 system brings an additional glue to the system and so limits and delays the viscosity drop.

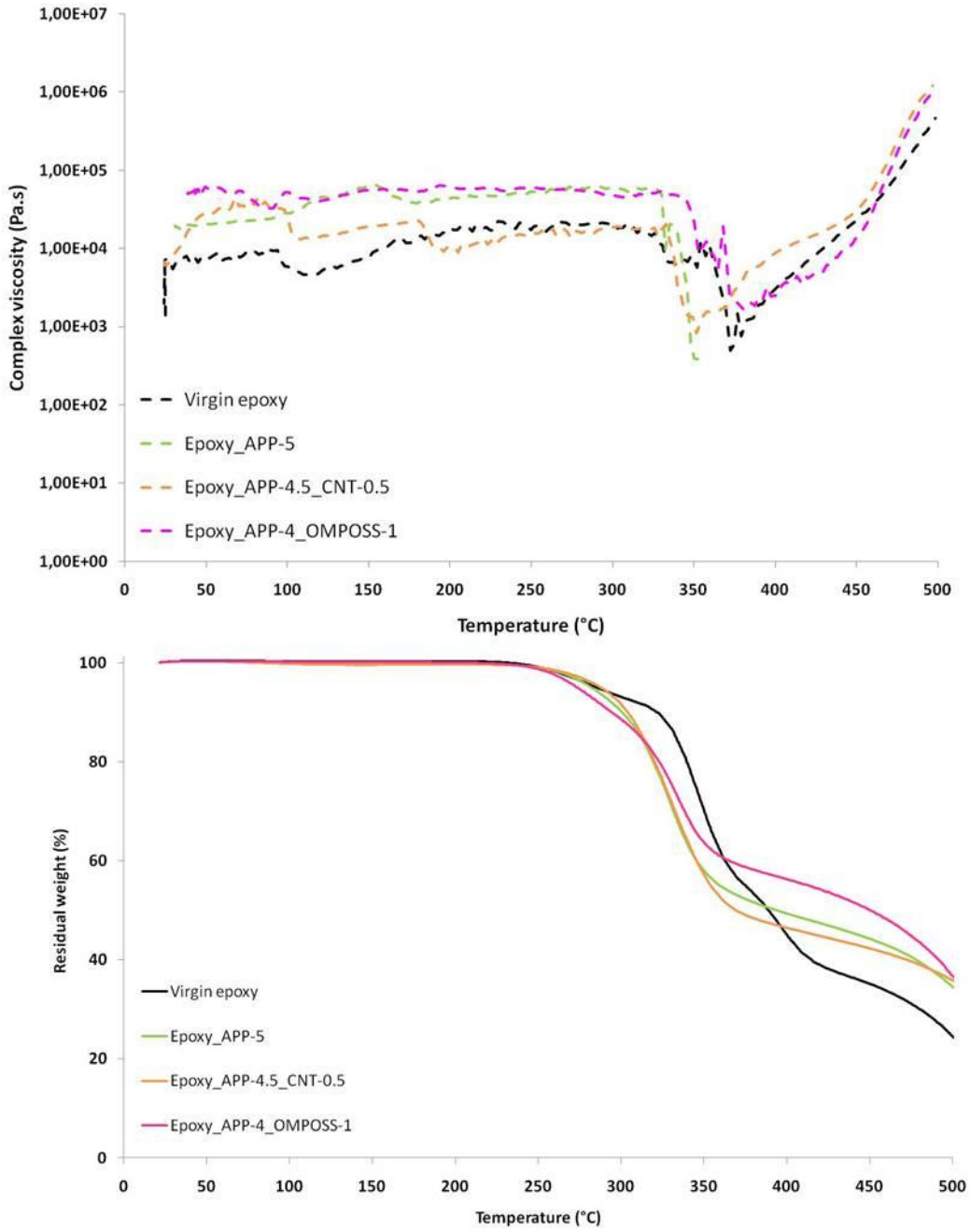

Figure 144: Complex viscosity and TG curve of intumescent formulations as a function of temperature.

V.2.2. Evaluation of the insulation efficiency

Intumescent formulations act by forming an insulating layer on top of materials. This layer, apart from limiting fuel flows between the inside of the material and the environment, should act as a heat insulator. Therefore, thermocouples recording the temperatures during the testing were inserted in the sample at three different locations. Simultaneously, the swelling of the sample was recorded by means of an infrared

camera associated to an image analysis protocol. In order to see most of the swelling, thin samples were tested at a longer distance from the cone heater than in the standard protocol with the heat flux set at 35 kW/m².

V.2.2.a. Mass-loss calorimetry

In order to ensure that the performances of the flame-retarded samples were similar when thermocouple and infrared camera were used or in the standard conditions, the reaction to fire of the materials was assessed at a longer distance from the cone heater than in the standard conditions. First, an important fact is that the time to ignition values are less reliable than when the samples are closer to the cone heater. Heat transfer via convection and radiation is then modified and the heating of the sample is changed. Furthermore, fumes are partially lost outside the chimney. All of this modifies the explosion diagram of the system, and since these modifications are partially erratic, the time to ignition is less reliable. For all these reasons, the times to ignition will not be compared in this section, but only be used for knowing when the sample is starting to burn. The tendency between the efficiency of thin formulations observed in Chapter IV is not modified at this higher distance from the cone compared to standard conditions: the reductions of HRR are different but the formulation ranking is kept.

The major conclusions concerning the efficiency of the thin flame-retarded formulations are not modified when the distance from the cone is higher than in standard conditions. Therefore, in these conditions, the mass-loss calorimeter can be instrumented in order to get a better knowledge of the behavior of our epoxy formulations.

V.2.2.b. Temperatures inside the samples

Three thermocouples are inserted in the sample (Chapter II, p.107). One of them is located one cm above the sample and will be incorporated in the char for intumescent samples. The second one is inserted at the top surface of the sample, whereas the third one lies at the bottom of the sample. For each location, the results of the different formulations are compared.

The experiments with the thermocouple located one centimeter above were only carried out with intumescent formulations (Figure 145). Before ignition, the samples show a similar temperature rate. The ignition results in a quick and large temperature increase. The temperature of Epoxy_APP-5 slightly increases after the ignition, up to 600 °C, then it cools down and the final temperature reaches 510 °C. Epoxy_APP-4.5-0.5 behaves very similarly and the final temperature is 450 °C, in the error margins of the experiment. Finally, the combination between APP and POSS leads to a much lower final temperature: 351 °C.

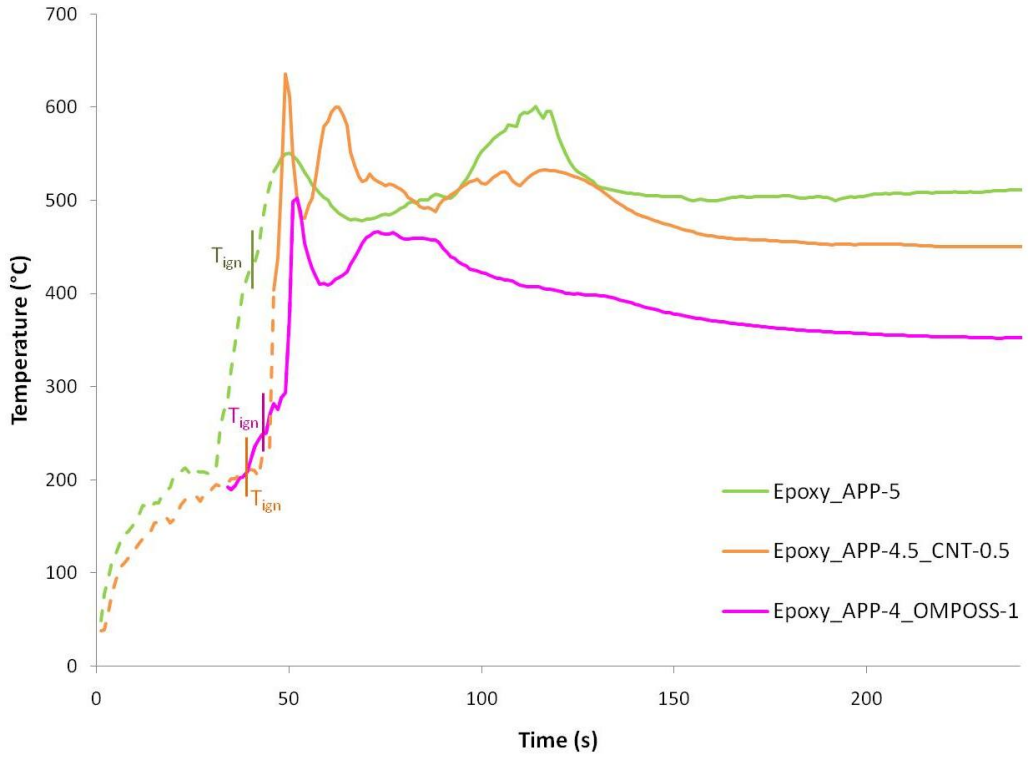

Figure 145: Top temperature as a function of time during mass-loss calorimetry on thin intumescent samples (Heat flux: 35 kW/m², thickness = 25 mm, distance=35 mm, T_{ign}=time to ignition). Dotted lines are used when thermocouples are not in the material.

The maximum temperatures reached during the experiment give also interesting information. Epoxy_APP-5 reaches 601 °C at its maximum, whereas Epoxy_APP-4.5_CNT-0.5 goes up to 636 °C. This is in good accordance with mass-loss calorimeter results where these two formulations have similar performances. Furthermore, Epoxy_APP-4_OMPOSS-1 only reaches 502 °C during the experiment and provides better fire performances. Finally, it is noteworthy that only the thermocouple

for Epoxy_APP-4_OMPOSS-1 is already in the matter when ignition occurs (i.e., the swelling is already important before ignition for this formulation).

For all formulations, the same analysis was conducted for the thermocouples on the surface of the samples (Figure 146). Therefore, thermocouples are in the material from the very beginning of the sample. The trends are very similar between all samples except for virgin epoxy. At the end of the experiment, the highest temperature is measured for virgin epoxy (473 °C) but there is no residue left on it since the sample is almost completely destroyed, whereas it is lower for Epoxy/POSS (385 °C). Intumescent Epoxy_APP-5 reaches 416 °C at the end. The temperatures are lower for Epoxy_APP-4.5_CNT-0.5 and Epoxy_APP-4_OMPOSS-1 (351 °C and 289 °C respectively). An interesting feature is the maximum temperature reached. Virgin epoxy goes up to 766 °C, probably because the material is destroyed (and burns with high flames) and the thermocouple is in the fire. The samples containing POSS alone, APP alone and the combination between APP and CNTs reach similar temperatures (424 °C, 431 °C and 433 °C respectively). Epoxy_APP-4_OMPOSS-1 still remains in a lower temperature range (375 °C). Interestingly, the temperature for this last formulation decreases immediately and continuously after reaching its highest temperature, whereas a kind of plateau is observed for other formulations.

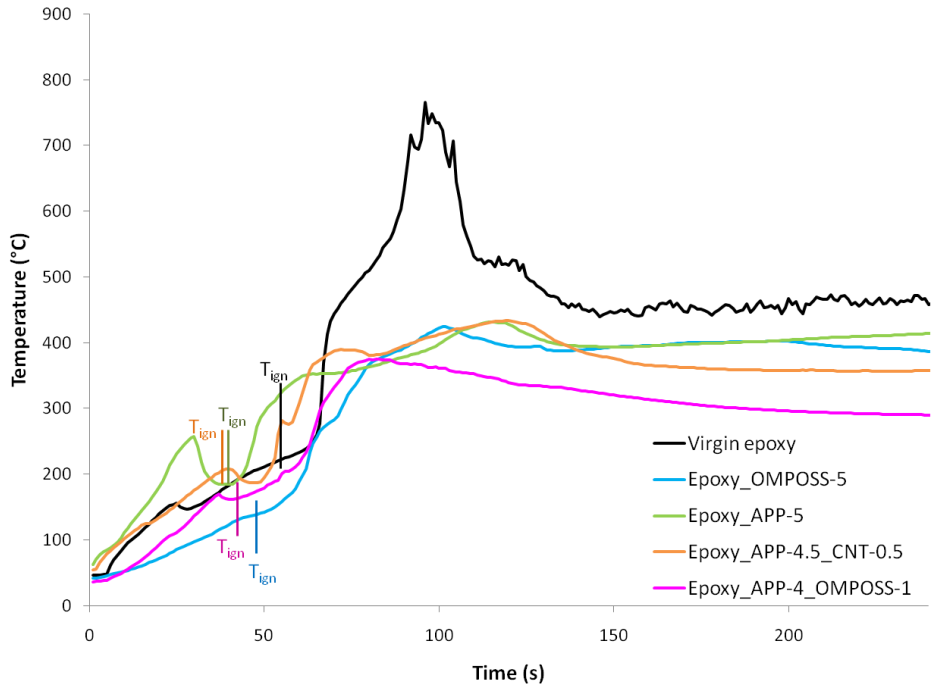

Figure 146: Middle temperature as a function of time during mass-loss calorimetry on thin intumescent samples (Heat flux: 35 kW/m², thickness = 25 mm, distance=35 mm, T_{ign}=time to ignition).

Finally, temperatures at the bottom of the samples were recorded (Figure 147). Temperatures at the end of the experiment for epoxy containing OMPOSS, APP and APP/CNTs are close and reach respectively 310 °C, 305 °C and 282 °C. For Virgin epoxy, it is higher (428°C), since there is almost no residue. On the contrary, Epoxy_APP 4_OMPOSS 1 leads to lower temperatures (264 °C).

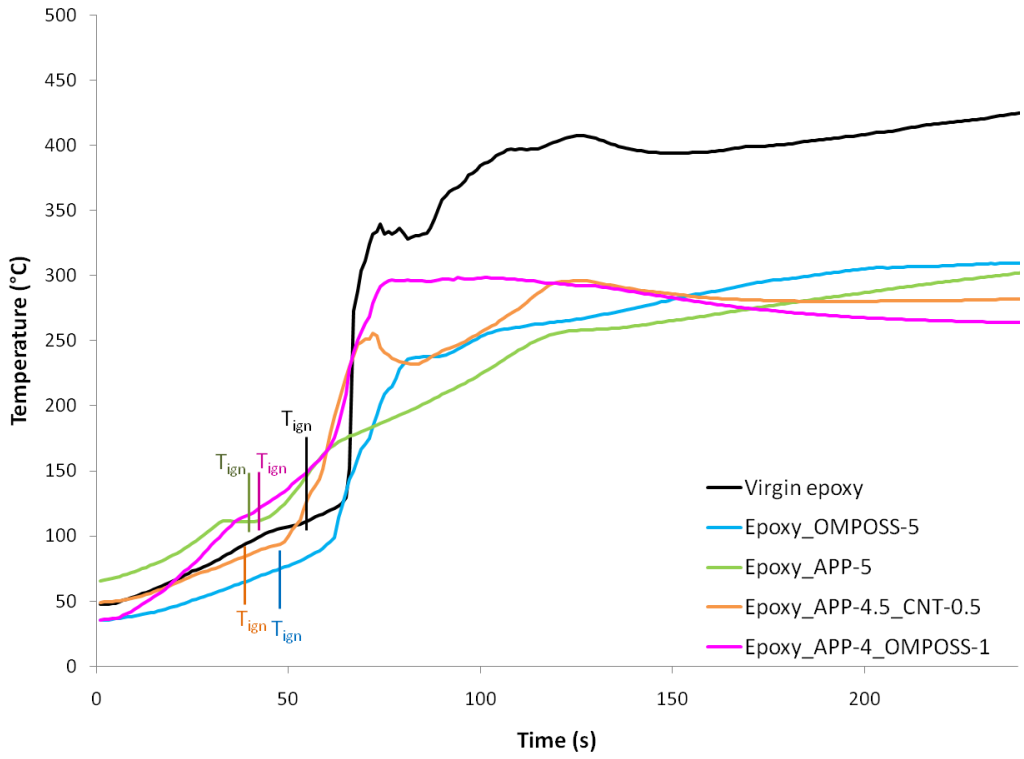

Figure 147: Bottom temperature as a function of time during mass-loss calorimetry on thin intumescent samples (Heat flux: 35 kW/m², thickness = 25 mm, distance=35 mm, T_{ign}=time to ignition).

Differences are more important when looking at the maximum temperatures recorded. The temperature of Virgin epoxy always increases during the whole experiment and the final temperature is also the highest one (428 °C). This is consistent with the almost complete degradation of the sample (only ashes at the end). The temperature increase rate during the main increase is almost vertical for Virgin epoxy (23 °C/s between 65 s and 74 s). This rate is lower for Epoxy_APP-4_OMPOSS-1, Epoxy_OMPOSS-5 and Epoxy_APP-4.5_CNT-0.5 (respectively 6 °C/s between 45 s and 75 s, 7 °C/s between 63 s and 80 s and 7 °C/s between 49 s and 72 s). It is even more reduced for Epoxy_APP-5 (2 °C/s between 41 s and 120 s). The maximum temperature reached by Epoxy_OMPOSS-5 is 322 °C, only 12 °C more than the final temperature for this formulation. For Epoxy_APP-5 and Epoxy_APP-4.5_CNT-0.5, the sample slightly

cools down after the maximum temperature is reached (differences of 16 °C and 13 °C respectively). This difference is higher for Epoxy_APP-4_OMPOSS-1: 35 °C. However, this sample has the second highest maximum temperature after virgin epoxy. This apparent drawback could be the cause of the early protection formation observed in the first part of this chapter (early degradation causing the formation of the protective structure more quickly).

V.2.3. Swelling

Figure 148 shows the swelling of intumescent systems as a function of time. At the beginning, a first increase is recorded for all samples and remains below 100 %. This phenomenon is likely due to the distortion of the sample (shrinkage) under the heat flux and cannot really be considered as a real expansion of the sample. This first artefact is then followed by the major development of the intumescent structure in a single step. This major increase begins at the same time for Epoxy_APP-5 and Epoxy_APP-4_OMPOSS-1 but the increase rate is higher in the presence of OMPOSS (40 %/s for Epoxy_APP-4_OMPOSS-1 instead of 17 %/s for Epoxy_APP-5). Taking into account that these POSS are known for subliming when heated [163], they should promote the quick development of the intumescent structure. On the contrary, the sample containing CNTs begins to swell later, with a still high swelling rate (48 %/s). However, it should be kept in mind that this high rate often ends with the cracking of the Epoxy_APP-4.5_CNT-0.5 residue. Concerning the swelling extent, APP alone leads to the lowest expansion (580 %), quickly followed by Epoxy_APP-4.5_CNT-0.5 (687 %). Epoxy_APP-4_OMPOSS-1 has the highest expansion with 918%. However, the final expansions are very similar for Epoxy_APP-5 and Epoxy_APP-4.5_CNT- 0.5. Indeed, the samples are thin at the beginning (2.5 mm) and the char surface is not regular at the end: the difference between Epoxy_APP-5 and Epoxy_APP-4.5_CNT-0.5 is therefore only 3 mm and the final height can be considered as similar between these two formulations. These results on the swelling show that the development of the protection is affected by the presence of nanoparticles. OMPOSS enhances it, whereas CNT is a hindrance.

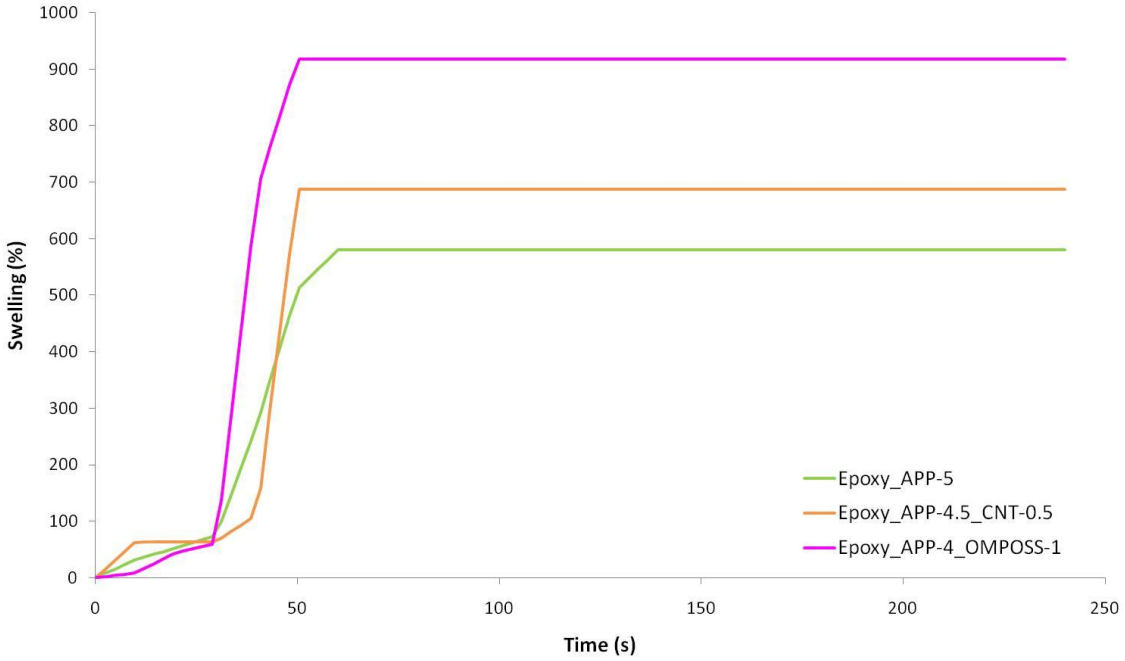

Figure 148: Swelling as a function of time for thin intumescent systems (Heat flux: 35kW/m², thickness: 25mm, distance: 35mm).

Figure 149 links the swelling to the weight lost during the burning. Indeed, if gases are not trapped during thermal decomposition, they may contribute to the development of fire (production of evolving flammable gases). If their trapping occurs, this should result in the swelling of the residue. Therefore, if the expansion is important with a low weight loss, gases are efficiently trapped in the samples. Furthermore, it means that the intumescent protection is created before most of the sample has degraded and the trapped gases contribute to the foaming (more foam in the char is supposed to enhance the thermal insulation).

The combination between APP and OMPOSS seems to have the most efficient swelling. Only 21 wt.% loss leads to a 687 % swelling. 21 wt.% more are lost for reaching the maximum swelling. Epoxy_APP-5 has an intermediate behavior, while Epoxy_APP-4.5-CNT-0.5 has the worst. Losing 24 wt.% only leads to a 273 % swelling for Epoxy_APP-5 and even less (97 %) for Epoxy_APP-4.5_CNT-0.5. The maximum swelling is reached when 59 wt.% of the APP sample and 48 wt.% of the APP/CNTs one are lost. It is also noteworthy that the final residues are very similar for Epoxy_APP-5 and Epoxy_APP-4_OMPOSS-1.Indeed, there is not more material remaining at the end of the experiment with OMPOSS than without, but the presence of OMPOSS delays the degradation and the instant release of fuels is lower. Subsequently, the flames are less

energetic and the HRR is decreased. On the contrary, when CNTs are incorporated, a higher weight loss is needed for developing the protection.

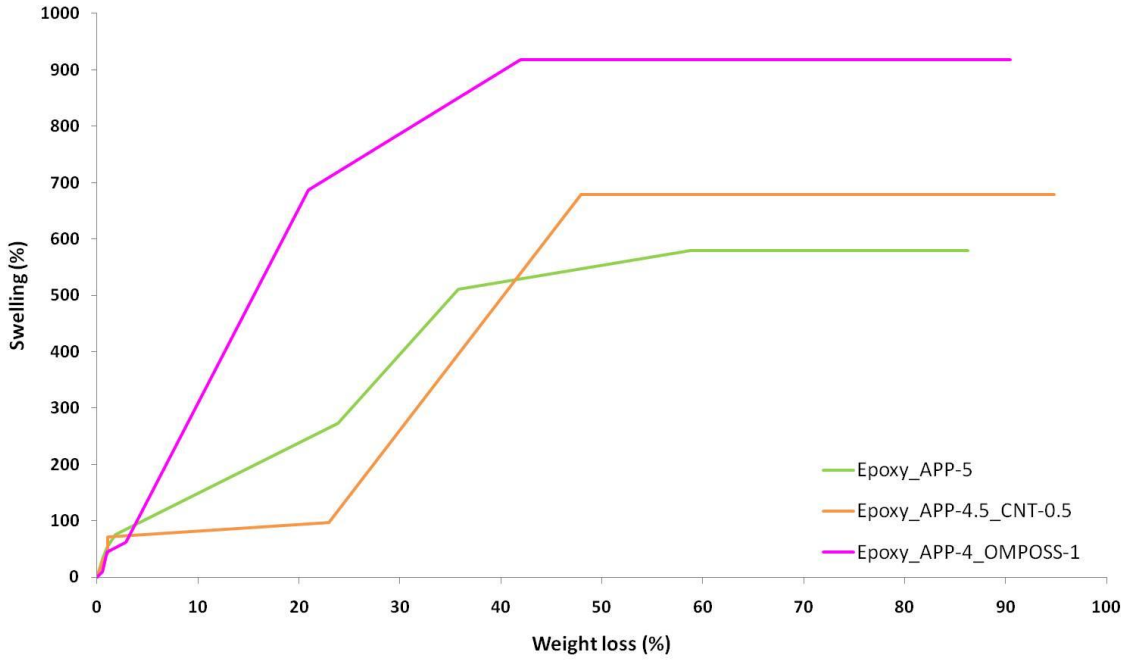

Figure 149: Swelling as a function of weight loss for thin intumescent systems (Heat flux: 35kW/m², thickness: 25mm, distance: 35mm).

V.2.4. Swelling/temperature relationship

The previous experiments have revealed different phenomena. First, from the chemical point of view, no additional species is created when samples burn. Then, the physical characterization has shown that the structures of the residues created during the burning are different. Furthermore, it seems that intumescence occurs at slightly different times, which may explain why the temperatures reached inside the samples are lower for the most efficient formulations. The next figures propose to correlate these phenomena.

Figure 150 shows the temperatures corresponding to the different thermocouples inside virgin epoxy, as well as the heat release rate. Briefly after ignition (determined with infrared camera), the two temperatures rise dramatically. The heat release rate begins to increase slightly later. In fact, epoxy often ignites with small flames on a limited area of the sample and the flames spread slowly on the whole sample. This may explain the shift between the ignition seen by infrared camera (direct observation of the flame at the surface of the sample) and on the HRR curve (measurement of fume

temperature on top of the chimney). The middle temperature increases then steadily until pHRR is reached. After the first increase, the bottom temperature increases much slower up to the end of the experiment.

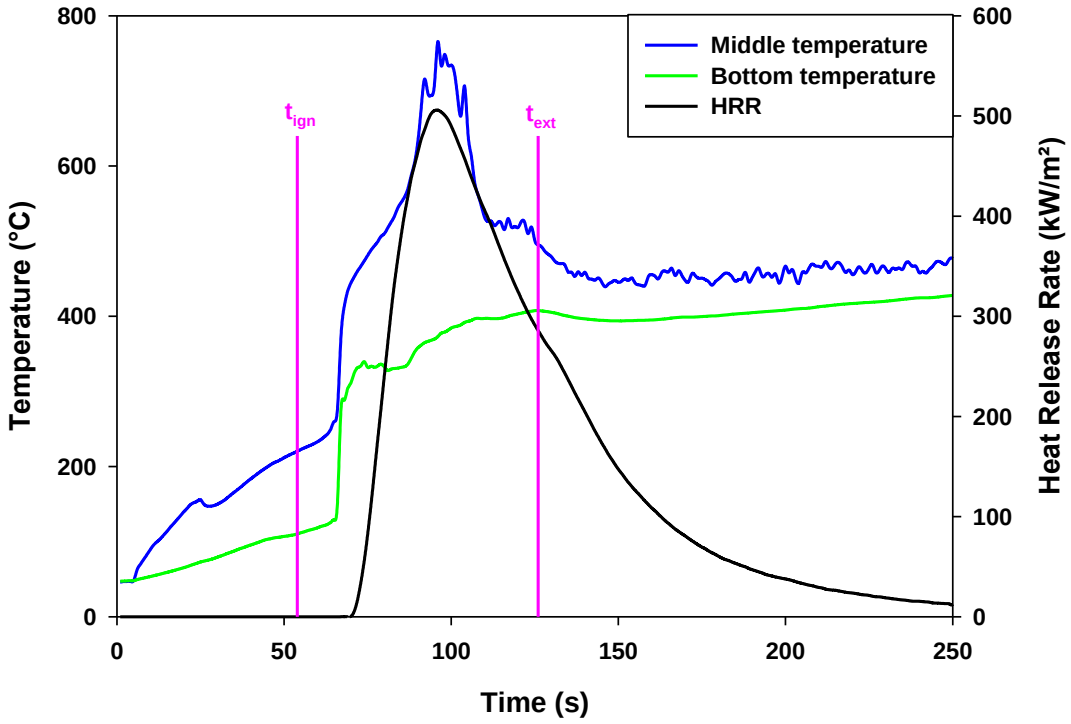

Figure 150: Temperatures reached inside virgin epoxy and Heat Release Rate as a function of time (Heat flux: 35kW/m², thickness: 25mm, distance: 35mm, t_{ign}: time to ignition, t_{ext}: time to extinction).

Similar observations were conducted on Epoxy_OMPOSS-5 (Figure 151). An interesting feature is that the temperatures increase less quickly after ignition: the increase rate is 7 °C/s for Epoxy_OMPOSS-5 instead of 23 °C/s for Virgin epoxy. This suggests that the residue created by OMPOSS provides a better protection and that the system may also been cooled down by the endothermal sublimation of OMPOSS.

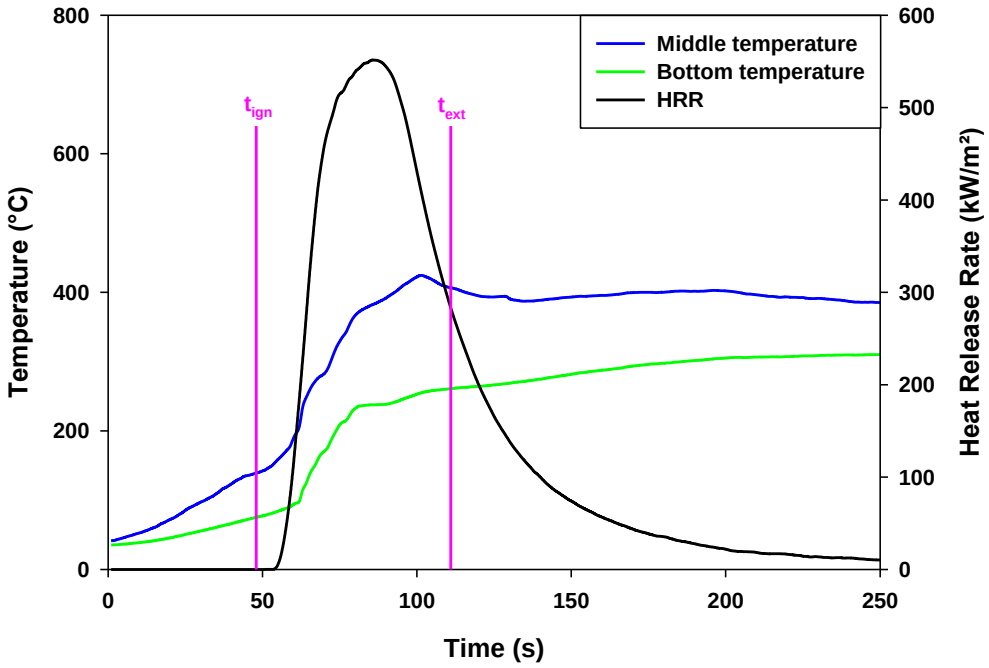

Figure 151: Temperatures reached inside Epoxy_OMPOSS-5 and Heat Release Rate as a function of time (Heat flux: 35kW/m², thickness: 25mm, distance: 35mm, t_{ign}: time to ignition, t_{ext}: time to extinction).

Epoxy_APP-5 is the first intumescent sample considered (Figure 152). Contrary to previous samples, the ignition occurs simultaneously to the HRR increase, probably because of the intumescence, which set the surface of the sample closer to the spark igniter. At this time, all thermocouples are already in the material. The three temperatures evolve in parallel and continue to slightly increase until the end of the experiment. It is noteworthy that intumescence begins before ignition and that the maximum expansion is reached just before the pHRR. An additional small peak is recorded for the top and the middle temperatures: it results probably from the partial cracking of the intumescent structure and the inflammation of released gases.

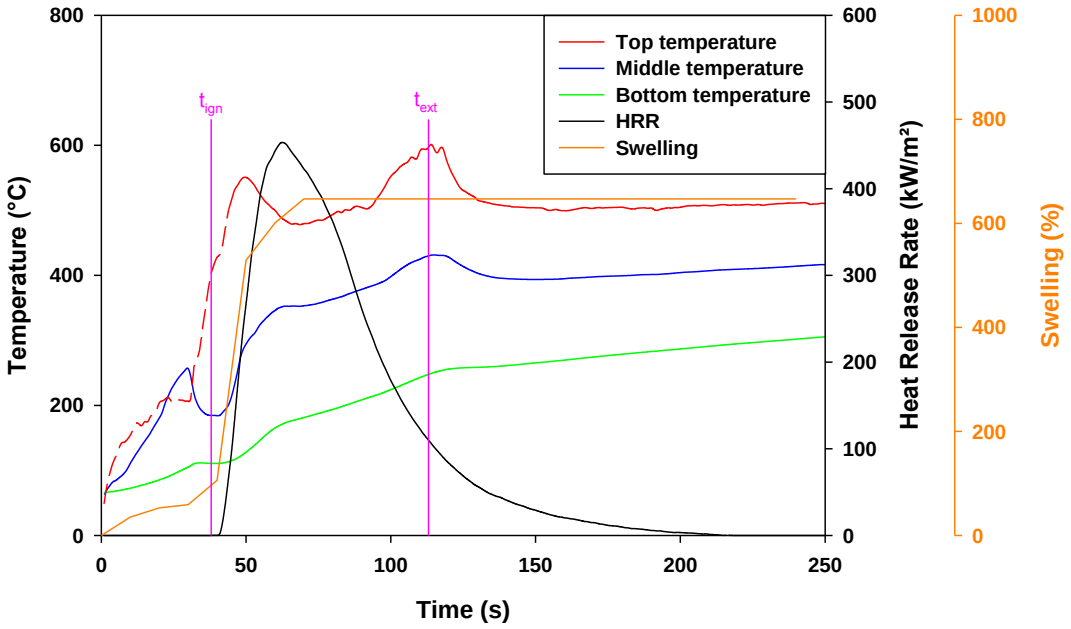

Figure 152: Temperatures reached inside Epoxy_APP-5, Heat Release Rate and swelling as a function of time. (Heat flux: 35kW/m², thickness: 25mm, distance: 35mm, t_{ign}: time to ignition, t_{ext}: time to extinction). The dotted line is used when the thermocouple is not in the material.

The presence of CNTs slightly modifies the previous behavior (Figure 153). The main difference is that HRR increases shortly after the ignition, and the temperatures do the same. An important fact is the expansion begins when the sample ignites and the maximum expansion is reached very quickly. It seems therefore that the structure created with APP and CNTs does not trap correctly the gases evolved during the combustion. This is consistent with the previous study linking the expansion and the weight loss: expansion is initiated with a higher weight loss in this sample. Taking into account the morphology of the different residues, the hollow structure of Epoxy_APP-4.5_CNT-0.5, combined with the presence of small holes on top of the specimen support this hypothesis.

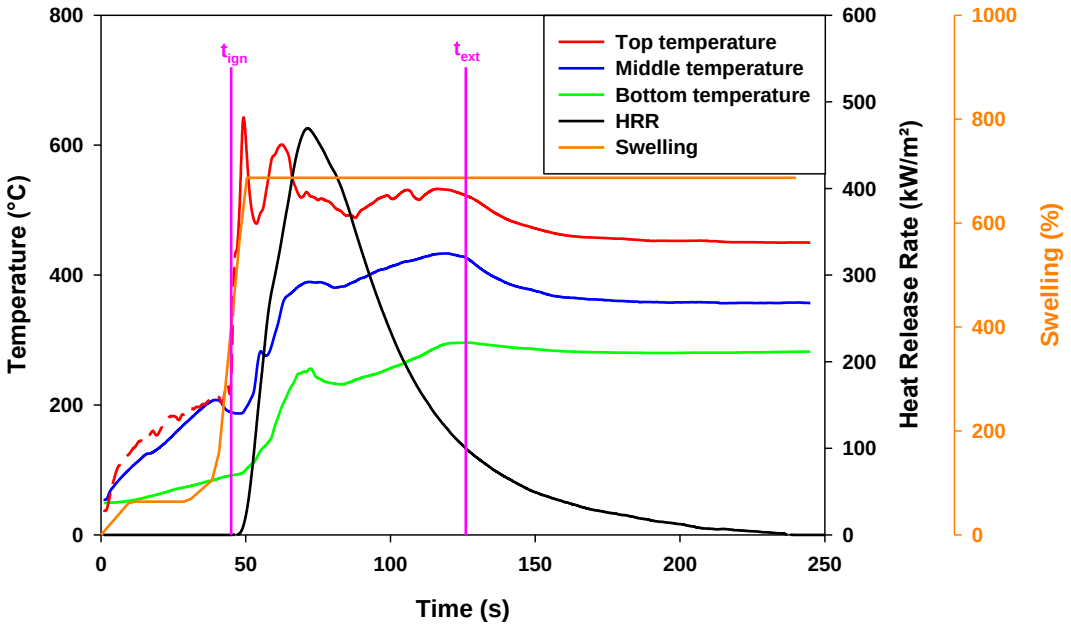

Figure 153: Temperatures reached inside Epoxy_APP-4.5_CNT-0.5, Heat Release Rate and swelling as a function of time. (Heat flux: 35kW/m², thickness: 25mm, distance: 35mm, t_{ign}: time to ignition, t_{ext}: time to extinction). The dotted line is used when the thermocouple is not in the material.

Finally, the sample containing both APP and OMPOSS was studied (Figure 154). Ignition occurs before the HRR increases, and the reached temperatures remain low. The main information is that the swelling occurs well before ignition and continues shortly thereafter. Comparing this to the behavior of Epoxy_APP-5, it can be concluded that the early development of intumescence is useful but also that the intumescent structure has to be created before most of the sample is burnt. In the case of Epoxy_APP-5, the maximum expansion is reached too late. TGA experiments showed that OMPOSS sublimes shortly above 200 °C, whereas APP decomposes around 275 °C. Therefore, OMPOSS are trapped in the structure and contribute to the blowing of the structure. Indeed, between 200 and 300 °C, the resin has already begun to degrade and the shortened network should be able to trap these gases. This is well-correlated with the observations in Figure 153. The swelling is initiated when the top and middle thermocouples reach 200 °C. Another important fact is that the temperatures decrease just after pHRR is reached, whereas it went down long after for other intumescent formulations. A thicker structure is more easily created thanks to the presence of OMPOSS and better insulates the system.

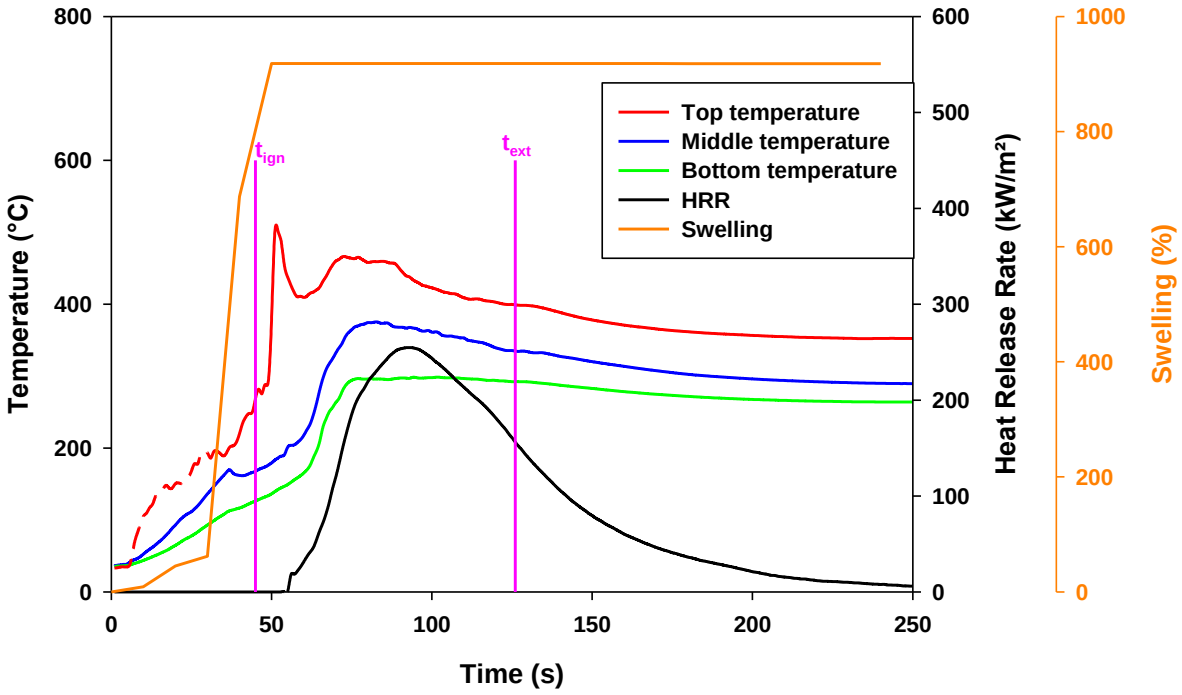

Figure 154: Temperatures reached inside Epoxy_APP-4_OMPOSS-1, Heat Release Rate and swelling as a function of time. (Heat flux: 35kW/m², thickness: 25mm, distance: 35mm, t_{ign}: time to ignition, t_{ext}: time to extinction). The dotted line is used when the thermocouple is not in the material.

V.3. DISCUSSION AND CONCLUSION – PROTECTION MECHANISMS

The study of the species formed during the burning of Epoxy_OMPOSS-5 and Epoxy_APP-5 as well as the properties of the structure created have confirmed the mechanisms suggested by the literature. The thermal degradation of the sample containing OMPOSS is slowed down, as shown by thermogravimetric analyses under air and nitrogen in Chapter IV. The better behavior of polymers containing POSS is generally attributed to the formation of silica in the sample. Wu et al.[65] have also suggested that a POSS bearing isobutyl moieties on part of its corners may act as a radical trap. The isobutyl radical would capture the hydrogen radicals formed during the combustion of the polymer and the silicon radical of the POSS would act similarly for hydroxyl radicals. A char with improved properties would be formed thereafter. This mechanism could be transposed to OMPOSS. However, without proof of the aforementioned mechanism, the main phenomenon occurring remains the formation of the silica layer, as observed on

residues pictures. It should be pointed out that the fragility of the produced residue limits the enhancement of the reaction to fire.

The mechanism of action of APP is relatively well-known in thermoplastics but it is limited in thermosets. It degrades at temperatures lower than that of the polymer and releases ammonia in the gas phase while phosphoric acid is formed from its degradation and remains in the condensed phase. Phosphoric acid is combined with the polymer in order to form a carbonaceous residue, whereas the release of ammonia makes it swell. The addition of CNTs to the Epoxy_APP-5 system modifies this otherwise well-organized mechanism. The species identified in the solid residue along the combustion do not differ from those observed in Epoxy_APP-5. CNTs do not therefore chemically interact with the other constituents. The swelling begins similarly as with APP alone, but it occurs very briefly. The thermal diffusivity is also significantly reduced compared to Epoxy_APP-5. These modifications may explain the antagonism between APP and CNTs. The development of the protective structure due to APP is not initially hindered by the presence of CNTs, but the char formed is not as resistant as before, and the continuous release of gases, which should expand it, gives cracks in the char. CNTs seem therefore to induce defects in the structure of the char resulting in its cracking and less efficient structure.

Finally, it has been shown that the intumescence occurs earlier with Epoxy_APP-4_OMPOSS-1, therefore offering a protection to the underlying material before further degradation. The development of this intumescent structure before ignition can be attributed to the combination between the release of ammonia by APP and the partial sublimation of OMPOSS. The lower temperatures reached by this formulation also give more time for the structure to foam, and to be subsequently better insulated. A char with improved mechanical resistance is produced. The better protection offered by this formulation is therefore due to the earlier formation of the char, which permits its better structuring.

All these mechanisms are summarized in Figure 155. Epoxy_APP-5 begins to swell before ignition with a relatively low swelling rate. Therefore, when ignition occurs and flames spread, the maximum expansion is not already reached. In the case of Epoxy_APP-4.5_CNT-0.5, the swelling is initiated relatively late. Furthermore, even if the protection develops with a high swelling rate, the structure does not resist to the

internal pressure involved by the presence of gases and cracks appear. Finally, in the case of Epoxy_APP-4_OMPOSS-1, swelling occurs early and with a high swelling rate. Therefore, the maximum expansion is reached before fire spreads. Furthermore, the internal structure of the char provides better insulation.

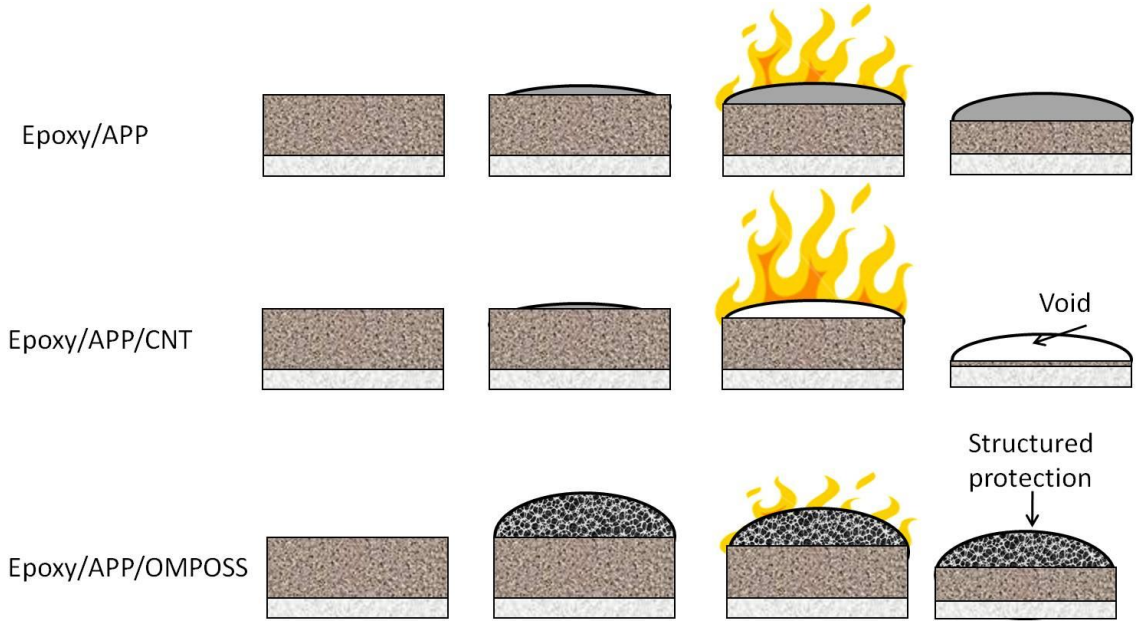

Figure 155: Main protection mechanisms involved by the intumescent formulations

In this chapter, the composition of the samples has been characterized at different times of the burning. OMPOSS alone in the epoxy matrix produces silica. The species identified in Epoxy_APP-4_OMPOSS-1 and Epoxy_APP-4.5_CNT-0.5 do not differ from those present in Epoxy_APP-5. The antagonism between APP and CNTs, and the synergy between APP and OMPOSS do not therefore originate in the creation of new species, even if phosphosilicates reinforcing the char may be produced in the case of Epoxy_APP-4_OMPOSS-1. Indeed, the dynamic study of the burning of the three intumescent samples reveals that the better behavior of Epoxy_APP-4_OMPOSS-1 results mainly from an adequate viscosity that facilitates the trapping of degradation gases in the material and favors its structured expansion. On the contrary, the excessive stiffness of the residue of Epoxy_APP-4.5_CNT-0.5 does not allow the correct development of the protective structure.

General conclusion and outlooks

The work described in this thesis was carried out in the frame of the LAYSA European project and aimed at improving the reaction to fire of epoxy systems by using nanoparticles. Indeed, epoxy-based composite structures are gaining interest for the design of aircrafts, but they are simultaneously easily flammable. There is therefore a need for low-flammability composite materials: one of the goals of the project was to reduce the pHRR by 50 % compared to base resin. First, the potential effect of different nanoparticles as flame-retardants was assessed (POSS and CNTs). Then, formulations combining phosphorus-based flame-retardants and nanoparticles were evaluated for their reaction to fire and interactions were identified: APP and OMPOSS act in synergy whereas APP and CNTs are antagonistic. Different experiments were then carried out in order to fully understand the mechanisms lying behind these interactions.

In this work, different nanofillers were incorporated in the epoxy resin and the resulting materials were characterized in terms of dispersion, crosslinking degree, thermal stability and reaction to fire. The use of different types of POSS and CNTs did not modify the material morphology. However, the thermal stability and the reaction to fire were affected. The nature of the organic moieties linked to the corners of POSS had an influence on the reaction to fire: the reduction of the pHRR compared to the virgin material lay between 21 % (Epoxy_FQ-POSS-5) and 46 % (Epoxy_OMPOSS-5). The incorporation of CNTs alone also changed the reaction to fire (pHRR decreased by 27%). The aforementioned nanoparticles were poorly dispersed in the materials and this parameter has often an influence on the flame retardant properties of nanoparticles in thermoplastics. Since the same conclusion may apply to thermosets, CNTs were functionalized by two flame-retardant moieties. CNT-POSS were completely original whereas CNT-melamine had already been synthesized in our laboratory. Complete characterization of these modified CNTs via TGA, FTIR, XPS and liquid-state NMR was carried out. Once incorporated in the epoxy matrix, it was found that the dispersion state of functionalized-CNTs in the matrix was not enhanced compared to unmodified ones, and that the reaction to fire was neither improved. Therefore, nanofillers are not suitable for strongly flame-retarding epoxy matrices when used alone.

Unmodified CNTs and OMPOSS were then combined with APP in the next part. The APP/CNTs combination showed an antagonistic effect in mass-loss calorimetry, whereas APP/OMPOSS led to a synergy. These effects could not be explained solely by modification of the thermal stability. Furthermore, the characterization by PCFC suggested that condensed-phase mechanisms were mostly involved.

The last part of this thesis aimed therefore at fully understanding these mechanisms. The identification of the species in the residues after burning did not show differences between the samples containing APP alone or in combination. However, it was proven that APP and OMPOSS may react together to yield silicophosphates that could reinforce the char structure. The system viscosity as a function of temperature, the swelling rates and the temperatures recorded inside the burning samples were analyzed and led to the following conclusions: synergistic and antagonistic effects observed when nanoparticles are incorporated in the intumescent Epoxy_APP-5 system result mainly from the modified ability of the degraded material for trapping gases. Epoxy_APP-4.5_CNT-0.5 char has an increased rigidity and many cracks and holes appear at the surface of the residue due to an excessive internal pressure when gases are released. On the contrary, the viscosity of Epoxy_APP-4_OMPOSS-1 drops at higher temperatures than for Epoxy_APP-5 and the minimum viscosity is higher than for other formulations. This allows the better trapping of gases. Furthermore, gases released by OMPOSS upon degradation/sublimation are added to ammonia from APP, and improving the swelling capability of this formulation.

Many issues have been addressed in this work. One of them is the potential of nanoparticles as efficient flame retardants in epoxy systems. Our work showed that when a simple process is used, no outstanding fire performance can be achieved with nanoparticles alone. It would however be interesting to improve the dispersion of these fillers in the matrix, since it may have an influence on the flame retardant capability. One way to achieve this would be the use of high-shear mixer or the addition of dispersants in the system: the use of polyoxyethylene-8-lauryl in order to disperse CNTs was reported as efficient [75]. Finding the good combination (nature of dispersant, quantity, type of mixing blade and mixing time) could be achieved through the use of experimental design. If possible, the dispersion of CNTs in the Epoxy_APP-4.5_CNT-0.5

formulation should also be enhanced by using these optimized conditions. Testing the reaction to fire of this new sample would show if well-dispersed CNTs still act as defects at the surface of the char.

A promising system, Epoxy_APP-4_OMPOSS-1, has been identified and its mechanism of action has been studied. It would however be worth investigating more precisely some parameters. It is not clear in the literature if OMPOSS sublime upon heating or if the evolved gases are decomposition products. Our work suggests that the gases evolved during thermal degradation and analyzed by FTIR are not intact POSS. It would therefore be interesting to deeply analyze these evolved gases by Gas Chromatography-Mass Spectroscopy (GC-MS pyrolyzer).

Another aspect of this work was the analysis of solid residues during burning. The repartition of phosphorus-containing species was examined by EPMA. It would also be useful to assess the repartition of silicon-containing species. However, silicon-containing particles were too small for being detected by EPMA, but the use of other techniques may solve this problem. In particular, elemental analyses would give the composition of samples taken in different parts of the residues.

Finally, since this work is part of a more global program, the reaction to fire of the full multilayer composite developed in the LAYSA project should be evaluated in the next months. It will show if the incorporation of CNTs in a fiber-reinforced composite will act similarly as in the model resin and be therefore a weak point for flame retardancy. If so, the APP/OMPOSS system may be an adequate alternative.

References

1. S. Bourbigot and S. Duquesne, *Fire retardant polymers: Recent developments and opportunities.* Journal of Materials Chemistry, **2007**. 17(22): p. 2283-2300.
2. M. Jimenez, S. Duquesne, and S. Bourbigot, *High-throughput fire testing for intumescent coatings.* Industrial and Engineering Chemistry Research, **2006**. 45(22): p. 7475-7481.
3. A. Vannier, S. Duquesne, S. Bourbigot, A. Castrovinci, G. Camino, and R. Delobel, *The use of POSS as synergist in intumescent recycled poly(ethylene terephthalate).* Polymer Degradation and Stability, **2008**. 93(4): p. 818-826.
4. X. Wang, Y. Hu, L. Song, W. Xing, and H. Lu, *Thermal degradation behaviors of epoxy resin/poss hybrids and phosphorus-silicon synergism of flame retardancy.* Journal of Polymer Science, Part B: Polymer Physics, **2010**. 48(6): p. 693-705.
5. G. Fontaine and S. Bourbigot, *Intumescent polylactide: A nonflammable material.* Journal of Applied Polymer Science, **2009**. 113(6): p. 3860-3865.
6. Available from: http://www.plasticseurope.org/documents/document/20101028135906-final_plasticsthefacts_26102010_lr.pdf. Accessed in March 2011
7. Available from: http://www.plasticseurope.org/documents/document/20110125093302-plasticseurope,_statistical_monitoring,_pemrg,_2011-01a_-_summary.pdf. Accessed in March 2011
8. H.F. Mark, *Epoxy resins*, in *Encyclopedia of polymer science and technology*. **2011**, Wiley. p. 378-804.
9. Available from: http://www.acmite.com/market-reports/chemicals/world-epoxy-resin-market.html. Accessed in March 2011
10. R.E. Lyon, *Materials with reduced flammability in aerospace and aviation*, in *Advances in fire retardant materials*, A.R. Horrocks and D. Price, Editors. **2008**, Woodhead Publishing. p. 573-598.
11. Available from: www.laysa.eu. Accessed in March 2011
12. H.Q. Pham and M.J. Marks, *Epoxy resins*, in *Encyclopedia of Polymer Science and Technology*, H.F. Mark, Editor. **2011**, Wiley. p. 678-804.
13. C. Barrère and F. Dal Maso, *Résines époxy réticulées par des polyamines : structures et propriétés.* Revue de l'Institut Français du Pétrole, **1997**. 52(3): p. 317-335.
14. P. Bardonnet, *Résines époxydes (EP) - Composants et propriétés* in *Techniques de l'Ingénieur*. **1992**.
15. S.V. Levchik and E.D. Weil, *Thermal decomposition, combustion and flame-retardancy of epoxy resins - A review of the recent literature.* Polymer International, **2004**. 53(12): p. 1901-1929.
16. T. Dyakonov, P.J. Mann, Y. Chen, and W.T.K. Stevenson, *Thermal analysis of some aromatic amine cured model epoxy resin systems - II: Residues of degradation.* Polymer Degradation and Stability, **1996**. 54(1): p. 67-83.

17. M. Iji and Y. Kiuchi, *Flame-retardant epoxy resin compounds containing novolac derivatives with aromatic compounds.* Polymers for Advanced Technologies, **2001**. 12(7): p. 393-406.
18. D.P. Bishop and D.A. Smith, *Combined pyrolysis and radiochemical gas chromatography for studying the thermal degradation of epoxy resins and polyimides- % 1.* Journal of Applied Polymer Science, **1970**. 14(1): p. 205-223.
19. M.A. Keenan and D.A. Smith, *Further aspects of the thermal degradation of epoxide resins.* Journal of Applied Polymer Science, **1967**. 11: p. 1009-1026.
20. B.K. Kandola, A.R. Horrocks, P. Myler, and D. Blair, *Thermal Characterization of Thermoset Matrix Resins*. **2001**. p. 344-360.
21. B.L. Burton, *Thermooxidative stability of cured epoxy resins. I.* Journal of Applied Polymer Science, **1993**. 47(10): p. 1821-1837.
22. S. Bourbigot and X. Flambard, *Heat resistance and flammability of high performance fibres: A review.* Fire and Materials, **2002**. 26(4-5): p. 155-168.
23. M. Spontón, G. Lligadas, J.C. Ronda, M. Galià, and V. Cádiz, *Development of a DOPO-containing benzoxazine and its high-performance flame retardant copolybenzoxazines.* Polymer Degradation and Stability, **2009**. 94: p. 1693-1699.
24. N. Rose, *Etude de la dégradation thermique et du comportement au feu de résines époxydes utilisées dans l'aéronautique*. **PhD thesis, 1995**, Université des Sciences et Technologies de Lille.
25. M. Iji and Y. Kiuchi, *Self-extinguishing epoxy molding compound with no flame-retarding additives for electronic components.* Journal of Materials Science: Materials in Electronics, **2001**. 12(12): p. 715-723.
26. J. Choi, A.F. Yee, and R.M. Laine, *Organic/inorganic hybrid composites from cubic silsesquioxanes. Epoxy resins of octa(dimethylsiloxyethylcyclohexylepoxide) silsesquioxane.* Macromolecules, **2003**. 36(15): p. 5666-5682.
27. J.M. Laza, E. Bilbao, M.T. Garay, J.L. Vilas, M. Rodríguez, and L.M. León, *Thermal properties and fire behaviour of materials produced from curing mixed epoxy and phenolic resins.* Fire and Materials, **2008**. 32(5): p. 281-292.
28. Available from: http://www.cefic-efra.com/Content/Default.asp?PageName=openfile&DocRef=2006-02-10-00005. Accessed in June 2010
29. Available from: http://www.cefic-efra.com/Content/Default.asp?PageName=openfile&DocRef=2008-04-07-00001. Accessed in April 2010
30. Available from: http://www.sriconsulting.com. Accessed in March 2011
31. J.J. Pitts, *Antimony/halogen synergistic reactions in fire retardants.* Journal of Fire and Flammability, **1972**. 3: p. 51.
32. C.-P. Yang and T.-W. Lee, *Synthesis and properties of 4-hydroxy-2,3,5,6-tetrabromobenzyl phosphonates and effects of their flame retardance on impact polystyrene.* Journal of Applied Polymer Science, **1986**. 32(1): p. 3005-3025.
33. R.V. Petrella, *Flame Retardant Polymeric Materials*, ed. M. Lewin, S.M. Atlas, and E.M. Pearce. **1978**: Plenum.
34. Available from: http://www.specialchem4polymers.com. Accessed in March 2011
35. S. Zhang and A.R. Horrocks, *A review of flame retardant polypropylene fibres.* Progress in Polymer Science (Oxford), **2003**. 28(11): p. 1517-1538.

36. Y. Kiuchi, M. Iji, H. Nagashima, and T. Miwa, *Increase in flame retardance of glass-epoxy laminates without halogen or phosphorous compounds by simultaneous use of incombustible-gas generator and charring promoter.* Journal of Applied Polymer Science, **2006**. 101(5): p. 3367-3375.
37. P.R. Hornsby, *Fire retardant fillers for polymers.* International Materials Reviews, **2001**. 46(4): p. 199-210.
38. F. Carpentier, S. Bourbigot, M. Le Bras, and R. Delobel, *Rheological investigations in fire retardancy: Application to ethylene-vinyl-acetate copolymer-magnesium hydroxide/zinc borate formulations.* Polymer International, **2000**. 49(10): p. 1216-1221.
39. P. Ducrocq, S. Duquesne, S. Magnet, S. Bourbigot, and R. Delobel, *Interactions between chlorinated paraffins and melamine in intumescent paint-investing a way to suppress chlorinated paraffins from the formulations.* Progress in Organic Coatings, **2006**. 57(4): p. 430-438.
40. T. Ishii, H. Kokaku, A. Nagai, T. Nishita, and M. Kakimoto, *Calcium borate flame retardation system for epoxy molding compounds.* Polymer Engineering and Science, **2006**. 46(6): p. 799-806.
41. A. De Fenzo, C. Formicola, V. Antonucci, M. Zarrelli, and M. Giordano, *Effects of zinc-based flame retardants on the degradation behaviour of an aerospace epoxy matrix.* Polymer Degradation and Stability, **2009**. 94(9): p. 1354-1363.
42. L.A. Mercado, J.A. Reina, and M. Galià *Flame Retardant Epoxy Resins Based on Diglycidyloxymethylphenylsilane.* Journal of Polymer Science, Part A: Polymer Chemistry, **2006**. 44: p. 5580-5587.
43. M. Harada, S. Minamigawa, and M. Ochi, *Thermal properties and flame retardancy of polyglycidyloxypropyl silsesquioxane/layered titanate nanocomposites.* Journal of Applied Polymer Science, **2008**. 110(5): p. 2649-2655.
44. M. Harada, S. Minamigawa, K. Tachibana, and M. Ochi, *Flame retardancy and thermomechanical properties of the poly-(glycidyloxypropyl) phenyl silsesquioxane/ layered titanate nanocomposites.* Journal of Applied Polymer Science, **2007**. 106(1): p. 338-344.
45. E. Manias, G. Polizos, H. Nakajima, and M.J. Heidecker, *Fundamentals of Polymer Nanocomposite Technology*, in *Flame Retardant Polymer Nanocomposites*, A.B. Morgan and C.A. Wilkie, Editors. **2007**, John Wiley and Sons.
46. Available from: http://www.hort.purdue.edu/newcrop/tropical/lecture_06/02m.jpg. Accessed in November 2010
47. Available from: http://serc.carleton.edu/images/NAGTWorkshops/mineralogy/montmorillonite_structure.jpg. Accessed in November 2010
48. M. Alexandre and P. Dubois, *Polymer-layered silicate nanocomposites: Preparation, properties and uses of a new class of materials.* Materials Science and Engineering R: Reports, **2000**. 28(1): p. 1-63.
49. F. Samyn, S. Bourbigot, C. Jama, and S. Bellayer, *Fire retardancy of polymer clay nanocomposites: Is there an influence of the nanomorphology?* Polymer Degradation and Stability, **2008**. 93(11): p. 2019-2024.
50. A. Hartwig, D. Pütz, B. Schartel, M. Bartholmai, and M. Wendschuh-Josties, *Combustion Behaviour of Epoxide Based Nanocomposites with Ammonium and*

Phosphonium Bentonites. Macromolecular Chemistry and Physics, **2003**. 204(18): p. 2247-2257.

51. B. Schartel, U. Knoll, A. Hartwig, and D. Pütz, *Phosphonium-modified layered silicate epoxy resins nanocomposites and their combinations with ATH and organo-phosphorus fire retardants.* Polymers for Advanced Technologies, **2006**. 17(4): p. 281-293.
52. B.W. Schartel, A.; Sturm, H.; Kleemeier, M.; Hartwig, A.; Vogt, C.; Fischer, R. X. , *Layered silicate epoxy nanocomposites: formation of the inorganic-carbonaceous fire protection layer.* Polymers for Advanced Technologies, **2010**.
53. G. Camino, G. Tartaglione, A. Frache, C. Manferti, and G. Costa, *Thermal and combustion behaviour of layered silicate-epoxy nanocomposites.* Polymer Degradation and Stability, **2005**. 90(2 SPEC. ISS.): p. 354-362.
54. M. Zammarano, *Thermoset Fire Retardant Nanocomposites*, in *Flame Retardant Polymer Nanocomposites*, A.B. Morgan and C.A. Wilkie, Editors. **2007**, John Wiley & Sons: Hoboken. p. 235-284.
55. L. Torre, E. Frulloni, J.M. Kenny, C. Manferti, and G. Camino, *Processing and characterization of epoxy-anhydride-based intercalated nanocomposites.* Journal of Applied Polymer Science, **2003**. 90(9): p. 2532-2539.
56. Available from: http://tresen.vscht.cz/min/en/research-team-mineralogy. Accessed in March 2011
57. M. Zammarano, M. Franceschi, S. Bellayer, J.W. Gilman, and S. Meriani, *Preparation and flame resistance properties of revolutionary self-extinguishing epoxy nanocomposites based on layered double hydroxides.* Polymer, **2005**. 46(22): p. 9314-9328.
58. J. Brus, M. Urbanova, and A. Strachota, *Epoxy networks reinforced with polyhedral oligomeric silsesquioxanes: Structure and segmental dynamics as studied by solid-state NMR.* Macromolecules, **2008**. 41(2): p. 372-386.
59. J. Fu, L. Shi, Y. Chen, S. Yuan, J. Wu, X. Liang, and Q. Zhong, *Epoxy nanocomposites containing mercaptopropyl polyhedral oligomeric silsesquioxane: Morphology, thermal properties, and toughening mechanism.* Journal of Applied Polymer Science, **2008**. 109(1): p. 340-349.
60. Z. Zhang, G. Liang, J. Wang, and P. Ren, *Epoxy/POSS organic-inorganic hybrids: Viscoelastic, mechanical properties and micromorphologies.* Polymer Composites, **2007**. 28(2): p. 175-179.
61. A. Vannier, S. Duquesne, S. Bourbigot, J. Alongi, G. Camino, and R. Delobel, *Investigation of the thermal degradation of PET, zinc phosphinate, OMPOSS and their blends-Identification of the formed species.* Thermochimica Acta, **2009**. 495(1-2): p. 155-166.
62. S. Bourbigot, S. Duquesne, G. Fontaine, S. Bellayer, T. Turf, and F. Samyn, *Characterization and Reaction to Fire of Polymer Nanocomposites with and without Conventional Flame Retardants.* Molecular Crystals and Liquid Crystals, **2008**. 486: p. 325-339.
63. T. Lu, G. Liang, Y. Peng, and T. Chen, *Blended hybrids based on silsesquioxane-OH and epoxy resins.* Journal of Applied Polymer Science, **2007**. 106(6): p. 4117-4123.

64. T. Lu, T. Chen, and G. Liang, *Synthesis, thermal properties, and flame retardance of the epoxy-silsesquioxane hybrid resins.* Polymer Engineering and Science, **2007**. 47(3): p. 225-234.
65. K. Wu, L. Song, Y. Hu, H. Lu, B.K. Kandola, and E. Kandare, *Synthesis and characterization of a functional polyhedral oligomeric silsesquioxane and its flame retardancy in epoxy resin.* Progress in Organic Coatings, **2009**. 65(4): p. 490-497.
66. Q. Wu, C. Zhang, R. Liang, and B. Wang, *Combustion and thermal properties of epoxy/phenyltrisilanol polyhedral oligomeric silsesquioxane nanocomposites.* Journal of Thermal Analysis and Calorimetry, **2009**: p. 1-7.
67. E. Franchini, J. Galy, J.F. Gérard, D. Tabuani, and A. Medici, *Influence of POSS structure on the fire retardant properties of epoxy hybrid networks.* Polymer Degradation and Stability, **2009**. 94: p. 1728-1736.
68. Ijima S., *Helical microtubules of graphitic carbon.* Nature, **1991**. 354: p. 56-57.
69. O. Breuer and U. Sundararaj, *Big returns from small fibers: A review of polymer/carbon nanotube composites.* Polymer Composites, **2004**. 25(6): p. 630-645.
70. R. Saito, G. Dresselhaus, and M.S. Dresselhaus, *Physical Properties of Carbon Nanotubes*. **1998**: World Scientific Publishing Company.
71. M.S. Dresselhaus, G. Dresselhaus, P. Eklund, and R. Saito, *Carbon nanotubes.* Physics World, **1998**. 33.
72. I. Kang, Y.Y. Heung, J.H. Kim, J.W. Lee, R. Gollapudi, S. Subramaniam, S. Narasimhadevara, D. Hurd, G.R. Kirikera, V. Shanov, M.J. Schulz, D. Shi, J. Boerio, S. Mall, and M. Ruggles-Wren, *Introduction to carbon nanotube and nanofiber smart materials.* Composites Part B: Engineering, **2006**. 37(6): p. 382-394.
73. J.M. Moon, K.H. An, Y.H. Lee, Y.S. Park, D.J. Bae, and G.S. Park, *High-yield purification process of singlewalled carbon nanotubes.* Journal of Physical Chemistry B, **2001**. 105(24): p. 5677-5681.
74. M. Moniruzzaman and K.I. Winey, *Polymer nanocomposites containing carbon nanotubes.* Macromolecules, **2006**. 39(16): p. 5194-5205.
75. X. Gong, J. Liu, S. Baskaran, R.D. Voise, and J.S. Young, *Surfactant-assisted processing of carbon nanotube/polymer composites.* Chemistry of Materials, **2000**. 12(4): p. 1049-1052.
76. J. Shen, W. Huang, L. Wu, Y. Hu, and M. Ye, *The reinforcement role of different amino-functionalized multi-walled carbon nanotubes in epoxy nanocomposites.* Composites Science and Technology, **2007**. 67(15-16): p. 3041-3050.
77. J. Wang, Z. Fang, A. Gu, L. Xu, and F. Liu, *Effect of amino-functionalization of multi-walled carbon nanotubes on the dispersion with epoxy resin matrix.* Journal of Applied Polymer Science, **2006**. 100(1): p. 97-104.
78. S. Wang, Z. Liang, T. Liu, B. Wang, and C. Zhang, *Effective amino-functionalization of carbon nanotubes for reinforcing epoxy polymer composites.* Nanotechnology, **2006**. 17(6): p. 1551-1557.
79. J. Sandler, M.S.P. Shaffer, T. Prasse, W. Bauhofer, K. Schulte, and A.H. Windle, *Development of a dispersion process for carbon nanotubes in an epoxy matrix and the resulting electrical properties.* Polymer, **1999**. 40(21): p. 5967-5971.
80. J. Liu, A.G. Rinzler, H. Dai, J.H. Hafner, R. Kelley Bradley, P.J. Boul, A. Lu, T. Iverson, K. Shelimov, C.B. Huffman, F. Rodriguez-Macias, Y.S. Shon, T.R. Lee, D.T.

Colbert, and R.E. Smalley, *Fullerene pipes.* Science, **1998**. 280(5367): p. 1253-1256.

81. H.Y. Ma, L.F. Tong, Z.B. Xu, and Z.P. Fang, *Functionalizing carbon nanotubes by grafting on intumescent flame retardant: nanocomposite synthesis, morphology, rheology, and flammability.* Advanced Functional Materials, **2008**. 18(3): p. 414-421.
82. T. Kashiwagi, F. Du, K.I. Winey, K.M. Groth, J.R. Shields, S.P. Bellayer, H. Kim, and J.F. Douglas, *Flammability properties of polymer nanocomposites with single-walled carbon nanotubes: Effects of nanotube dispersion and concentration.* Polymer, **2005**. 46(2): p. 471-481.
83. T. Kashiwagi, E. Grulke, J. Hilding, K. Groth, R. Harris, K. Butler, J. Shields, S. Kharchenko, and J. Douglas, *Thermal and flammability properties of polypropylene/carbon nanotube nanocomposites.* Polymer, **2004**. 45(12): p. 4227-4239.
84. C.F. Kuan, W.J. Chen, Y.L. Li, C.H. Chen, H.C. Kuan, and C.L. Chiang, *Flame retardance and thermal stability of carbon nanotube epoxy composite prepared from sol-gel method.* Journal of Physics and Chemistry of Solids, **2010**. 71(4): p. 539-543.
85. S.S. Rahatekar, M. Zammarano, S. Matko, K.K. Koziol, A.H. Windle, M. Nyden, T. Kashiwagi, and J.W. Gilman, *Effect of carbon nanotubes and montmorillonite on the flammability of epoxy nanocomposites.* Polymer Degradation and Stability, **2010**. 95(5): p. 870-879.
86. M. Jimenez, S. Duquesne, and S. Bourbigot, *Characterization of the performance of an intumescent fire protective coating.* Surface and Coatings Technology, **2006**. 201(3-4): p. 979-987.
87. V. Babushok and W. Tsang, *Inhibitor rankings for alkane combustion.* Combustion and Flame, **2000**. 123(4): p. 488-506.
88. L.S. Wang, X.L. Wang, and G.L. Yan, *Synthesis, characterization and flame retardance behaviour of poly(ethylene terephthalate) copolymer containing triaryl phosphine oxide.* Polymer Degradation and Stability, **2000**. 69(1): p. 127-130.
89. G. Fontaine, S. Bourbigot, and S. Duquesne, *Neutralized flame retardant phosphorus agent: Facile synthesis, reaction to fire in PP and synergy with zinc borate.* Polymer Degradation and Stability, **2008**. 93(1): p. 68-76.
90. F. Samyn, S. Bourbigot, C. Jama, S. Bellayer, S. Nazare, R. Hull, A. Fina, A. Castrovinci, and G. Camino, *Characterisation of the dispersion in polymer flame retarded nanocomposites.* European Polymer Journal, **2008**. 44(6): p. 1631-1641.
91. S. Levchik, A. Piotrowski, E. Weil, and Q. Yao, *New developments in flame retardancy of epoxy resins.* Polymer Degradation and Stability, **2005**. 88(1): p. 57-62.
92. S.V. Levchik and E.D. Weil, *A review of recent progress in phosphorus-based flame retardants.* Journal of Fire Sciences, **2006**. 24(5): p. 345-364.
93. P. Jain, V. Choudhary, and I.K. Varma, *Flame retarding epoxies with phosphorus.* Journal of Macromolecular Science Polymer Reviews, **2002**. 42(2): p. 139-183.
94. M. Hussain, R.J. Varley, Z. Mathys, Y.B. Cheng, and G.P. Simon, *Effect of Organo-Phosphorus and Nano-Clay Materials on the Thermal and Fire Performance of Epoxy Resins.* Journal of Applied Polymer Science, **2004**. 91(2): p. 1233-1253.

95. C.S. Wang and C. Lin Hsuan, *Synthesis and properties of phosphorus-containing epoxy resins by novel method.* Journal of Polymer Science, Part A: Polymer Chemistry, **1999**. 37(21): p. 3903-3909.
96. C.H. Lin and C.S. Wang, *Novel phosphorus-containing epoxy resins Part I. Synthesis and properties.* Polymer, **2001**. 42(5): p. 1869-1878.
97. J. Artner, M. Ciesielski, M. Ahlmann, O. Walter, M. Döring, R.M. Perez, V. Altstädt, J.K.W. Sandler, and B. Schartel, *A novel and effective synthetic approach to 9,10-dihydro-9-oxa-10- phosphaphenanthrene-10-oxide (DOPO) derivatives.* Phosphorus, Sulfur and Silicon and the Related Elements, **2007**. 182(9): p. 2131-2148.
98. J. Artner, M. Ciesielski, O. Walter, M. Döring, R.M. Perez, J.K.W. Sandler, V. Altstädt, and B. Schartel, *A novel DOPO-based diamine as hardener and flame retardant for epoxy resin systems.* Macromolecular Materials and Engineering, **2008**. 293(6): p. 503-514.
99. R.M. Perez, J.K.W. Sandler, V. Altstädt, T. Hoffmann, D. Pospiech, J. Artner, M. Ciesielski, M. Döring, A.I. Balabanovich, and B. Schartel, *Effective halogen-free flame retardancy for a monocomponent polyfunctional epoxy using an oligomeric organophosphorus compound.* Journal of Materials Science, **2006**. 41(24): p. 8347-8351.
100. R.M. Perez, J.K.W. Sandler, V. Altstädt, T. Hoffmann, D. Pospiech, M. Ciesielski, and M. Döring, *Effect of DOP-based compounds on fire retardancy, thermal stability, and mechanical properties of DGEBA cured with 4,4'-DDS.* Journal of Materials Science, **2006**. 41(2): p. 341-353.
101. B. Schartel, U. Braun, A.I. Balabanovich, J. Artner, M. Ciesielski, M. Döring, R.M. Perez, J.K.W. Sandler, and V. Altstädt, *Pyrolysis and fire behaviour of epoxy systems containing a novel 9,10-dihydro-9-oxa-10-phosphaphenanthrene-10-oxide-(DOPO)-based diamino hardener.* European Polymer Journal, **2008**. 44(3): p. 704-715.
102. M. Ciesielski, A. Schäfer, and M. Döring, *Novel efficient DOPO-based flame-retardants for PWB relevant epoxy resins with high glass transition temperatures.* Polymers for Advanced Technologies, **2008**. 19(6): p. 507-515.
103. A. Schäfer, S. Seibold, W. Lohstroh, O. Walter, and M. Döring, *Synthesis and properties of flame-retardant epoxy resins based on DOPO and one of its analog DPPO.* Journal of Applied Polymer Science, **2007**. 105(2): p. 685-696.
104. P.M. Hergenrother, C.M. Thompson, J.G. Smith Jr, J.W. Connell, J.A. Hinkley, R.E. Lyon, and R. Moulton, *Flame retardant aircraft epoxy resins containing phosphorus.* Polymer, **2005**. 46(14): p. 5012-5024.
105. U. Braun, A.I. Balabanovich, B. Schartel, U. Knoll, J. Artner, M. Ciesielski, M. Döring, R. Perez, J.K.W. Sandler, V. Altstädt, T. Hoffmann, and D. Pospiech, *Influence of the oxidation state of phosphorus on the decomposition and fire behaviour of flame-retarded epoxy resin composites.* Polymer, **2006**. 47(26): p. 8495-8508.
106. W. Liu, R.J. Varley, and G.P. Simon, *Understanding the decomposition and fire performance processes in phosphorus and nanomodified high performance epoxy resins and composites.* Polymer, **2007**. 48(8): p. 2345-2354.
107. P. Kiliaris and C.D. Papaspyrides, *Polymer/layered silicate (clay) nanocomposites: An overview of flame retardancy.* Progress in Polymer Science, **2010**.

108. A. Toldy, N. Toth, P. Anna, and G. Marosi, *Synthesis of phosphorus-based flame retardant systems and their use in an epoxy resin.* Polymer Degradation and Stability, **2006**. 91: p. 585-592.
109. G.H. Hsiue, W.J. Wang, and F.C. Chang, *Synthesis, characterization, thermal and flame-retardant properties of silicon-based epoxy resins.* Journal of Applied Polymer Science, **1999**. 73(7): p. 1231-1238.
110. M. Jimenez, S. Duquesne, and S. Bourbigot, *Intumescent fire protective coating: Toward a better understanding of their mechanism of action.* Thermochimica Acta, **2006**. 449(1-2): p. 16-26.
111. M. Jimenez, S. Duquesne, and S. Bourbigot, *Kinetic analysis of the thermal degradation of an epoxy-based intumescent coating.* Polymer Degradation and Stability, **2009**. 94(3): p. 404-409.
112. G. Wang and J. Yang, *Influences of binder on fire protection and anticorrosion properties of intumescent fire resistive coating for steel structure.* Surface and Coatings Technology. 204(8): p. 1186-1192.
113. Z. Wang, E. Han, and W. Ke, *Influence of nano-LDHs on char formation and fire-resistant properties of flame-retardant coating.* Progress in Organic Coatings, **2005**. 53(1): p. 29-37.
114. Z. Wang, E. Han, and W. Ke, *Effect of nanoparticles on the improvement in fire-resistant and anti-ageing properties of flame-retardant coating.* Surface and Coatings Technology, **2006**. 200(20-21): p. 5706-5716.
115. Z. Wang, E. Han, F. Liu, and W. Ke, *Thermal behavior of nano-TiO_2 in fire-resistant coating.* Journal of Materials Science and Technology, **2007**. 23(4): p. 547-550.
116. A. Castrovinci, G. Camino, C. Drevelle, S. Duquesne, C. Magniez, and M. Vouters, *Ammonium polyphosphate-aluminum trihydroxide antagonism in fire retarded butadiene-styrene block copolymer.* European Polymer Journal, **2005**. 41(9): p. 2023-2033.
117. J.T. Thurston, J.R. Dudley, D.W. Kaiser, I. Hechenbleikner, F.C. Schaefer, and D. Holm-Hansen, *Cyanuric chloride derivatives. I. Aminochloro-s-triazines.* Journal of the American Chemical Society, **1951**. 73(7): p. 2981-2983.
118. J.M.E. Quirke, *1,3,5-Triazines*, in *Comprehensive heterocyclic chemistry* A.R. Katritzky and C.W. Rees, Editors. **1984**. p. 457-530.
119. M. Bugajny, M. Le Bras, and S. Bourbigot, *New approach to the dynamic properties of an intumescent material.* Fire and Materials, **1999**. 23(1): p. 49-51.
120. P. Anna, G. Marosi, I. Csontos, S. Bourbigot, M. Le Bras, and R. Delobel, *Influence of modified rheology on the efficiency of intumescent flame retardant systems.* Polymer Degradation and Stability, **2001**. 74(3): p. 423-426.
121. M. Hellenbrandt, *The inorganic crystal structure database (ICSD) - Present and future.* Crystallography Reviews, **2004**. 10(1): p. 17-22.
122. T. Kashiwagi, E. Grulke, J. Hilding, R. Harris, W. Awad, and J. Douglas, *Thermal degradation and flammability properties of poly(propylene)/carbon nanotube composites.* Macromolecular Rapid Communications, **2002**. 23(13): p. 761-765.
123. S. Bourbigot, F. Samyn, T. Turf, and S. Duquesne, *Nanomorphology and reaction to fire of polyurethane and polyamide nanocomposites containing flame retardants.* Polymer Degradation and Stability, **2010**. 95(3): p. 320-326.
124. S. Bourbigot, G. Fontaine, A. Gallos, C. Gérard, and S. Bellayer, *Functionalized-carbon multiwall nanotube as Flame Retardant for Polylactid Acid*, in *Fire and*

Polymers V, C.A. Wilkie, A.B. Morgan, and G.L. Nelson, Editors. **2009**, ACS. p. 25-34.

125. S. Bourbigot, T. Turf, S. Bellayer, and S. Duquesne, *Polyhedral oligomeric silsesquioxane as flame retardant for thermoplastic polyurethane.* Polymer Degradation and Stability, **2009**. 94(8): p. 1230-1237.
126. Y.S. Song and J.R. Youn, *Influence of dispersion states of carbon nanotubes on physical properties of epoxy nanocomposites.* Carbon, **2005**. 43(7): p. 1378-1385.
127. K. Tao, S. Yang, J.C. Grunlan, Y.S. Kim, B. Dang, Y. Deng, R.L. Thomas, B.L. Wilson, and X. Wei, *Effects of carbon nanotube fillers on the curing processes of epoxy resin-based composites.* Journal of Applied Polymer Science, **2006**. 102(6): p. 5248-5254.
128. W. Zou, Z.j. Du, Y.x. Liu, X. Yang, H.q. Li, and C. Zhang, *Functionalization of MWNTs using polyacryloyl chloride and the properties of CNT-epoxy matrix nanocomposites.* Composites Science and Technology, **2008**. 68(15-16): p. 3259-3264.
129. X.L. Xie, Y.W. Mai, and X.P. Zhou, *Dispersion and alignment of carbon nanotubes in polymer matrix: A review.* Materials Science and Engineering R: Reports, **2005**. 49(4).
130. R.A. Venditti and J.K. Gillham, *A relationship between the glass transition temperature (Tg) and fractional conversion for thermosetting systems.* Journal of Applied Polymer Science, **1997**. 64(1): p. 3-14.
131. J.P. Pascault and R.J.J. Williams, *Glass transition temperature versus conversion relationships for thermosetting polymers.* Journal of Polymer Science, Part B: Polymer Physics, **1990**. 28(1): p. 85-95.
132. Y. Ni, S. Zheng, and K. Nie, *Morphology and thermal properties of inorganic-organic hybrids involving epoxy resin and polyhedral oligomeric silsesquioxanes.* Polymer, **2004**. 45(16): p. 5557-5568.
133. Y. Liu, S. Zheng, and K. Nie, *Epoxy nanocomposites with octa(propylglycidyl ether) polyhedral oligomeric silsesquioxane.* Polymer, **2005**. 46(25): p. 12016-12025.
134. T.H. Hsieh, A.J. Kinloch, A.C. Taylor, and S. Sprenger, *The effect of silica nanoparticles and carbon nanotubes on the toughness of a thermosetting epoxy polymer.* Journal of Applied Polymer Science, **2011**. 119(4): p. 2135-2142.
135. A. Allaoui and N. El Bounia, *How carbon nanotubes affect the cure kinetics and glass transition temperature of their epoxy composites? - A review.* Express Polymer Letters, **2009**. 3(9): p. 588-594.
136. C. Ramirez, M. Rico, A. Torres, L. Barral, J. LÃ³pez, and B. Montero, *Epoxy/POSS organic-inorganic hybrids: ATR-FTIR and DSC studies.* European Polymer Journal, **2008**. 44(10): p. 3035-3045.
137. B. Mailhot, S. Morlat-Thérias, P.O. Bussière, and J.L. Gardette, *Study of the degradation of an epoxy/amine resin, 2 kinetics and depth-profiles.* Macromolecular Chemistry and Physics, **2005**. 206(5): p. 585-591.
138. F. Fraga, E.C. Vazquez, E. Rodríguez-Núñez, and J.M. Martínez-Ageitos, *Curing kinetics of the epoxy system diglycidyl ether of bisphenol A/isophoronediamine by Fourier transform infrared spectroscopy.* Polymers for Advanced Technologies, **2008**. 19(11): p. 1623-1628.

139. B.K. Kandola and W. Pornwannachai, *Enhancement of passive fire protection ability of inorganic fire retardants in vinyl ester resin using glass frit synergists.* Journal of Fire Sciences, **2010**. 28(4): p. 357-381.
140. C. Manzi-Nshuti, J.M. Hossenlopp, and C.A. Wilkie, *Fire retardancy of melamine and zinc aluminum layered double hydroxide in poly(methyl methacrylate).* Polymer Degradation and Stability, **2008**. 93(10): p. 1855-1863.
141. D. Yang, G. Guo, J. Hu, C. Wang, and D. Jiang, *Hydrothermal treatment to prepare hydroxyl group modified multi-walled carbon nanotubes.* Journal of Materials Chemistry, **2008**. 18(3): p. 350-354.
142. V. Datsyuk, M. Kalyva, K. Papagelis, J. Parthenios, D. Tasis, A. Siokou, I. Kallitsis, and C. Galiotis, *Chemical oxidation of multiwalled carbon nanotubes.* Carbon, **2008**. 46(6): p. 833-840.
143. H.J. Wang, X.K. Xi, A. Kleinhammes, and Y. Wu, *Temperature-induced hydrophobic-hydrophilic transition observed by water adsorption.* Science, **2008**. 322(5898): p. 80-83.
144. F. Hennrich, K. Arnold, S. Lebedkin, A. Quintilla, W. Wenzel, and M.M. Kappes, *Diameter sorting of carbon nanotubes by gradient centrifugation: Role of endohedral water.* Physica Status Solidi (B) Basic Research, **2007**. 244(11): p. 3896-3900.
145. Q. Chen, J.L. Herberg, G. Mogilevsky, H.J. Wang, M. Stadermann, J.K. Holt, and Y. Wu, *Identification of endohedral water in single-walled carbon nanotubes by 1H NMR.* Nano Letters, **2008**. 8(7): p. 1902-1905.
146. G.X. Chen and H. Shimizu, *Multiwalled carbon nanotubes grafted with polyhedral oligomeric silsesquioxane and its dispersion in poly(l-lactide) matrix.* Polymer, **2008**. 49(4): p. 943-951.
147. J. Shen, W. Huang, L. Wu, Y. Hu, and M. Ye, *Thermo-physical properties of epoxy nanocomposites reinforced with amino-functionalized multi-walled carbon nanotubes.* Composites Part A: Applied Science and Manufacturing, **2007**. 38(5): p. 1331-1336.
148. S. Hayashi, F. Hoshi, T. Ishikura, M. Yumura, and S. Ohshima, *^{13}C NMR study of ^{13}C-enriched single-wall carbon nanotubes synthesized by catalytic decomposition of methane.* Carbon, **2003**. 41(15): p. 3047-3056.
149. F. Liang, L.B. Alemany, J.M. Beach, and W.E. Billups, *Structure analyses of dodecylated single-walled carbon nanotubes.* Journal of the American Chemical Society, **2005**. 127(40): p. 13941-13948.
150. L.B. Alemany, L. Zhang, L. Zeng, C.L. Edwards, and A.R. Barron, *Solid-state NMR analysis of fluorinated single-walled carbon nanotubes: Assessing the extent of fluorination.* Chemistry of Materials, **2007**. 19(4): p. 735-744.
151. R.R. Nayak, K.Y. Lee, A.M. Shanmugharaj, and S.H. Ryu, *Synthesis and characterization of styrene grafted carbon nanotube and its polystyrene nanocomposite.* European Polymer Journal, **2007**. 43(12): p. 4916-4923.
152. Q. Yang, L. Shuai, J. Zhou, F. Lu, and X. Pan, *Functionalization of multiwalled carbon nanotubes by pyrene-labeled hydroxypropyl cellulose.* Journal of Physical Chemistry B, **2008**. 112(41): p. 12934-12939.
153. A. Kitaygorodskiy, W. Wang, S.Y. Xie, Y. Lin, K.A. Shiral Fernando, X. Wang, L. Qu, B. Chen, and Y.P. Sun, *NMR detection of single-walled carbon nanotubes in solution.* Journal of the American Chemical Society, **2005**. 127(20): p. 7517-7520.

154. R. Marega, V. Aroulmoji, F. Dinon, L. Vaccari, S. Giordani, A. Bianco, E. Murano, and M. Prato, *Diffusion-ordered NMR spectroscopy in the structural characterization of functionalized carbon nanotubes.* Journal of the American Chemical Society, **2009**. 131(25): p. 9086-9093.
155. T.I.T. Okpalugo, P. Papakonstantinou, H. Murphy, J. McLaughlin, and N.M.D. Brown, *High resolution XPS characterization of chemical functionalised MWCNTs and SWCNTs.* Carbon, **2005**. 43(1): p. 153-161.
156. J. Zhu, H. Peng, F. Rodriguez-Macias, J.L. Margrave, V.N. Khabashesku, A.M. Imam, K. Lozano, and E.V. Barrera, *Reinforcing epoxy polymer composites through covalent integration of functionalized nanotubes.* Advanced Functional Materials, **2004**. 14(7): p. 643-648.
157. Z. Han and A. Fina, *Thermal conductivity of carbon nanotubes and their polymer nanocomposites: A review.* Progress in Polymer Science (Oxford), **2011**.
158. S. Bourbigot and S. Duquesne, *Intumescence-base Fire Retardants*, in *Fire Retardancy of Polymeric Materials*, C.A. Wilkie and A.B. Morgan, Editors. **2009**, CRC Press.
159. E. Bugnicourt, J. Galy, J.F. Gérard, and H. Barthel, *Effect of sub-micron silica fillers on the mechanical performances of epoxy-based composites.* Polymer, **2007**. 48(6): p. 1596-1605.
160. Z. Zhang, G. Liang, P. Ren, and J. Wang, *Curing behavior of epoxy/POSS/DDS hybrid systems.* Polymer Composites, **2008**. 29(1): p. 77-83.
161. C.C. Teng, C.C.M. Ma, K.C. Chiou, T.M. Lee, and Y.F. Shih, *Synergetic effect of hybrid boron nitride and multi-walled carbon nanotubes on the thermal conductivity of epoxy composites.* Materials Chemistry and Physics.
162. B. Biswas, B.K. Kandola, A.R. Horrocks, and D. Price, *A quantitative study of carbon monoxide and carbon dioxide evolution during thermal degradation of flame retarded epoxy resins.* Polymer Degradation and Stability, **2007**. 92(5): p. 765-776.
163. A. Fina, D. Tabuani, F. Carniato, A. Frache, E. Boccaleri, and G. Camino, *Polyhedral oligomeric silsesquioxanes (POSS) thermal degradation.* Thermochimica Acta, **2006**. 440(1): p. 36-42.
164. G. Camino and M.P. Luda, in *Fire Retardancy of Polymers-The use of intumescence*, G. Camino, et al., Editors. **1998**, Royal Society of Chemistry: Cambridge. p. 48.
165. S. Bourbigot, M. Le Bras, R. Delobel, R. Decressain, and J.P. Amoureux, *Synergistic effect of zeolite in an intumescence process: Study of the carbonaceous structures using solid-state NMR.* Journal of the Chemical Society - Faraday Transactions, **1996**. 92(1): p. 149-158.
166. A.B. Morgan and M. Galaska, *Microcombustion calorimetry as a tool for screening flame retardancy in epoxy.* Polymers for Advanced Technologies, **2008**. 19(6): p. 530-546.
167. M.I.B. Tavares, J.R.M. D'Almeida, and S.N. Monteiro, *^{13}C solid-state NMR analysis of the DGEBA/TETA epoxy system.* Journal of Applied Polymer Science, **2000**. 78(13): p. 2358-2362.
168. N. Grassie, M.I. Guy, and N.H. Tennent, *Degradation of epoxy polymers: Part 4-Thermal degradation of bisphenol-A diglycidyl ether cured with ethylene diamine.* Polymer Degradation and Stability, **1986**. 14(2): p. 125-137.

169. H. Assaaoudi, I.S. Butler, J. Kozinski, and F. Bélanger-Gariépy, *Crystal structure, vibrational spectra and thermal decomposition study of a new, dicationic, acidic pyrophosphate: $KHMgP_2O_7 \cdot 2H_2O$.* Journal of Chemical Crystallography, **2005**. 35(10): p. 809-820.
170. S. Bourbigot, M. Le Bras, R. Delobel, and J.M. TrÃ©millon, *Synergistic effect of zeolite in an intumescence process: Study of the interactions between the polymer and the additives.* Journal of the Chemical Society - Faraday Transactions, **1996**. 92(18): p. 3435-3444.
171. A. Karrasch, E. Wawrzyn, B. Schartel, and C. Jäger, *Solid-state NMR on thermal and fire residues of bisphenol A polycarbonate/silicone acrylate rubber/bisphenol A bis(diphenyl-phosphate)/(PC/ SiR/BDP) and PC/SiR/BDP/zinc borate (PC/SiR/BDP/ZnB) - Part I: PC charring and the impact of BDP and ZnB.* Polymer Degradation and Stability, **2010**. 95(12): p. 2525-2533.
172. J.R. Van Wazer, *Phosphorus and its compounds, Vol.1:Chemistry*: Interscience Publishers Inc.
173. S. Bourbigot, M.L. Bras, and R. Delobel, *Carbonization mechanisms resulting from intumescence association with the ammonium polyphosphate-pentaerythritol fire retardant system.* Carbon, **1993**. 31(8): p. 1219-1230.
174. M. Bugajny, S. Bourbigot, M. Le Bras, and R. Delobel, *The origin and nature of flame retardance in ethylene-vinyl acetate copolymers containing hostaflam AP 750.* Polymer International, **1999**. 48(4): p. 264-270.
175. A. Tuteja, P.M. Duxbury, and M.E. Mackay, *Multifunctional nanocomposites with reduced viscosity.* Macromolecules, **2007**. 40(26): p. 9427-9434.

Appendices

APPENDIX 1: SUMMARY OF THE PROPERTIES OF VIRGIN EPOXY AND INTUMESCENT FORMULATIONS

Experiment	Parameter	Virgin epoxy	Epoxy_APP-5	Epoxy_APP-4.5_CNT-0.5	Epoxy_APP-4_OMPOSS-1
TGA under air (10 °C/min)	$T_{max\ deg\ rate\text{-}step\ 1}$*	347	329	323	338
	Residual weight 1 (%)	40	50	46	55
	$T_{max\ deg\ rate\text{-}step\ 2}$*	510	510	539	508
	Residual weight 2 (%)	1	14	10	10
	$T_{max\ deg\ rate\text{-}step\ 3}$*	-	700	690	745
	Residual weight 3 (%)	-	3	2	3
TGA under nitrogen (10 °C/min)	$T_{max\ deg\ rate}$*	353	336	337	339
	Residual weight (%)	14	20	17	19
PCFC (1 °C/s, N2)	pHRR (W/g)	428	381	410	414
	ΔpHRR (%)	-	-11	-4	-3
	Temperature at pHRR (°C)	357	337	318	337
Apparent viscosity (10 °C/min)	$T_{onset\ decrease}$ (°C)*	355	326	330	342
	Minimum viscosity (Pa.s)	500	-	825	1616
	$T_{minimum\ viscosity}$ (°C)	369	-	352	381

Experiment	Parameter	Virgin epoxy	Epoxy_APP-5	Epoxy_APP-4.5_CNT-0.5	Epoxy_APP-4_OMPOSS-1
Mass-loss calorimetry (Heat Flux: 35kW/m², thickness: 5mm, d: 25mm)	tign (s)	94	75	55	75
	pHRR (kW/m²)	1077	536	776	326
	ΔpHRR (%)	-	-50	-28	-68
	THR (MJ/m²)	79	63	76	-
	ΔTHR (%)	-	-20	-4	-
	Residual weight (%)	0	19	8	21
Mass-loss calorimetry (Heat Flux: 35kW/m², thickness: 2.5mm, d: 25mm)	tign (s)	49	46	37	41
	pHRR (kW/m²)	813	557	587	408
	ΔpHRR (%)	-	-31	-28	-50
	THR (MJ/m²)	33	26	25	23
	ΔTHR (%)	-	-21	-24	-30
	Residual weight (%)	4	12	8	15
Swelling (Heat Flux: 35kW/m², thickness: 2.5mm, d: 35mm)	$t_{beginning}$ (s)	-	31	38	29
	t_{end} (s)	-	60	50	50
	Swelling rate (%/s)	-	17	48	40
	Maximum swelling (%)	-	380	687	918

* $T_{max\ deg\ rate\text{-}step\ x}$ = Temperature for which the mass loss rate is the highest for step x,

$T_{onset\ decrease}$ = Temperature for which the viscosity begins to drop

APPENDIX 2: PUBLICATIONS AND COMMUNICATIONS

Publications

Bourbigot, S., Fontaine, G., Gallos, A., Gérard, C., Bellayer, S.,
Functionalized-carbon multiwall nanotube as Flame Retardant for Polylactid Acid.
in *Fire and Polymers V*, Wilkie, C. A., Morgan, A. B., Nelson, G. L., Editors. **2009**, ACS, p.25-34.

Gérard, C., Fontaine, G., Bourbigot, S.,
New trends in reaction and resistance to fire of fire-retarded epoxies.
Materials, **2010,** *3*, 4476-4499.

Gérard, C.; Fontaine, G.; Bourbigot, S.;
Synergistic and antagonistic effects in flame retardancy of an intumescent epoxy resin.
Polymers for Advanced Technologies, **2011**, accepted.

Oral communication with proceedings

Fontaine, G., Gérard, C., Gallos, A., Mamède, A.-S., Bourbigot, S.
(Chemically-modified) nanoparticles for flame-retarded polymeric materials.
21st Annual Recent Advances in Flame Retardancy of Polymeric Materials, Stamford, USA, 24-26 May **2010**, 10p.

Fontaine, G., Gérard, C., Bellayer, S., Bourbigot, S.
Intumescent epoxy resin: impressive synergistic effect of APP/POSS combination.
International Symposium on Flame-Retardant Materials & Technologies, Chengdu, China, 17-20 Septembre **2010,** 4p.

Fontaine, G., Gérard, C., Bellayer, S., Bourbigot, S.
POSS a synergist for fire retardant epoxy resin /APP system: Mecanism of action.
22nd Annual Recent Advances in Flame Retardancy of Polymeric Materials, Stamford, USA, 23-25 May **2011**, 10p.

Oral communication without proceedings

Gérard, C., Fontaine, G., Bourbigot, S.
Synthèse de nanotubes fonctionalisés pour l'amélioration des propriétés retard au feu de matrices polymères.
Journée des Jeunes Polymeristes du Nord, Lille, 2 December 2009

Gérard, C., Fontaine, G., Bourbigot, S.
Flame-retarding epoxy resins
Joint working group, Sippenaeken, Belgium, 14-17 June 2010

Apport des nanoparticules à l'ignifugation des résines époxydes

Ce mémoire porte sur l'étude de l'ignifugation d'une résine époxyde grâce à l'utilisation de nanoparticules. L'incorporation de Polyhedral Oligomeric Silsesquioxanes (POSS) ou de nanotubes de carbone seuls dans la matrice apporte une amélioration très limitée des propriétés feu. La fonctionnalisation covalente de nanotubes de carbone par des fonctions retardatrices de flamme a été réalisée et caractérisée, mais elle n'augmente pas les performances feu de la matrice chargée en nanotubes de carbone. La combinaison entre un retardateur de flamme phosphoré (APP) et les nanotubes de carbone révèle l'existence d'un effet antagoniste entre ces deux charges. Au contraire, l'utilisation de POSS en combinaison avec l'APP apporte une synergie. L'étude de la dégradation thermique de ces systèmes montre que les interactions entre ces constituants modifient la viscosité de la matrice dégradée. La capture des gaz de dégradation est améliorée dans le cas APP/POSS, ce qui résulte en la création d'une couche protectrice plus tôt qu'avec le système de référence contenant l'APP seul. De plus, la présence de POSS rend possible la création de silicophosphates renforçant le résidu. Au contraire, le résidu du système à base de nanotubes de carbone est très rigide et se fissure durant la combustion, ce qui empêche la bonne formation de la couche protectrice.

Mots-clefs: Résine époxyde, ignifugation, dégradation thermique, ammonium polyphosphate, nanoparticules, POSS, nanotubes de carbone

Contribution of nanoparticles to the flame retardancy of epoxy resins

This thesis aims at flame-retarding an epoxy resin through the use of nanoparticles. Incorporation of Polyhedral Oligomeric Silsesquioxane (POSS) or carbon nanotubes alone in the matrix provides little enhancement of the reaction to fire. The covalent functionalization of carbon nanotubes by grafting fire-retardant moieties has been carried out and characterized, but it does not enhance the reaction to fire of the epoxy matrix filled with carbon nanotubes. The combination between a phosphorus-based flame-retardant (APP) and carbon nanotubes reveals an antagonistic effect between these two fillers. On the contrary, using POSS in combination with APP provides a synergy. The study of the thermal degradation of these systems shows that the interactions between these fillers modify the viscosity of the degraded matrix. The trapping of degradation gases is enhanced in the case of APP/POSS, which results in the creation of a protective layer earlier than with the reference system containing APP alone. Furthermore, the presence of POSS permits the creation of silicophosphates which reinforce the residue. On the contrary, the residue of the formulation containing carbon nanotubes is excessively stiff and it cracks during combustion, hindering the proper formation of the protective layer.

Keywords: Epoxy resins, flame retardancy, thermal degradation, ammonium polyphosphate, nanoparticles, POSS, carbon nanotubes

Adresse du laboratoire :
Unité Matériaux Et Transformations (UMET) – CNRS UMR 8207
ENSCL, Bâtiment C7, Cité Scientifique
BP 90108
59652 Villeneuve d'Ascq Cedex - FRANCE